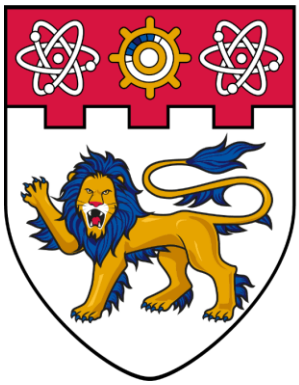

NANYANG TECHNOLOGICAL UNIVERSITY
SINGAPORE

EXPOSURE, BIOACTIVATION AND METABOLIC TOXICITY OF BISPHENOL A DIGLYCIDYL ETHER

LIU MIN

SCHOOL OF CIVIL AND ENVIRONMENTAL ENGINEERING

2020

EXPOSURE, BIOACTIVATION AND METABOLIC TOXICITY OF BISPHENOL A DIGLYCIDYL ETHER

LIU MIN

School of Civil and Environmental Engineering

A thesis submitted to the Nanyang Technological University in partial fulfilment of the requirement for the degree of Doctor of Philosophy

Statement of Originality

I hereby certify that the work embodied in this thesis is the result of original research, is free of plagiarised materials, and has not been submitted for a higher degree to any other University or Institution.

15/1/2020

…… ……

Date LIU MIN

Supervisor Declaration Statement

I have reviewed the content and presentation style of this thesis and declare it is free of plagiarism and of sufficient grammatical clarity to be examined. To the best of my knowledge, the research and writing are those of the candidate except as acknowledged in the Author Attribution Statement. I confirm that the investigations were conducted in accord with the ethics policies and integrity standards of Nanyang Technological University and that the research data are presented honestly and without prejudice.

15/01/2020

…… ……

Date Fang Mingliang

Authorship Attribution Statement

Please select one of the following; *delete as appropriate:
*(B) This thesis contains material from [1] paper(s) published in the following peer-reviewed journal(s)

Chapter 3 is published as Liu, M., Jia, S., Dong, T., Han, Y., Xue, J., Wanjaya, E. R., & Fang, M. (2019). The occurrence of bisphenol plasticizers in paired dust and urine samples and its association with oxidative stress. *Chemosphere*, 216, 472-478.

The contributions of the co-authors are as follows:
 Asst/Prof Fang provided the initial project direction and edited the manuscript drafts.

 I prepared the manuscript drafts. The manuscript was revised by Dr.Jia, Dr.Dong, Dr.Han and Dr. Xue and Miss Wanjaya.

 I co-designed the study with Asst/Prof Fang and performed all the laboratory work at the School of Civil and Environmental Engineering and Nanyang Environment and Water Research Institute. I also analysed the data.

 Dr. Jia and Dr. Dong assisted in the sample preparation and method development.

 Dr. Han and Miss. Wanjaya assisted in the instrument method development.

 Dr. Xue provided substantial advice and manuscript revision.

15/1/2020
……
Date

……
LIU MIN

ACKNOWLEDGEMENT

The dissertation was compiled at School of Civil and Environmental Engineering, Nanyang Technological University. I would like to express my sincere gratitude to those who have accompanied and provided continuous support during my PhD study.

I am deeply indebted to my supervisor Prof. Fang Mingliang, who always tries his best to help and encourage me during my study. His invaluable advice and enlightenment have led me to go forward and complete my study.

Sincere thanks also go to our lovely technical staff in the Environmental Lab and the R3C lab, especially to Ong Chee Yung, Tan Han Khiang, Lim-Tay Chew Wang, Wong Yuet Mun and Lo Siew Cheng, for their professional assistance and kind helps during my experiments.

I thank our group members, Dr. Jia Shenglan and Dr. Shang Hongtao and Dr. Wang Bei, Dr. Zhao Fangrong, Dr. Xu Tengfei and Ms. Tharushi Prabha Keerthisinghe and many other groupmates for their patience and help in my research works.

Lastly, I'd like to express my sincere thanks to my parents and husband, who give me encourage and supports to help me complete my study.

TABLE OF CONTENTS

ACKNOWLEDGEMENTS····· i
TABLE OF CONTENT ····· ii
SUMMARY·····v
LIST OF PUBLICATIONS·····vii
LIST OF TABLES·····ix
LIST OF FIGURES ·····x
LIST OF ABBREVIATIONS ·····xv

Contents

Chapter 1. Introduction 1
1.1 Background 1
1.2 Purpose and Scope 3
1.3 Dissertation Overview 4
Chapter 2. Literature Review 6
2.1 Production, Application and Sources 6
2.1.1 Production 6
2.1.2 Applications and Indoor Sources 7
2.2 Physicochemical Properties and Structures of BADGEs 8
2.3 Analytical Method of BADGEs 12
2.4 Occurrences in Environmental Matrix and Human Specimen 16
2.4.1 Occurrence in Indoor Dust 16
2.4.2 Occurrence in Air Samples 16
2.4.3 Occurrences in Wastewater and River Water Samples 16
2.4.4 Occurrence in Sewage Sludge 17
2.4.5 Occurrences in Dental Sealants 17
2.4.6 Occurrences in Textiles 17
2.4.7 Occurrences in Human Urine 17
2.4.8 Occurrences in Adipose and Plasma Samples 18
2.4.9 Occurrences in Marine Mammals 18
2.5 Biotransformation and Toxicity 25
2.5.1 Biotransformation 25
2.5.2 In Vitro Toxicological Studies 25
2.5.3 In Vivo Toxicological Studies 27
2.6 Summary of Literature Review 28
Chapter 3. The Occurrence of Bisphenol Plasticizers in Paired Dust and Urine Samples and its Association with Oxidative Stress 30
3.1 Overview 30

3.2 Introduction 30
3.3 Methodology 32
3.3.1 Sample Collection 32
3.3.2 Chemical Analysis 32
3.3.3 Quality Assurance and Quality Control (QA/QC) 35
3.3.4 Statistical Analysis 36
3.4 Results and Discussion 36
3.4.1 BADGE/BFDGE Stability Test and Water-free Method Development for Dust Analysis 36
3.4.2 Bisphenol Plasticizers in Indoor House Dust 38
3.4.3 Bisphenol Plasticizers in Human Urine 41
3.4.4 Correlation of Bisphenol Plasticizers in Paired Samples and its Association with Oxidative Stress 44
3.5 Conclusions 45
Chapter 4. Complementing Experiment with Prediction to Identify the Biotransformation Products of BADGE 47
4.1 Overview 47
4.2 Introduction 47
4.3 Methodology 48
4.3.1 Chemicals and Materials 48
4.3.2 Liver Microsomal Incubation 49
4.3.3 Cell Culture, Exposure Experiment and Metabolite Extraction 49
4.3.4 Instrumental Analysis 50
4.3.5 Reaction with Amino Acids 50
4.3.6 General Workflow to Identify Biotransformation Products 50
4.3.7 Empirical Knowledge Acquirement through Prediction and Identification of Potential Reaction Products with Amino Acids 52
4.3.8 In Silico Biotransformation Prediction using SyGMa 56
4.3.9 Knowledge-based Prediction 59
4.4 Results & Discussions 64
4.4.1 Identification and MS/MS Fragmentation Behavior of BADGE and Amino Acids Reaction Products 64
4.4.2 Kinetics of BADGE and Amino Acids Reaction Products 65
4.4.4 In Vitro Metabolism of BADGE in Rat Liver Microsomal 67
4.4.5 Detected Biotransformation Products in HepG2 Cells 72
4.5 Short Summary 74
Chapter 5. Comparison of Metabolic Toxicity between Bisphenol A Diglycidyl Ether (BADGE) and Bisphenol A 75
5.1 Overview 75
5.2 Introduction 75
5.3 Methodology 76
5.3.1 Cell Culture and Reagent Preparation 76
5.3.2 Cytotoxicity Test 76
5.3.3 Mixture Exposure and Metabolite Extraction 77
5.3.4 Metabolite Profiling and QA/QC 78
5.3.5 Metabolites and Metabolic Pathway Analysis 78
5.4 Results &Discussion 79
5.4.1 Cytotoxicity of BADGE and its Derivatives 79

5.4.2 Metabolomics Profiling....80
5.4.3 Dysregulated Metabolites Identification....81
5.4.4 Metabolomics Pathway Analysis....86
5.5 Short Summary....88
Chapter 6. Significant "Mixture Effect" Upon Exposure to 23 Chemicals at Human-relevant Levels....90
6.1 Overview....90
6.2 Introduction....90
6.3 Methodology....92
6.3.1 Chemicals and Materials....92
6.3.3 Experimental Workflow....93
6.3.4 Xenobiotic Mixture Preparation....96
6.3.5 Resazurin Assay, Protein and DNA quantification....99
6.3.6 Mixture Exposure and Metabolite Extraction....99
6.3.7 Metabolite Profiling and QA/QC....100
6.3.8 Metabolites and Metabolic Pathway Analysis....101
6.3.9 RNA Preparation Sequencing Preparation and Data Analysis....101
6.3.10 Differential Expression Analysis, Functional Enrichment and Joint Pathway Analysis....102
6.3.11 "Counting-out" Method to Evaluate the Relative Contribution of each Chemical in the Mixture....103
6.4 Results....104
6.4.1 Mixture Cell Viability and DNA Quantification....104
6.4.2 Metabolomics Profiling....104
6.4.3 Dysregulated Metabolite Identification....105
6.4.4 Metabolomics Pathway Analysis....109
6.4.5 Transcriptomic Profiling....109
6.4.6 Gene Ontology (GO) Analysis and Unsupervised Pathway Analysis....110
6.4.7 Supervised Pathway Analysis....112
6.4.8 Integration of Metabolome and Transcriptome through Joint Pathway Analysis....112
6.4.9 Relative Contribution of Each Chemical in the Mixture Effect....115
6.5 Discussions....118
6.6 Short Summary....121
Chapter 7. Conclusions and Recommendations....122
7.1 Conclusions....122
7.2 Recommendations....123
References....125
Appendix A....137
Appendix B....144

Summary

Bisphenol A diglycidyl ether (BADGE) is an emerging organic contaminant (EOC) with unique epoxide structure and also known as an endocrine-disrupting chemical (EDC). BADGE and its derivatives (BADGEs) are widely used as epoxy resins and emerging plasticizers in food packages and material coating. Unlike its precursor bisphenol A (BPA) that has been intensely investigated, little information is available on its occurrence, biotransformation and toxicity. In addition, the analysis of BADGEs has always been a challenge due to their reactive chemical properties.

My thesis first started from the development of a novel water-free method to analyze BADGEs in dust samples. Based on this method, the study measured the bisphenol plasticizer levels in paired dust and urine samples collected from Singapore. To tentatively explore the human health effects from exposure to these bisphenol plasticizers, this thesis further assessed the correlation between urinary concentrations of these compounds and oxo-2'-deoxyguanosine (8-OHdG), an oxidative stress biomarker.

Considering the reactive properties and limited biotransformation information of BADGE, this thesis further investigated its *in vitro* biotransformation products. We first developed a novel discovery platform to predict and identify potential metabolites of BADGE in rat liver microsomal and human liver cancer cell HepG2. Prior to knowledge-based prediction and identification, this study built an "empirical knowledge acquirement" method through investigating BADGE's potential reaction and kinetics with 17 amino acids and the MS/MS fragmentation patterns of those reaction products. Furthermore, this study employed both *in silico* and knowledge-based method to predict the possible biotransformation products of BADGE. Lastly, the potential metabolites and metabolism pathway were proposed through experimental analysis and data deconvolution derived from high-resolution mass spectrometry (HRMS).

To compare the metabolic toxicity between two structurally similar compounds, this study further explored the possible cellular disturbances induced by different levels of BADGE and BPA exposure upon a hormone-responsive breast cancer cell line MCF-7 using a global metabolomics approach. The endogenous metabolite profiling after BADGE or BPA treatment was conducted. Their respective affected biochemical pathways were figured out and compared at system-biological levels.

To understand the potential effects after exposure to BADGEs at human-relevant level, this study has employed omics method (e.g. metabolomics and transcriptomic) to characterize the biological effect after exposure to 23 xenobiotics 'cocktail' (e.g., BPA and BADGEs, flame retardants, phthalates and etc.) at human-relevant levels upon breast cancer cell MCF-7. Furthermore, this study also developed a novel "counting out" method to evaluate the relative contribution of each compound including BADGE to the observed mixture effect.

List of Publications

Liu, M., Jia, S., Dong, T., Han, Y., Xue, J., Wanjaya, E. R., & Fang, M.* (2019). The occurrence of bisphenol plasticizers in paired dust and urine samples and its association with oxidative stress. *Chemosphere*, *216*, 472-478. doi: 10.1016/j.chemosphere.2018.10.090.

Min Liu, Shenglan Jia, Ting Dong, Qin Yang, Mingliang Fang*. Exposure of MCF-7 cells to Mixture of 23 Chemicals at Human-relevant Levels: Metabolomic and Transcriptomic Analysis and Prioritization of Individual Contribution. *Environmental Health Perspectives, **Under Revision***.

Zhang, Y. [#], **Liu, M.** [#,*], Peng, B., Jia, S., Koh, D., Wang, Y., ... & Fang, M. (2020). Impact of Mixture Effects between Emerging Organic Contaminants on Cytotoxicity: A systems-biological Understanding of Synergism between TDCPP and TPP. Environmental Science & Technology. ([#] Co-first and [*]co-corresponding author)

Min Liu, Mingliang Fang*. Complementing Experiment with Prediction to Identify Biotransformation Products of BADGE. ***To be Submitted.***

Min Liu, Mingliang Fang*. Comparison of Metabolic Toxicity between Bisphenol A Diglycidyl Ether and Bisphenol A. ***To be Submitted.***

Bo Peng, **Min Liu**, Yuan Han, Elvy Riani Wanjaya, Mingliang Fang*. (2019). Competitive Biotransformation among Phenolic Xenobiotic Mixtures: Underestimated Risks for Toxicity Assessment. *Environmental Science & Technology*, *53* (20), 12081-12090. doi: 10.1021/acs.est.8b02629.

Yingdan Zhang, Tharushi Prabha Keerthisinghe, Yuan Han, **Min Liu**, Elvy Riani Wanjaya, Mingliang Fang*. (2018). “Cocktail” of xenobiotics at human relevant levels reshapes the gut bacterial metabolome in a species-specific manner. *Environmental Science & Technology*, *52* (19), 11402-11410. doi: 10.1021/acs.est.8b02629.

Shenglan Jia, Tengfei Xu, Tao Huan, Maria Chong, **Min Liu**, Wenjuan Fang, Mingliang Fang*. (2019). Chemical Isotope Labeling Exposome (CIL-EXPOSOME): one High-throughput Platform for Human Urinary Global Exposome Characterization. *Environmental Science & Technology*, *53* (9), 5445-5453. doi: 10.1021/acs.est.9b00285.

JJ Yang, Y Han, CH Mah, E Wanjaya, B Peng, TF Xu, **M Liu**, T Huan, ML Fang*. (2019). Streamlined MRM Method Transfer between Instruments Assisted with HRMS Matching and Retention-time Prediction. *Analytica Chimica Acta*, doi: 10.1016/j.aca.2019.12.002.

Shenglan Jia, Gayatri Sankaran, Bei Wang, Hongtao Shang, Sze Tat Tan, Hooi Ming Yap, Joanna Shen, Ramona Alikiiteaga Gutiérrez, Wenjuan Fang, **Min Liu**, Victor Wei-Chung Chang, Lee Ching Ng, Mingliang Fang*. (2019). Exposure and Risk Assessment of Volatile Organic Compounds and Airborne Phthalates in Singapore's Child Care Centers, *Chemosphere*, *224*, 85-92. doi: 10.1016/j.chemosphere.2019.02.120.

List of Tables

Table 2-1. Physicochemical properties and structures of bisphenol plasticizers

Table 2-2. Extraction, purification and analytical methods of BADGEs in different sample matrix using Liquid Chromatography and Mass Spectrometry detection.

Table 2-3. The concentration of BADGEs in environmental and human samples collected from different countries.

Table 3-1. Concentrations, detection rate (DR%) and method detection limit (MDL) of bisphenol plasticizers in indoor dust (ng/g) and urine (ng/mL) from Singapore

Table 4-1. Knowledge-based prediction of reaction products of BADGE with amino acids and the observed retention time.

Table 4-2. Prediction on the potential metabolites of BADGE-2H_2O using Python library SyGMa.

Table 4-3. Knowledge-based metabolic prediction on potential metabolites.

Table 4-4. Experimentally determined rate constants (K) for BADGE's reaction products in pH=7.4 at 37 ºC.

Table 5-1. Dysregulated metabolites of MCF-7 cells after BPA or BADGE exposure (Significance Criteria: |Fold change(FC)| >1.3 & *p*-value <0.05)

Table 6-1. Summary of the maximum (Max), geometric mean (GM) and 95th percentile mean urinary or blood concentration of 23 chemicals.

List of Figures

Figure 2-1. The synthesis of BADGE and reactions for the formation of BADGE-related compounds; modified from (Wang et al. 2012) and dash line represents the products were likely to form during PVC production.

Figure 2-2. The widespread applications and sources of bisphenol diglycidyl ether (BADGE).

Figure 3-1. Hydrolysis and product formation of (a) BADGE; (b) BFDGE for pH=7 at 25°C

Figure 3-2. (a) Scatter plot of bisphenol plasticizers (ng/g) in indoor house dust from Singapore; (b) Box plot of relative distribution (%) of BADGEs in indoor dust; (c) Spearman correlation between BPA and BADGE-H_2O in indoor dust; (d) Spearman correlation between BADGE and BADGE-$2H_2O$ in indoor dust.

Figure 3-3. Scatter plot representing the total form concentration (ng/mL) of bisphenol plasticizers in urine samples (deconjugated by β-glucuronidase treatment) from Singapore (n=33).

Figure 3-4. Pearson Correlation between BPA concentration in paired house dust and human urine samples (n=32)

Figure 3-5. (a) Spearman Correlation between urinary BPA concentration and oxidative stress biomarker 8-OHdG (n=32); (b) Pearson correlation between urinary oxidative stress biomarker and body mass index (BMI) (n=33)

Figure 4-1. Workflow for the prediction and identification of biotransformation products of BADGE.

Figure 4-2. Proposed workflow for 'empirical knowledge acquirement' through reaction of amino acids with BADGE.

Figure 4-3. Knowledge-based prediction of BADGE glucuronide and sulfate conjugates based on the validated biotransformation for BPA.

Figure 4-4. Fragmentation pattern of reaction products of BADGE and amino acids with a collision energy of 20 eV under ESI (+) mode. **A.** BADGE-H_2O-Cys; **B.** BADGE-H_2O-Methionine; **C.** BADGE-H_2O-Proline; **D.** BADGE-H_2O-Alanine; **E.** BADGE-H_2O-isoleucine; **F.** BADGE-H_2O-glutamic acid

Figure 4-5. The formation [%] of reaction products of BADGE with **A.** cysteine and **B.**

methionine over time (hours); pH=7.4 at 37 ºC.

Figure 4-6. Cloud plot of filtered features for microsomes samples.

Figure 4-7. Two one-side BADGE glucuronide conjugates in microsomes and their potential structures eluted in **A.** 7.5 min; **B.** 8.7 min and their MS/MS fragments in ESI (+) mode with a collision energy of 20 eV.

Figure 4-8. The proposed structure for BADGE two-side glucuronide conjugates in microsomes and its MS/MS fragments in ESI (+) mode with a collision energy of 20 eV

Figure 4-9. Proposed structure for **A.** BADGE sulfate conjugates and **B.** BADGE glutathione conjugation products in microsomes and their MS/MS fragments in ESI (+) mode with a collision energy of 20 eV.

Figure 4-10. Proposed potential metabolites for BADGE metabolism by rat liver microsomal.

Figure 4-11. Cloud plot of filtered features in HepG2 cell samples.

Figure 4-12. Proposed structure for BADGE glucose adduct (m/z 556.2742 was the $[M+NH4]^+$ adduct) in HepG2 and its MS/MS fragments in ESI (+) mode with a collision energy of 20 eV.

Figure 4-13. Proposed potential metabolites for BADGE metabolism by HepG2 cell.

Figure 5-1. Cell viability of MCF-7 cells exposed to BADGE and its derivatives at varying concentrations (0.01, 0.1, 1, 5, 10, 50 and 100μM) by Resazurin Assay.

Figure 5-2. Global metabolite profiling of MCF-7 cell in response to 10μM BADGE, 25μM BADGE, 50μM BADGE, 10μM BPA, 25μM BPA and 50μM BPA **A.** Up and down regulated significant features detected by global profiling (percentage was calculated based on total detected feature numbers); **B.** Classic Venn diagram summarizing the number of shared and distinct features for BADGE and BPA at 25 μM and 50 μM.

Figure 5-3. A. Heatmap of the identified metabolites for different concentrations of BADGE and BPA. Scales in color key represent $\log_2$ (Fold Change) value of metabolites (Fold Change: treatment over control samples). Red indicates upregulation; Purple indicates downregulation. **B.** Bar graphs represent the dysregulation of metabolites as examples in treatment (y-axis is the fold changes by comparing the treatment to the control). "*" and "**" represent $p \leqslant 0.05$ and $p \leqslant 0.01$.

Figure 5-4. Metabolic pathway analysis for **A.** BPA and **B.** BADGE exposure using

Metaboanalyst ($p \leq 0.05$); Up and down regulation of metabolites at different concentrations (10μM BADGE, 25μM BADGE, 50μM BADGE, 10μM BPA, 25μM BPA, 50μM BPA) in **C.** the dysregulation of arginine and proline metabolism with exposure to BPA and BADGE at different concentrations (Mean ± S.D.; n=4; red-horizontal dash line represents the fold change equals to 1)

Figure 6-1. Workflow for metabolome and transcriptome characterization and assessment of relative contribution on mixture effect using "Counting-out" Method.

Figure 6-2. A. Cell viability of MCF-7 after exposed to different levels (0.5 GM, GM, 5GM, Max, 5Max and 10Max) of the xenobiotic mixture by Resazurin Assay (N=4; mean ± S.D.); **B.** Normalized DNA concentration (% of control samples) of cells exposing to different levels of mixture (N=3; mean ± S.D.) "*" and "**" represent $p \leqslant 0.05$ and $p \leqslant 0.01$ when treatment groups is statistically different non-treated control using One-way *ANOVA* and *Duncan* post-hoc analysis; Global metabolite profiling of MCF-7 cell in response to the xenobiotic cocktail mixture at GM, 2GM, 5GM, Max and 5Max levels. **C.** Up and down regulated significant features detected by global profiling (percentage was calculated based on total detected feature numbers); Classic Venn diagram summarizing the number of shared and distinct features in **D.** ESI-negative mode and **E.** ESI-positive mode.

Figure 6-3. A. Heatmap of the identified significantly dysregulated metabolites for different mixture treatment level (GM, 2GM, 5GM, Max and 5Max). Scales in color key represent $\log_2$ (Fold Change) value of metabolites (Fold Change: treatment over control samples; N=4). Red indicates upregulation; Purple indicates downregulation. **B.** Box and whiskers plots represent the dysregulation of metabolites as examples in different mixture level (y-axis is the fold changes by comparing the treatment to the control; mid-line: median; upper and lower box boundaries represent 75^{th} percentile and 25^{th} percentile values; upper and lower whisker boundaries represent maximum and minimum values). "*" and "**" represent $p \leqslant 0.05$ and $p \leqslant 0.01$ when one treatment group is statistically different from non-treated control using One-way *ANOVA* and *Duncan* post-hoc analysis.

Figure 6-4. Significantly dysregulated pathways of xenobiotic mixture exposure at Max. **A.** Metabolic pathway analysis for the xenobiotic mixture at Max using Metaboanalyst ($p \leqslant 0.05$); Up and down regulation of metabolites at different concentrations (GM,

2GM, 5GM, Max and 5Max, N=4) in **B.** Pyrimidine metabolism; **C.** Purine metabolism.

Figure 6-5. A. Gene ontology (GO) analysis results from DAVID Bioinformatics Resources 6.8 for Max level mixture (N=3); **B.** The gene pathway enrichment analysis for differentially expressed genes (DEGs) of Max level mixture exposure using KOBAS 3.0 in three databases PANTHER, KEGG and REACTOME; **C.** The *in vitro* supervised pathway enrichment analysis for DEGs of Max level mixture exposure.

Figure 6-6. A. Significantly dysregulated pathways through integration of metabolites and genes data using joint pathway analysis in Metaboanalyst; Dysregulated metabolites and genes in **B.** "Pyrimidine metabolism" and **C.** "Purine metabolism" in MCF-7 cells under the exposure of xenobiotic mixture at Max; Red and green indicate upregulation and downregulation.

Figure 6-7. Assessment on the relative contribution of each component to the observed effect using the high-throughput metabolomics-based "counting-out" method (N=3). Total 25 groups: including 23 treatment groups with one component removed with the others remaining at Max level, one 23 chemical mixture at Max level labeled as All Compounds and one DMSO control. **A.** Intuitive hierarchical clustering analysis for grouping similar objects among the targeted 19 metabolites across 25 groups; each colored cell on the map corresponds to a concentration value; clustering of metabolites was based on Ward's clustering method with the Euclidean distance. Bar graph of the fold change (mean ± SEM) of **B.** UDP; **C.** Lactic acid; **D.** ATP after the removal of each component; y-axis represents the fold change by comparing treated samples with control samples; each color/pattern represents a chemical category; symbol a indicates one treatment group is statistically different from the DMSO controls by One-way *ANOVA* and *Duncan* post-hoc analysis, "a" denotes $p \leq 0.05$ and "aa" denotes $p \leq 0.01$; symbol b indicates one treatment group is statistically different from the All Compounds group, "b" denotes $p \leq 0.05$ and "bb" denotes $p \leq 0.01$; Abbreviations: MnBP, mono-n-butyl phthalate; BzBP, benzylbutyl phthalate; DHB: 2,4-dihydroxybenzophenone; BPA, bisphenol A; TDCPP, tris (1,3-dichloroisopropyl) phosphate; BPS, bisphenol S; TPhP, triphenyl phosphate; DBP, dibutyl phthalate; MEHP, mono-ethylhexyl phthalate; PFOA, perfluorooctanoic acid; DiNP, di-iso-nonyl phthalate; DiDP, diisodecyl phthalate; BFDGE, bisphenol F-diglycidyl ether; TBBPA, tetrabromobisphenol A; MBzP, monobenzyl phthalate; BADGE, bisphenol A diglycidyl ether; BADGE-2H_2O,

bisphenol A bis(2,3-dihydroxypropyl) ether; UDP-glucose, uridine diphosphate glucose; UDP, uridine diphosphate; CTP, cytidine triphosphate; GTP, guanosine triphosphate; UDP-glucuronic acid, uridine diphosphate glucuronic acid; GDP, guanosine diphosphate; ATP, adenosine triphosphate; ADP, adenosine diphosphate; CDP, cytidine 5'-diphosphate; UTP, uridine 5'triphosphate; b-G6P, beta-D-glucose-6-phosphate; GDP-mannose, guanosine diphosphate mannose.

List of Abbreviations

Abbreviation	Description
AGMs	Axon Guidance Molecules
AR	Androgen Receptor
BADGE	Bisphenol A Diglycidyl Ether
BADGEs	Bisphenol A Diglycidyl Ether-related Compounds
BaP	Benzo[a]pyrene
BFDGE	Bisphenol F Diglycidyl Ether
BMI	Body Mass Index
BPA	Bisphenol A
BPS	Bisphenol S
BzBP	Benzybutyl Phthalate
DBP	Di-n-butyl Phthalate
DDA	Data-dependent Acquisition
DEGs	Differentially Expressed Genes
DHB	2,4-dihydroxybenzophenone
DiDP	Di-isodecyl Phthalate
DiNP	Di-isononyl Phthalate
DMSO	Dimethyl Sulfoxide
EDCs	Endocrine-disrupting Chemicals
EDI	Estimated Daily Intake
EOCs	Emerging Organic Contaminants
ERα	Estrogen Receptor (α)
ESI	Electrospray Ionization
FBS	Fetal Bovine Serum
FC	Fold Change
GM	Geometric Mean
GO	Gene Ontology
HepG2	Human Liver Cancer Cells
HPV	High Production Volume
IRIS	Integrated Risk Information System
LC-MS/MS	Liquid Chromatography-Tandem Mass Spectrometry
LD50	Median Lethal Dose
LLE	Liquid-liquid Extraction
MBzP	Mono-benzyl Phthalate
MCF-7	Breast Cancer Cell
MCM	Minichromosome Maintenance Protein
MCNP	Mono-(-carboxynonyl) Phthalate
MDL	Method Detection Limit
MEHP	Mono-2-ethylhexyl Phthalate
MHBP	Mono-3-hydroxybutyl Phthalate
MiNP	Mono-isononyl Phthalate

MnBP	Mono-n-butyl Phthalate
MNT	Micronucleus Test
MOA	Mode of Action
MRM	Multiple Reaction Monitoring Mode
MSCs	Mesenchymal Stromal Stem Cells
NIST	National Institute of Standards and Technology
ORC	Origin Recognition Complex
PAHs	Polycyclic Aromatic Hydrocarbon
PBDEs	Poly-brominated Diphenyl Ethers
PBS	Phosphate-buffered Saline
PCPs	Personal Care Products
PFOA	Perfluorooctanoic Acid
PPARγ	Peroxisome Proliferator-activated Receptor gamma
PVC	Polyvinyl Chloride
QA/QC	Quality Assurance and Quality Control
qTOF	Quadrupole Time-of Flight
ROS	Reactive Oxygen Species
SG	Specific Gravity
SOMs	Site of Metabolites
SPE	Solid Phase Extraction
SRM	Standard Reference Material
SVOCs	Semi-volatile Compounds
TBBPA	Tetrabromobisphenol A
TCS	Triclosan
TDCPP	Tris (1,3-dichloro-2-propyl) Phosphate
TPhP	Triphenyl Phosphate
WWTPs	Wastewater Treatment Plants

Chapter 1. Introduction

1.1 Background

Many bisphenol plasticizers are known as endocrine-disrupting chemicals (EDCs) such as bisphenol A (BPA) and bisphenol a diglycidyl ether (BADGE). BPA is a manufacture precursor for BADGE and BADGE can be used as replacement for BPA in many applications. In terms of chemical structure, the backbone of BADGE is similar with BPA. Its side chain contains two epoxides, a cyclic ether with a three-atom ring, which makes it reactive. In addition, these electrophilic oxirane rings are subject to reaction with nucleophilic species (Petersen et al. 2008). BADGE is one of the most widely used epoxy resins in the world (Chamorro-García et al. 2012) and relative production of the glycidyl ethers covered in this monograph was reported to be 'ultra-high' for BADGE (Association 1984). It is used in epoxy surface coatings that provide superior adhesion, flexibility and corrosion resistance in metal surfaces (Cancer 1989).

The presence of BADGE-related compounds (BADGEs) is ubiquitous in our daily life. They are used in a variety of applications, such as protective coatings and reinforced plastics, as well as bonding materials and adhesives (Cancer 1989). The major application fields of BADGEs are primarily in PVC, sealants, coating, textiles, packaging materials or dental sealants (Møller et al. 2012). Unlike BPA has been intensely investigated, only a few studies documented the occurrences of BADGEs in the environmental matrix (Wang et al. 2012, Xue et al. 2015, Xue et al. 2016) and human specimens (Wang et al. 2012, Wang et al. 2015). A study raised the concern of BADGE's safety that it was reported may be equally or more harmful than BPA in triggering specific toxic effects such as cytotoxicity (Rosso et al. 2018). Therefore, further environmental and toxicological studies on BADGE are of great significance to human health and regulation guidance.

The chemical structure of BADGE is quite unique with two epoxides (electrophilic

oxirane rings), resulting in its reactive property. This property has been confirmed in an earlier study on the reaction of BADGE with food components such as oil, protein and amino acids that leads to its 'disappearance' in food packaging materials (Petersen et al. 2008). The analysis of BADGEs has always been a challenge due to these reasons and the laboratory background contamination. So far, for current available analytical protocols, since water is frequently used during the sample extraction/cleanup, the hydrolysis potentials of BADGEs may cause high uncertainty for the absolute quantification.

Xenobiotic transformation is known as a primary detoxification strategy in organisms, but in many cases some bioactivated metabolites could be even more toxic than their parent compounds. As an emerging organic contaminant (EOC), very few studies have documented the biotransformation of BADGE *in vitro* and *in vivo*. Although it is generally presumed that its main metabolites are its hydrolysis products (Wang et al. 2012), some studies revealed that a large proportion of BADGE has been bio-transformed to many unknown metabolites which yet to be thoroughly investigated. For examples, F344 rats were given oral 2-^{14}C-propane-labelled BADGE doses of 2.7 mg/kg body weight. The results showed less than 10% was unchanged BADGE in plasma (Nolan et al. 1981). In another study, the bis-diol of BADGE (BADGE-2H_2O) was excreted in both free and conjugated forms with the total amount ~5% of the dose to mouse (Climie et al. 1981). Overall, its metabolism may be quite complicated considering the reactivity and covalent binding potentials. Therefore, the development of an unbiased platform to robustly predict and identify the known and unknown metabolites was very important in its toxicity assessment.

Unlike accumulated toxicological evidences have suggested the pleiotropic toxic effect of BPA (Ortiz-Villanueva et al. 2017), less is known regarding the toxicity of BADGE. Up to date, BADGE has been reported to be an antagonist of peroxisome proliferator-activated receptor gamma (PPAR γ) (Wright et al. 2000). It was reported

mutagenic, genotoxic and cytotoxic in the cell model (Suárez et al. 2000, Ramilo et al. 2006, Sueiro et al. 2006). However, its toxic action mechanism on biological events at system-biological level is yet unknown and warranted further exploration. Besides, BPA and BADGE show high similarity on their backbones while side chains are different (e.g. epoxide groups versus hydrophenol groups). Therefore, it will be interesting to compare the cellular perturbations upon exposure to each of them, which will enhance our understanding of chemical structure's effect on metabolic toxicity.

Lastly, another knowledge gap is whether BADGE or its similar compounds at environmentally or human-relevant concentration can induce some adverse effects. As is well-known, the results generated from traditional toxicology assessment with high dose usually have less relevance to human. The real-life exposure scenarios for BPA and BADGEs are alongside with inorganics and other ever-increasing organic contaminants such as flame retardants and phthalates at very low-level. Although each chemical may be at non-effective concentration, the co-exposure raises the major concern from the possibility that chemicals have either additive or even synergistic effects (Carpenter et al. 2002, Kortenkamp 2007). Several earlier mixture studies have revealed the ability of chemicals to act together to induce some observable effects at non-lethal levels (Silva et al. 2002, Brian et al. 2007). Therefore, whether "chemical mixture" of higher complexity at the low human-relevant levels would trigger any health effects remains unaddressed and it is an ongoing challenge for toxicological risk assessment. In addition, there is also a pressing demand to develop more effective "proof-of-concept" for elucidating the contribution of each component in the mixture, which could enhance our understanding on BADGE' relative toxicity contribution at human-relevant level.

1.2 Purpose and Scope

The objectives of this PhD work are to:

(i) Develop a sensitive and water-free method for BADGE analysis in the dust; determine their occurrences in paired dust and urine samples collected from Singapore; tentatively explore the association of all typical bisphenol plasticizers between paired dust and urine samples as well as their correlation with oxidative stress biomarkers.

(ii) Develop an effective biotransformation product discovery platform for BADGE; robustly identify possible transformation products and propose metabolism pathway of BADGE in liver microsomes and *in vitro* liver cells (HepG2).

(iii) Use global metabolomics to compare the metabolic toxicity between two structurally similar compounds BADGE and BPA; compare their affected pathways and elucidate their underlying toxicity mechanism.

(iv) Characterize the mixture effect after exposure to 23 common organic contaminants (e.g. BADGE and bisphenol A etc.) at human-relevant levels upon breast cancer cell (MCF-7); develop a high-throughput metabolomics-based "counting out" method to evaluate the relative contribution of BADGEs to the observed mixture effect.

1.3 Dissertation Overview

This dissertation includes seven chapters. Chapter 1 and 2 are introduction and literature review. Chapter 7 is the conclusions and recommendations.

Chapter 3 developed and validated a novel water-free method for BADGEs analysis in dust samples. It also investigated the occurrences of these bisphenol plasticizers in 33 paired dust and urine samples collected from Singapore. The urinary oxidative stress biomarker oxo-2'-deoxyguanosine (8-OHdG) was also quantified to explore its possible association with bisphenol plasticizer exposure.

Chapter 4 developed a useful biotransformation product discovery platform with the integration of experimental analysis with *in silico* and knowledge-based prediction. It has investigated the reaction kinetics and MS/MS fragmentation behavior for those

formed products of BADGE with 17 amino acids. Lastly, it has proposed several novel biotransformation products and metabolism pathways for BADGE in liver microsomal and HepG2.

Chapter 5 compared the possible cellular disturbances induced by different levels of BADGE and BPA exposure upon a hormone-responsive cell line MCF-7 using the global metabolomics. It has further characterized the metabolic profiles of both chemicals and their affected biochemical pathways to elucidate the underlying mechanism at system-biological levels.

Chapter 6 utilized omics approach (e.g. metabolomics and transcriptomic) to characterize the biological effects of 23 xenobiotics 'cocktail' (e.g. including bisphenol plasticizers such as BPA and BADGEs, flame retardants and phthalates) at human-relevant level upon MCF-7. It also developed a novel "counting out" method to evaluate the relative contribution of bisphenol plasticizers to the observed mixture effect.

Chapter 2. Literature Review

2.1 Production, Application and Sources

2.1.1 Production

The world's consumption of epoxy resin was 1,093 kilotons in 2009 (Møller et al. 2012). Bisphenol A diglycidyl ether (BADGE) is one of the most widely used epoxy resins in the world (Chamorro-García et al. 2012). It has been listed as a high production volume (HPV) chemical in U.S. that had a production volume of 1 to 10 million pounds in 2006. It is a reactive pre-polymer of bisphenol A (BPA) that was produced through the O-alkylation of BPA with epichlorohydrin **(Figure 2-1)**. Besides, BADGE has many derivatives (mainly its hydrolysis and chlorohydroxy products) and they can be transformed to each other under specific conditions **(Figure 2-1)**. BADGE can be readily hydrolyzed (nucleophilic addition of water) in aqueous solutions, forming BADGE-H_2O and BADGE-$2H_2O$. The chlorohydroxy products (BADGE-HCl, BADGE-2HCl and BADGE-HCl-H_2O) are likely to form during polyvinyl chloride (PVC) production, which is also unstable and ready to be hydrolyzed.

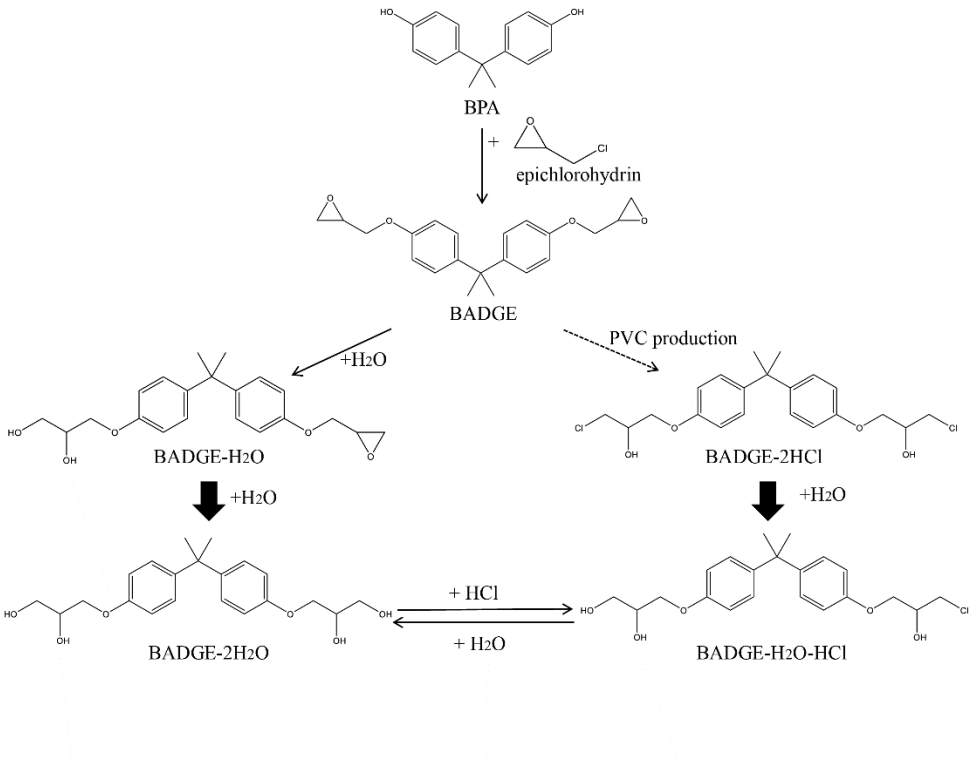

Figure 2-1. The synthesis of BADGE and reactions for the formation of BADGE-related compounds; modified from (Wang et al. 2012) and dash line represents the products were likely to be form during PVC production.

2.1.2 Applications and Indoor Sources

The presence of BADGE-related compounds (BADGEs) is ubiquitous in our daily life. The major application fields of BADGEs are primarily in PVC, sealants, coating, paints, textiles, packaging materials or even dental filling material **(Figure 2-2) (Møller et al. 2012)**. One big concern to BADGE was raised by its use in canned food coating/food packaging materials that can migrate into foods when heated and further consumed by human (Coulier et al. 2010). Besides, they had wide applications in indoor environments such as in paints, varnishes and furniture coatings. BADGEs are semi-volatile compounds (SVOCs) and can migrate from the product to the indoor environments via vaporization, deposition or product decaying processes.

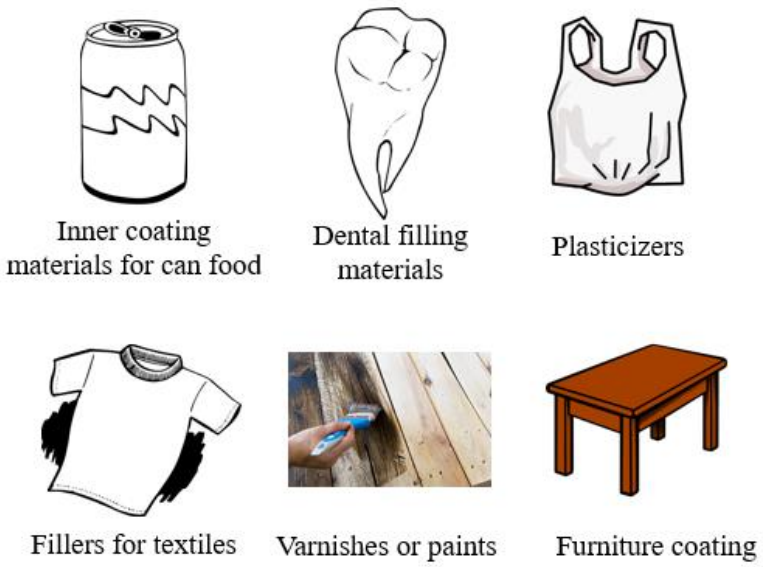

Figure 2-2. The widespread applications and sources of bisphenol diglycidyl ether (BADGE).

2.2 Physicochemical Properties and Structures of BADGEs

The general physicochemical properties and structures of BADGEs were summarized in **Table 2-1.** In general, the structures of these compounds show high similarity in backbones containing two benzenes, but their side-chain functional groups were quite different. For examples, BADGE/BFDGE have two epoxides, a cyclic ether with a three-atom ring, which makes them highly reactive. Besides, these electrophilic oxirane rings are subject to reaction with nucleophilic species (Petersen et al. 2008). In terms of physicochemical properties, BADGE itself is a pale yellow or colorless transparent solid which has low volatility (log K_{OA} =12.59) at room temperature. These chemicals have high similarity in the physicochemical properties and are semi-volatile compounds (SVOCs).

Table 2-1. Physicochemical properties and structures of bisphenol plasticizers

Compound	Abbreviation	Structure	Molecular Formula	CAS #	M.W.	Log K_{OW}	Log K_{OA}	Solubility (mg/L) at 25 °C
Bisphenol A bis(3-chloro-2-hydroxypropyl) ether	BADGE· 2HCl	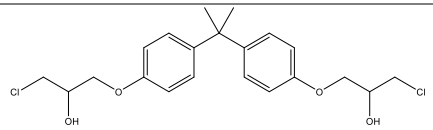	$C_{21}H_{26}Cl_2O_4$	4809-35-2	411.34	4.57	14.77	0.31
Bisphenol A (3-chloro-2-hydroxypropyl) (2,3-dihydroxypropyl) ether	BADGE·HCl·H_2O	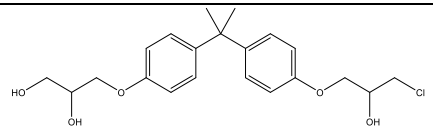	$C_{21}H_{27}ClO_5$	227947-06-0	394.89	3.25	14.44	5.54
Bisphenol A bis(2,3-dihydroxypropyl) ether	BADGE·H_2O	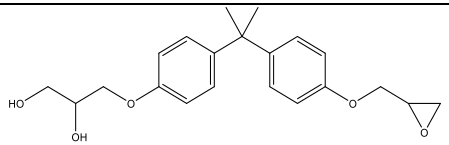	$C_{21}H_{26}O_5$	76002-91-0	358.43	1.93	14.10	96.18

Bisphenol A (3-chloro-2-hydroxypropyl) glycidyl ether	BADGE·HCl	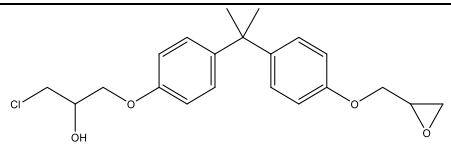	$C_{21}H_{25}ClO_4$	13836-48-1	376.87	4.00	15.22	5.25
Bisphenol A bis(2,3-dihydroxypropyl) ether	BADGE·$2H_2O$	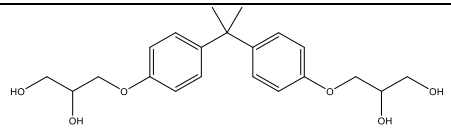	$C_{21}H_{28}O_6$	5581-32-8	376.44	1.93	14.10	96.18
bisphenol F diglycidyl-ether	BFDGE	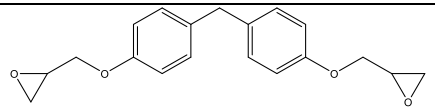	$C_{19}H_{20}O_4$	2095-03-6	312.36	3.26	12.25	17.20
Bisphenol F bis(2,3-dihydroxypropyl) ether	BFDGE·$2H_2O$	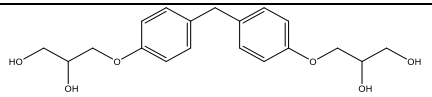	$C_{19}H_{24}O_6$	72406-26-9	348.39	1.34	13.76	452.60
Bisphenol A diglycidyl ether	BADGE	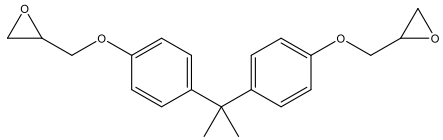	$C_{21}H_{24}O_4$	1675-54-3	340.42	3.84	12.59	3.69
Bisphenol A	BPA	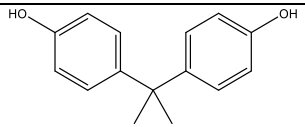	$C_{15}H_{16}O_2$	80-05-7	228.3	3.64	172.70	12.75

Bisphenol S	BPS	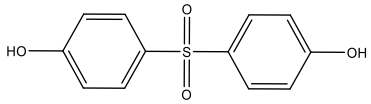	$C_{12}H_{10}O_4S$	80-09-1	250.27	1.65	14.61	3518.00
Bisphenol F bis(2-chloro-1-propanol) ether	BFDGE-2HCl	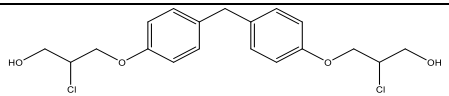	$C_{19}H_{22}Cl_2O_4$	374772-79-9	385.28	3.98	14.43	1.51

Notes: Log k_{OW}, Log k_{OA} and solubility were calculated using EPI Suite ^{TM}-Estimation program interface.

2.3 Analytical Method of BADGEs

BADGEs are a group of emerging organic contaminants and their analysis can be quite challenging for a couple of reasons. Above all, the first concern is the hydrolysis potentials of BADGEs. BADGE itself contains two epoxides that are reactive and can be hydrolyzed with half-lives of approximately 2 days at pH 7 and 35°C (Lane et al. 2015). For samples (e.g. dust etc.) that don't contain water, a water-free environment during the sample extraction/clean-up steps must be ensured, otherwise can lead to the low recovery issues. The second major concern is the widespread uses of BADGEs in the laboratory environment (e.g. plastic consumables etc.). This usually cause background contamination for the trace level analysis (e.g. urine, blood etc.).

To date, only a few studies that attempted to investigate their environmental/human occurrences in different sample matrix and the applied analytical methods were summarized in **Table 2-2**. For sample preparation, the dried solid samples (e.g. dust) were prepared by solvent extraction, followed up with purification using solid phase extraction (SPE). So far, only two studies have investigated the occurrences in indoor dust samples (Wang et al. 2012, Tran et al. 2016). Briefly, the dust samples were firstly extracted by a combination of water and methanol and further diluted with 0.2 % formic acid in water before loading to a Waters MCX cartridge. This acidified environment, accelerating the hydrolysis (Lane et al. 2015), creates great uncertainty to the absolute quantification and results in low recovery of BADGEs. For liquid samples (e.g. urine and blood etc.), the common treatment approach is liquid-liquid extraction using ethyl acetate, followed by a drying process to further concentrate the samples.

For instrumental analysis of BADGEs **(Table 2-2)**, Liquid Chromatography (LC) is the most frequently used instrument to quantify BADGEs in different sample matrix (Gallart-Ayala et al. 2011, Xue et al. 2016). Among many LC instruments, Liquid Chromatography-tandem Mass Spectrometry (LC-MS/MS) offers good sensitivity

and suits for the quantification analysis at trace-level. In addition, a reverse-phase column is usually incorporated with LC-MS/MS for the separation. In electrospray ionization (ESI), BADGEs and BFDGEs were analyzed in positive ionization mode while the negative mode is employed to analyze BPA and BPS. In terms of mobile phase, BADGEs and BFDGEs showed a high tendency to form adducts with the mobile phase components $[M+NH_4]^+$ ions. Therefore, the ammonium buffer is used as an additive in the mobile phase by enabling the ammonium adducts formation and ensuring signal reproducibility.

Table 2-2. Extraction, purification and analytical methods of BADGEs in different sample matrix using Liquid Chromatography and Mass Spectrometry detection.

Sample type (Size) Country	Analytes	Sample Treatment	Separation & Detection	References
Indoor Dust (150 um) Vietnam	BADGE, BADGE-H_2O, BADGE-$2H_2O$, BADGE-HCl-H_2O	Solid-Liquid Extraction (Methanol: Milli-Q Water 2:1 v/v); Solid phase extraction (Oasis MCX Cartridge)	C18, (100×2.1mm); Methanol (A) and 10% methanol in Milli-Q Water that contained 2 mM ammonium acetate (B)	(Tran et al. 2016)
Indoor Dust (2 mm) U.S. China Korea Japan	BADGE, BADGE-H_2O, BADGE-$2H_2O$, BADGE-HCl-H_2O	Solid-Liquid extraction (Methanol: Milli-Q Water 5:3, v/v); Solid phase extraction (Oasis MCX Cartridge)	C18, (100×2.1mm); Methanol (A) and 10% methanol in Milli-Q Water that contained 2 mM ammonium acetate (B)	(Wang et al. 2012)
Indoor Air U.S.	BPA, BPS, BPF, BPZ, BADGE, BADGE-H_2O, BADGE-$2H_2O$, BADGE-HCl-H_2O, BADGE-HCl, BFDGE, BFDGE-2HCl, BFDGE $2H_2O$	Samples were extracted by ethyl acetate;	C18 (2.1 mm ×100 mm, 5 um) Negative mode: methanol (A) and Milli-Q Water that contained 1%(v/v) ammonium hydroxide(B) Positive mode: methanol (A) and 10% methanol with 2 mM ammonium acetate(B)	(Xue et al. 2016)

Human Urine U.S. China	BADGE, BADGE-H_2O, BADGE-$2H_2O$, BADGE-HCl-H_2O	Deconjucation with β-glucuronidase and sulfatase; Liquid-Liquid Extraction by Ethyl Acetate	C18 (100×2.1 mm) methanol (A) and 10% methanol with 2 mM ammonium acetate(B)	(Wang et al. 2012)
Human Urine Greece	BADGE, BADGE-H_2O, BADGE-$2H_2O$, BADGE-HCl-H_2O, BADGE-HCl	Deconjucation with β-glucuronidase and sulfatase; Liquid-Liquid Extraction by Ethyl Acetate	C18 (100×2.1 mm) methanol (A) and 10% methanol with 2 mM ammonium acetate(B)	(Asimakopoulos et al. 2014)
Human Urine Indian	BADGE, BADGE-H_2O, BADGE-$2H_2O$, BADGE-HCl-H_2O, BADGE-HCl, BFDGE, BFDGE-2HCl, BFDGE $2H_2O$	Deconjugation by 22 units of β-glucuronidase; Liquid-Liquid Extraction by ethyl acetate	C18 (100×2.1 mm) methanol (A) and 10% methanol with 2 mM ammonium acetate(B)	(Xue et al. 2015)
Human Blood U.S.	BPA, BADGE, BADGE-H_2O, BADGE-$2H_2O$, BADGE-HCl-H_2O, BADGE-HCl, BFDGE, BFDGE-2HCl, BFDGE $2H_2O$	Liquid-liquid extraction with ethyl acetate	C18 (100×2.1 mm) methanol (A) and 10% methanol with 2 mM ammonium acetate(B)	(Wang et al. 2015)
Adipose Fat U.S.	BPA, BADGE, BADGE-H_2O, BADGE-$2H_2O$, BADGE-HCl-H_2O, BADGE-HCl, BFDGE, BFDGE-2HCl, BFDGE-$2H_2O$	Homogenized in a mortar with acetone	C18 (100×2.1 mm) methanol (A) and 10% methanol with 2 mM ammonium acetate(B)	
Sewage Sludge U.S.	BADGE, BFDGE BADGE-$2H_2O$, BADGE-H_2O, BADGE-HCl-H_2O, BADGE-2HCl, BADGE-HCl, BFDGE-$2H_2O$, BFDGE-2HCl	Samples were freeze-dried and extracted with methanol; purified by ENVI-Carb solid phase extraction	C18 (100×2.1 mm) methanol (A) and 10% methanol with 2 mM ammonium acetate(B)	(Xue et al. 2015)

2.4 Occurrences in Environmental Matrix and Human Specimen

2.4.1 Occurrence in Indoor Dust

The occurrences of BADGE and its derivatives (BADGE-H_2O, BADGE-$2H_2O$ and BADGE-HCl-H_2O) in indoor house dust have been found in several limited studies from some countries like U.S., China, Korea, Japan and Vietnam **(Table 2-3)**. Their occurrences in indoor dust samples have been firstly investigated in four countries U.S.A., China, Japan and Korea (Wang et al. 2012). For all countries, the general distribution profiles of BADGEs are quite similar with BADGE-$2H_2O$ and BADGE-HCl-H_2O as the predominant ones in dust samples. The hydrolysis compound BADGE-$2H_2O$ was found with the highest median concentrations of 1,920 ng/g in Korea followed by Japan, U.S. and China. The estimated daily intake (EDI) via dust ingestion for BADGEs is 6.5 ng/kg-bw/day. In Vietnam (Tran et al. 2016), the concentrations of total BADGEs in indoor dust ranged from 23 to 1,750 ng/g (median 184 ng/g) and the estimated daily intake ranged from 0.158 to 0.736 ng/kg-bw/day.

2.4.2 Occurrence in Air Samples

To date, only one study from U.S. reported the occurrence of BADGE and BFDGE as well as their derivatives in indoor air **(Table 2-3)**. Among these compounds, BADGE-$2H_2O$ was the main compound found in indoor air (detection rate [DR]:85.5%) with a concentration as high as 6.71 ng-m^{-3}. The inhalation exposure to BADGE-$2H_2O$ of teenagers was estimated as 3.84 ng-day^{-1} (Xue et al. 2016).

2.4.3 Occurrences in Wastewater and River Water Samples

BADGE and BFDGE were determined in wastewater samples (n=4) and river samples (n=3) collected from Spain (Ballesteros-Gómez et al. 2007). None of the targeted compounds were detected in river water samples **(Table 2-3)**. BADGE was detected in all wastewater treatment plant (WWTP) influent samples with the concentration ranged from 0.57 ± 0.04 ~ 1.15 ± 0.1 μg/L. BFDGE was detected in two WWTP influent samples with the concentration ranged from non-detected to 0.41

± 0.06 μg/L. Only BADGE was detected in one WWTP effluents sample with a concentration of 0.25 ± 0.02 μg/L. In another study, BADGE and its hydrolysis compounds as well as BADGE-HCl-H_2O were determined in wastewater samples from two WWTP in the Albany area of New York State, U.S. **(Table 2-3)**. BADGE-$2H_2O$ was the predominant compound and its GM concentrations in influents was 4.36 ng/L. BADGE-HCl-H_2O was the second most abundant chemical found at a GM concentration of 1.72 ng/L (Xue et al. 2019).

2.4.4 Occurrence in Sewage Sludge

BADGE, BFDGE and eight of their derivatives were determined in archived biosolid samples collected from 68 wastewater treatment plants (WWTPs) from U.S. **(Table 2-3)**. BADGE-$2H_2O$ was the most frequently detected (DR=99%) with the highest abundance (median: 93.6 ng/g dry weight [dw]) among these compounds (Xue et al. 2015).

2.4.5 Occurrences in Dental Sealants

Concentrations of BADGEs were determined in 70 dental sealants collected from the U.S. market (Xue et al. 2018). Among all the tested compounds, BADGE-$2H_2O$ was the most abundant compound, found at concentrations of up to 1,780 μg/g. The GM concentration of total BADGEs was 48.7 μg/g. Leaching of these compounds into saliva can be a pathway of exposure by humans.

2.4.6 Occurrences in Textiles

Concentrations of BADGEs and BFDGEs were determined in 77 textiles and infant clothing collected from Albany, New York, USA (Xue et al. 2017). BFDGE was the predominant compound, with a mean concentration of 13.6 ng/g, followed by BADGE-HCl-H_2O (7.32 ng/g) and BADGE-$2H_2O$ (1.92 ng/g).

2.4.7 Occurrences in Human Urine

The occurrences of BADGEs have been found in human urine samples collected from U.S., China, Greece and Indian **(Table 2-3)**. In the urine samples collected from U.S.

and China, BADGE-2H_2O was the predominant compound, accounting for 45-60% of the total BADGEs concentration, followed by BADGE (17-24%) (Wang et al. 2012). The urinary concentrations of total BADGEs in U.S. ranged from 1.24 to 9.03 ng/mL, with a GM concentration of 3 ng/mL. The concentrations of BADGEs in urine from adults (GM: 1.36 ng/mL) and children (1.02 ng/mL) in China were 3-fold higher than U.S.. In another study, the occurrence of five BADGE-related compounds BADGE, BADGE-H_2O, BADGE-2H_2O, BADGE-HCl-H_2O and BADGE-HCl were found in Greece (Asimakopoulos et al. 2014), with urinary concentrations of total BADGEs 0.3-20.9 (GM: 0.9) ng/mL. The estimated daily intakes (EDI urine) is 0.023 μg/kg-bw/day for total BADGEs calculating on the basis of measured urinary concentrations. In another study investigated the urinary BADGEs and BFDGEs in Indian children (Xue et al. 2015), similarly, BADGE and BADGE-2H_2O were the predominant compounds among all these analytes. The GM urinary concentrations of BADGE-2H_2O and BADGE in Indian children were 12.2 and 24.8 ng/mL, respectively, which were one order of magnitude higher than those reported for Chinese children (0.594 and 0.175 ng/mL).

2.4.8 Occurrences in Adipose and Plasma Samples

BADGE, BFDGE and seven of their derivatives were determined in human adipose fat and blood plasma samples collected from New York City (Wang et al. 2015). Similar to the urinary distribution profile, BADGE-2H_2O was predominant and detected in 60% and 70% of the adipose and plasma samples. High concentrations and detection frequencies of BFDGE were also found in both adipose (19.1-4,500 ng/g) and plasma samples (23.3-180 ng/g).

2.4.9 Occurrences in Marine Mammals

The occurrence and bioaccumulation of BADGEs or BFDGEs were also examined in 121 tissue (liver, kidney, blubber and brain) samples from eight species of marine mammals collected from the U.S. coastal waters of Florida, California, Washington

and Alaska (Xue et al. 2016). Among all tested compounds, BADGE-HCl was detected in 78.5 % of the samples, at concentrations of up to 2,950 ng/g (wet weight). The favorable accumulated organ of BADGEs was livers, but considerable concentrations of BADGE-2HCl also occurred in brains and kidneys.

Table 2-3. The concentration of BADGEs in environmental and human samples collected from different countries.

Sample Type	Matrix	Country	Conc.	BADGE	BADGE-H_2O	BADGE-H_2O-HCl	BADGE-$2H_2O$	Reference
Environmental Samples	Indoor Dust (ng/g)	U.S. (n=40)	Range	<LOQ-12	0.700-486	14-2,260	51-29,800	(Wang et al. 2012)
			Median	2.40	27	127	1,110	
		China (n=55)	Range	0.900-7,750	2-8,850	5-1,720	35-38,300	
			Median	51	67	124	1,074	
		Korea (n=41)	Range	0.100-98	3.9-2,440	56-13,100	564-30,500	
			Median	18	91	270	1,920	
		Japan (n=22)	Range	<LOQ-8.21	<LOQ-421	56-24,300	291-59,900	
			Median	2.600	27	267	1,410	
		Vietnam (n=46)	Range	<LOQ-172	1.790-255	<LOQ-417	7.58-1,630	(Tran et al. 2016)

			Median	11.100	28	11.400	129	
	Air (ng/m^3)	U.S. (n=52)	Range	N.A.	N.A.	N.A.	<LOQ-153	(Xue et al. 2016)
			Median	N.A.	N.A.	N.A.	0.10	
	Wastewater (ng/L)	U.S. (n=2)	Range	N.A.	N.A.	N.A.	N.A.	(Xue et al. 2019)
			GM	Effluent: 0.77	n.d.	Influent: 1.72	Influent: 4.36 Effluent: 6.43	
		Spain (n=4)	Range	Influent :0.57 ± 0.04 -1.15±0.1 Effluent: n.d.-0.25±0.02	N.A.	N.A.	N.A.	(Ballesteros-Gómez et al. 2007)
			Median	N.A.	N.A.	N.A.	N.A.	
		Spain (n=3)	Range	N.A.	N.A.	N.A.	N.A.	

	River Water(ng/ mL)		Median	n.d.	N.A.	N.A.	N.A.	
	Sludge (ng/g dry weight)	U.S. (n=84)	Range	<LOQ-1,980	<LOQ-20,90	<LOQ-121	<LOQ-2,290	(Xue et al. 2015)
			Median	9.66	<LOQ	3.66	93.6	
	Dental Sealants (µg/g)	U.S.(n=70)	GM	0.29	1.43	2.76	13.7	(Xue et al. 2018)
	Textiles (ng/g)	U.S. (n=77)	Range	<0.74-4.37	N.A.	<1.47-62.9	<1.47-13.1	(Xue et al. 2017)
			Mean	0.23	N.A.	7.32	1.92	
Human Specimens	Urine (ng/mL)	U.S. (n=31)	Range	0.105-2.231	0.121-1.361	<LOQ-3.412	0.150-4.604	(Wang et al. 2012)
			Median	0.682	0.428	0.308	1.082	
			Range	0.042-0.709	0.030-1.671	<LOQ-0.352	0.228-2.192	

		China (Adult; n=26)	Median	0.241	0.245	0.106	0.629	
		China (Children; n=70)	Range	0.075-1.226	<LOQ-0.360	<LOQ-1.340	0.333-5.810	
			Median	0.182	0.139	0.101	0.550	
		Greece (n=100)	Range	<LOQ-0.600	<LOQ-0.600	<LOQ	<LOQ-18.700	(Asimakopoulos et al. 2014)
			Median	<LOQ	<LOQ	<LOQ	0.600	
		Indian (Children; n=76)	Range	0.070-295	N.A.	N.A.	0.070-1,450	(Xue et al. 2015)
			Geometric Mean	24.800	N.A.	N.A.	12.200	
	Blood (ng/mL)	U.S. (n=20)	Range	<LOQ	<LOQ-9.54	<LOQ-1.41	<LOQ-65.1	(Wang et al. 2015)
			Median	<LOQ	2.26	<LOQ	7.15	
		U.S. (n=20)	Range	<LOQ-5.16	<LOQ-4.33	<LOQ-28.2	<LOQ-45.4	

	Adipose (ng/g wet weight)		Median	<LOQ	<LOQ	<LOQ	3.44	

2.5 Biotransformation and Toxicity

2.5.1 Biotransformation

Although metabolism is one of the important detoxification strategies in organisms (Kluger et al. 2013), the bioactivity profiles of biotransformation products can sometimes cause more adverse and toxic effects (Kirchmair et al. 2013). Comparing with bisphenol A, much less information is available on the metabolism and toxicity of BADGEs. The degree of their toxicity is believed to depend mainly on the fractional concentrations of unreacted epoxy groups (Suarez 2000). Till now, very few studies have documented the metabolism of BADGE and its main metabolites were presumed to be the hydrolysis products (Wang et al. 2012). In an *in vivo* study, F344 rats were given orally 2-^{14}C-propane-labelled BADGE doses of 2.7 mg/kg body weight. The results showed less than 10% was unchanged BADGE in plasma (Nolan et al. 1981). In another mouse study, the bis-diol of BADGE (BADGE-2H_2O) was excreted in both free and conjugated forms in total amounts representing 5% of the original dose (Climie et al. 1981). Both studies suggested that a large proportion of parent compound has been bio-transformed to some unknown metabolites. In addition, the biotransformation mechanism can be quite complex considering the reactivity of epoxides that can react with many nucleophile species. Therefore, the potential bioactivation of BADGE is warranted for further investigation.

2.5.2 In Vitro Toxicological Studies

In vitro bioassays have reported that BADGEs exhibit endocrine-disrupting potentials as well as mutagenicity, genotoxicity and cytotoxicity (Suárez et al. 2000, Ramilo et al. 2006, Sueiro et al. 2006). Regarding endocrine-disrupting potentials, BADGE and its derivatives exhibit anti-androgenic and estrogenic effects as well as obesogenic properties. For examples, the chlorohydroxy derivatives of BADGE and BFDGE (BADGE-2HCl and BFDGE-2HCl) can act as androgen antagonist through the process of binding to the androgen receptor in CHO-K1 cell lines (Satoh et al.

2004). Besides, BADGE, BADGE-2H_2O and BADGE-2HCl exhibited breast cancer (T47D) cell proliferation at concentrations of 10^{-14}-10^{-4} M. However, they did not bind to estrogen receptor (ERα) in the binding assay (Nakazawa et al. 2002). Besides, more and more studies have investigated BADGE's obesogenic properties, but the results suggested these cellular processes may be cell-type specific. For examples, BADGE was shown to be an antagonist of PPARγ in 3T3-L1 and 3T3-F442A cells (Wright et al. 2000). In contrast, a recent study also revealed BADGE exhibits PPARγ agonistic activities in ECV403 cell line (Bishop-Bailey et al. 2000). Although BADGE was considered as low-affinity ligand that required very high concentrations to demonstrate PPARγ antagonism (half maximal inhibitory concentration: IC_{50} of approximately 100 μM), a study has revealed its ability to induce adipogenic differentiation in both mesenchymal stromal stem cells (MSCs) and preadipocytes at low nanomolar concentrations (Fehlberg et al. 2002).

In addition to its endocrine-disrupting potentials, many *in vitro* endpoints screening tests suggested BADGEs exhibit genotoxicity and mutagenicity. For examples, a study has reported the increase in the frequency of chromosomal aberration as well as the percentage of cells chromatid gaps and chromatid exchanges figures in rat liver cells exposed to 3.75-15 μg/mL of BADGE (Laboratory 1981). In another study, a toxicological screening assay micronucleus test (MNT) was conducted to examine the genotoxicity of BADGE, BADGE-H_2O, BADGE-2H_2O and BADGE-2HCl to human peripheral blood lymphocytes in the presence or absence of an exogenous metabolizing system S9 rat liver (Suárez et al. 2000). The results suggested that all tested chemicals are able to induce both cytotoxic and genotoxic effects, but their triggered effects are varied. BADGE itself is stronger than its hydrolysis products BADGE-H_2O and BADGE-2H_2O while the genotoxicity of BADGE-2HCl is comparable to BADGE-H_2O. A study has also reported BADGE and BADGE-H_2O's ability to cause genetic alterations using *Escherichia coli* tryptophan reverse mutation

test with strains WP2, WP2uvrA and IC3327 (Sueiro et al. 2006). The results suggest these compounds are able to induce mutagenic effects in WP2uvrA and IC3327.

BADGEs were also able to induce *in vitro* overt cytotoxicity at specific dose. A study reported BADGE and BFDGE are able to induce morphological changes, cell detachment from the substratum and to inhibit cell proliferation of Caco-2 cells (Ramilo et al. 2006). Moreover, they found that both chemicals at 200 µM can induce F-actin depolymerization and the effect is potent at 24 h of incubation. A newly published study examined the toxicity, endocrine and lipid disruption potentials of BADGE, BADGE-H_2O and BADGE-2HCl in human placental cells. In general, BADGE-2HCl and BADGE show higher cytotoxicity than BADGE-H_2O. Besides, BADGE-2HCl alters the cell lipidome by decreasing the amount of neutral lipids while exposure to BADGE increases the intracellular concentration of triacylglycerides (Marqueño et al. 2019).

2.5.3 In Vivo Toxicological Studies

The *in vivo* systemic toxicity of BADGE has been examined as early as 1958 for both single-dose and full-dose tests (Hine et al. 1958). In single-dose oral toxicity test, a median lethal dose (LD_{50}) of BADGE was upper than 1,000 mg/kg, which has been recorded in studies with rats, mice and rabbits. In full-dose test, the oral LD_{50} for a commercial BADGE-based epoxy resin was reported to be 11,400 mg/kg in rats, 15,600 mg/kg in mice, and 19,800 mg/kg in rabbits.

In addition to the acute oral toxicity, accumulated *in vivo* evidence suggested BADGE can seriously damage the reproductive systems and endocrine systems in pigs, rats and native amphibian species. For examples, a study found the plastic bags used for semen storage lead to a significant decrease in fertility for a group of pig farms (Nerin et al. 2014). The main causal compound responsible for the failures was BADGE (adhesive used to manufacture the multilayer plastic bags). Besides, they also found a synergistic reproductive toxicity effect developed between BADGE, its derivatives

and the cyclic lactone. Another study investigated the developmental effects of prenatal and postnatal exposures to BADGE at 375 mg/kg/day orally in male rat offsprings (Hyoung et al. 2007). Their body weight and relative organ weight (lung, adrenal gland, epididymis, prostate, spleen testis and brain) have changed in 6 or 9 weeks and testicular toxicity appeared in 9 weeks. BADGE also exhibits acute testis toxicity for male rats (Yang et al. 2010). This study found an increasing number of immature and maturing sperm on the testis when the male rats were exposed to single-dose of BADGE at 750; 1,000 and 2,000 mg/kg/day. However, if below 1,000 mg/kg/day, no significant differences between treatment group and control group were observed with respect to sperm count, sperm headcount, sperm motility and sperm abnormality. In addition, BADGE has been reported to have adverse effects on *Rhinella arenarum* in an embryo-larval development study through standardized bioassays (Wolkowicz et al. 2016). The results showed that BADGE was more toxic to embryos (96 hours post fertilization with median lethal concentrations: 0.04 mg/L) than larvae (2.2 mg/L) at all exposure times. Significant lethality rates were also observed for embryos and larvae when exposed to 0.0005 mg/L and 10 mg/L of BADGE; respectively.

2.6 Summary of Literature Review

From the literature review, the following research gaps are identified:

(i) The unique structure makes BADGEs highly reactive and unstable, which creates great challenges to analyze these chemicals in environmental or human samples. Therefore, a water-free method should be developed for solid sample (e.g. dust) analysis. Up to date, the information on their occurrences is still very scarce. More information is needed to understand their human exposure and potential health impact considering their widespread applications in our daily life.

(ii) To date, very few studies have investigated the biotransformation of BADGE. A

feasible and robust discovery platform is needed to assist the identification of reactive compound BADGE's potential metabolites. Considering its reactivity and covalent binding potentials (e.g. can react with proteins, amino acids etc.), fully understanding their metabolism pathways would provide a more comprehensive view to the assessment of its toxicity and potential health consequences. Besides, BADGE can also serve as a model chemical to study the biological fate of reactive chemicals.

(iii) Comparing with BPA, the toxicology information of BADGEs is still limited. A more systematic approach (e.g. omics) should be employed to compare the toxicity between these two structurally similar compounds. Among the omics methods, metabolomics is feasible, which enables us to understand the major dysregulated metabolites and pathways triggered by these compounds.

(iv) Most of current available toxicology assessment studies of BADGEs have little human health implication due to the application of high dosing concentrations. Considering the companion with many other xenobiotics for real-life BADGEs exposure, it would be meaningful to explore the possible consequences and evaluate the contribution from BADGEs when after exposure to a chemical mixture that mimics human exposure.

Chapter 3. The Occurrence of Bisphenol Plasticizers in Paired Dust and Urine Samples and its Association with Oxidative Stress

3.1 Overview

Chapter 3 developed and validated a novel water-free method for BADGEs analysis in dust samples. It also investigated the occurrences of these bisphenol plasticizers in 33 paired dust and urine samples collected from Singapore. The urinary oxidative stress biomarker oxo-2'-deoxyguanosine (8-OHdG) was also quantified to explore its possible association with bisphenol plasticizer exposure. This chapter has been published as: **Liu, M.**, Jia, S., Dong, T., Han, Y., Xue, J., Wanjaya, E. R., & Fang, M.* (2019). The occurrence of bisphenol plasticizers in paired dust and urine samples and its association with oxidative stress. *Chemosphere*, *216*, 472-478. doi: 10.1016/j.chemosphere.2018.10.090.

3.2 Introduction

Many bisphenol plasticizers are known as endocrine-disrupting chemicals (EDCs) such as bisphenol A (BPA), bisphenol S (BPS) and bisphenol a diglycidyl ether (BADGE) that are widely used in the manufacture of polycarbonate plastic and epoxy resins. BPA, as a most well-known bisphenol, the maximum allowable dose levels for causing reproductive toxicity is 3 μg/day according to the guideline values in EPA Integrated Risk Information System (IRIS). As emerging contaminants, BADGE and bisphenol F diglycidyl ether (BFDGE) are the most commonly used epoxy resin monomers and some studies have documented that BADGE may be equally or more harmful than BPA in some toxicological effects such as cytotoxicity (Russo et al. 2018)

Studies have also shown that BADGE and its derivatives can induce cytotoxic effect, mutagenicity as well as adverse reproductive and developmental effects (Suárez et al.

2000, Ramilo et al. 2006, Sueiro et al. 2006, Wolkowicz et al. 2016). Besides, BADGE is an androgen receptor (AR) and peroxisome proliferator-activated receptor gamma (PPARγ) antagonist (Wright et al. 2000, Satoh et al. 2004). Therefore, further environmental and toxicological studies on BADGE are of great significance for human health. However, to date, only a few studies have documented the occurrence of BADGE and its derivatives in the environmental matrix and human specimens (Wang et al. 2012, Asimakopoulos et al. 2014, Wang et al. 2015, Xue et al. 2016) due to the analytical challenges including highly reactive properties and laboratory background contamination. Furthermore, in the current available analytical protocols, water is used during the sample extraction/cleanup in those studies, thus the result might be of great uncertainties due to the hydrolysis potentials of BADGE.

The ubiquity of these bisphenol plasticizers indicates that people are exposed to them on a daily basis (Vandenberg et al. 2007, Xue et al. 2016). Most of these plasticizers will sink into the dust due to their semi-volatile properties and the levels of semi-volatile organic compounds (SVOCs) in indoor dust can be used as a surrogate of indoor environmental quality. Dust ingestion has been pointed as an important exposure pathway for some compounds such as flame retardant poly-brominated diphenyl ethers (PBDEs) (Stapleton et al. 2005, Wilford et al. 2005, Harrad et al. 2006). Bisphenol plasticizers have a large number of application, which allows multiple exposure routes. Some studies have suggested that food ingestion is the major exposure route for these compounds (Geens et al. 2012, Asimakopoulos et al. 2014), whereas little evidence is available until now.

In this study, we investigated the occurrences of BADGE and its related compounds together with BPA and BPS in paired indoor house dust and urine samples collected from Singapore. Additionally, since the involvement of oxidative stress is believed to be a key mechanism of inducing health effects for many xenobiotics, we further measured the concentration of urinary oxidative stress biomarker and investigated its

association with urinary bisphenol plasticizer levels. In summary, the primary aims of this study were to (i) develop a sensitive and water-free method for BADGE analysis in dust samples; (ii) determine their occurrence in paired dust and urine samples collected from Singapore; and (iii) tentatively explore the association of all typical bisphenol plasticizers between paired dust and urine samples as well as the correlation between oxidative stress with bisphenol plasticizers.

3.3 Methodology

3.3.1 Sample Collection

In this study, 33 participants (Healthy; Age: 22~37 years old; Male participants: 20; Female participants: 13) were recruited from Singapore and their information were listed in **Table A1 in Appendix A.** Indoor house dust samples were collected using a vacuum cleaner during November 2017 (n=32) following our previous method (Fang et al. 2013). Samples were wrapped in aluminum foil and then placed in a glass jar at 4°C until analysis. In the meantime, the early morning urine samples (n=33) from the residents were collected in glass tubes and immediately placed in a cooler with ice for storage and transport. Urine samples were measured for specific gravity (SG) by a refractometer for future concentration normalization and stored at -40°C within 24 h of collection. Institutional Review Board approvals were obtained for human specimen analysis from Singapore (IRB-2017-02-023).

3.3.2 Chemical Analysis

All the chemical standards were purchased with a purity higher than 95% and reagents used were HPLC grade (Text S1). LC/MS grade Methanol and HPLC grade Ethyl Acetate were purchased from Aik Moh Paints & Chemicals (Singapore). Analytical standards of BADGE (≥95%) and its derivatives, BADGE-H_2O (≥95%), BADGE-2H_2O (≥97%), BADGE-HCl-H_2O (≥95%), BADGE-HCl (≥90%), BADGE-2HCl (≥97%), BFDGE (≥95%), BFDGE- 2HCl (≥95%), 8-Oxo-2'-deoxyguanosine (≥98%) as well as β-glucuronidase from Helix (≥85,000 units/mL)

were purchased from Sigma-Aldrich (Singapore). BFDGE-2HCl (≥98%), 8-Oxo-2'-deoxyguanosine-$^{13}C,^{15}N_2$, d6-isotopically labeled bisphenol diglycidyl ether (d_6-BADGE) (98%) and BFDGE-2HCl (≥98%) were purchased from Toronto Research Chemicals (Toronto, Canada) and $^{13}C_{12}$-BPA was purchased from Cambridge Isotope Laboratories (MA, U.S.A). Milli-Q water was prepared using an ultrapure water system. The stock solutions of target analytes and internal standards were prepared at 2 mg/mL in methanol and stored at -40°C.

In this study, a novel water-free method was developed to analyze BADGE and its related compounds. Dust samples were extracted by methanol and purified by a solid phase extraction (SPE) method. Prior to analysis, dust samples were sieved and homogenized by passage through a 150 μm sieve. Approximately 50~60 mg of dust was weighed and spiked with d_6-BADGE (20 ng). The spiked dust samples were equilibrated for 30 min at room temperature and 5 mL of methanol were added for extraction. The mixture was centrifuged at 3,000 *g* for 10 min after sonication for 15 min. The supernatant was transferred into a polypropylene tube and the extraction was repeated twice. The combined extracts were concentrated to near-dryness under a gentle nitrogen stream and reconstituted in 0.5 mL 3% ethyl acetate in hexane. The extract was purified by passage through silica gel cartridge (200 mg/cm^3, baked at 180°C overnight) and pre-conditioned with 5 mL of hexane. The sample extracts were loaded, followed by passage of 10 mL of hexane. The target compounds were eluted with 10 mL of ethyl acetate/methanol (4:1, v/v). Furthermore, the extract was concentrated under a gentle nitrogen stream and then spiked with 60 ng $^{13}C_{12}$-BPA and reconstituted in 500 μL methanol. After filtration through a 0.45 μm PTFE filter, the samples were ready for instrumental analysis. For urinary bisphenol plasticizers analysis, samples were extracted using a liquid-liquid extraction (LLE) method after deconjugation with β-glucuronidase, as described in a previous study with minor modifications (Wang et al. 2012). For bisphenol plasticizers in urine samples,

enzymatic deconjugation was performed for all urine samples prior to liquid-liquid extraction. 5 mL of urine sample was transferred into a 15-mL PP tube and 3 mL of 100 mM sodium acetate buffer which contained 330 units of β-glucuronidase (prepared by spiking 150 µL of β-glucuronidase into 120 mL of 100mM sodium acetate buffer) was added. Since sulfatase solution was found trace level of BADGE-$2H_2O$ contamination, we only use β-glucuronidase for deconjugation. After incubation and shaking at 37°C for 18 hours, urine samples were extracted three times with 3 mL of ethyl acetate. For each extraction, the mixture was well-mixed for 2 min and then centrifuged at 4,000 g for 10 mins. The supernatant was transferred to a glass tube. After extraction, d_6-BADGE (10 ng) was added and concentrated to near-dryness by a Speed vac (Labconco, Inc. Singapore). The residues were reconstituted in 0.5 mL of methanol and were transferred to a 1.5 mL Eppendorf tube. Samples were further concentrated to around 200 µL under a gentle nitrogen stream and centrifuged at 13,000 g for 15 min. Supernatant was transferred into an LC vials with insert and ready for analysis by LC/MS-MS. To determine urinary Oxo-2'-deoxyguanosine (8-OHdG) concentration (Ma et al. 2016), urine samples were spiked with 20 ng internal standard 8-Oxo-2'-deoxyguanosine-$^{13}C,^{15}N_2$ and were purified using solid phase extraction. In brief, 0.5 mL of urine sample was centrifuged to remove the particulates before loading on the Strata-X cartridge (30 mg, Phenomenex) which was previously conditioned with methanol and water. After loading the samples, the cartridges were washed with water and finally were eluted with 35% methanol in water. The samples were stored in -80 °C fridge until being fully froze and further dried in a freeze dryer. Afterwards, the sample was re-dissolved in 80% of acetonitrile in water.

Separation and detection of target analytes were accomplished using an Agilent 1290 infinity II Series HPLC (Agilent Technologies Inc., Singapore) interfaced with an Agilent 6460 electrospray triple quadrupole mass spectrometer (ESI-MS/MS; Agilent

Technologies Inc., Singapore) using multiple reaction monitoring mode (MRM). For bisphenol plasticizers analysis, an Atlantis T3 column (3 μm, 2.1 ×100 mm) was used for separation. While for 8-OHdG analysis, an Acquity BEH amide (1.7 μm, 2.1×100 mm) was used for separation. The mobile phase comprised of 10% Methanol in Milli-Q Water with 2 mM of ammonium acetate (A) and 100% Methanol (B). A gradient elution at a flow rate of 0.4 mL/min was used for the separation：0-5 min: 50% of B; increase to 70% B at 20 min; 20-20.1 min: decrease from 70% to 50% B and 3 min was used as a post run equilibrium. For urinary oxidative stress biomarker 8-Oxo-2'-deoxyguanosine (8-OHdG) analysis, 10 μl of samples were injected onto an analytical column (ACQUITY BEH amide, 1.7 μm, 2.1×100 mm, Waters Corporation, Milford, USA) coupled with ACQUITY BEH Amide Vanguard (1.7 μm, 2.1 mm×5 mm). The mobile phase comprised of water containing acetic acid pH=3 (A) and acetonitrile with 0.2 mM formic acid (B). The gradient elution at a flow rate of 0.3 mL/min were used for the separation: 0-1 min: 95% B; 1-6 min: decrease from 95% to 50% of B; maintain at 50% B until 9 min; 9-10 min: increase from 50% to 95% of B and 3 min was used as a post run equilibrium. The MS/MS was operated in the multiple reaction monitoring mode (MRM). Parameters were optimized by infusion of individual analyte **(Table A2)**.

3.3.3 Quality Assurance and Quality Control (QA/QC)

Sodium sulfate powder and phosphate buffered saline were used as procedural blanks for dust samples and urine samples, respectively. As part of our quality assurance criteria, levels of target compounds were analyzed in field, laboratory blanks (n=2 for each batch) and house dust Standard Reference Material (SRM) 2585 (National Institute of Standards and Technology (NIST), Gaithersburg, MD) (n=1 for each batch). Method detection limit (MDL) was estimated from 3 times of standard deviation calculated from procedural blanks **(Table 3-1)**.

3.3.4 Statistical Analysis

SPSS statistics 22 was used for the statistical analysis. Concentrations below MDL were substituted with a value equal to the half MDL for statistical analysis. Bisphenol plasticizers levels in dust and urine samples were tested for normality using the Shapiro-Wilk test. Pearson correlation coefficients were used for the analysis of the relationship between two sets of data with normal distribution. Otherwise, Spearman correlation coefficients were used. A value of p <0.05 denoted significance. Differences between groups were analyzed by one-way *ANOVA* with Duncan post-hoc analysis. One outlier of urinary BPA concentration was identified by Dixon's test and Grubb's test thus was excluded from correlation analysis.

3.4 Results and Discussion

3.4.1 BADGE/BFDGE Stability Test and Water-free Method Development for Dust Analysis

In our preliminary experiment, we found a relatively low recovery (30 ~ 50%) of BADGE/BFDGE in the SPE columns such as HLB cartridge (Waters) and WCX cartridge (Phenomenex). Suspecting that these compounds may be readily hydrolyzed in the purification process, we further tested their stability by monitoring their hydrolysis products (BADGE-H_2O and BADGE-$2H_2O$, BFDGE-$2H_2O$) for pH =7 at 25°C. A steady decay of BADGE and an increase of BADGE-H_2O and BADGE-$2H_2O$ were observed in the hydrolysis and BFDGE was also observed with the same trend **(Figure 3-1)**. The half-lives of BADGE and BFDGE was approximately 3 days, which is close to 2 days as estimated in an earlier study (Lane et al. 2015).

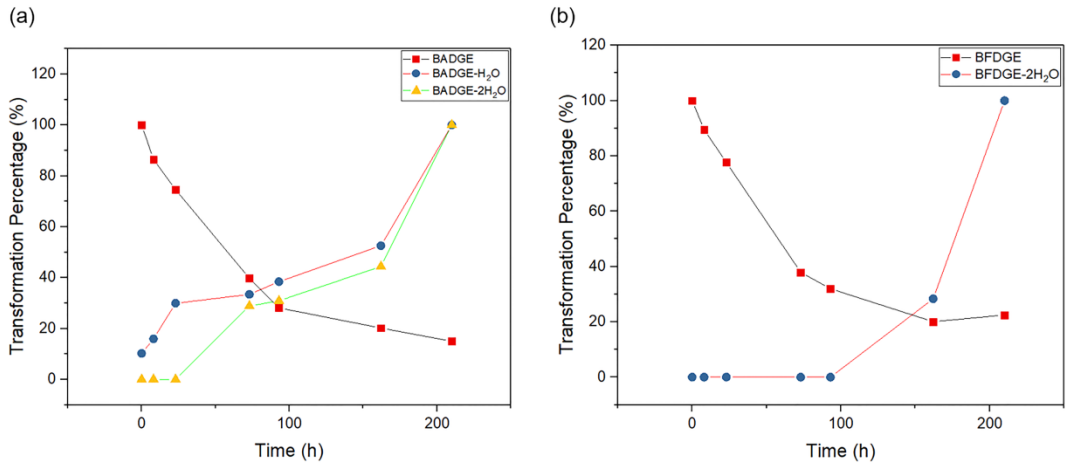

Figure 3-1. Hydrolysis and product formation of (a) BADGE; (b) BFDGE for pH=7 at 25°C

Since water-free environment is of considerable importance to the dust analysis, we optimized clean-up steps using silica gel cartridge as mentioned in section 3.2.2 Chemical Analysis. We found that 10 mL of 20% methanol in ethyl acetate was sufficient for the elution of all tested compounds without great increase in matrix effect **(Figure A1)**. The recovery of BADGE-related compounds in dust samples was assessed by spiking different levels of the pure standard onto a homogeneous dust sample (SRM2585). In this experiment, 1 ng (low), 20 ng (median) and 200 ng (high) of BADGEs were spiked to 50 mg of SRM2585 (in triplicate). The average recovery in spiked dust samples was Average ± S.D: 76 ± 2%, 71 ± 6% and 88 ± 23% for the high, medium and low spiking samples, respectively **(Figure A2)** and no obvious hydrolysis were observed. The matrix effect for dust samples were further evaluated based on the ratio of the signal for the internal standard in the dust samples to that of the calibration standard in pure solvent. The matrix effect of dust samples ranged from 33 to 72% with an average of 53%. All compounds were detected in SRM 2585 (n=5) except BFDGE-2HCl and BFDGE-2H_2O. BPA was detected with the highest concentration (5780 ± 13 ng/g) followed by BPS (4,486 ± 1,201 ng/g) and BADGE-2H_2O (486 ± 105 ng/g). Intra-day variabilities of all compounds ranged from 1~25%

and inter-day variabilities ranged from 18~28% **(Table A3)**.

3.4.2 Bisphenol Plasticizers in Indoor House Dust

Table 3-1 summarizes the bisphenol plasticizers concentration and detection rate in the dust from Singapore. Among all targeted analytes, BPA was the most abundant in the house dust samples, ranging from <1,972 to 22,516 ng/g dust with a geometric mean (GM) of 3,420 ng/g. The BPA concentrations in dust samples from Singapore was relatively higher than those reported in U.S (GM: 1,700 ng/g) and China (GM: 360 ng/g) while comparable with Japan (GM: 2,830 ng/g) and Korea (GM: 4,070 ng/g) (Liao et al. 2012). BPS was also detected in all dust samples ranging from 153 to 5,053 ng/g with a GM of 714 ng/g dust, which is comparable with U.S (GM: 130 ng/g), Japan (GM: 820 ng/g) and Korea (GM: 430 ng/g) (Liao et al. 2012). As a simple factor to reflect the substitution degree, the ratio of BPS to BPA in Singapore was around 0.2 which was comparable to those found in U.S.(0.39) and China (0.26) (Liao et al. 2012). For BADGEs, BADGE-2H_2O was the dominant compounds ranging from 214 to 35,419 ng/g with an GM concentration of 1,843 ng/g. The contribution of BADGE-2H_2O to total BADGEs ranged from 34 to 96% with an average of 61% **(Figure 3-2b)**. Besides BADGE-2H_2O, BADGE-2HCl concentration in dust samples ranged from < 56 to 2,474 ng/g with a GM concentration of 223 ng/g. In terms of BADGE-2HCl concentration in total BADGEs the value ranged from 0 to 49% with an average of 17 % **(Figure 3-2b)**. Another transformation product BADGE-HCl-H_2O was dectected with concentration ranging from 66 to 1,832 ng/g with a GM of 233 ng/g. Compared with other BADGEs, BADGE, BADGE-H_2O and BADGE-HCl were the minor contributors and detected with a GM concentration of 16, 93 and 3 ng/g; respectively **(Table 3-1)**.

Since the water-free methods limited the hydrolysis of reactive BADGEs, we revealed some new distribution profiles of all BADGEs in indoor dust **(Figure 3-2b)**. We found that BADGE-2HCl accounted for approximately 17% of total BADGE

concentrations while previous study did not include BADGE chlorinated compounds for dust analysis. Besides, the contribution of native compound BADGE was observed with relatively higher standard deviation that ranged from below MDL to 23% with an average of 5%, which was comparably higher than those found in U.S. (0%), Japan (0%), Korea (1%) and China (4%) (Wang et al. 2012).

This is the first study reporting the occurrence of BFDGEs in indoor dust samples **(Table 3-1)**. Parent compound BFDGE concentration in dust samples (detection rate: 44%) ranged from < 4.9 to 421 ng/g with a GM concentration of 2.5 ng/g, which was one order of magnitude less than BADGE. BFDGE-2H_2O concentration in dust samples ranged from < 7.2 to 130.0 ng/g with a GM concentration of 0.3 ng/g while BFDGE-2HCl was only detected in one sample with a concentration of 903.2 ng/g **(Table 3-1).** In contrast with BADGEs, native compound BFDGE was dominant (average relative contribution >50%) in 12 of 17 dust samples where BFDGEs were detected. Although the half-lives in hydrolysis test were similar, it seems that the environmental transformation of BFDGE may not as rapid as BADGE.

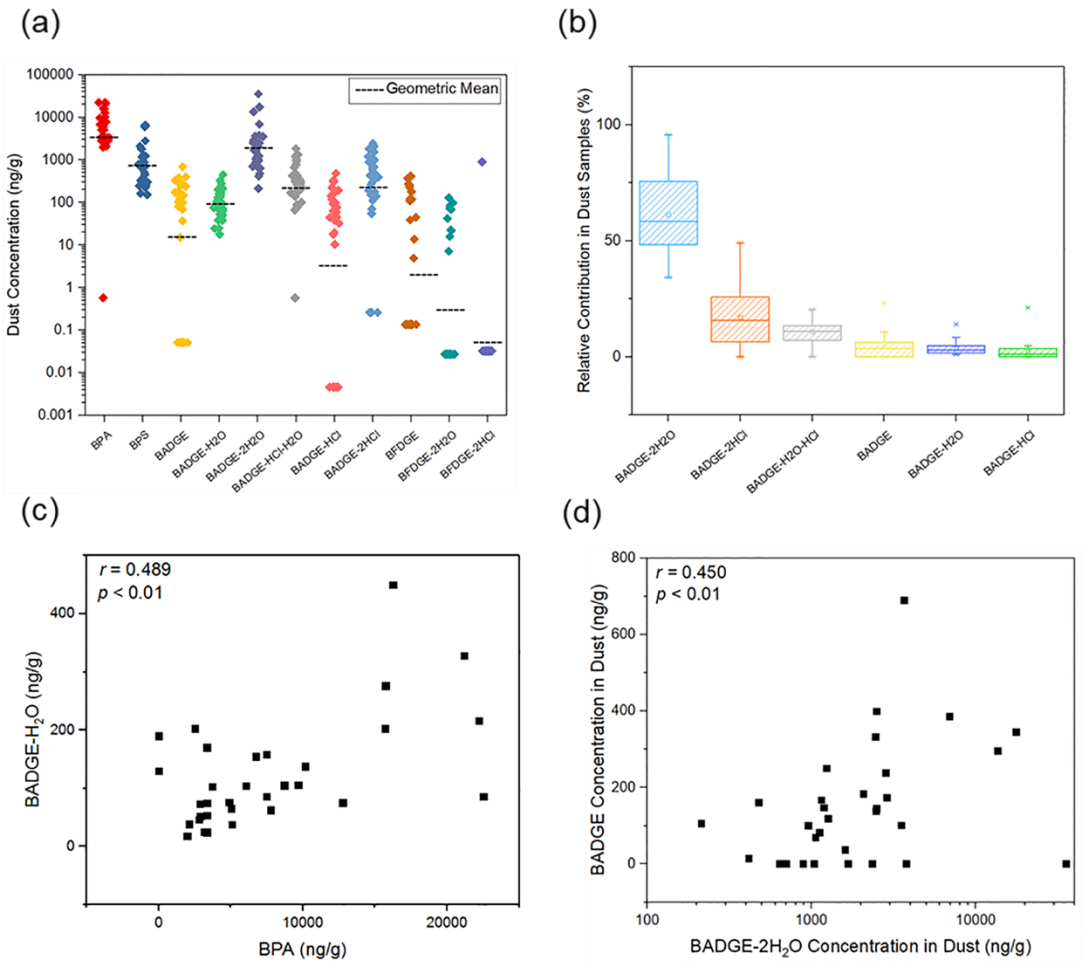

Figure 3-2. (a) Scatter plot of bisphenol plasticizers (ng/g) in indoor house dust from Singapore; (b) Box plot of relative distribution (%) of BADGEs in indoor dust; (c) Spearman correlation between BPA and BADGE-H_2O in indoor dust; (d) Spearman correlation between BADGE and BADGE-$2H_2O$ in indoor dust.

To understand the association between each bisphenol plasticizer in indoor dust, we conducted the Spearman correlation analysis in this study **(Table A4)**. Though no significant correlation was found between BPA and BPS, these two compounds were found significantly correlated with some BADGE-related compounds. For example, the concentrations of BPA in dust samples (n=32) was positively correlated with BADGE hydrolysis products such as BADGE-H_2O (r = 0.489; p < 0.01) **(Figure 3-2c)**, BADGE-$2H_2O$ (r = 0.378; p < 0.05) and BADGE-HCl-H_2O (r = 0.453; p < 0.01).

This finding is consistent with an earlier study suggesting that BAGDE-based epoxy resin is a source of BPA (Schmalz et al. 1999) and the common source for BPA and BADGE (Wang et al. 2012). Interestingly, BADGE was associated with BADGE-2H_2O (r = 0.396; p < 0.05) and BADGE-2H_2O (r = 0.450; p < 0.01) **(Figure 3-2d)** but was not significantly related to BADGE-H_2O (r = 0.254; p > 0.05). These results may be explained by considering the fact that BADGE-H_2O itself is unstable and can be readily hydrolyzed in the dust. Lastly, the concentrations of BFDGE in dust samples (n = 32) was positively correlated with BADGE-HCl (r = 0.430; p < 0.05) and BADGE-2HCl (r = 0.365; p < 0.05) while was not significantly correlated with BADGE.

3.4.3 Bisphenol Plasticizers in Human Urine

Table 3-1 summarizes the urinary concentrations of bisphenol plasticizers and detection rate in this study. Similar to dust, BPA is the most abundant plasticizer in urine samples, ranging from < 0.52 to 31.92 ng/mL with a GM concentration of 2.6 ng/mL **(Figure 3-3)**, which was slightly higher than other countries such as U.S. (GM: 0.70 ng/mL) (Ye et al. 2015) and several Asian countries (GM: 0.84~2.0 ng/mL) (Zhang et al. 2011). Consistent with the findings in dust, BPS, another important contributor, ranging from < 0.012 to 1.97 ng/mL with a GM concentration of 0.070 ng/mL, which was slightly lower than those found in some countries like U.S. (GM: 0.299 ng/mL), China (GM: 0.226 ng/mL), Japan (GM: 1.180 ng/mL), Kuwait (GM: 0.172 ng/mL) and Vietnam (GM: 0.160 ng/mL) but was comparable with the concentrations found in India (GM: 0.072 ng/mL) and Korea (GM: 0.030 ng/mL). Total BADGEs were detected in 50% of the urine samples ranging from < 0.016 to 0.889 ng/mL with a GM concentration of 0.03 ng/mL, which was lower than those found in U.S. (GM: 1.010 ng/mL), China (GM: 1.073 ~ 1.328 ng/mL) (Wang et al. 2012) and Greece (GM: 0.900 ng/mL) (Asimakopoulos et al. 2014). As expected, BADGE-2H_2O was dominant in urine samples among all BADGE and its derivatives.

Besides, no other positive correlation was found. In our study, total BFDGEs were only detected in 5 urine samples ranged from < 0.65 to 1.733 ng/mL.

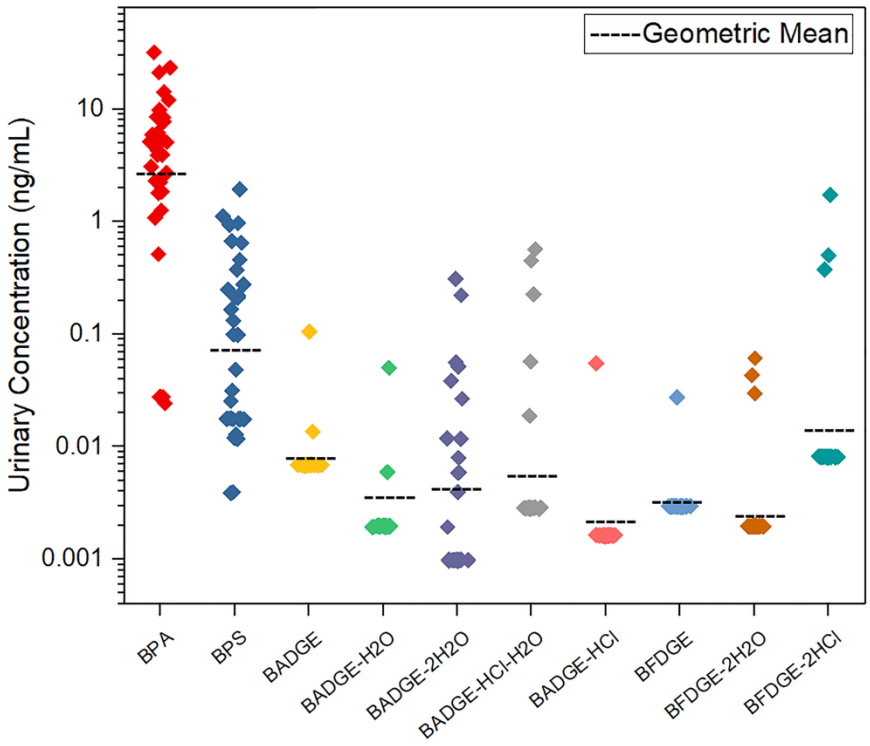

Figure 3-3. Scatter plot representing the total form concentration (ng/mL) of bisphenol plasticizers in urine samples (deconjugated by β-glucuronidase treatment) from Singapore (n=33).

Table 3-1. Concentrations, detection rate (DR%) and method detection limit (MDL) of bisphenol plasticizers in indoor dust (ng/g) and urine (ng/mL) from Singapore

		BPA	BPS	BADGE	BADGE - H_2O	BADGE-$2H_2O$	BADGE-H_2O-HCl	BADGE-HCl	BADGE-2HCl	BFDGE	BFDGE-$2H_2O$	BFDGE-2HCl
Dust ng/g	GM[a]	3,420	714	16	93	1,843	233	3	223	2.5	0.27	0.04
	Range	<MDL-22,516	153-6,491	<MDL-690	18-450	214-35,419	<MDL-1,832	<MDL-480	<MDL-2,474	<MDL-421	<MDL-130	<MDL-2,473
	DR %[b]	93	100	72	100	100	94	66	91	44	31	3
	MDL	1.555	0.173	0.103	0.293	1.066	0.579	0.009	0.527	0.274	0.055	0.065
Urine ng/mL	GM	2.61	0.077	0.0076	0.0022	0.0032	0.0052	0.0018	N.A.	0.0032	0.0026	0.0122
	Range	<MDL-31.92	<MDL-1.93	<MDL-0.10	<MDL-0.05	<MDL-0.3	<MDL-0.56	<MDL-0.05	<MDL	<MDL-0.02	<MDL-0.06	<MDL-1.71
	DR %	88	94	9	9	39	15	3	0	3	9	9
	MDL	0.151	0.007	0.014	0.004	0.006	0.002	0.003	0.017	0.006	0.004	0.017

[a] GM: geometric mean;

[b] MDL for 8-OHdG is 0.015 ng/mL in Urine samples;

3.4.4 Correlation of Bisphenol Plasticizers in Paired Samples and its Association with Oxidative Stress

To tentatively explore the relationship between indoor environment pollution and human exposure, we further conducted the Pearson correlation analysis of bisphenol plasticizers between paired dust and urine samples. For most compounds, we did not observe positive correlations. Interestingly, the urinary BPA concentration was positively correlated with indoor dust concentration (n = 32; $r = 0.491$; $p < 0.01$) **(Figure 3-4)** but this correlation might be driven by the highest two urine samples. Therefore, a larger scale sample size is warranted to validate this correlation. Previous studies suggested that food ingestion was one of the major routes for BPA exposure (Von Goetz et al. 2010) and account for > 90% of total BPA exposure for all age groups (Geens et al. 2012). The correlation result suggests the possible contribution of non-dietary BPA exposure to human exposure.

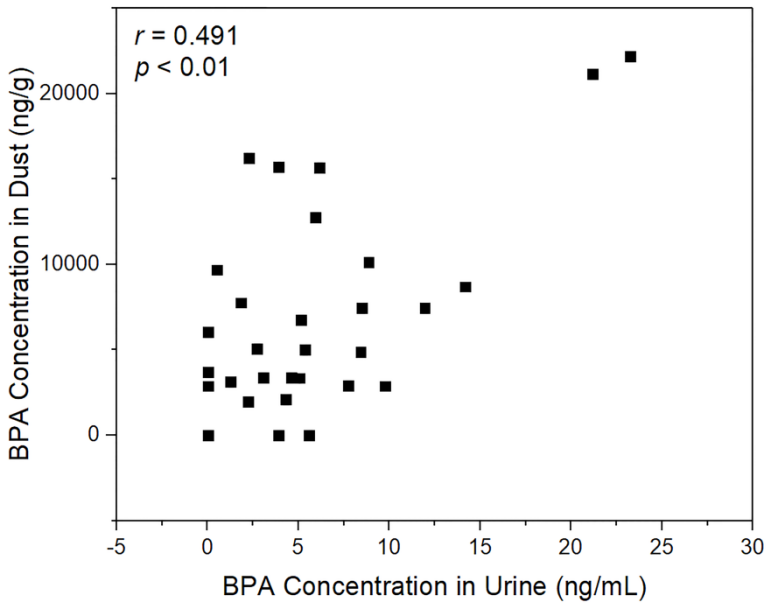

Figure 3-4. Pearson Correlation between BPA concentration in paired house dust and human urine samples (n=32)

We also conducted the Spearman correlation analysis to assess the association between bisphenol plasticizers exposure with oxidative stress levels in human urine. A positive correlation was found between BPA concentration in urine (n = 32) and oxidative stress biomarker 8-OHdG ($r = 0.353$; $p < 0.05$) **(Figure 3-5a).** This is consistent with earlier findings suggesting that BPA exposure induces oxidative stress in animal studies

(Vandenberg et al. 2007 , Lang et al. 2008) and associates with elevated oxidative stress in human specimens (Yang et al. 2009, Asimakopoulos et al. 2016, Zhang et al. 2016). Since 8-OHdG is also known as an index of DNA oxidation (Kasai 1997), it is possible to suggest that exposure to BPA may be an enhancing factor of DNA damage. Interestingly, urinary 8-OHdG (n = 33) was also positively correlated with participants' body mass index (BMI) (r = 0.431; p < 0.05) **(Figure 3-5b).** This finding agrees with previous studies suggesting that oxidative stress increases with increasing BMI (Keaney et al. 2003, Wonisch et al. 2012) and higher BMI tended to have significantly decreased levels of antioxidants (Vincent et al. 2007).

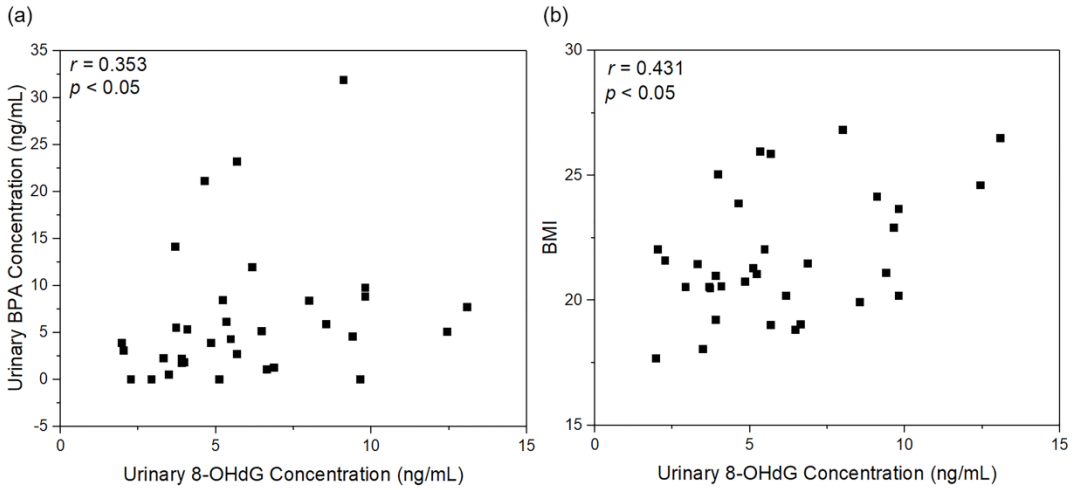

Figure 3-5. (a) Spearman Correlation between urinary BPA concentration and oxidative stress biomarker 8-OHdG (n=32); (b) Pearson correlation between urinary oxidative stress biomarker and body mass index (BMI) (n=33)

3.5 Conclusions

In this study, a novel water-free method was developed for dust samples analysis of bisphenol plasticizers and the concentrations of these compounds were measured in paired indoor house dust and urine samples. Besides, the concentration of urinary oxidative stress biomarker was also measured to examine its association with urinary bisphenol plasticizers levels. In this study, most of the bisphenol plasticizers such as BPA, BPS could be well-detected in the dust and urine samples. Meanwhile, BPA concentrations in paired dust and urine samples were positively correlated and elevated oxidative stress were found associated with BPA exposure/BMI. The results of this study provide baseline information on exposures to environmental estrogenic chemicals

for the Singapore population. The present study also offers evidence that the indoor environment is of considerable importance to human exposure and elevated oxidative stress may be associated with BPA exposure and obesity. A larger scale study for different populations as well as more other EDCs is warranted due to the limited sample size in this study. It would also be beneficial to investigate the mechanism on the association of BPA exposure with elevated oxidative stress and the combinatory toxic effects of these EDCs in the exposome-scale investigation.

Chapter 4. Complementing Experiment with Prediction to Identify the Biotransformation Products of BADGE

4.1 Overview

Chapter 4 developed a useful biotransformation product discovery platform with the integration of experimental analysis with *in silico* and knowledge-based prediction. It has investigated the reaction kinetics and MS/MS fragmentation behavior for those formed products of BADGE with 17 amino acids. Lastly, it has proposed several novel biotransformation products and metabolism pathways for BADGE in liver microsomal and HepG2. The manuscript is under preparation and to be submitted.

4.2 Introduction

Metabolism enables organisms to perform the complex biochemical transformations that maintain homeostasis. It is one of the main factors to mediate the activation, deactivation, toxication and detoxification of small molecules (Rudik et al. 2017). As a detoxification strategy, xenobiotics are frequently metabolized and subsequently conjugated to more polar derivatives in organisms including animals and plants (Kluger et al. 2013). However, the xenobiotic transformation products can be significantly different from their parent compounds on bioactivity profiles, sometimes causing even higher adverse and toxic effects (Kirchmair et al. 2013). For examples, for some polycyclic aromatic hydrocarbon (PAHs) compounds like Benzo[a]pyrene (BaP), it was believed the bioactivation of OH-BaP can be the DNA or protein adducts that leads to the toxicity (Souza et al. 2016). Therefore, the development of an unbiased method to predict and identify unknown biotransformation products has been assumed to have increasing importance in toxicology assessment.

Good prediction provides on-target candidates and enhances the discovery potentials of biotransformation products through previously established knowledge on biotransformation rules. Currently available *in silico* prediction tools require established knowledge, often generating a combinatorial explosion of prediction, which lead to many difficulties on further compound identification. It would be even more difficult to predict the metabolites for those emerging organic contaminants (EOCs) that have little metabolism information on current databases. As some EOCs are quite reactive and can form reaction products with other compounds (e.g. nutrients) in an environment that is

similar to human body. The acquirement on their reaction products enables us to generalize the similar fragmentation rules in mass spectrometry and makes it feasible to identify and narrow down the potential candidates.

BADGE itself is one of the reactive EOCs and widely used in the manufacture of epoxy resins. So far, limited information is available on its metabolism. Its reactivity comes from the unique structure that contains two epoxides (electrophilic oxirane rings). An earlier study reported its 'disappearance' in food packaging materials, which was found to be resulted from its reaction with food components such as oil, protein and amino acids (Petersen et al. 2008). Up to date, it is generally believed that its main metabolites are the hydrolysis products with two water molecules (Wang et al. 2012). There are possibilities that its metabolism could be much more complicated due to its reactive property and covalent binding potentials. For these reasons, BADGE is a suitable model compound to acquire 'prerequisite knowledge' by reaction with nutrients/metabolites. These prerequisite knowledges assist further potential metabolites filtering and study of fragmentation patterns in mass spectrometry.

This study proposed a novel discovery platform to predict and identify *in vitro* biotransformation products for BADGE that have incorporated both prediction and experimental mass spectrometry deconvolution. Due to its reactivity and covalent binding potentials, BADGE was used as a model chemical to find its potential biotransformation products in rat liver microsomal and human liver cancer cell HepG2. Prior to knowledge-based prediction and identification, we built up an 'empirical knowledge acquirement' method through investigating BADGE's potential reaction and kinetics with seventeen amino acids as well as the MS/MS fragmentation patterns of their reaction products. Furthermore, this study employed both *in silico* and knowledge-based prediction to find the possible biotransformation products of BADGE. Lastly, the potential metabolites and metabolism pathway of BADGE were proposed through experimental analysis in rat liver microsomal and HepG2 cell.

4.3 Methodology

4.3.1 Chemicals and Materials

All the solvents and reagents in this study are of High-performance Liquid Chromatography (HPLC) grade or higher. Analytical grade of all amino acids standards

and bisphenol a diglycidyl ether (BADGE) were purchased from Sigma-Aldrich (Singapore).

4.3.2 Liver Microsomal Incubation

The incubation with rat liver microsomes (RLM, Invitrogen Life Technologies, SG) was modified from previous studies (Fang et al. 2014, Peng et al. 2019). Prepared in DMSO (50 mM), BADGE was diluted at concentration of 50 µM in a final reaction mixture volume of 1 mL. This mixture contains 50 mM phosphate-buffered saline (PBS) at pH 7.4, 10 mM magnesium chloride, 10 mM DL-dithiothreitol and 0.05 mg/mL of the RLM protein. The mixtures were placed on ice during sample preparation. Then they were pre-warmed for 5 min at 37 ºC prior to reaction. The reaction was started with the addition of mixture containing uridine 5'-diphosphate-glucuronic acid (final concentration: 5 mM), 3'-phosphoadenosine-5'-phosphosulfate (final concentration: 50 µM), reduced glutathione (final concentration: 10 µM) and nicotinamide adenine dinucleotide phosphate (final concentration: 5 mM). After 1-hour incubation, reaction was terminated with addition of 1 mL of ice-cold methanol and further transferred to -40 ºC fridge for 30 min. The supernatant was transferred to another tube after being centrifuged at 13,000 rpm for 15 min. After the addition of 2 mL water and being froze in -80 ºC, the samples were dried completely using a freeze-dryer. The samples were reconstituted in 250 µL acetonitrile: water (1:1; v/v) and filtered prior to analysis.

4.3.3 Cell Culture, Exposure Experiment and Metabolite Extraction

HepG2 human liver cancer cells (ATCC HB-8065) were grown in Dulbecco's modified Eagle's medium (Gibco, SG) containing 10% fetal bovine serum (FBS, Gibco Invitrogen) and maintained in a humidified 37 ºC incubator with 5% CO_2. For the experiment, cells were seeded with 2.1×10^6 cells per T75 flusk containing a final volume of 13 mL medium. Cells were exposed with 50 µM BADGE for 24 hours.

The metabolite extraction was modified from a previous study (Beyer et al. 2018). Briefly, cell metabolites were extracted with 4 mL ice-cold methanol: acetonitrile: water (2:2:1, v/v/v) and further collected by a cell scraper. The intracellular metabolites were extracted by three times' freeze-thaw steps using liquid nitrogen followed by sonication in an ice bath for 10 min. The samples were placed at -40°C for 1 h, followed by 15-min centrifugation at 13,000 rpm at 4°C to precipitate proteins. The supernatants were

dried using a freeze-dryer and further reconstituted in 250 µL acetonitrile: water (1:1; v/v) and filtered prior to analysis.

4.3.4 Instrumental Analysis

Analysis of all samples was performed using an Agilent 1260 HPLC system coupled with a 6550 Q-ToF mass spectrometer (Agilent Technologies, Singapore). Samples were analysed with an Atlantis T3 column (3 mm, 2.1 ×100 mm) for separation in electrospray ionization (ESI) in both negative and positive modes. The mobile phase comprised water with 5 mM ammonium acetate (A) and acetonitrile (B). A gradient elution at a flow rate of 0.3 mL/min was used for separation: 0~2.5 min, 5% B; 2.5~10 min, increased to 95% B (hold for 2-min); 12~15 min, decreased from 95 to 5% B and 2 min was used as a post-run equilibrium. The compounds and their metabolites were identified using accurate mass and MS/MS fragmentations. All samples were in triplicates in this study. For each batch, one procedural blank was run alongside to correct for the background level during sample preparation and analysis. Any peaks with signal/noise ratio (S/N) < 10 were considered as noise.

4.3.5 Reaction with Amino Acids

The reaction of amino acids was slightly modified based on an earlier method (Petersen et al. 2008). Seventeen amino acids (final concentration: 10 ppm) were mixed in 50 mL water (adjusted to pH=7.4 by phosphoric acid or sodium hydroxide). BADGE (500 µg) was added and incubated in an orbital shaker at 37 ºC and procedural blanks were also prepared without the addition of BADGE. After 2 hours as well as after 1, 3 and 14 days, 1 mL of each mixture was analyzed. For kinetics of selected amino acids after the first screening, cysteine and methionine were added in 50 mL water with 10 ppm final concentrations (pH=7.2~7.4) and procedural control was also prepared. Approximately ~75 µg BADGE was added in each tube. After 2 hours as well as after 14, 24, 41, 64 and 86 hours, 1 mL of each tube was sampled and further analyzed. The formation of reaction products with BADGE over time (hour) was fitted to non-linear, least-squares regression to determine the rate constants (K) with different exponential fitting method accordingly (e.g., one phase decay, one phase association, or growth) using GraphPad Prism 7.04.

4.3.6 General Workflow to Identify Biotransformation Products

The overall workflow of the method was designed with the following steps **(Figure 4-**

1). (1) The reaction of BADGE and amino acid mixture under pH=7.4 in water; (2) Predicting reaction products *m/z* and filtering out possible candidates for targeted MS/MS analysis; (3) Reaction products MS/MS identification incorporating with *in silico* MS/MS fragments prediction with CFM-ID; (4) Studying the fragmentation behaviors/rules; (5) Summarizing in-house fragments database (e.g. some typical BADGE and their product fragments); (6) Culturing rat liver microsomes and HepG2 cell line with BADGE and analysis of samples by LC-QToF; (7) Importing raw MS data to the cloud-based XCMS Online platform (http://xcmsonline.scripps.edu) and filtering the possible candidates with several criteria such as a peak intensity (maxint) > 10,000; much larger than control samples (fold change >10), p <0.01 and a good peak shape; (8) Prediction of possible transformation products *m/z* using *in silico* tool SyGMa or knowledge-based enzymatic reaction rules; (9) Searching the predicted *m/z* values by Step 8 along with the possible reaction products with amino acids in *in vitro* samples under mass accuracy tolerance of 10 ppm and peak intensity (maxint) >5,000; (10) Targeted MS/MS analysis for all the possible candidates filtered in Steps 7, 8 and 9; (11) Identifying the metabolite candidates with the assistance of *in silico* predicted MS/MS fragmentation patterns and summarized MS/MS fragmentation rules.

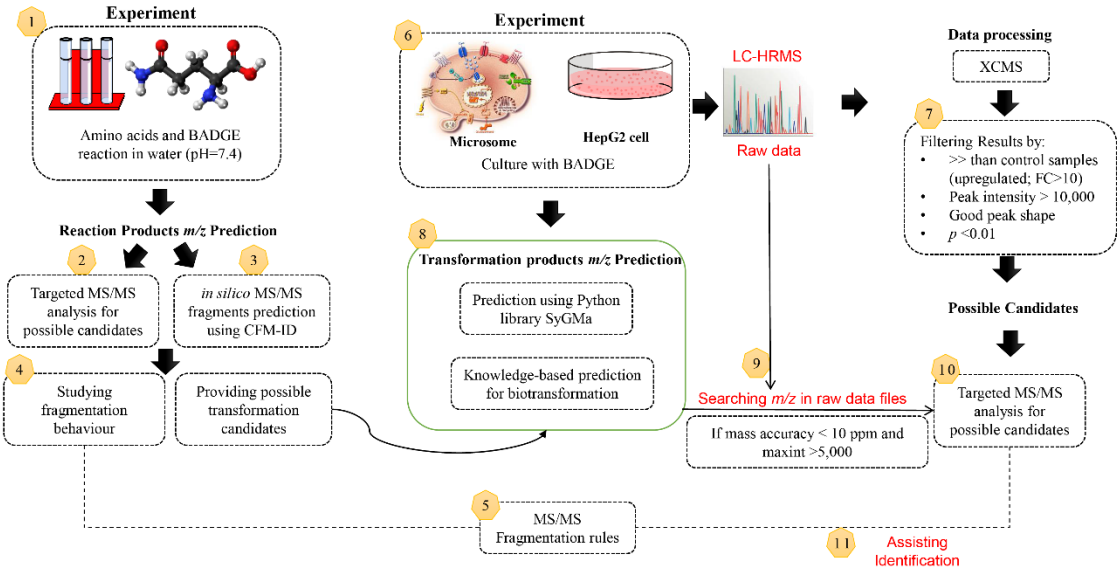

Figure 4-1. Workflow for the prediction and identification of biotransformation products of BADGE (LC-HRMS: Liquid Chromatography-High Resolution Mass Spectrometry)

4.3.7 Empirical Knowledge Acquirement through Prediction and Identification of Potential Reaction Products with Amino Acids

Due to the limited available biotransformation data for BADGE, the acquirement of empirical knowledge was performed through investigating the reaction of BADGE and 17 amino acids and studied their reaction products' MS/MS fragmentation behaviors as described in **Section 4.2.6 Step 1 to 4**. The detailed steps and rationale of this 'empirical knowledge acquirement' were summarized in **Figure 4-2.** (1) Predicting reaction products' *m/z* values based on the prerequisite knowledge that BADGE has two electrophilic epoxides which subject to reaction with nucleophilic species (Petersen et al. 2008). Therefore, its potential reaction usually starts with the open of three-membered ring followed by the hydrolysis or covalent binding with other molecules (the *m/z* could be predicted by [Elemental composition after subtraction of adducts and BADGE] + [BADGE-H_2O] as detailed **in Table 4-2**); (2) Preparing samples for the reaction of amino acid mixture with model compound and collecting samples at different time points, which were further analyzed by LC-QToF; (3) Searching the predicted *m/z* values in the amino acid mixture experiment with mass accuracy tolerance of 10 ppm and performing targeted MS/MS analysis for those candidates with a significant increase in abundance overtime and maxint >5,000; (4) Prior to identification, predicting the *in silico* MS/MS fragments at different collision energy using a machine-learning method CFM-ID (Allen et al. 2014) to assist the identification of reaction products; (5) Studying fragmentation pattern of reaction products; (6) For selected amino acids (e.g. thiol-containing metabolites), investigating the kinetics of their reaction products with BADGE.

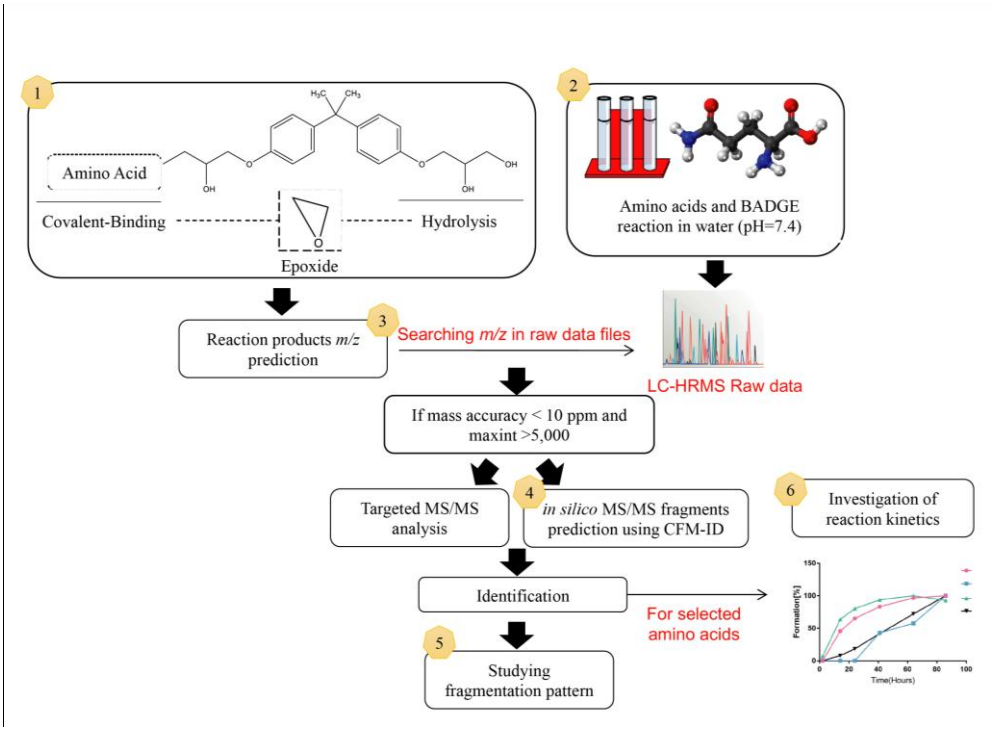

Figure 4-2. Proposed workflow for 'empirical knowledge acquirement' through reaction of amino acids with BADGE.

Table 4-1. Knowledge-based prediction of reaction products of BADGE with amino acids and the observed retention time.

No.	Amino Acids	Reaction Products with BADGE	Predicted Formula [b]	Elemental composition after subtraction [c]	Predicted *m/z*		Retention Time
					$[M+H]^+$	$[M+NH4]^+$	
1	Methionine [a]	BADGE-H_2O-SCH_3	$C_{22}H_{30}O_5S$	SCH_3	-	424.2145	6.9
		BADGE-2SCH_3	$C_{23}H_{32}O_4S_2$	$S_2C_2H_6$	-	454.2117	-
		BADGE-H_2O-Met	$C_{26}H_{37}NO_7S$	$C_5H_{11}O_2N_1S_1$	508.2359	-	6.6
2	Cysteine [a]	BADGE-H_2O-Cys	$C_{24}H_{33}NO_7S$	$C_3H_7NO_2S_1$	480.2049	-	6.5
		BADGE-2Cys	$C_{27}H_{38}N_2O_8S_2$	$C_6H_{14}N_2O_4S_2$	583.2141	-	6.25
3	Lysine	BADGE-H_2O-Lys	$C_{27}H_{40}O_7N_2$	$C_3H_6NO_2S$	505.2905	522.3173	6.3
4	Arginine	BADGE-H_2O-Arg	$C_{27}H_{40}N_4O_7$	$C_6H_{13}N_4O_2$	533.2969	550.3235	-
5	Glycine	BADGE-H_2O-Gly	$C_{23}H_{31}NO_7$	$C_2H_4NO_2$	434.2173	451.2438	6.8
6	Alanine	BADGE-H_2O-Ala	$C_{24}H_{33}NO_7$	$C_3H_6NO_3$	448.2329	465.2595	6.9
7	Serine	BADGE-H_2O-Ser	$C_{24}H_{33}NO_8$	$C_3H_8O_2N_1$	464.2278	481.2544	6.8
8	Proline	BADGE-H_2O-Pro	$C_{26}H_{35}O_7N_1$	$C_5H_8O_2N_1$	474.2486	491.2751	7
9	Valine	BADGE-H_2O-Val	$C_{26}H_{37}O_7N_1$	$C_5H_{10}O_2N_1$	476.2642	493.2908	-
10	Threonine	BADGE-H_2O-Thr	$C_{25}H_{35}O_8N_1$	$C_4H_8O_3N_1$	478.2435	495.27	-
11	Isoleucine	BADGE-H_2O-Ile	$C_{27}H_{39}O_7N_1$	$C_6H_{12}O_2N_1$	490.2799	507.3064	7.7
12	Aspartic Acid	BADGE-H_2O-Asp	$C_{25}H_{33}O_9N$	$C_4H_6O_4N$	492.2228	509.2493	6.4
13	Glutamic Acid	BADGE-H_2O-Glu	$C_{26}H_{35}O_9N_1$	$C_5H_8O_4N_1$	506.2384	523.265	6.5
14	Histidine	BADGE-H_2O-His	$C_{27}H_{35}N_3O_7$	$C_6H_8N_3O_2$	514.2547	531.2813	-
15	Phenylalanine	BADGE-H_2O-Phe	$C_{30}H_{37}O_9N_2$	$C_9H_{10}O_4N_2$	570.2571	587.2837	-
16	Tyrosine	BADGE-H_2O-Tyr	$C_{30}H_{37}O_8N_1$	$C_9H_{10}O_3N_1$	540.2591	557.2857	7.3
17	Tryptophan	BADGE-H_2O-Trp	$C_{32}H_{38}O_7N_2$	$C_{11}H_{11}O_2N_2$	563.2751	580.3017	7.8

Note:

[a] the prediction of reaction products with methionine and cysteine was referred from an earlier study (Coulier et al. 2010).

[b] the predicted formula of reaction products = [BADGE-H_2O: $C_{21}H_{27}O_5$] + [Elemental composition after subtraction]

[c] for predictions except methionine, the [Elemental composition after subtraction of BADGE-H_2O] is equally to [the chemical formula of amino acids] – H.

4.3.8 In Silico Biotransformation Prediction using SyGMa

Firstly, we employed a Python library SyGMa (Systematic Generation of Potential Metabolites) to predict the xenobiotic chemical modifications and conjugations of BADGE-H_2O (Ridder et al. 2008) as summarized in **Table 4-2**. (BADGE-H_2O was chosen to ensure one epoxide being hydrolyzed). SyGMa mainly focuses on CYP enzymes (Phase I enzymes) and transferase (Phase II enzymes) that has been derived from metabolic reactions reported in the metabolites database to occur in humans. This tool predicts the structure without preliminary prediction of site of metabolites (SOMs). An empirical probability score is assigned to refine the rules and to rank predicted metabolites. Generally, 36 potential candidates were generated through *in silico* prediction (18 glucuronide conjugates; 3 sulfate conjugates; 2 glycine conjugates; others were hydroxylation, methylation, acetylation products). Through the prediction, one predicted compound BADGE-$2H_2O$ was found in the further cell/microsomes experiment.

Table 4-2. Prediction on the potential metabolites of BADGE-H_2O using Python library SyGMa.

S	Smile String	Score	Molecular Formula	$[M+H]^+$	$[M+NH4]^+$
1	CC(C)(c1ccc(OCC(O)CO)cc1)c1ccc(OCC(O)CO)cc1	1	$C_{21}H_{28}O_6$	377.1958	394.2224
2	CC(C)(c1ccc(OCC(O)CO)cc1)c1ccc(OCC(O)C(=O)O)cc1	0.199	$C_{21}H_{26}O_7$	391.176	408.202
3	CC(C)(c1ccc(OCC(O)CO)cc1)c1ccc(OCC(CO)OC2OC(C(=O)O)C(O)C(O)C2O)cc1	0.101	$C_{27}H_{36}O_{12}$	553.228	570.255
4	CC(C)(c1ccc(OCC(O)CO)cc1)c1ccc(OCC(O)COC2OC(C(=O)O)C(O)C(O)C2O)cc1	0.101	$C_{27}H_{36}O_{12}$	553.228	570.255
5	CC(C)(c1ccc(O)cc1)c1ccc(OCC(O)CO)cc1	0.087	$C_{18}H_{22}O_4$	303.160	320.186
6	OCC(O)CO	0.087	$C_3H_8O_3$	93.055	110.082
7	CC(CO)(c1ccc(OCC(O)CO)cc1)c1ccc(OCC(O)CO)cc1	0.061	$C_{21}H_{28}O_7$	393.191	410.218
8	CC(C)(c1ccc(OCC(O)CO)cc1)c1ccc(OCC(O)CO)c(O)c1	0.032	$C_{21}H_{28}O_7$	393.191	410.218
9	CC(C)(c1ccc(OCC(O)CO)cc1)c1ccc(OCC(O)C(=O)OC2OC(C(=O)O)C(O)C(O)C2O)cc1	0.02985	$C_{27}H_{34}O_{13}$	567.208	584.234
10	CC(C)(c1ccc(OCC(O)CO)cc1)c1ccc(OC2OC(C(=O)O)C(O)C(O)C2O)cc1	0.02175	$C_{24}H_{30}O_{10}$	479.192	496.218
11	CC(C)(c1ccc(OCC(O)CO)cc1)c1ccc(OCC(OC2OC(C(=O)O)C(O)C(O)C2O)C(=O)O)cc1	0.020099	$C_{27}H_{34}O_{13}$	567.208	584.234
12	CC(C)(c1ccc(OCC(CO)OC2OC(C(=O)O)C(O)C(O)C2O)cc1)c1ccc(OCC(O)C(=O)O)cc1	0.020099	$C_{27}H_{34}O_{13}$	567.208	584.234
13	CC(C)(c1ccc(OCC(O)COC2OC(C(=O)O)C(O)C(O)C2O)cc1)c1ccc(OCC(O)C(=O)O)cc1	0.020099	$C_{27}H_{34}O_{13}$	567.208	584.234
14	CC(C(=O)O)(c1ccc(OCC(O)CO)cc1)c1ccc(OCC(O)CO)cc1	0.013	$C_{21}H_{26}O_8$	407.171	424.197
15	CC(C)(c1ccc(OCC(O)CO)cc1)c1ccc(OS(=O)(=O)O)cc1	0.010353	$C_{18}H_{22}O_7S$	383.116	400.143
16	CC(C)(c1ccc(O)cc1)c1ccc(OCC(CO)OC2OC(C(=O)O)C(O)C(O)C2O)cc1	0.008787	$C_{24}H_{30}O_{10}$	479.192	496.218
17	CC(C)(c1ccc(O)cc1)c1ccc(OCC(O)COC2OC(C(=O)O)C(O)C(O)C2O)cc1	0.008787	$C_{24}H_{30}O_{10}$	479.192	496.218
18	O=C(O)C1OC(OCC(O)CO)C(O)C(O)C1O	0.008787	$C_9H_{16}O_9$	269.087	286.114

Continued on next page

19	O=C(O)C1OC(OC(CO)CO)C(O)C(O)C1O	0.008787	$C_9H_{16}O_9$	269.087	286.114
20	CC(C)(c1ccc(OCC(O)CO)cc1)c1ccc(OCC(O)CO)c(OC2OC(C(=O)O)C(O)C(O)C2O)c1	0.008	$C_{27}H_{36}O_{13}$	569.223	586.250
21	CC(C)(c1ccc(OCC(O)CO)cc1)c1ccc(OCC(O)C(=O)NCC(=O)O)cc1	0.007164	$C_{23}H_{29}NO_8$	448.197	465.224
22	CC(COC1OC(C(=O)O)C(O)C(O)C1O)(c1ccc(OCC(O)CO)cc1)c1ccc(OCC(O)CO)cc1	0.006161	$C_{27}H_{36}O_{13}$	569.223	586.250
23	CC(CO)(c1ccc(OCC(O)CO)cc1)c1ccc(OCC(CO)OC2OC(C(=O)O)C(O)C(O)C2O)cc1	0.006161	$C_{27}H_{36}O_{13}$	569.223	586.250
24	CC(CO)(c1ccc(OCC(O)CO)cc1)c1ccc(OCC(O)COC2OC(C(=O)O)C(O)C(O)C2O)cc1	0.006161	$C_{27}H_{36}O_{13}$	569.223	586.250
25	COc1ccc(C(C)(C)c2ccc(OCC(O)CO)cc2)cc1	0.004698	$C_{19}H_{24}O_4$	317.175	334.202
26	CC(C)(c1ccc(OCC(O)CO)cc1)c1ccc(OCC(O)CO)c(OS(=O)(=O)O)c1	0.003808	$C_{21}H_{28}O_{10}S$	473.148	490.175
27	CC(C)(c1ccc(OCC(O)CO)cc1)c1ccc(OCC(CO)OC2OC(C(=O)O)C(O)C(O)C2O)c(O)c1	0.003232	$C_{27}H_{36}O_{13}$	569.223	586.250
28	CC(C)(c1ccc(OCC(O)CO)cc1)c1ccc(OCC(O)COC2OC(C(=O)O)C(O)C(O)C2O)c(O)c1	0.003232	$C_{27}H_{36}O_{13}$	569.223	586.250
29	CC(C)(c1ccc(OCC(CO)OC2OC(C(=O)O)C(O)C(O)C2O)cc1)c1ccc(OCC(O)CO)c(O)c1	0.003232	$C_{27}H_{36}O_{13}$	569.223	586.250
30	CC(C)(c1ccc(OCC(O)COC2OC(C(=O)O)C(O)C(O)C2O)cc1)c1ccc(OCC(O)CO)c(O)c1	0.003232	$C_{27}H_{36}O_{13}$	569.223	586.250
31	CC(C(=O)OC1OC(C(=O)O)C(O)C(O)C1O)(c1ccc(OCC(O)CO)cc1)c1ccc(OCC(O)CO)cc1	0.00195	$C_{27}H_{34}O_{14}$	583.203	600.229
32	COc1cc(C(C)(C)c2ccc(OCC(O)CO)cc2)ccc1OCC(O)CO	0.001728	$C_{22}H_{30}O_7$	407.207	424.234
33	CC(C(=O)O)(c1ccc(OCC(O)CO)cc1)c1ccc(OCC(CO)OC2OC(C(=O)O)C(O)C(O)C2O)cc1	0.001313	$C_{27}H_{34}O_{14}$	583.203	600.229
34	CC(C(=O)O)(c1ccc(OCC(O)CO)cc1)c1ccc(OCC(O)COC2OC(C(=O)O)C(O)C(O)C2O)cc1	0.001313	$C_{27}H_{34}O_{14}$	583.203	600.229
35	CC(COS(=O)(=O)O)(c1ccc(OCC(O)CO)cc1)c1ccc(OCC(O)CO)cc1	0.001098	$C_{21}H_{28}O_{10}S$	473.148	490.175
36	CC(C(=O)NCC(=O)O)(c1ccc(OCC(O)CO)cc1)c1ccc(OCC(O)CO)cc1	0.000468	$C_{23}H_{29}NO_9$	464.192	481.219

4.3.9 Knowledge-based Prediction

As mentioned above, the rule-based prediction usually generates a combinatorial explosion of results that were hard to evaluate and interpret since they rely on the generic transformation rules heavily. Therefore, the empirical knowledge on potential transformation products could give the rational basis underlying a prediction and increase the discovery rate. In this study, the prediction of substrate modification is based on the empirical knowledge of BADGE's reaction with amino acids and the common biotransformation *m/z* changes following enzymatic reactions summarized by an earlier study (Anari et al. 2004). For glucuronide conjugates prediction, *in silico* tool SyGMa proposed 18 possible glucuronide conjugates but none of them was detected in the experimental samples. Due to the similarity of structure between bisphenol A (BPA) and BADGE, it is possible that their xenobiotic transformation products can share some common patterns. Hereby, we first summarized all the possible validated biotransformation pathway for BPA from previous studies (Schmidt et al. 2013, Yousofshahi et al. 2015). As shown in **Figure 4-3**, the identified glucuronide conjugation rules of BPA were referred for further prediction for BADGE. Besides, based on the empirical knowledge on BADGE's reaction with amino acids, the epoxides tend to react with metabolites containing the thiol group. Here, this study proposed the possible transformation products with thiol-containing metabolites S-glutathione and N-Acetyl-L-cysteine. It also included the adduct formation of BADGE and glucose as it has been reported in an earlier study (Petersen et al. 2008). All the predicted reaction products as well as their potential structures were summarized in **Table 4-3**.

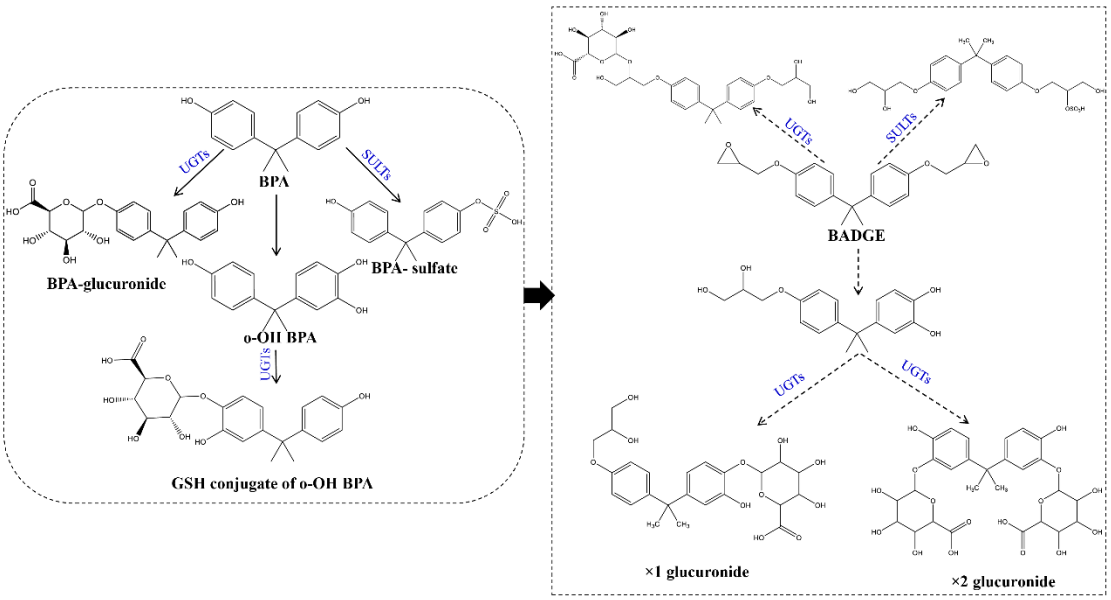

Figure 4-3. Knowledge-based prediction of BADGE glucuronide and sulfate conjugates based on the validated biotransformation for BPA.

Table 4-3. Knowledge-based metabolic prediction on potential metabolites.

Description	Metabolic Reaction	Predicted Chemical Formula	m/z		Proposed Metabolites Structure	Identified in Samples/ Retention time
			$[M+H]^+$	$[M+NH4]^+$		
Sulfate conjugation	R-OH->R-OSO_3H	$C_{21}H_{28}O_9S$	457.1526	474.1792	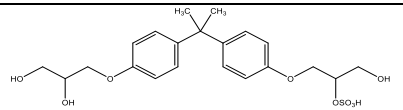	Microsome 6.2 min
	×2 sulfate conjugation	$C_{21}H_{28}O_{12}S_2$	537.1094	554.136	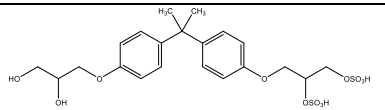	n.d.
	×3 sulfate conjugation	$C_{21}H_{28}O_{15}S_3$	617.0663	634.0928	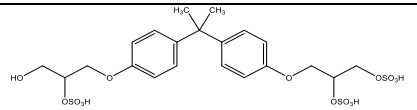	n.d.
	×4 sulfate conjugation	$C_{21}H_{28}O_{18}S_4$	697.0231	714.0496	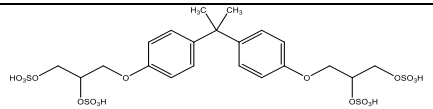	n.d.
Glucuronide conjugation (Based on BPA-glucuronide conjugates)[a]	+$C_6H_9O_7$ (Based on $C_{18}H_{21}O_4$)	$C_{24}H_{30}O_{11}$	495.1860	533.1419	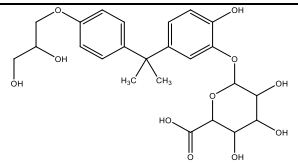	Microsome 8.7 min
	×2 glucuronide conjugation (Based on $C_{15}H_{16}O_2$)	$C_{27}H_{32}O_{16}$	613.1763	630.2028	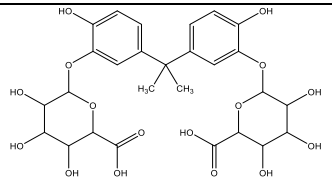	n.d.

S-Glutathione conjugation	$+C_{10}H_{16}N_3O_6S$	$C_{31}H_{43}N_3O_{11}S$	666.2691	683.2956	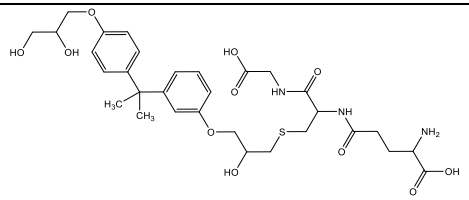	Microsome, Cell 6.2 min
	×2 S-glutathione conjugation	$C_{41}H_{58}N_6O_{16}S_2$	955.3423	972.3688	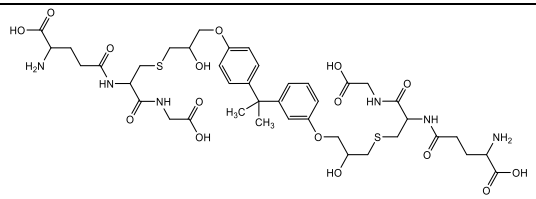	n.d.
Acetylcysteine conjugation	$+C_5H_8NO_3S$	$C_{26}H_{35}NO_8S$	522.2156	539.2421	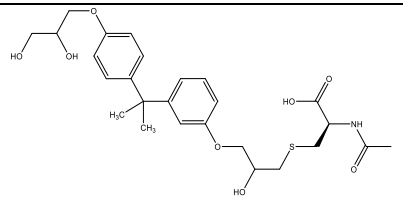	n.d.
	×2 Acetylcysteine	$C_{31}H_{42}N_2O_{10}S_2$	667.2353	684.2619	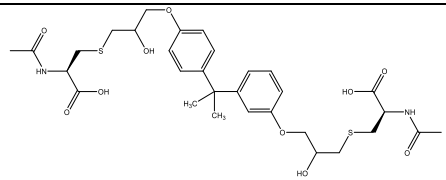	n.d.
Glucose adduct [b]	×1 glucose	$C_{27}H_{38}O_{11}$	539.2486	556.2752	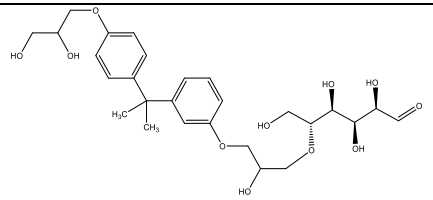	Cell 6.6 min

[a] predicted structure based on the BPA-glucuronide conjugate from an earlier study (Yousofshahi et al. 2015).

[b] predicted from earlier reported reaction of BADGE's reaction with food components (Petersen et al. 2008).

4.4 Results & Discussions

4.4.1 Identification and MS/MS Fragmentation Behavior of BADGE and Amino Acids Reaction Products

Through the reaction of amino acid mixture with BADGE, we observed several suspicious adduct formation with amino acids under the condition of pH=7.4 in water for 14 days. Their retention time ranged from 6.25 to 7.8 min and were also summarized in **Table 4-1**. It should be noted that many of these suspected candidates' signal were too low to perform high quality targeted MS/MS analysis. Therefore, we only conducted the targeted MS/MS analysis for those peaks with maxint >5,000 (BADGE-H_2O-Cys, BADGE-H_2O-Methionine, BADGE-H_2O-Proline, BADGE-H_2O-Alanine, BADGE-H_2O-isoleucine and BADGE-H_2O-glutamic acid).

We summarized the MS/MS of these candidates under positive electrospray ionization mode at a collision energy of 20 eV in **Figure 4-1**. We have also generalized the similar fragmentation rules for these reaction products. Firstly, either side of the bond connecting two benzenes has high chance to be fragmented, generating characteristic daughter ions major *m/z* 209.1168 (the hydrolysis side) or minor *m/z* 312.1263/322.2007 **(Figure 4-4. A and E)** for cysteine/isoleucine (the amino acid side). Furthermore, BADGE's reaction products with cysteine, methionine, alanine and isoleucine, these fragments tend to form another characteristic daughter ion *m/z* 135.0798 (Note: 135.0798 is formed under collision energy of 40 eV for isoleucine). Interestingly, we also observed the *m/z* 102.0548, 116.0708 and 130.0495 which equal to the *m/z* of amino acids for methionine, proline and glutamic acid, respectively **(Figure 4-4 B, C and F)**. Overall, 'prerequisite knowledge' on these characteristic fragmentation patterns make it feasible to identify and narrow down the potential candidates.

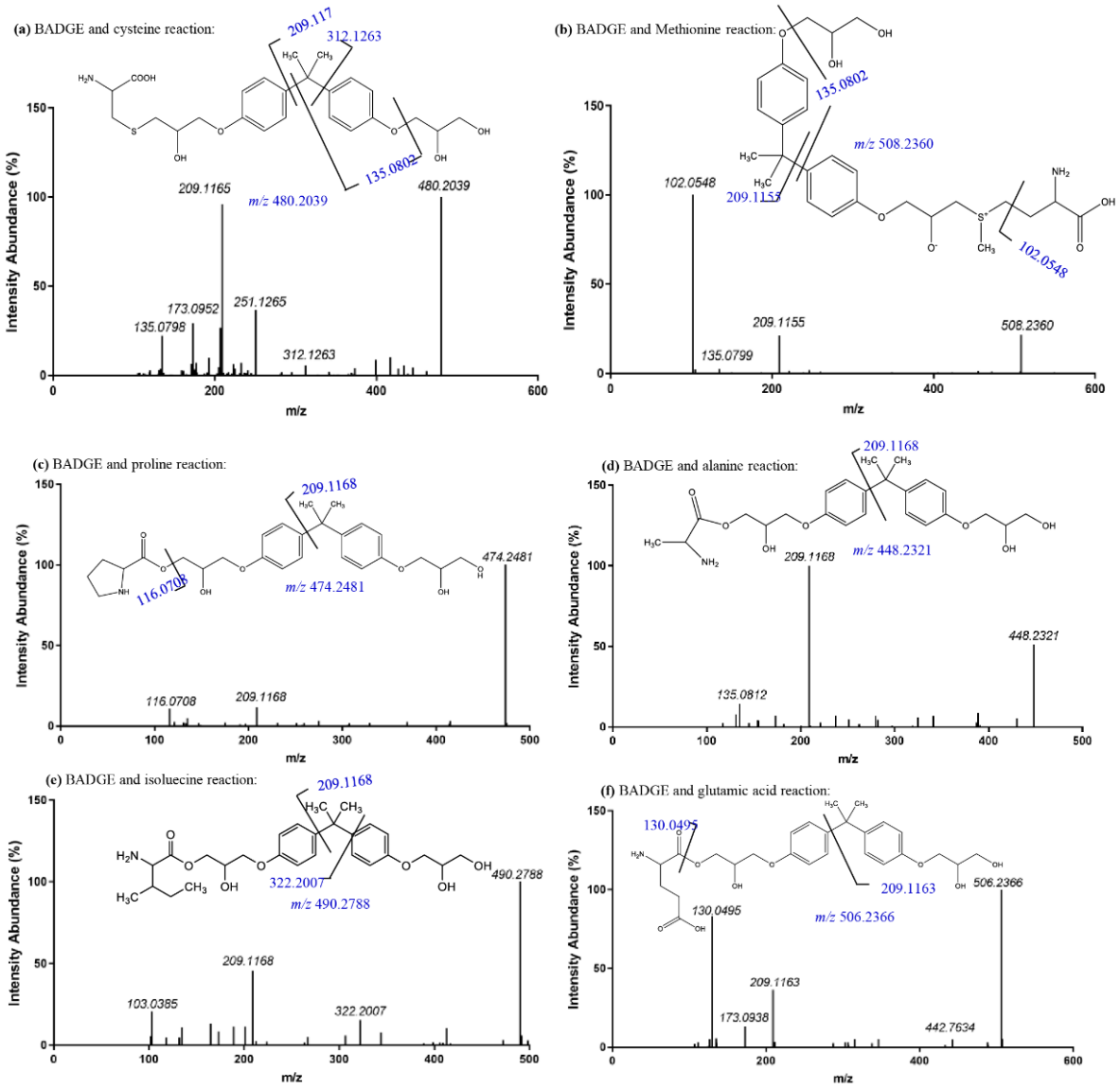

Figure 4-4. Fragmentation patterns of reaction products of BADGE and amino acids with a collision energy of 20 eV under ESI (+) mode. **A.** BADGE-H_2O-Cys; **B.** BADGE-H_2O-Methionine; **C.** BADGE-H_2O-Proline; **D.** BADGE-H_2O-Alanine; **E.** BADGE-H_2O-isoleucine; **F.** BADGE-H_2O-glutamic acid.

4.4.2 Kinetics of BADGE and Amino Acids Reaction Products

We further investigated the reaction kinetics of BADGE with Cysteine and Methionine in pH=7.4 at 37 ºC in water. Cysteine and Methionine were selected because they all have a thiol (nucleophilic properties) which can react with electrophilic epoxides of BADGE. Under both reactions, the BADGE hydrolysis products BADGE-H_2O and

BADGE-2H_2O were detectable with considerable amounts. The formation trends of these hydrolysis products were identical for both reactions. BADGE-H_2O formed rapidly within 24 hours and slowed down gradually afterwards while BADGE-2H_2O formed in a quite opposite manner.

Regarding BADGE's reaction with cysteine, both BADGE-2Cys and BADGE-H_2O-Cys were detected. Interestingly, the maximal concentration of BADGE-2Cys occurred in the initial sampling point (2h) and decreased rapidly in the following 80 hours, suggesting its instability. In contrast, its stable adduct BADGE-H_2O-Cys formed rapidly in the first 14 hours then decreased drastically until 40 hours. Afterwards, it increased steadily from 40 ~80 hours. For the reaction products with methionine, only one-side reaction products (BADGE-H_2O-Met and BADGE-H_2O-SCH_3) were detected. The overall formation trends of both intermediates (BADGE-H_2O-Met) and its stable form (BADGE-H_2O-SCH_3) were consistent but their reaction rates were different.

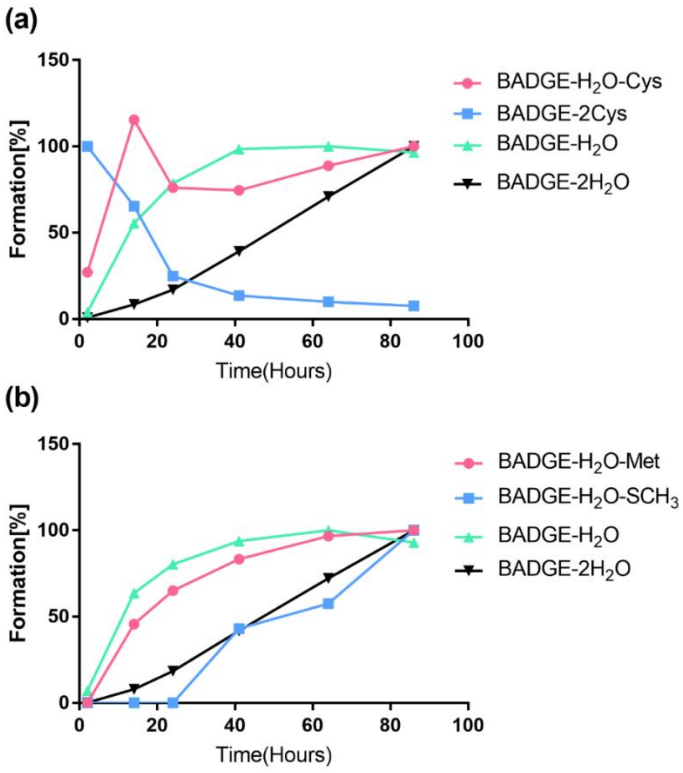

Figure 4-5. The formation [%] of reaction products of BADGE with **A.** cysteine and **B.** methionine over time (hours); pH=7.4 at 37 ºC.

The formation of reaction products with BADGE over time were fitted to non-linear, least-squares regression to determine the rate constants (K) **(Table 4-4)**. Firstly, the BADGE-$2H_2O$ hydrolysis rates at both conditions were nearly identical (cysteine: 0.026; methionine: 0.025). While the BADGE-H_2O hydrolysis rates for cysteine (0.068) were slightly lower than methionine (0.082). In addition, for BADGE and methionine reaction, the constant rate for reaction intermediates BADGE-H_2O-Met (0.047) was higher than its final products BADGE-H_2O-SCH_3 (0.030). Overall, the kinetics of these reaction products suggested the rapid reaction between epoxide and thiol group.

Table 4-4. Experimentally determined rate constants (K) for BADGE's reaction products in pH=7.4 at 37 ºC.

Reaction	Reaction Products	Fitting Method	Rate constant (K, 1/h)	% RSD	Half-life or doubling time (h)
Cysteine	BADGE-H_2O-Cys [a]	Exponential One phase association	0.992	-	-
	BADGE-2Cys	Exponential One phase decay	-0.560	2	12.390
	BADGE-H_2O	Exponential One phase association	0.068	10	10.210
	BADGE-$2H_2O$	Exponential Growth	0.026	16	26.570
Methionine	BADGE-H_2O-Met	Exponential One phase association	0.047	5	14.810
	BADGE-H_2O-SCH_3	Exponential Growth	0.030	24	22.130
	BADGE-H_2O	Exponential One phase association	0.082	10	8.5050
	BADGE-$2H_2O$	Exponential Growth	0.025	17	27.200

[a] BADGE-H_2O-Cys formation percentage [%] were log-transformed first and then fitted with exponential one phase association curve.

4.4.4 In Vitro Metabolism of BADGE in Rat Liver Microsomal

In microsomes samples, we have found 160 potential features after filtering as illustrated in a cloud plot **(Figure 4-6)**. These features were manually examined and those with

good peak shapes were further performed targeted MS/MS analysis. Incorporating with predictions, we have identified 5 biotransformation products of BADGE in microsomes incubations including 2 hydrolysis products, 1 sulfate conjugate, 1 glutathione conjugate and 3 glucuronide conjugates.

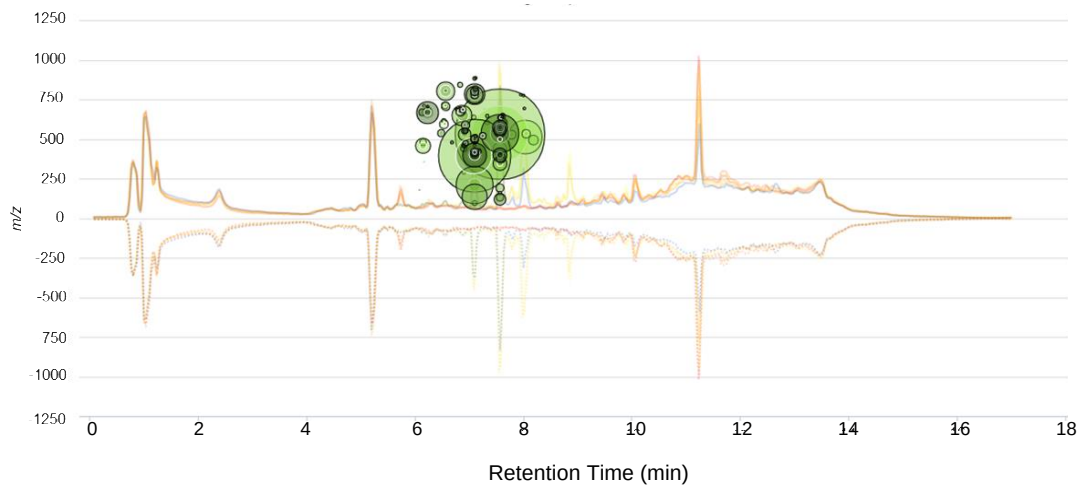

Figure 4-6. Cloud plot of filtered features for microsomes samples (x-axis represents retention time and y-axis represents *m/z* of features; Radius scale represents peak intensity; filtering criteria: Fold Change >10; Peak intensity > 10,000; p <0.01)

Two possible glucuronide conjugates were found in the microsome samples. The *m/z* observed 513.1972 was presumed to be the glucuronide conjugation product of BADGE (with one-side glucuronidation) following hydroxylation with a formula of $C_{24}H_{32}O_{12}$ with a theoretical $[M+H]^+$ *m/z* 513.1966. Through MS/MS fragmentation, the structure was proposed in **Figure 4-7 A** on the basis of both daughter ions and high-resolution molecular mass. Through prediction based on validated BPA metabolism pathway, in microsomal incubation samples, the *m/z* 495.185 was presumed to be the glucuronide conjugation products of BADGE (one-side glucuronidation) following hydroxylation with a formula of $C_{24}H_{30}O_{11}$ and with a predicted theoretical $[M+H]^+$ *m/z* 495.1860. The structure was proposed based on the validated biotransformation for BPA. The *m/z* eluted from retention time = 8.7 min presumably were the glucuronide conjugate of BADGE. Through MS/MS fragmentation, the structure was proposed as follows **(Figure 4-7 B)**. On the basis of both daughter ions and high-resolution molecular mass, it is plausible to conclude that these two detected peaks could be BADGE-glucuronide conjugates. It should be noted that the position of OH-group substitution could not be

elucidated yet.

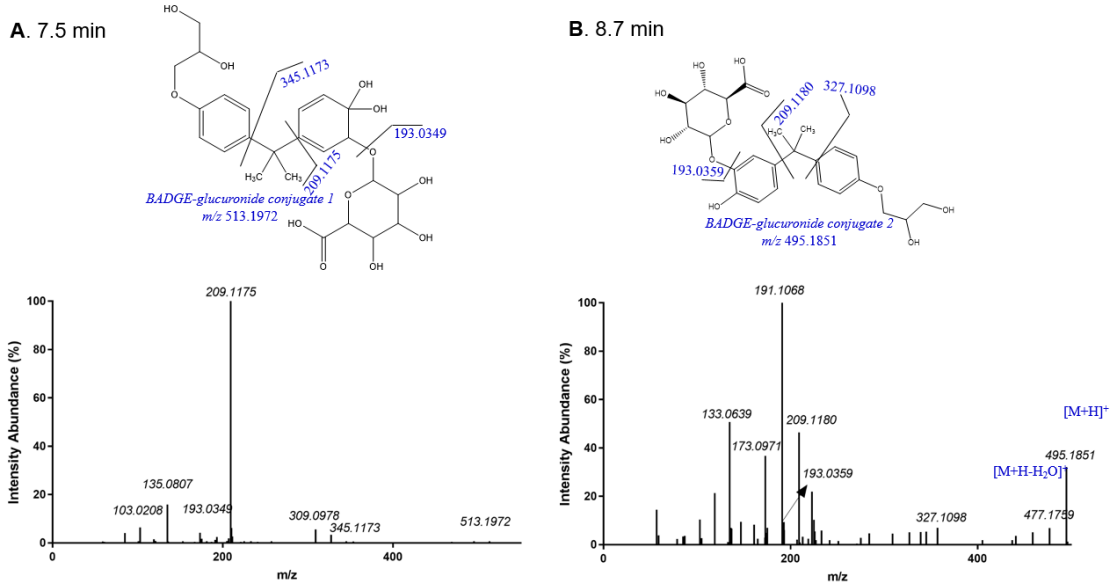

Figure 4-7. Two one-side BADGE glucuronide conjugates in microsomes and their potential structures eluted in **A.** 7.5 min; **B.** 8.7 min and their MS/MS fragments in ESI (+) mode with a collision energy of 20 eV.

The m/z 649.1971 was a potential BADGE transformation product with two sides being conjugated with glucuronides **(Figure 4-8)**. It was presumed with a formula of $C_{27}H_{36}O_{18}$ and with theoretical $[M+H]^+$ *m/z* 649.1974. In MS/MS mode, no daughter ion *m/z* 209.117 was observed, which implied this biotransformation product may not contain the typical BADGE-hydrolysis fragment and both benzene sides have been transformed. Besides, this compound generated one significant daughter ions *m/z* 345.1188, which is precisely the mass of the presumed structure if the bond connecting two benzenes was broken. These accumulated results suggested that it is a two-side glucuronide conjugate of BADGE.

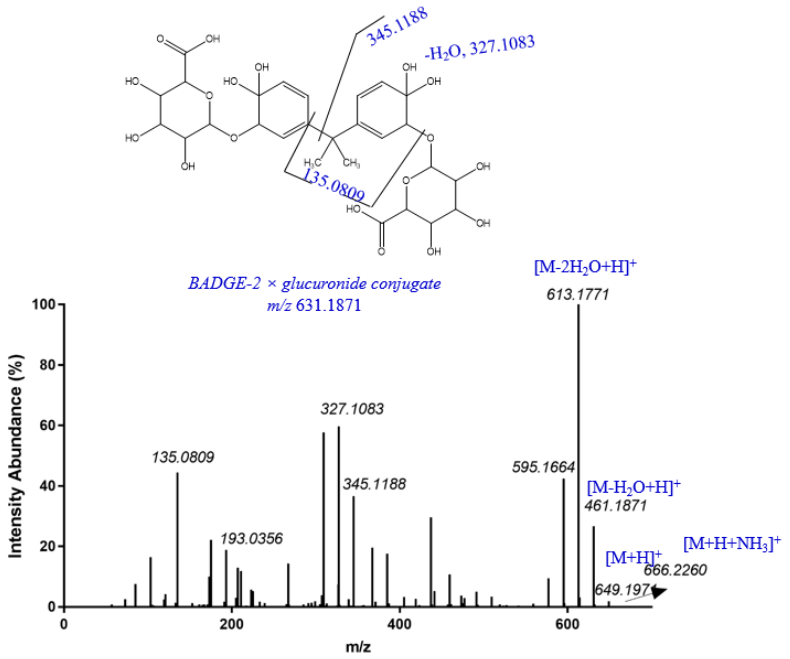

Figure 4-8. The proposed structure for BADGE two-side glucuronide conjugates in microsomes and its MS/MS fragments in ESI (+) mode with a collision energy of 20 eV.

Furthermore, we also found two possible conjugates through knowledge-based prediction. One is BADGE sulfate conjugate **(Figure 4-9 A)** that was predicted with a formula of $C_{21}H_{28}O_9S$ and a theoretical $[M+H]^+$ *m/z* 457.1526. The presumed reaction products generate several daughter ions. Main fragment *m/z* 209.1174's appearance suggests the hydrolysis of one epoxide. Considering the exact mass of fragment *m/z* 98.9846 is the same as sulfate ($-OSO_3H$), it is very likely to be a sulfate conjugate (one-side). It should be noted that the position of $–OSO_3H$ could not be elucidated yet. Another one is BADGE glutathione conjugate eluted in 6.2 min, which was predicted with a formula of $C_{24}H_{30}O_{11}$ and a theoretical $[M+H]^+$ *m/z* 666.2691 **(Figure 4-9 B)**. Glutathione also has a thiol group that could react with the epoxide group. The *m/z* 666.2685 could generate daughter ions *m/z* 209.1174 and 537.2262. Through CFM-ID prediction, the *m/z* 537.2262 might be resulted from the fragmentation of glutathione, which is consistent with the glutathione's fragmentation behavior.

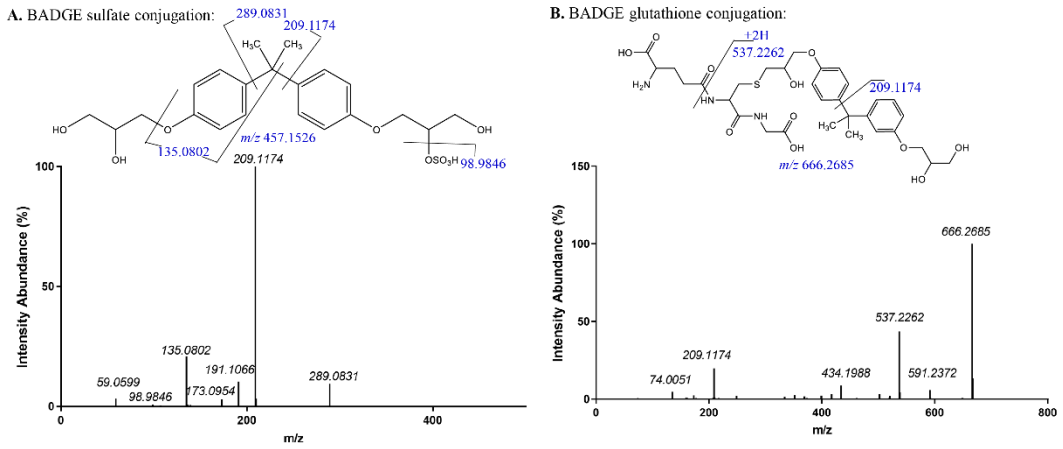

Figure 4-9. Proposed structure for **A.** BADGE sulfate conjugates and **B.** BADGE glutathione conjugation products in microsomes and their MS/MS fragments in ESI (+) mode with a collision energy of 20 eV.

Overall, the potential biotransformation products of BADGE in rat liver microsomal were outlined **(Figure 4-10)**. Both epoxides could be hydrolyzed readily in microsomes. In addition, BADGE can form sulfate and glutathione conjugates with another epoxide being hydrolyzed. Furthermore, BADGE may undergo Phase I hydroxylation with the addition of –OH group and further form glucuronide conjugates. This is interesting and warrants further investigation in the future.

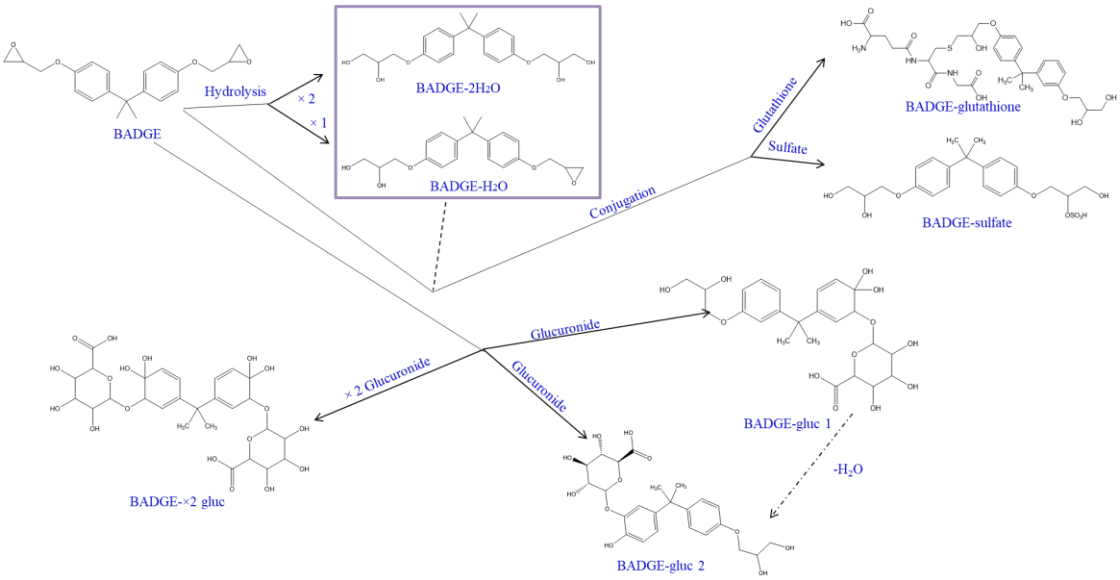

Figure 4-10. Proposed potential metabolites for BADGE metabolism by rat liver microsomal.

4.4.5 Detected Biotransformation Products in HepG2 Cells

In cell samples, 142 potential candidates' features were found after filtering and were illustrated in a cloud plot **(Figure 4-11)**. These features were manually examined and those with good peak shapes were further performed targeted MS/MS analysis. We have identified 7 biotransformation products of BADGE in cell incubations. Except 2 hydrolysis products and 1 glutathione conjugate that were found in microsomes samples, the other identified metabolites were adducts with cysteine, methionine and glucose.

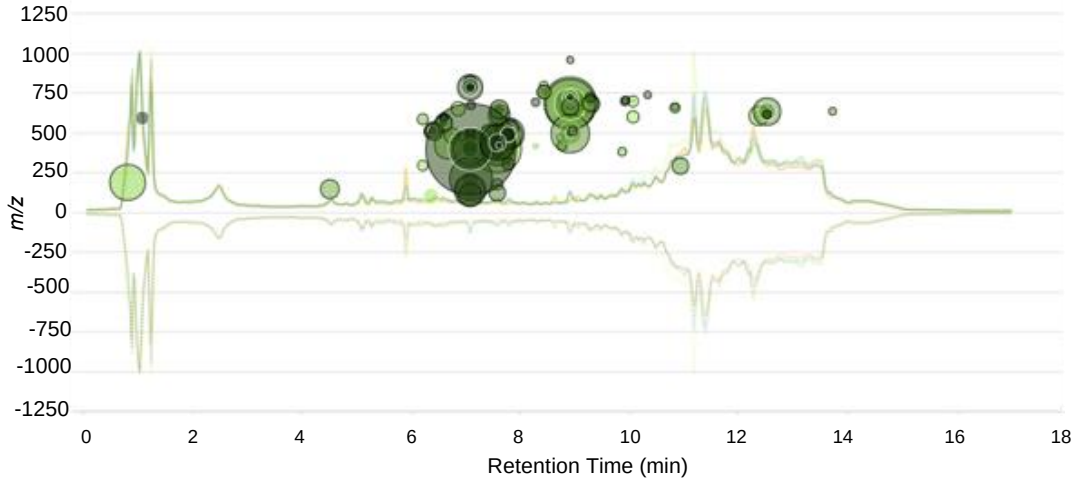

Figure 4-11. Cloud plot of filtered features in HepG2 cell samples (x-axis represents retention time and y-axis represents *m/z* of features; Radius scale represents peak intensity; filtering criteria: Fold Change >10; Peak intensity > 10,000; p <0.01)

In comparison with microsomes samples, cell samples have a rather complicated matrix. Most of the suspected metabolites' signals could be quite low, which resulted in the difficulties in identification. In this case, the prerequisite knowledge-based prediction could provide more targeted candidates for further identification and validation. Above all, we found the vigorous reaction between BADGE and the thiol-containing metabolites in HepG2. For examples, biotransformation products BADGE-H_2O-Cys (RT=6.6 min) and BADGE-2Cys (RT= 6.3 min) as well as BADGE-H_2O-Methionine intermediate (RT=6.6 min) were found in cell samples with an almost identical retention time as the reaction products of BADGE and amino acids. The glutathione conjugate was also found eluted in 6.19 min, which was identical with that in microsomes samples (RT= 6.2 min). Besides, we also found an adduct formation of BADGE and glucose,

which was predicted with a formula of $C_{27}H_{32}O_{16}$ and a theoretical $[M+NH_4]^+$ *m/z* 556.2748 **(Figure 4-12)**. It was found to be eluted in retention time of 6.7 min. The *m/z* 556.2742 could generate daughter ions *m/z* 209.1171 and 377.1956. Through CFM-ID prediction, the *m/z* 377.1956 might be resulted from the fragmentation of glucose. It should be noted that the position of glucose could not be elucidated yet.

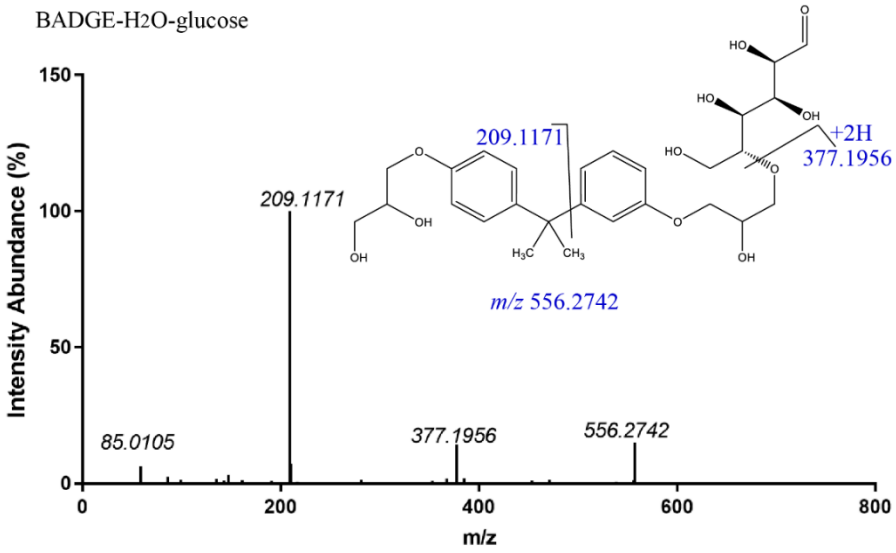

Figure 4-12. Proposed structure for BADGE glucose adduct (m/z 556.2742 was the $[M+NH4]^+$ adduct) in HepG2 and its MS/MS fragments in ESI (+) mode with a collision energy of 20 eV.

In general, the potential metabolites of BADGE in HepG2 cell was also outlined **(Figure 4-13)**. The potential metabolites discovered through HepG2 metabolism were those adducts formed by thiol-containing metabolites with BADGE such as BADGE-H_2O-Cys, BADGE-2Cys as well as BADGE-Methionine intermediate. Interestingly, BADGE tends to form an adduct with glucose. In contrast, all these adducts with nutrient were not found in microsome samples. Since none of these nutrients were added in the microsome experiment, it is possible the contents of these nutrients were too low in rat liver microsome to form adducts. Considering culture medium of HepG2 containing these nutrients, another possible reason is that these adducts were formed in the medium first and then transported into cells. The question of whether these adducts formed in the medium and then transported into cells or purely synthesized in the cells remains for further exploration. Glutathione conjugate was found in both microsome samples and cell samples. Since no adduct formed in the reaction of BADGE with glutathione at pH

7.4, 37 ºC in water, this suggest the glutathione conjugate cannot form without the presence of enzyme.

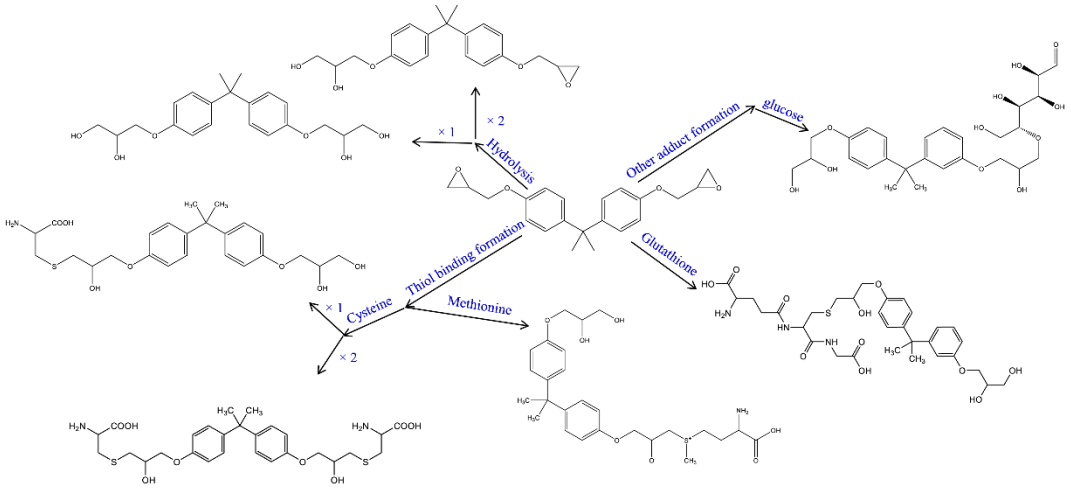

Figure 4-13. Proposed potential metabolites for BADGE metabolism by HepG2 cell.

4.5 Short Summary

In this study, we have developed a novel discovery platform to predict and identify the potential metabolites for emerging organic pollutants (EOCs). A new approach was adopted to acquire 'empirical knowledge' through amino acids' reaction with model compound. The results showed that incorporating experimental analysis with both *in silico* and knowledge-based prediction can greatly enhance the discovery potentials. We have successfully identified the BADGE's glucuronide, sulfate and glutathione conjugates and reaction products with thiol-containing metabolites in microsomes or HepG2 cell.

Chapter 5. Comparison of Metabolic Toxicity between Bisphenol A Diglycidyl Ether (BADGE) and Bisphenol A

5.1 Overview

Chapter 5 compared the possible cellular disturbances induced by different levels of BADGE and BPA exposure upon a hormone-responsive cell line MCF-7 using the global metabolomics. It has further characterized the metabolic profiles of both chemicals and their affected biochemical pathways to elucidate the underlying mechanism at system-biological levels. This manuscript is under preparation and to be submitted.

5.2 Introduction

Many bisphenol plasticizers are known as endocrine-disrupting chemicals (EDCs) such as bisphenol A (BPA) and bisphenol a diglycidyl ether (BADGE). BADGE is made by the O-alkylation of BPA with epichlorohydrin and can be used as replacement for BPA in many applications. Therefore, the backbones of BPA and BADGE are similar, but their side-chain functional groups are quite different (epoxides for BADGE and hydrophenyl groups for BPA). In addition, both compounds are quite ubiquitous in our daily life and widely used in the synthesis of polycarbonates (e.g. plasticizers) and epoxy resins. Both chemicals have been found their widespread occurrences in the indoor environments as well as human specimens (Wang et al. 2012, Asimakopoulos et al. 2014, Wang et al. 2015, Xue et al. 2016).

More and more toxicological studies raised the safety concern on BPA. Its exposure is linked with pleiotropic toxic effects such as affecting estrogenic, androgenic, thyroid, retinoid and prostaglandin signaling pathways as well as cholesterol and lipid homeostasis (Ortiz-Villanueva et al. 2017). In contrast, less is known regarding the toxicity mechanism of BADGE though it was found to be an antagonist of peroxisome proliferator-activated receptor gamma (PPARγ) (Wright et al. 2000) and to exhibit mutagenicity, genotoxicity and cytotoxicity (Suárez et al. 2000, Ramilo et al. 2006, Sueiro et al. 2006). Further study is needed on biological events in the cellular response of BADGE to elucidate the underlying mechanism and its differences from BPA. Since both compounds are EDCs, MCF-7, a hormone-responsive cell line, is a suitable model to further investigate their toxicology mechanism and potential influences from different

functional groups.

Metabolomics, a method of understanding metabolic regulations by studying small molecule metabolites at a specified time point, is ideal to address these questions and provide valuable information for risk assessment. The integration of metabolomics and traditional toxicological approach enables us to understand both chemicals' phenotypical fingerprints (Leon 2013) and their affected biochemical pathways (Griffin 2004). Since metabolomics could detect even slight changes of endogenous metabolites within the cell, examining the biological process triggered by BPA and BADGE through a global view could deepen our understanding of their toxicology mechanism. Up to date, no metabolomics assessment for BADGE toxicity has been conducted.

In this study, we seek to understand the possible cellular disturbances induced by different levels of BADGE and BPA exposure upon a hormone-responsive cell line MCF-7 using a global metabolomics approach. We will first determine the cytotoxicity of BADGE and its eight derivatives (BADGE, BADGE-H_2O, BADGE-$2H_2O$, BADGE-HCl-H_2O, BADGE-HCl, BADGE-2HCl, BFDGE, BFDGE-$2H_2O$ and BFDGE-HCl). Furthermore, it will characterize the metabolic profiles of BADGE and BPA and their affected biochemical pathways to understand their underlying mechanism at system-biological levels.

5.3 Methodology

5.3.1 Cell Culture and Reagent Preparation

Human breast cancer cell (MCF-7) was obtained from the American Type Culture Collection (ATCC, Rockville, MD, USA). Cells were stored in the liquid nitrogen vapor phase and were revived and maintained in humidified 37°C atmosphere containing 5% CO_2. Dulbecco's modified eagle medium (DMEM; with 4.5 g/L glucose, 10% fetal bovine serum (FBS) and L-glutamine) (Gibco, Thermo Fisher Scientific, Singapore) was applied as the growth medium. The chemicals applied for cell treatment were purchased from Sigma-Aldrich (Singapore) or Toronto Research Chemicals (Canada). The single-compound stock solution of each chemical was prepared in dimethyl sulfoxide (DMSO).

5.3.2 Cytotoxicity Test

The cytotoxicity of BADGE and its derivatives (BADGE, BADGE-H_2O, BADGE-

$2H_2O$, BADGE-HCl-H_2O, BADGE-HCl, BADGE-2HCl, BFDGE, BFDGE-$2H_2O$ and BFDGE-HCl) on MCF-7 cell was evaluated by resazurin assay (Fang et al. 2015). Briefly, the cells were seeded in 96-well flat-bottomed plates (Thermo Fisher Scientific, Singapore) with a seeding density of 30,000 cells/well in 100 µL DMEM for 7 h. Subsequently, 100 µL medium dissolved with chemicals were added into each well. The cells were exposed to each chemical with final concentrations of 0.01, 0.1, 1, 5, 10, 50 and 100 µM. Non-treated negative control samples were prepared by adding DMSO with a final concentration at 0.1% and positive control samples were prepared by adding 50µM tamoxifen. After exposure for 40h, 20 µL resazurin (0.50 mg/mL) were added into cells to further incubate for 8 h. The activity was measured by fluorescence using 530 EX nm/ 590 EX nm filter setting. The cell viability was calculated by setting the viability of the negative DMSO control cells as 100%.

5.3.3 Mixture Exposure and Metabolite Extraction

MCF-7 cells were seeded in 6-well plates with a density of 0.4×10^6 in each well. After the cell reached 60 ~70% confluency, they were exposed to BADGE and BPA (each level with four replicates, N=4) with varying concentrations (10 µM, 25 µM and 50 µM) in the culture medium for 24 hours. Non-treated control samples were prepared by adding DMSO with a final concentration at 0.1%. Metabolite extraction was modified version of that used in our previous studies (Fang et al. 2015, Beyer et al. 2018). Cell metabolites were extracted with 1.6 mL ice-cold methanol: acetonitrile: water (2:2:1, v/v/v) and then collected by a cell scraper. The intracellular metabolites were extracted by freeze-thaw steps conducted thrice using liquid nitrogen followed by sonication in an ice bath for 10 min. Afterwards, the samples were placed at -40 °C for 1 hour, followed by 15-min centrifugation at a speed of 13,000 rpm at 4 °C to precipitate proteins. The protein concentration of the cells was measured in the final pellet after centrifugation using Pierce BCA assay (N=3) according to kit protocols. A 100µL diluted sample (100 times) was mixed with 100 µL of working reagents in 96-well plates and incubated at 37 °C for 4 hours. The absorbance was measured at 562 nm on a plate reader. The resulting supernatant was removed and evaporated to dryness by a CentriVap centrifugal vacuum concentrator (Labconco, USA). The dried extracts were then reconstituted in the appropriate volume of acetonitrile: water (1:1, v/v), normalized by the protein concentration with the lowest concentration of 50 µL, sonicated for 10

min, and centrifuged for 15 min at 13,000 rpm and 4 °C to remove insoluble debris. The supernatants were transferred to HPLC vials with inserts and stored in -40 °C before analysis.

5.3.4 Metabolite Profiling and QA/QC

Instrumental analysis was performed using a High-performance Liquid Chromatography (HPLC) system (1200 series, Agilent Technologies) coupled to a 6550 quadrupole Time-of Flight (qToF) mass spectrometer (Agilent Technologies, Singapore). Details of the profiling method were modified based on our previous study (Fang et al. 2015, Beyer et al. 2018). A Phenomenex Luna NH_2 Column (3 µm, 2×150 mm, for hydrophilic metabolites) was used for separation in negative mode. The injection volume was 6 µL and the mobile phase was composed of A= 20 mM ammonium acetate and 40 mM ammonium hydroxide in 95% water and 5% acetonitrile and B= 95% acetonitrile and 5% water. The flow rate was 0.25 mL/min and the column temperature was 30 °C. The linear gradient was set as follows: 0~2 min: 100% B; 2~15 min: 100% B to 10% B; 15~17 min: 10% B to 0% B; 17~33 min: 0% B; 33~55 min: 0% B to 100% B. Other parameters were set as follows: gas temperature: 225°C; gas flow: 14 L/min; sheath gas temperature: 275°C; sheath gas flow: 11 L/min; nozzle voltage: 1000 V; nebulizer pressure: 35 psig; capillary voltage: 3500V and -3500V for positive (ESI+, electrospray ionization) and negative mode (ESI-); nozzle voltage: 1000 V; fragmentor: 175 V, collision energy: 0 V and scan rate: 1 spectra/second. To correct the mass, retention time and response drift, a mix of metabolites (QC sample) was prepared by pooling all treated and control cell samples. QC analysis was conducted once for every six injections of biological samples and a blank sample (acetonitrile: water, 1:1, v/v). Data-dependent acquisition (DDA) auto-MS/MS and targeted MS/MS of selected precursors were run with the QC sample to confirm the identity of metabolites. To compare the metabolic changes under different dosing levels, one-way *ANOVA* and *Duncan post-hoc* analysis were used to test whether one treatment group is statistically different from non-treated controls; a p-value $\leqslant 0.05$ was considered statistically significant.

5.3.5 Metabolites and Metabolic Pathway Analysis

The metabolite profiling data were converted to mzXML files using Agilent Masshunter Acquisition Software 6.0 and were then uploaded to the cloud-based XCMS Online

platform (http://xcmsonline.scripps.edu). After alignment and annotation, the significant features were first screened with *p*-value ≤0.05, maximal intensity >10,000 and |fold change| >1.3. Metabolites identification was carried out using a few filters including MS/MS fragment match (auto/targeted MS/MS), accurate mass match and in-house retention time match if available. Moreover, the metabolite standard verification by the identical HPLC method was applied to support the metabolite identification process if available. Besides, metabolite features were searched against several open-source platforms, including METLIN (https://metlin.scripps.edu/), KEGG (http://www.genome.jp/kegg/), and HMDB (www.hmdb.ca/). Pathway analysis was conducted using Metaboanalyst (http://www.metaboanalyst.ca). Graphs were made using GraphPad Prism (version 7) and statistical analyses were performed by SPSS Statistics (version 22).

5.4 Results &Discussion

5.4.1 Cytotoxicity of BADGE and its Derivatives

For all the tested concentrations, only several compounds at 100 µM produced significant cell lethality comparing with the negative control samples **(Figure 5-1)**. Among these compounds, BADGE itself exhibited the lowest cell viability of 37%, following by BADGE-2HCl (45%), BFDGE (65%) and BADGE-H_2O (71%) at 100 µM. We did not observe a significant cytotoxic effect for other tested compounds or concentrations. It is interesting to note the difference in cytotoxic effects at 100 µM triggered by BADGE (37%) and its hydrolysis derivatives BADGE-H_2O (71%) and BADGE-$2H_2O$ (97%). This is in line with the earlier findings suggesting their degree of toxicity mainly depends on the fractional concentrations of unreactive epoxy groups (Suarez 2000). Since the half-lives of BADGE at pH 7 and 35°C is 2 days (Lane et al. 2015), it is possible that its toxicity could be mediated correspondingly through transforming to its hydrolysis products. The same trend was also observed for BFDGE (65%) and its derivatives BFDGE-$2H_2O$ (97%) and BFDGE-2HCl (93%). Besides, among all the chlorohydroxy derivatives of BADGE or BFDGE, only 100 µM BADGE-2HCl has produced significant cell lethality (45% cell viability).

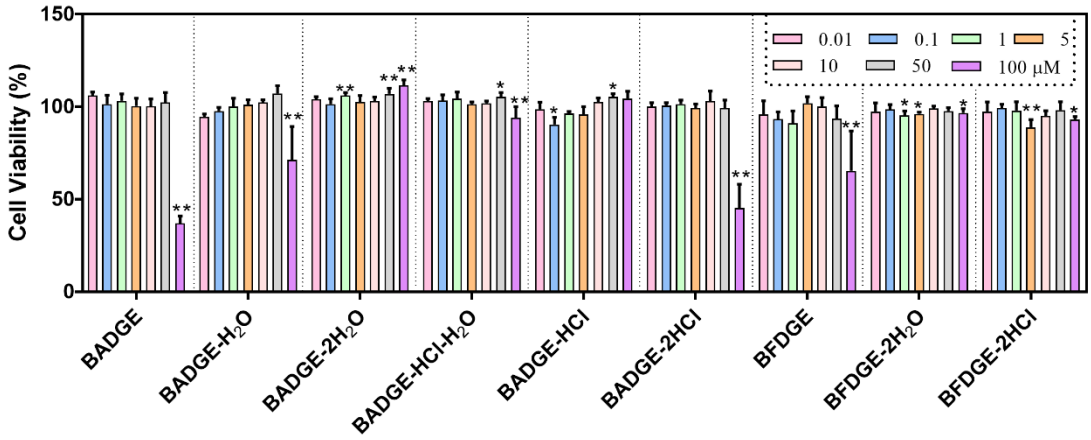

Figure 5-1. Cell viability of MCF-7 cells exposed to BADGE and its derivatives at varying concentrations (0.01, 0.1, 1, 5, 10, 50 and 100 µM) by Resazurin Assay (The cell viability was calculated by setting the viability of the negative DMSO control cells as 100%, Mean ± S.D., n=4; "*" or "**" indicates if individual chemicals treatment were statistically significant from dual treatment condition using one way *ANOVA* and *LSD post-hoc* analysis; "*" represents p <0.05 and "**" represents p <0.01)

5.4.2 Metabolomics Profiling

We semi-quantitatively evaluated the dose-response effect of BADGE and BPA using manually confirmed feature numbers (**Figure 5-2A**). Overall, increasing dosing concentrations of chemicals induced more responsive metabolite features especially for BADGE in ESI negative mode. We also summarized the overlapping and distinct feature numbers for 25, 50 µM of BADGE and BPA in a *Venn* diagram. Among all treatment groups, the overlapped percentage for significant dysregulated features were dominant for 25 µM, 50 µM BADGE and 50 µM BPA (97%, 93% and 89%; respectively) while for 25 µM BPA only accounted for 19%. If regardless of the concentrations, BADGE and BPA have a great number of overlapped features, which account for 68% and 56% of their total features respectively.

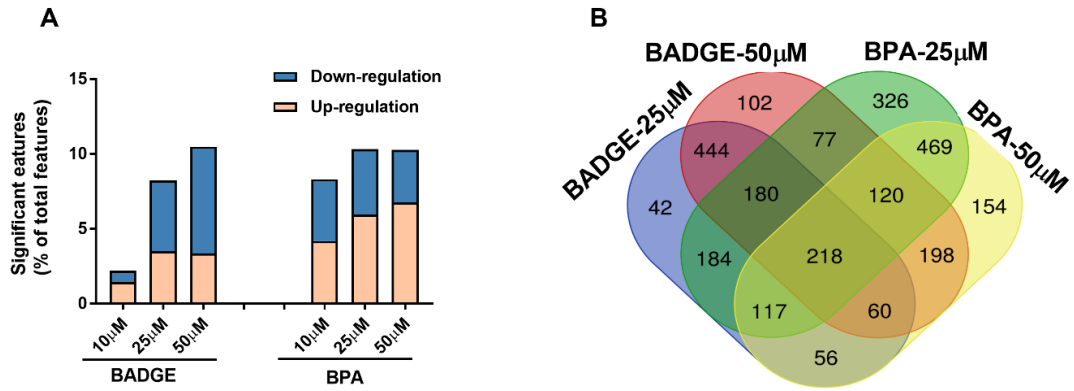

Figure 5-2. Global metabolite profiling of MCF-7 cell in response to 10μM BADGE, 25μM BADGE, 50μM BADGE, 10μM BPA, 25μM BPA and 50μM BPA **A.** Up and down regulated significant features detected by global profiling (percentage was calculated based on total detected feature numbers); **B.** Classic Venn diagram summarizing the number of shared and distinct features for BADGE and BPA at 25 μM and 50 μM.

5.4.3 Dysregulated Metabolites Identification

In total, we have identified 45 significantly dysregulated metabolites across all treatment conditions, including nucleoside phosphate compounds, lipids, fatty acids and amino acids **(Table 5-1)**. In general, BPA showed higher dysregulation potency than BADGE **(Figure 5-3A)**. Many amino acids were interrupted in higher doses of (>10 μM) BPA or BADGE, such as the upregulation of glutamine, tyrosine, proline, histidine, lysine as well as the downregulation of leucine and aspartic acid. Approximately 47% and 67% of detected metabolites were observed with a significant dose-response relationship for BADGE and BPA, respectively.

Table 5-1. Dysregulated metabolites of MCF-7 cells after BPA or BADGE exposure (Significance Criteria: |Fold change(FC)| >1.3 & *p*-value <0.05)

Compound Name	**KEGG**	**BADGE**						**BPA**					
		10 μM		**25 μM**		**50 μM**		**10 μM**		**25 μM**		**50 μM**	
		FC	***p***	**FC**	***p***	**FC**	***p***	**FC**	***p***	**FC**	***p***	**FC**	***p***
NADH	C00004	1.65	0.02	1.48	0.22	1.64	0.06	2.31	0.01	2.67	0.02	2.99	0
ADP	C00008	1.27	0.19	-1.11	0.61	1.21	0.26	1.24	0.1	1.66	0.05	1.92	0.01
UDP	C00015	1.17	0.16	-1.17	0.26	1.05	0.43	1.07	0.23	1.33	0.11	1.39	0.02
Uridine-disphosphate-N-acetylglucosamine	C00043	-1.13	0.07	-1.18	0.06	-1.34	0.01	-1.09	0.41	-1.17	0.1	-1.2	0.04
Lysine	C00047	1.05	0.79	1.27	0.11	-1.03	0.83	1.04	0.5	1.51	0	1.46	0.02
Aspartic acid	C00049	-1.11	0.23	-1.15	0.2	-2.35	0	-1.26	0.05	-1.19	0.17	-1.8	0
Glutathione	C00051	1	0.99	1.23	0.02	1.31	0.01	1.03	0.71	1.18	0.06	1.01	0.82
Glutamine	C00064	-1.02	0.91	1.35	0.02	1.3	0.03	-1.64	0.11	1.32	0.03	1.12	0.51
Tyrosine	C00082	-1.02	0.91	1.36	0.02	1.15	0.36	-1.54	0.14	1.44	0.01	1.32	0.06
CDP	C00112	1.34	0.15	-1.29	0.34	1.01	0.92	1.45	0.03	1.68	0.04	1.93	0
Fumaric acid	C00122	1.01	0.84	1.03	0.67	-1.23	0.03	1.15	0.07	1.47	0	1.44	0
Leucine	C00123	1	1	1.01	0.63	-1.04	0.37	1.06	0.06	-1.3	0.14	-1.55	0
Histidine	C00135	1.09	0.24	1.37	0.04	1.1	0.48	1.09	0.65	1.41	0.01	1.22	0.28
Adenine	C00147	1.06	0.7	1.17	0.08	-1.36	0.03	1.01	0.9	1.16	0.07	1.17	0.2
Proline	C00148	1.05	0.43	1.24	0.02	1.12	0.23	1.1	0.41	1.31	0.02	1.31	0.01
Citric acid	C00158	1.09	0.44	1	0.97	1.05	0.43	-1.13	0	1.45	0.04	1.5	0.01
UDP-D-glucuronic acid	C00167	1.17	0.28	-1.28	0.13	1.06	0.02	1.11	0.19	1.43	0.07	1.52	0

Xylose	C00181	1.25	0.09	1.41	0	1.53	0.01	1.3	0.01	2.04	0	2.82	0
Lactic acid	C00186	1.29	0.2	1.61	0.03	1.74	0.03	1.58	0.12	2.39	0	3.41	0
Adenosine	C00212	1.17	0.49	1.32	0.34	1.63	0.03	-1.76	0.05	-1.14	0.48	-1.01	0.94
Thymidine	C00214	-1.26	0.38	1.1	0.28	2.3	0	-1.27	0.07	-1.27	0.02	-1.02	0.68
DGMP	C00362	1.28	0.09	-1.06	0.48	1.5	0.01	1.16	0.12	1.39	0.01	1.47	0
Deoxyuridine	C00526	1.23	0.34	-1.32	0.09	-1.58	0.02	1.9	0.22	-1.31	0.2	-1.16	0.33
CDP-ethanolamine	C00570	-1.13	0.12	-1.01	0.86	-1.34	0.02	-1.1	0.31	1.29	0.02	1.54	0.01
3-Phosphoglycerate	C00597	1.26	0.35	1.17	0.44	1.49	0.01	1.35	0.01	2.38	0.01	2.72	0
Acetyl-Glutamic acid	C00624	-1.02	0.54	1.23	0.01	1.14	0.02	1.31	0.01	1.66	0.01	1.92	0
Glycerophosphocholine	C00670	-1.01	0.8	-1.14	0.01	-1.25	0	-1.15	0.04	-1.24	0	-1.55	0
(3S)-3-Methyl-2-oxopentanoic acid	C00671	1.59	0.41	1.54	0.01	1.31	0.66	1.27	0.31	1.25	0.57	1.17	0.57
Malic acid	C00711	-1.03	0.35	1	0.97	-1.24	0	1.1	0.03	1.34	0.01	1.39	0.01
Pantothenic acid	C00864	1.09	0.6	1.43	0.08	1.09	0.5	-1.29	0.04	1.53	0	1.14	0.64
O-Succinyl-L-homoserine	C01118	1.1	0.04	1.44	0	1.67	0	1.46	0.01	2.27	0	3.12	0
4-Hydroxyproline	C01157	-1.06	0.43	-1	0.97	-1.33	0.03	-1.1	0.41	1.03	0.78	-1.01	0.94
Pyroglutamic acid	C01879	1.12	0.67	1.51	0.02	1.42	0.04	-1.67	0.11	1.47	0.04	1.17	0.51
Citraconic acid	C02226	-1.04	0.63	1.03	0.78	-1.36	0.01	-1.18	0.13	1.07	0.68	1.38	0.02
Cystathionine	C02291	-1.03	0.51	-1.08	0.12	-1.79	0	-1.09	0.28	1.12	0.18	-1.03	0.57
Phosphocreatine	C02305	-1.14	0.07	-1.16	0.05	-1.58	0	-1.28	0.02	-1.26	0.04	-1.92	0
Argininosuccinic acid	C03406	1.11	0.11	1.03	0.03	-1.24	0.01	1.45	0	1.98	0	2.14	0
3-hydroxy-3-methyl-	C03761	1.1	0.3	1.25	0.03	2.05	0	-1.08	0.43	1.1	0.28	1.26	0.04

glutaric acid													
Myristic acid	C06424	1.28	0.04	1.1	0.29	1.48	0.19	1.32	0.01	1.21	0.01	1.38	0.01
Hexadecenoic acid	C08362	1.35	0.04	2.04	0.02	1.47	0.16	1.24	0.09	1.27	0.08	1.59	0.05
N-acetylaspartylglutamic acid	C12270	-1.13	0.15	1.06	0.39	-1.36	0.02	1.01	0.93	1.3	0.01	1.24	0.01
PC(14:0/0:0)		1.09	0.11	1.11	0.01	1.09	0.18	1.08	0.19	1.45	0	1.75	0
PE (18:1(9Z)/0:0)	-	1.18	0.3	1.39	0.05	1.25	0.36	-1.28	0.12	1.13	0.22	1.41	0.02
(3S)-3-Methyl-2-oxopentanoic acid	-	1.17	0.41	1.42	0.03	1.18	0.2	1.25	0.37	1.45	0.01	1.81	0
PC(P-17:0/0:0)	-	1.06	0.31	1.19	0	-1.4	0.01	-1.17	0.26	-1.05	0.26	-1.28	0.04

Among these metabolites **(Figure 5-3B)**, it is interesting to note that the dysregulating patterns of specific metabolites after exposure to these compounds were quite similar. For examples, the upregulation for lactic acid, NADH, aspartic acid and the downregulation of glycerophosphocholine. The upregulation of NADH and lactic acid suggest the biological activities after exposure to BADGE and BPA maybe associate with sugar/energy metabolism. The NADH accumulation implied the reduced expression of the mitochondrial electron transport system, which was on the other hand to facilitate anaerobic glucose metabolism that further resulted in excess lactic acid (Vemuri et al. 2007). Since glycerophosphocholine is a metabolite precursor of phospholipids, it's depletion after exposure to these compounds (25 µM and 50 µM) suggest their possible impact on lipid metabolism. The dysregulating trend of certain metabolites such as argininosuccinic acid was quite different after exposure to these chemicals, suggest their different impact on specific pathways. Overall, both BPA and BADGE have triggered significant dose-response metabolome changes for many metabolites.

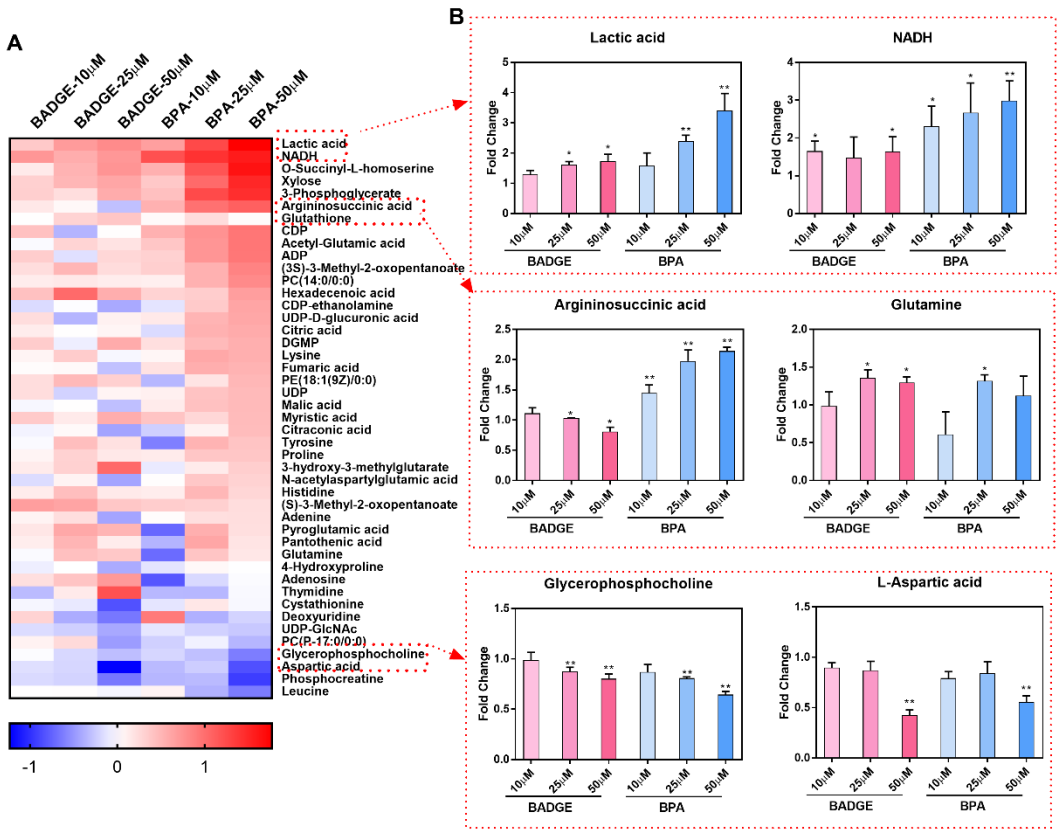

Figure 5-3. A. Heatmap of the identified metabolites for different concentrations of BADGE and BPA. Scales in color key represent $\log_2$(Fold Change) value of metabolites (Fold Change: treatment over control samples). Red indicates upregulation; Purple indicates downregulation. **B.** Bar graphs represent the dysregulation of metabolites as examples in treatment (y-axis is the fold changes by comparing the treatment to the control). "*" and "**" represent $p \leq 0.05$ and $p \leq 0.01$.

5.4.4 Metabolomics Pathway Analysis

Pathway analysis was conducted through mapping for dysregulated metabolites after exposure to BPA and BADGE respectively **(Figure 5-4 A, B)**. The top dysregulated pathways for BPA **(Figure 5-4A)** are nitrogen metabolism, arginine and proline synthesis, alanine, aspartate and glutamate as well as cysteine and methionine metabolism. Similar with BPA, the top dysregulated pathways for BADGE **(Figure 5-4B)** are nitrogen metabolism, cysteine and methionine metabolism, aminoacyl-tRNA synthesis as well as arginine, proline metabolism. Among these pathways, the dysregulated metabolites for BADGE and BPA could be well mapped in arginine, proline metabolism **(Figure 5-4C)**. This is in line with an earlier study suggesting

developmental toxicants such as BPA exposure can cause arginine and proline metabolism, citrate cycle and glutamate metabolism (West et al. 2010). The perturbation of aminoacyl-tRNA synthesis was also consistent with earlier studies suggesting the increase in amino acid concentrations in BPA treated-embryos (Huang et al. 2017, Ortiz-Villanueva et al. 2017). Interestingly, although both compounds were observed with perturbation of arginine and proline metabolism, BPA comparably triggered more effects on this pathway. BPA>10 µM has significantly triggered the upregulation of argininosuccinic acid (FC=2.1 for 50 µM), fumaric acid (1.4) and proline (1.3) while BADGE has no significant changes. These metabolites' dysregulating trends are consistent with proliferating cells. The toxicity differences between BPA and BADGE could be possibly explained by their estrogenic activity differences that BPA is 100 times that of BADGE (Park et al. 2012). Many other evidence could further facilitate this explanation. For examples, uridine diphosphate glucuronic acid (1.5) and UDP (1.4) were two indicators of proliferation and were found upregulated after 50 µM BPA exposure. Besides, BPA exposure has comparably resulted in more amino acid dysregulation in amino acyl-tRNA synthesis pathway. For examples, BPA exposure (>10 µM) led to the upregulation of tyrosine, N-Acetylglutamic acid, proline, histidine and lysine while BADGE was not affected. The upregulation of amino acids after BPA exposure was probably due to the need of these nutrients in proliferating cells (Vander Heiden et al. 2009). As one of the most prominent estrogenic biomarker, proline was observed with an upregulation (FC=1.30 for 25 µM and 1.31 for 50 µM), which could clearly be related to estrogenic exposure and concomitant ERα-mediated induction of proliferation (Potratz et al. 2016).

BPA has been known for its pleiotropic toxic effect but less is known regarding the toxicity mechanism of BADGE. The similarity with BPA regarding changing patterns of some metabolites such as the upregulation of NADH, lactic acid and xylose suggested that BADGE can also lead to the dysregulation of sugar/energy metabolism. Besides, BADGE also showed some unique changing patterns. For examples, we observed the glutathione level of BADGE at 50 µM was significantly elevated (FC=1.3), suggesting a modulation of this detoxification pathway while we did not observe this dysregulation for BPA exposure. This further suggests BADGE may affect energy metabolism pathways. Besides, we observed the upregulation of fatty acids such as palmitoleic acid

(FC=1.3 at 10μM) and myristic acid (1.47 at 50μM). Another unique indicator is the downregulation (-1.34 at 50 μM) of Uridine-diphosphate-N-acetylglucosamine that has been found associated with insulin sensitivity (Fülöp et al. 2008). These findings suggest that BADGE exposure may have an impact on lipid metabolism. This is in line with the findings that BADGE is an antagonist of PPARγ (Wright et al. 2000), which is known to play an important role in lipid storage, adipocyte differentiation and anti-inflammation.

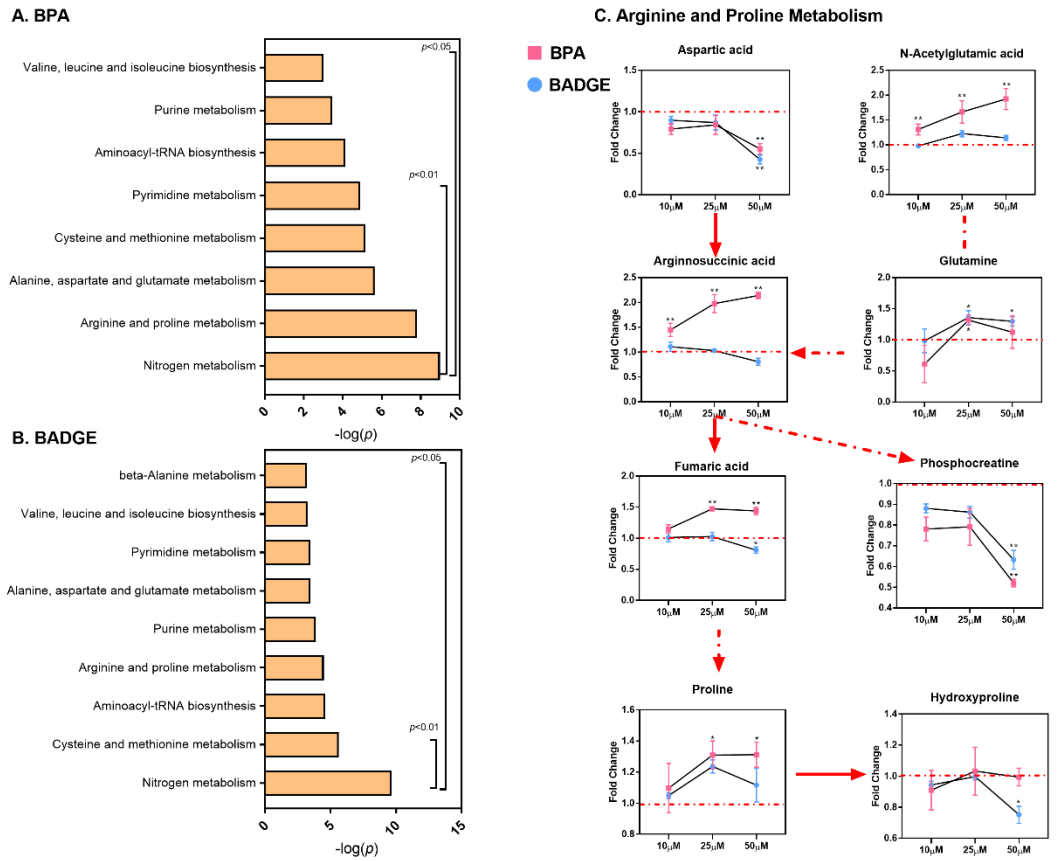

Figure 5-4. Metabolic pathway analysis for **A.** BPA and **B.** BADGE exposure using Metaboanalyst ($p \leq 0.05$); Up and down regulation of metabolites at different concentrations (10μM BADGE, 25μM BADGE, 50μM BADGE, 10μM BPA, 25μM BPA, 50μM BPA) in **C.** the dysregulation of arginine and proline metabolism with exposure to BPA and BADGE at different concentrations (Mean ± S.D.; n=4; red-horizontal dash line represents the fold change equals to 1)

5.5 Short Summary

In general, this study employed global metabolomics to examine the toxicity of BADGE and BPA at the system-biological level. Both BADGE and BPA exposure have affected

the energy/sugar metabolism with upregulation of NADH and lactic acid. Although both chemicals had affected the dysregulation of arginine and proline metabolism, BPA exposure triggered higher perturbations and toxicity on this pathway which could be explained by its stronger estrogenic activity (100 times that of BADGE). Besides, accumulating evidence suggested that BADGE may also disturb the lipid metabolism. Therefore, further investigation on its toxicity mechanism is warranted using more omics technologies (e.g. lipidomics, proteomics).

Chapter 6. Significant "Mixture Effect" Upon Exposure to 23 Chemicals at Human-relevant Levels.

6.1 Overview

Chapter 6 utilized omics approach (e.g. metabolomics and transcriptomic) to characterize the biological effects of 23 xenobiotics 'cocktail' (e.g. including bisphenol plasticizers such as BPA and BADGEs, flame retardants and phthalates) at human-relevant level upon MCF-7. It also developed a novel "counting out" method to evaluate the relative contribution of bisphenol plasticizers to the observed mixture effect. A manuscript entitled "Exposure of MCF-7 cells to Mixture of 23 Chemicals at Human-relevant Levels: Metabolomic and Transcriptomic Analysis and Prioritization of Individual Contribution" has been submitted to Environmental Health Perspectives and under revision.

6.2 Introduction

Humans are ubiquitously exposed to a large number of xenobiotics on a daily basis. These chemicals include personal care products (PCPs), pharmaceuticals, plasticizers and dietary additives, of which many are known to be toxic to humans and wildlife (Boxall et al. 2012, Guo et al. 2013). In a recent study, we have summarized over 300 chemicals and their concentrations in indoor dust with the implication of their widespread occurrences in our environment (Dong et al. 2019). The co-occurrence of over 1,000 small molecules in human blood was also reported before (Rappaport et al. 2014), suggesting human's ubiquitous exposure to chemicals with vast complexity. Furthermore, most environmental contaminants have very low biological concentration at sub-part-per-billion (ppb) or part-per-trillion (ppt) (Rappaport et al. 2014). Therefore, the question of whether 'chemical mixture' of higher complexity at the low human-relevant levels would trigger any health effects remains unaddressed and it is an ongoing challenge for toxicological risk assessment.

Though human expose to most chemicals at non-effective concentrations, the combined effects of mixture have been recognized as a concern due to the possibility that chemicals have additive or even synergistic effects (Carpenter et al. 2002, Kortenkamp 2007). Several previous mixture studies have revealed the ability of chemicals to act together to induce some observable effect at low or even environmentally relevant levels.

For example, eight weak estrogenic chemicals combined at concentrations below NOECs (no observed effect concentration) produce significant mixture effects *in vitro* (Silva et al. 2002). An *in vivo* study has also demonstrated that five estrogenic chemicals at low-effect concentrations have the capacity to act in combination to affect the fitness and reproductive performance of fish (Brian et al. 2007). In another example, our results showed that the metabolome of gut microbiota can be significantly perturbed by exposure to xenobiotic mixtures at human-relevant levels (Zhang et al. 2018). However, majority of these studies usually focused on several compounds with the same mode of action (MOA) and utilized single toxicological end point such as estrogenic effect (Silva et al. 2002, Brian et al. 2007, Repouskou et al. 2019).

Therefore, more work is needed to investigate the possible effect of complex mixture by involving more chemicals for those ever-increasing organic contaminants with diverse MOA. Among them, little work has been focused on mixture studies of organic contaminants such as flame retardants, phthalates and bisphenols that have been shown substantial contribution to human exposure due to their wide application in products and occurrences in the environment (Lioy et al. 2002, Meeker et al. 2013, Asimakopoulos et al. 2014, Yang et al. 2014, Wang et al. 2015, Liu et al. 2019). Besides, one challenge of mixture studies is to quantify each component's contribution to the total observed effect (Carpenter et al. 2002), which could be even more difficult for mixtures at human-relevant level considering the fact that the effect triggered by a single component may be too trivial to be distinguishable. The chemical interactions between each component with distinct MOA are very complex and the resulting experimental workload is tremendous. Therefore, it may not be feasible to use the traditional bioassay with specific end point or effect-directed analysis to figure out the causal compounds, which usually assume a couple of chemicals as the key drivers in the mixture effect (Fang et al. 2014, Fang et al. 2015). Generally, there is still a pressing demand to develop more effective "proof-of-concept" to elucidate the contribution of each component in the mixture.

To address these questions, we have utilized omics-technologies (i.e., the metabolomics and transcriptomic) to fully characterize the biological effect triggered by mixtures at human-relevant levels, on breast cancer cell (MCF-7), a known sensitive hormone-responsive and suitable cell model to study endocrine disruption chemical (EDCs). This

mixture ‘cocktail’ covered 23 organic contaminants with diverse MOA, including bisphenols, phthalates, personal care products, flame retardants and other xenobiotics. These chemicals were selected based on a few criteria including high-volume production, widely occurrences in the environmental and human samples, and endocrine-disrupting chemicals (EDCs). The dosing concentrations of these xenobiotics were referred to previous large cohort biomonitoring data as detailed in **Table 1**. Furthermore, we have also developed a high-throughput metabolomics based “counting-out” method to evaluate the relative contribution of each component in the mixture. This method can effectively characterize and compare the change of mixture effect before and after removing one compound. In sum, this present study has shown a “proof-of-principle” to use omics approaches to characterize the mixture effects and how to quantify the relative contribution of each chemical in the cocktail.

6.3 Methodology

6.3.1 Chemicals and Materials

Analytical standards of bisphenol A (BPA, ≥97%) and bisphenol S (BPS, ≥98%), 10 mM Tris pH 8 and ammonium hydroxide were purchased from VWR (Singapore). Bisphenol A diglycidyl ether (BADGE, ≥95%), Bisphenol A bis(2,3-dihyroxypropyl) ether (BADGE-2H_2O, ≥97%), bisphenol F diglycidyl ether (BFDGE, ≥95%), 2,4-dihyroxybenzophenone (DHB, ≥99%), Triphenyl phosphate (TPP, ≥99%), Di-n-butyl phthalate (DBP, ≥99%), Di-isononyl phthalate (DiNP, ≥99%), Di-isodecyl phthalate (DiDP, ≥99%), Genistein (≥98%), Perfluorooctanoic acid (PFOA, ≥95%), Tetrabromobisphenol A (TBBPA, ≥97%), Resazurin sodium salt (~80%), Ammonium acetate (≥97%), Triton X-100 and other analytical grade chemicals including Butyl paraben, Ethyl paraben and Methyl paraben, Triclosan (TCS), Triclocarban, Tris(1,3-dichloro-2-propyl)phosphate (TDCPP), Mono-n-butyl phthalate (MnBP), Benzybutyl phthalate (BzBP), Mono-benzyl phthalate (MBzP) were purchased from Sigma-Aldrich (Singapore). Quant-iT PicoGreen dsDNA Reagent, EDTA pH 8.0, Tris-Cl pH 8.0, Pierce BCA Protein Assay Kit, dimethyl sulfoxide (DMSO; ≥ 99.5%) were purchased from Thermo Fisher (Singapore). LC/MS grade Acetonitrile were purchased from Aik Moh Paints & Chemicals (Singapore).

MCF-7 was obtained from the American Type Culture Collection (ATCC, Rockville, MD, USA). Cells were cultured in humidified 37℃ atmosphere containing 5% CO_2 with

Dulbecco's modified eagle medium (DMEM; 10% fetal bovine serum (FBS), L-glutamine and sodium pyruvate) (Gibco, Thermo Fisher Scientific, Singapore).

6.3.3 Experimental Workflow

A mixture consisting of 23 xenobiotic chemicals at human-relevant concentrations based on earlier biomonitoring data was prepared to mimic their actual human exposure. MCF-7 cell was chosen as the experimental model because it is a sensitive hormone-responsive cell line (Levenson et al. 1997) and many selected chemicals in the mixture were xenoestrogens and endocrine-disrupting chemicals. In general, the study design and entire workflow were summarized in **Figure 6-1**. Firstly, we have employed metabolomics and transcriptomic to characterize the biological effect of this mixture at several human-relevant levels. Secondly, the changed genes and metabolites were integrated to further interpret the biological perturbation due to the cocktail exposure. Lastly, to evaluate the relative contribution of each chemical to the observed effect, we further developed a high-throughput targeted metabolomics method (i.e., "counting out" method, see below) to further screen the causal chemicals by characterizing the metabolome changes of the mixture with and without the each tested compound (resulting 24 treatment groups and one DMSO control).

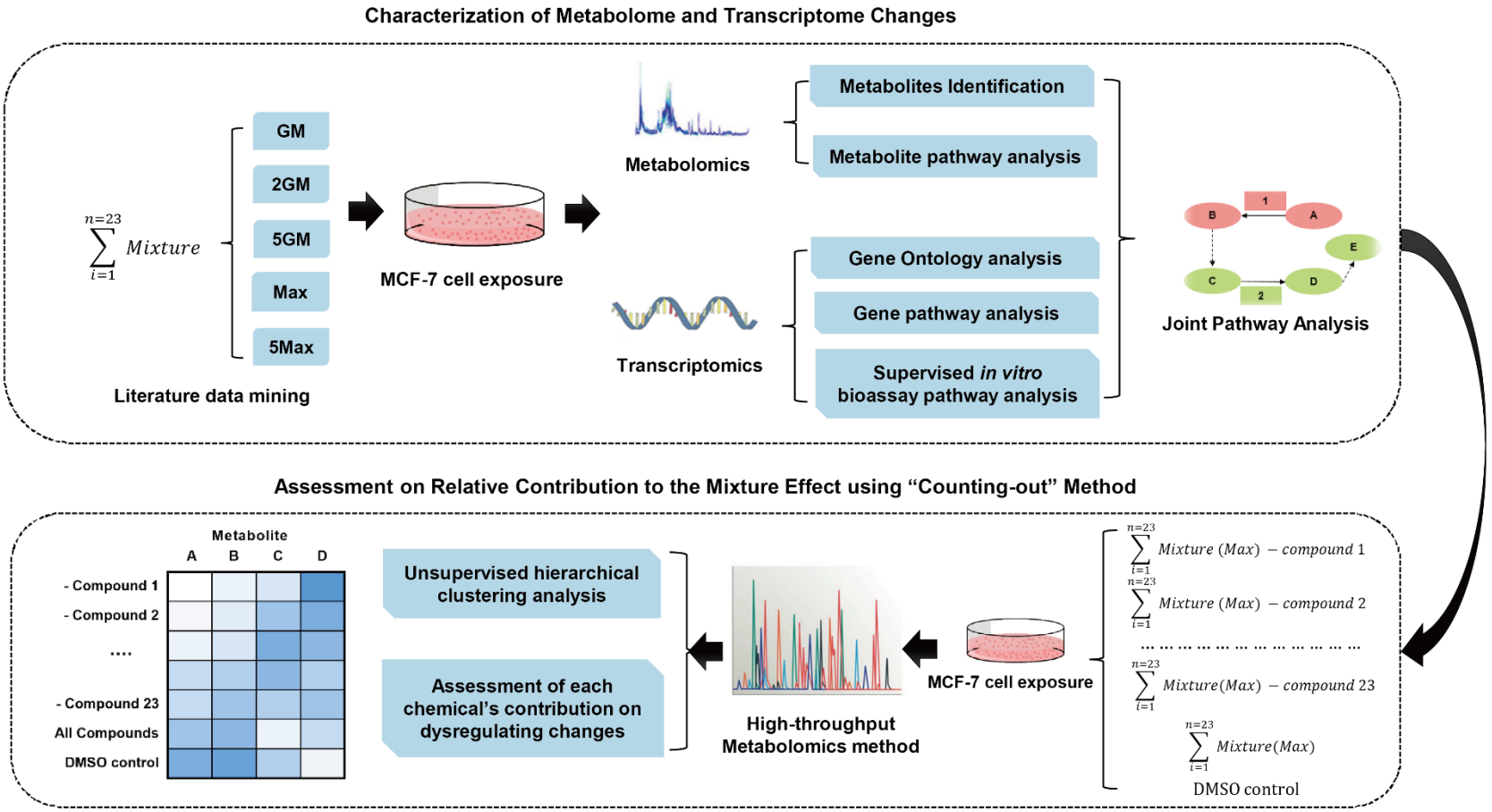

Figure 6-1. Workflow for metabolome and transcriptome characterization and assessment of relative contribution on mixture effect using

“Counting-out” Method.

6.3.4 Xenobiotic Mixture Preparation

This mixture 'cocktail' covered organic contaminants with diverse MOA, namely, bisphenol plasticizers (n=5); phthalate plasticizers (n=7); personal care products (PCPs, n=6); flame retardants (n=3), perfluorochemicals (n=1) and phytoestrogens (n=1). As mentioned above, these chemicals were selected based on a few characteristics such as high-volume manufacturing production, endocrine-disrupting chemicals (EDCs) (e.g. bisphenols, parabens, flame retardants), and widely occurrences in human or environmental samples. In order to better mimic human exposure, the concentration of these xenobiotics were referred to earlier large cohort biomonitoring data. All chemicals' urinary or blood geometric mean (GM), 95th percentile and maximum (Max) concentration at human-relevant level were summarized in **Table 6-1**. The urinary or blood concentrations of 17 chemicals or their metabolites were determined by the Fourth National Report on Human Exposure to Environmental Chemicals with cumulative biomonitoring data for U.S. population consisting of about 2,500 participants with wide age range (blood: 1 year and older; urine: 6 year and older) (CDC 2018). Chemical concentrations were calculated by the average of all detected maximum (Max)/geometric mean (GM) values from the year 1999 to 2016 (GM was replaced by 75th percentile concentration if below limit of quantification). The remaining chemicals were referred to some earlier biomonitoring studies and their concentration were calculated based on the sample size weighted Max/GM concentration (Nagayama et al. 2000, Thomsen et al. 2002, Högberg et al. 2007, Frederiksen et al. 2010, Xiao et al. 2011, Kim et al. 2015, Peng et al. 2015, Wang et al. 2015, Li et al. 2017, Zhao et al. 2017, Li 2018). In the present study, it should be noted that we did not convert the urinary concentration to blood one due to the high uncertainties of this calculation. The Single-compound stock solution was prepared in DMSO first and the mixture stocks were pooled with 1,000 times of its final concentration prior to dosing.

Table 6-1. Summary of the maximum (Max), geometric mean (GM) and 95th percentile mean urinary or blood concentration of 23 chemicals.

Applications	Compounds Name (Abbreviation if available)	Concentration for Urine or Blood (ng/mL)			Sample Type	Sample Size (n)	References
		Max	GM	95th Percentile			
Personal Care Products	2,4-dihydroxybenzophenone (DHB)[a]	1911.7	21.9	1191.8	Urine	15593	(CDC 2018)
	Triclocarban	24.5	0.2[c]	13.4	Urine	2686	(CDC 2018)
	Triclosan (TCS)	599.7	13.8	504.0	Urine	15593	(CDC 2018)
	Butyl Paraben	18.28	1.2[c]	13.9	Urine	13076	(CDC 2018)
	Ethyl Paraben	99.6	5.4[c]	71.5	Urine	13076	(CDC 2018)
	Methyl Paraben	1056.6	52.4	909.2	Urine	13076	(CDC 2018)
Flame Retardants	Tetrabromobisphenol A (TBBPA)	7.6	0.7	N.A.	Blood	265	(Nagayama et al. 2000, Thomsen et al. 2002, Xiao et al. 2011)
	Tris(1,3-dichloroisopropyl) phosphate (TDCPP)[b]	8.6	0.9	7.2	Urine	2646	(CDC 2018)
	Triphenyl phosphate (TPhP)[b]	16.6	2.7	N.A.	Blood	69	(Peng et al. 2015, Li et al. 2017, Zhao et al. 2017)
Phthalates	Di-n-butyl phthalate (DBP)[b]	13.9	3.5	N.A.	Blood	184	(Högberg et al. 2007, Frederiksen et al. 2010, Li 2018)
	Mono-n-butyl phthalate (MnBP)	110.2	16.8	97.1	Urine	21003	(CDC 2018)
	Benzylbutyl phthalate (BzBP)[b]	232.8	16.7	168.8	Urine	18462	(CDC 2018)
	Mono-2-ethylhexyl phthalate (MEHP)	31.3	2.7	23.8	Urine	21003	(CDC 2018)
	Mono-benzyl phthalate (MBzP)	70.0	8.3	59.6	Urine	21003	(CDC 2018)

	Di-isononyl phthalate (DiNP)[b]	13.8	2.0[c]	8.4	Urine	21003	(CDC 2018)
	Di-isodecyl phthalate (DiDP)[b]	20.9	2.7	16.6	Urine	13075	(CDC 2018)
Phytoestrogen	Genistein	781.3	29.7	598.2	Urine	15689	(CDC 2018)
Perluorochemicals	Perfluorooctanoic acid (PFOA)	10.7	3.5	8.8	Blood	14178	(CDC 2018)
Bisphenols	Bisphenol A Diglycidyl Ether (BADGE)	2.5	0.5	N.A.	Blood	223	(Kim et al. 2015)
	Bisphenol A bis(2,3-dihydroxypropyl) ether (BADGE-2H_2O)	9.5	2.3	N.A.	Blood	243	(Kim et al. 2015, Wang et al. 2015)
	Bisphenol A (BPA)	12.9	1.9	11.2	Urine	15593	(CDC 2018)
	Bipshenol S (BPS)	4.7	0.4	3.6	Urine	2682	(CDC 2018)
	Bisphenol-F-diglycidyl ether (BFDGE)	180	26.2	N.A.	Blood	20	(Wang et al. 2015)

[a] Using Metabolites as a replacement for the parent compounds: 2,4-dihydroxybenzophenone (DHB) replaces its parent compound benzophenone-3.

[b] Using parent compounds as a replacement for the metabolites: Di-n-butyl phthalate (DBP) replaced its urinary metabolites Mono-3-hydroxybutyl phthalate (MHBP), Tris (1,3-dichloroisopropyl)phosphate (TDCPP) replaced its metabolites Bis (1,3-dichloro-2-propyl) phosphate (BDCPP) , Di-isodecyl phthalate (DiDP) replaced its urinary metabolites Mono-(carboxynoyl) phthalate (MCNP), Di-isononyl phthalate (DiNP) replaced its urinary metabolite Mono-isononyl phthalate (MiNP), Benzylbutyl phthalate (BzBP) replaced its urinary metabolites Mono-benzyl phthalate (MBzP).

[c] The geometric mean of triclocarban, butyl paraben, ethyl paraben and Di-isononyl phthalate is below detection limit and is replaced with the mean value of 75th Percentile of samples.

6.3.5 Resazurin Assay, Protein and DNA quantification

The cell viability of the mixture on MCF-7 cell was evaluated by resazurin assay (Fang et al. 2015) with four replicates (N=4). Briefly, the cells were seeded in 96-well flat-bottomed plates (Thermo Fisher Scientific, Singapore) with a seeding density of 30,000 cells/well in 100 µL DMEM for 7 h. Subsequently, 100 µL medium dissolved with varying concentrations of the mixture were added into each well. The cells were exposed with final concentrations of GM, 2GM (i.e., 2 times of GM levels), 5GM, Max, 5Max (i.e., 5 times of the Max levels) and 10Max in each well. Non-treated negative control samples were prepared by adding DMSO with a final concentration at 0.1%. After exposure for 40h, 20 µL resazurin (0.50 mg/mL) were added into cells and further incubated for 8 h. The activity was measured by fluorescence using 530 EX nm/ 590 EX nm filter setting. The cell viability was calculated by setting the viability of the negative DMSO control cells as 100%. The DNA concentration was quantified using PicoGreen Assay with three replicates (N=3). Briefly, cells in 6-well plates were exposed with three replicates at varying concentrations (GM, 2 GM, 5GM, Max, 5Max) for 40 hours. After exposure, cells were detached in 1 mL lysis buffer (10 mM Tris pH 8, 1 mM EDTA and 0.2% (v/v) Triton X-100). Keeping on ice throughout, samples were vortexed for 10 seconds every five minutes for half an hour. Samples were diluted by adding 30 µL samples to 170 µL TE buffer (10 mM Tris-Cl pH 8.0, 1 mM EDTA pH 8.0). 50 µL of diluted samples and Picogreen working reagent (diluted 200 times) were added in 96-well plate and further measured by fluorescence using 485 EX nm/ 535 EX nm filter setting. The DNA concentrations of treatment groups were normalized by setting the concentration of the negative control cells as 100%. One-way *ANOVA* and *Duncan* post-hoc analysis was used to test whether one treatment group is statistically different from non-treated control.

6.3.6 Mixture Exposure and Metabolite Extraction

MCF-7 were seeded in 6-well plates with a density of 0.4×10^6 in each well. After reaching around 60% confluency, cells were exposed to the mixture (each with four replicates, N=4) with varying concentrations (GM, 2GM, 5GM, Max, 5Max) in the culture medium for 40 hours. Non-treated control samples were prepared by adding DMSO with a final concentration at 0.1%. Metabolite extraction was modified from our previous studies (Fang et al. 2015, Beyer et al. 2018). Briefly, cell metabolites were

extracted with 1.6 mL ice-cold methanol: acetonitrile: water (2:2:1, v/v/v) and further scraped by a cell lifter. The intracellular metabolites were extracted by three times' freeze-thaw steps using liquid nitrogen following by sonicating in an ice bath for 10-min. The samples were incubated for 1h at -40°C, followed by 15-min centrifugation at 13,000 rpm at 4°C to precipitate proteins. The supernatants were evaporated to dryness by CentriVap Centrifugal Vacuum Concentrator (Labconco, U.S.A) while the settled proteins were quantified using Pierce BCA assay (N=3) for future normalization according to kit protocols. Briefly, 100µL diluted samples (100 times) were well mixed with 100µL working reagents in 96-well plates and incubated at 37 °C for 4 hours. The absorbance was measured at 562 nm on a plate reader. Afterwards, the dry extracts were then reconstituted in a normalized volume of acetonitrile: water (1:1, v/v) based on protein content as detailed in **Table B1 in Appendix B**.

6.3.7 Metabolite Profiling and QA/QC

Instrumental analysis was performed using a high-performance liquid chromatography (HPLC) system (1200 series, Agilent Technologies) coupled to a 6550 quadrupole time-of flight (qTOF) mass spectrometer (Agilent Technologies, Singapore) in accordance with our previous studies (Fang et al. 2015, Beyer et al. 2018). Briefly, to have a better metabolite coverage, a Phenomenex Luna NH_2 Column (3 µm, 2×150 mm, for polar metabolites) and Atlantis T3 column ((3 µm, 2.1 × 100 mm, for hydrophobic metabolites) were used for separation in negative and positive mode; respectively. The mobile phase for NH_2 column was composed of A= 20 mM ammonium acetate and 40 mM ammonium hydroxide in 95% water and 5% acetonitrile, and B=95% acetonitrile and 5% water. T3 column method was slightly modified based on an earlier study (Ko et al. 2018). The mobile phase A was 0.1% formic acid in water and mobile phase B was 0.1% formic acid in acetonitrile. The linear gradient was set as follows: 0~1 min: 1% B; 1~8 min: 1% B to 100% B; 8~10 min: 100% B; 10~10.5 min: 100% B to 1% B; 10.5 ~ 12.5 min: 1% B. Other parameters were set as follows: gas temperature: 225°C; gas flow: 14 L/min; sheath gas temperature: 275°C; sheath gas flow: 11 L/min; nozzle voltage: 1000 V; nebulizer pressure: 35 psig; capillary voltage: 3500V and -3500V for positive and negative mode. QC samples were analyzed every six injections of biological samples and a blank sample (acetonitrile: water, 1:1, v/v) to correct the mass, retention time and response drift. Variation of the four biological replicates for each sample group was

manually checked with the relative standard error of most features being less than 20% as detailed **in Figure B1**. Data-dependent acquisition (DDA) auto-MS/MS and targeted MS/MS of selected precursors were run with QC sample to confirm the identity of the metabolites. To compare the metabolic changes under different dosing levels, one-way *ANOVA* and *Duncan* post-hoc analysis was used to identify the group between doses and controls.

6.3.8 Metabolites and Metabolic Pathway Analysis

The metabolite profiling data were converted to mzXML files using Agilent Masshunter Acquisition Software 6.0 and were then uploaded to the cloud-based XCMS Online platform (http://xcmsonline.scripps.edu). After alignment and annotation, the significant features were first screened with p-value ≤0.05, maximal intensity >10,000, and |fold change| >1.3. Metabolites identification was carried out using a few filters including MS/MS fragment match (auto/targeted MS/MS), accurate mass match and in-house retention time match if available. Moreover, the metabolite standard verification by the identical HPLC method was applied to support the metabolite identification process if available. Besides, metabolite features were searched against several open-source platforms, including METLIN (https://metlin.scripps.edu/) , KEGG (http://www.genome.jp/kegg/), and HMDB (www.hmdb.ca/). Pathway analysis was conducted using Metaboanalyst (http://www.metaboanalyst.ca). Graphs were made using GraphPad Prism (version 7) and statistical analyses were performed by SPSS statistics (version 22).

6.3.9 RNA Preparation Sequencing Preparation and Data Analysis

MCF-7 cells were exposed to the mixture at Max concentration for 40 hours with three biological replicates (N=3) as described above and were further fixed by RNAprotect reagent (Qiagen, Singapore) immediately. The total RNA extraction, mRNA purification, library preparation and library sequencing were carried out by a service company (Majorbio, Shanghai, China). For purification, total RNA was extracted using TRIzol® Reagent according to the experimental protocol (Invitrogen) and genomic DNA was removed using DNase I (TaKara). The RNA quality was determined by 2100 Bioanalyser (Agilent) and quantified using the ND-2000 (NanoDrop Technologies). Only high-quality RNA sample (OD260/280=1.8~2.2, OD260/230≥2.0, RIN≥6.5, 28S:18S≥1.0, >2μg) was used to construct sequencing library. Subsequently, RNA-seq

transcriptome library was prepared following TruSeqTM RNA sample preparation Kit from Illumina (San Diego, CA) using 1μg of total RNA. Briefly, messenger RNA was isolated according to polyA selection method by oligo (dT) beads and then fragmented by fragmentation buffer. Subsequently, double-stranded cDNA was synthesized using a SuperScript double-stranded cDNA synthesis kit (Invitrogen) with random hexamer primers (Illumina). Then the synthesized cDNA was subjected to end-repair, phosphorylation and 'A' base addition according to Illumina's library construction protocol. Libraries were size selected for cDNA target fragments of 200–300 bp on 2% Low Range Ultra Agarose followed by PCR amplified using Phusion DNA polymerase (NEB) for 15 PCR cycles. After quantified by TBS380, paired-end RNA-seq sequencing library was sequenced with the Illumina Novaseq 6000 (2×150bp read length). For read mapping, the raw paired end reads were trimmed and quality controlled by SeqPrep (https://github.com/jstjohn/SeqPrep) and Sickle (https://github.com/najoshi/sickle) with default parameters. Then clean reads were separately aligned to reference genome with orientation mode using TopHat software (http://tophat.cbcb.umd.edu/version2.1.1) (Trapnell et al. 2009). The mapping criteria of bowtie was as follows: sequencing reads should be uniquely matched to the genome allowing up to 2 mismatches, without insertions or deletions. Then the region of gene were expanded following depths of sites and the operon was obtained. In addition, the whole genome was split into multiple 15kb windows that share 5kb. New transcribed regions were defined as more than 2 consecutive windows without overlapped region of gene, where at least 2 reads mapped per window in the same orientation.

6.3.10 Differential Expression Analysis, Functional Enrichment and Joint Pathway Analysis

To identify DEGs (differential expression genes) between two different samples, the expression level of each transcript was calculated according to the fragments per kilobase of exon per million mapped reads (FPKM) method. RSEM (http://deweylab.biostat.wisc.edu/rsem/) (Li et al. 2011) was used to quantify gene abundances. R statistical package software EdgeR (Empirical analysis of Digital Gene Expression in R, http://www.bioconductor.org/packages/2.12/bioc/html/edgeR.html) (Robinson et al. 2010) was utilized for differential expression analysis. After gene annotation, a filter criteria of $|\log_2 (\text{Fold change})| \geq 0.68$ (i.e., the fold changes of 1.3 in

expression obtained by comparing treated samples with untreated control) with adjusted *p*-value ≤ 0.05 was applied to find the significantly dysregulated genes. The gene ontology (GO) analysis was conducted using DAVID Bioinformatic Resources 6.8 (https://david.ncifcrf.gov/) with *p*-value ≤ 0.05. The unsupervised pathways analysis was carried out using a web server for gene functional annotation KOBAS 3.0 (http://kobas.cbi.pku.edu.cn/) with an adjusted *p*-value ≤ 0.01 as the threshold and top 3 ranked enrichment for each database were listed for illustration. A supervised approach was used to assess the gene enrichment of the *in vitro* bioassays summary based on a previous study (Xia et al. 2017). The percentage of genes (%) was calculated by gene hit numbers divided by total gene numbers of a respective pathway. Besides, joint pathway analysis was conducted using Metaboanalyst by selecting 20 top -log (*p*-value of the hypergeometric test) and hit number less than 5 were excluded for discussion.

6.3.11 "Counting-out" Method to Evaluate the Relative Contribution of each Chemical in the Mixture

Considering the effect triggered by single chemicals at human-relevant level could be too low to be distinguishable from control samples (preliminary results as detailed in **Figure B2** showing metabolic responses of bisphenol A and bisphenol A diglycidyl ether at 10 μM), a "counting-out" approach was used to evaluate the relative contribution of each chemical to the observed mixture effect at Max. We characterized the metabolome changes of the mixture before and after the removal of one chemical from the 23 chemicals mixture (resulting 24 treatment groups and one DMSO control group). Due to the large sample size (N>90 for each batch), we further developed a high throughput metabolomics method with modification of the above-mentioned global metabolomics method. The chemical exposure and extraction is the same as mentioned above but with three replicates (N=3). For the instrumental analysis, a method slightly modified from an earlier method (Wang et al. 2018) using UPLC Acquity BEH amide (1.7 μm, 2.1×100 mm) in negative mode (ESI-) with an injection volume of 10 μL, reduced the run time from 50 to 12 min per sample. Briefly, the mobile phase A was 25 mM NH_4OH and 25 mM NH_4OAc in water and mobile phase B was acetonitrile. The linear gradient was set as follows: 0~0.5 min: 95% B; 0.5~7 min: 95% to 65% B; 7~8 min: 65% B to 40% B; 8~9 min: 40% B; 9~9.5 min: 40% B to 95% B; 9.5~12.5 min: 95% B. The new method could save several weeks in sample preparation and analysis.

Within 24 significantly altered metabolites that were identified atMax level, 19 could be well detected with good peak shape using this high-throughput method. These metabolites were further used as targeted compounds and their peaks were extracted and manually integrated using Agilent qTOF Quantitative analysis. Afterwards, the peak intensities of all groups were analyzed by unsupervised hierarchical clustering analysis using Eucidean distance as similarity metric after standardization (https://www.metaboanalyst.ca/).

6.4 Results

6.4.1 Mixture Cell Viability and DNA Quantification

Among all tested concentration in the resazurin assay, only 10 Max showed a significant decrease in cell viability (32% of control), compared with the DMSO control **(Figure 6-2A)**. The tested concentration of 2GM, 5GM, and Max exhibited cell viability of 124%, 127% and 118%; respectively, suggesting the possible proliferation of cells. There is no significant difference between 5Max and control samples. We further quantified the DNA concentration of cells exposed to different levels of mixture and normalized by comparing with control samples **(Figure 6-2B)**. The results were generally in compliance with the cell viability data. Though slight suppression on DNA concentration was observed at the 5Max level, DNA concentrations from GM to Max were comparably higher than control (GM: 124%; 2GM: 131%; 5GM: 134% and Max: 110%), which further confirmed the cell proliferation.

6.4.2 Metabolomics Profiling

Since it is difficult in completely identifying cell metabolites, we first semi-quantitatively evaluated the dose-response effect of the xenobiotic mixture using the manually confirmed feature numbers **(Figure 6-2C)**. In general, increasing dosing concentration of mixture induced more responsive metabolite features especially for ESI negative mode. Besides, more upregulated features (all over 50%) were generated regardless of dosing level and ESI mode. We also identified the distinct and shared significant features between different dosing levels in ESI negative **(Figure 6-2D)** and positive modes **(Figure 6-2E)**. Overall, more distinct features were found in 5Max, which accounted for 81% of its total features. In contrast, more overlapping features were found in Max, 5GM, 2GM and GM, which accounted for 58%, 60%, 64% and 62% of their total features; respectively.

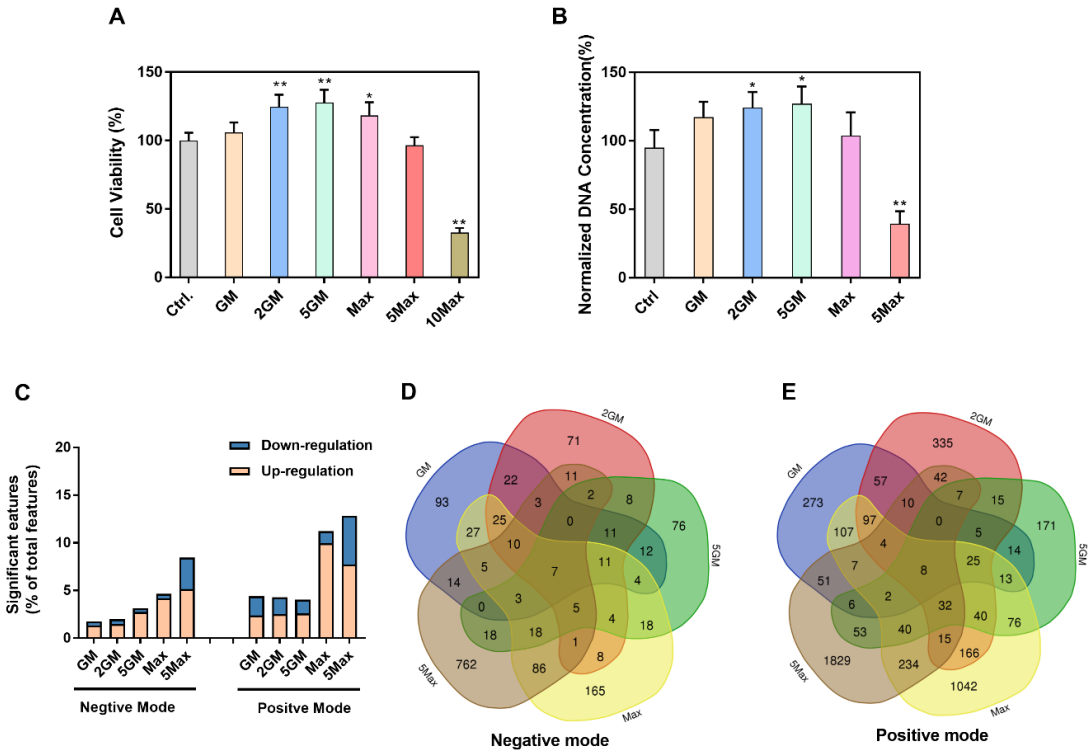

Figure 6-2. A. Cell viability of MCF-7 after exposed to different levels (0.5 GM, GM, 5GM, Max, 5Max and 10Max) of the xenobiotic mixture by Resazurin Assay (N=4; mean ± S.D.); **B.** Normalized DNA concentration (% of control samples) of cells exposing to different levels of mixture (N=3; mean ± S.D.) "*" and "**" represent $p \leq 0.05$ and $p \leq 0.01$ when treatment groups is statistically different non-treated control using One-way *ANOVA* and *Duncan* post-hoc analysis; Global metabolite profiling of MCF-7 cell in response to the xenobiotic cocktail mixture at GM, 2GM, 5GM, Max and 5Max levels. **C.** Up and down regulated significant features detected by global profiling (percentage was calculated based on total detected feature numbers); Classic Venn diagram summarizing the number of shared and distinct features in **D.** ESI-negative mode and **E.** ESI-positive mode.

6.4.3 Dysregulated Metabolite Identification

Overall, we have identified 54 significantly dysregulated metabolites across all treatment conditions **(Table B1 in Appendix B)**, including nucleoside phosphate compounds, lipids, carnitines and amino acids. In general, 5Max group showed higher dysregulation potency that were often downregulated and increasing numbers of

upregulated metabolites from GM to Max **(Figure 6-3A)**. For 5Max dosing, we observed the depletion for nearly all nucleoside phosphate compounds while several lipids (e.g. PC (16:0/0:0), PC (O-15:0/2:0)) and fatty acids (e.g. stearic acid and palmitic acid) were found significantly upregulated. From GM to Max, the dysregulated metabolites were mainly nucleoside phosphate compounds such as ATP, ADP and CTP as well as carnitines such as L-palmitoylcarnitine, octanoylcarnitine and L-carnitine. Approximately 40% of detected metabolites were observed with a significant dose-response relationship from GM to Max. For examples, the responses of UDP, CDP, CTP and CDP were significantly increased from GM to Max **(Figure 6-3B)**. Besides, we also observed a significantly elevated concentration of lactate for Max and 5Max **(Figure 6-3B)**. Overall, the mixture at different levels has triggered significant dose-response metabolome changes for many metabolites.

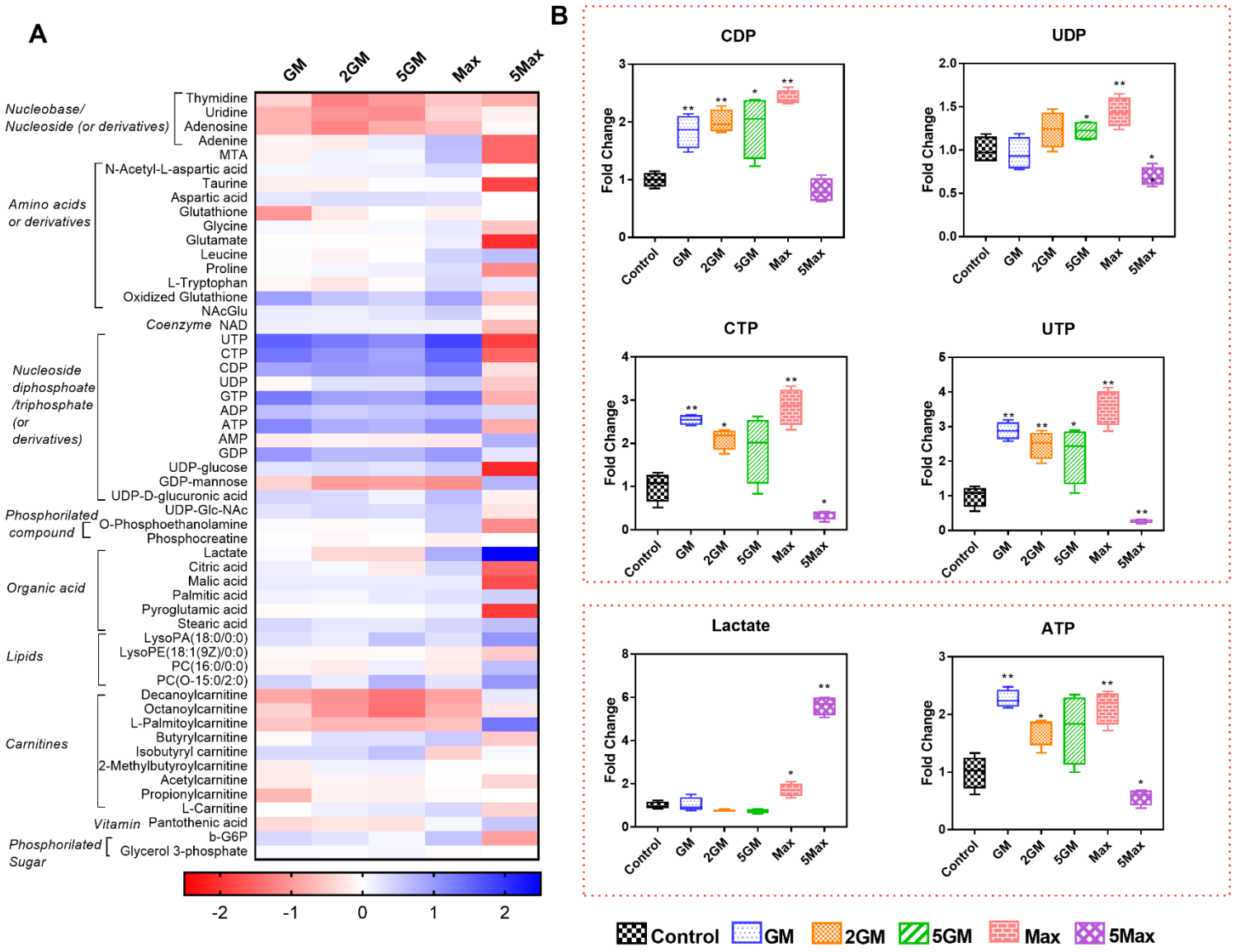
A
GM
2GM
5GM
Max
5Max
Nucleobase/ Nucleoside (or derivatives)
Thymidine
Uridine
Adenosine
Adenine
MTA
Amino acids or derivatives
N-Acetyl-L-aspartic acid
Taurine
Aspartic acid
Glutathione
Glycine
Glutamate
Leucine
Proline
L-Tryptophan
Oxidized Glutathione
NAcGlu
Coenzyme
NAD
Nucleoside diphosphoate /triphosphate (or derivatives)
UTP
CTP
CDP
UDP
GTP
ADP
ATP
AMP
GDP
UDP-glucose
GDP-mannose
UDP-D-glucuronic acid
Phosphorilated compound
UDP-Glc-NAc
O-Phosphoethanolamine
Phosphocreatine
Organic acid
Lactate
Citric acid
Malic acid
Palmitic acid
Pyroglutamic acid
Stearic acid
Lipids
LysoPA(18:0/0:0)
LysoPE(18:1(9Z)/0:0)
PC(16:0/0:0)
PC(O-15:0/2:0)
Carnitines
Decanoylcarnitine
Octanoylcarnitine
L-Palmitoylcarnitine
Butyrylcarnitine
Isobutyryl carnitine
2-Methylbutyroylcarnitine
Acetylcarnitine
Propionylcarnitine
L-Carnitine
Vitamin
Pantothenic acid
Phosphorilated Sugar
b-G6P
Glycerol 3-phosphate
-2
-1
0
1
2
B
CDP
UDP
CTP
UTP
Lactate
ATP
Fold Change
Control
GM
2GM
5GM
Max
5Max

Figure 6-3. A. Heatmap of the identified significantly dysregulated metabolites for different mixture treatment level (GM, 2GM, 5GM, Max and 5Max). Scales in color key represent $\log_2$ (Fold Change) value of metabolites (Fold Change: treatment over control samples; N=4). Red indicates upregulation; Purple indicates downregulation. **B.** Box and whiskers plots represent the dysregulation of metabolites as examples in different mixture level (y-axis is the fold changes by comparing the treatment to the control; mid-line: median; upper and lower box boundaries represent 75^{th} percentile and 25^{th} percentile values; upper and lower whisker boundaries represent maximum and minimum values). "*" and "**" represent $p \leq 0.05$ and $p \leq 0.01$ when one treatment group is statistically different from non-treated control using One-way *ANOVA* and *Duncan* post-hoc analysis.

6.4.4 Metabolomics Pathway Analysis

All the significantly dysregulated metabolites from Max **(Figure 6-4)** and 5Max **(Figure B3-A)** treatment were mapped into metabolic pathways. The majority of metabolic responses for Max mixture were involved in "Purine metabolism", "Pyrimidine metabolism" and "Ascorbate and Aldarate metabolism". Especially in pyrimidine **(Figure 6-4B)** and purine metabolism **(Figure 6-4C)**, the majority of metabolites (UTP, CDP, GDP, CDP, GTP, CTP, ATP and ADP) at GM, 2GM and 5GM are consistent with Max that all show a upregulated trend, while 5Max often exhibits downregulation or no responses. For 5Max, the main dysregulated pathways were "Nitrogen metabolism", "Glycerophospholipid metabolism" **(Figure B3-B)**, and "Glutathione metabolism" **(Figure B3-C)**.

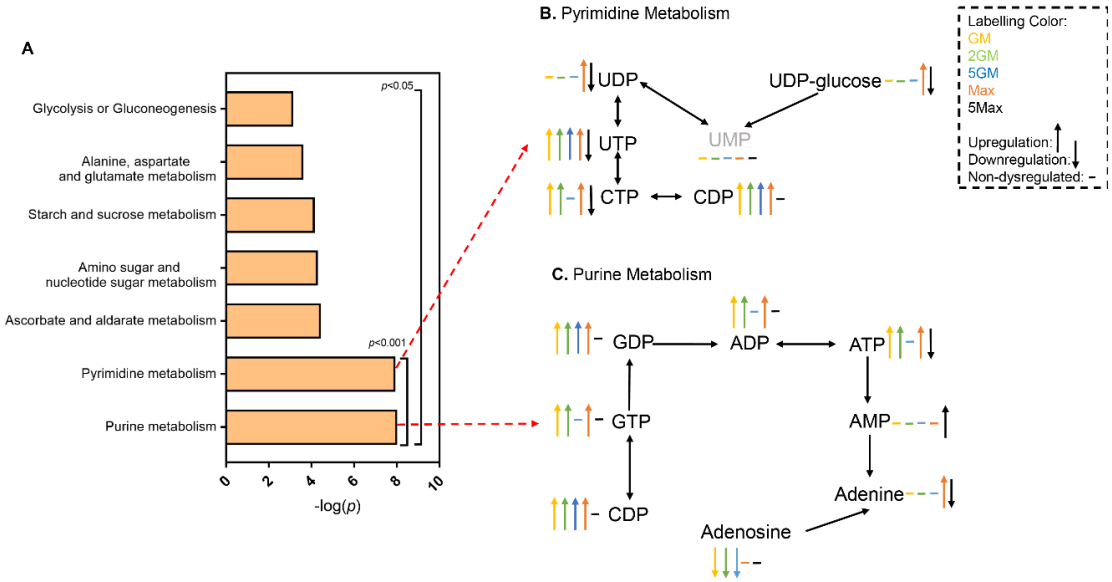

Figure 6-4. Significantly dysregulated pathways of xenobiotic mixture exposure at Max. **A.** Metabolic pathway analysis for the xenobiotic mixture at Max using Metaboanalyst ($p \leq 0.05$); Up and down regulation of metabolites at different concentrations (GM, 2GM, 5GM, Max and 5Max, N=4) in **B.** Pyrimidine metabolism; **C.** Purine metabolism.

6.4.5 Transcriptomic Profiling

HiSeq RNA sequencing was applied to profile the differentially expressed genes (DEGs) in MCF7 cells under Max mixture treatment and the heatmap were shown in **Figure B4**. In total, we have found 1,619 significantly dysregulated genes and 45% of them showed

upregulation **(Table B2).** The volcano plot further visualizes these DEGs in response to mixture exposure **(Figure B5)**. Among these genes, the maximally upregulated ones include imprinted maternally expressed transcript (H19, log2 (FC) = 2.39) and early growth response 3 (EGR3, 2.32) as well as the downregulated genes C-Type Lectin Domain Family 3 Member A (CLEC3A, -3.19) and Membrane Metalloendopeptidase (MME, -3.06).

6.4.6 Gene Ontology (GO) Analysis and Unsupervised Pathway Analysis

To better understand the function and pathway of these DEGs, we performed an unsupervised GO functional annotation and enrichment analysis **(Figure 6-5A)** as well as unsupervised pathway analysis **(Figure 6-5B)**. Most DEGs were involved in the biological process such as "cell proliferation", "cell division" and "DNA replication". The top three enriched GO terms of the cellular component are "cytoplasm", "extracellular exosome" and "membrane" and two additional GO terms were found for molecular function "protein binding" and "structural constituent of cytoskeleton". Through mapping these DEGs to the pathways from databases KEGG, PANTHER and REACTOME **(Figure 6-5B)**, the top enriched pathways across all databases are "Axon guidance mediated by Slit/Robo", "DNA replication" and "Cell cycle".

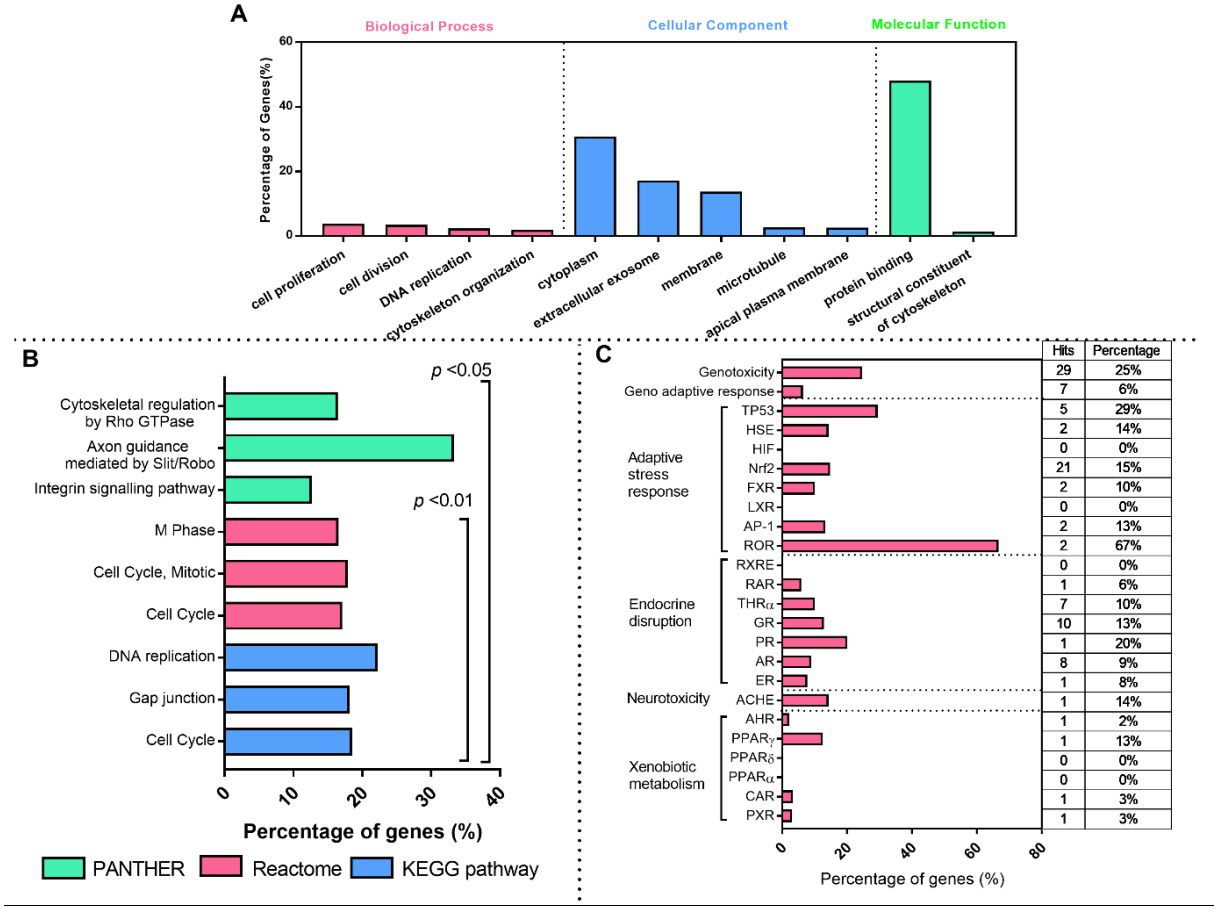

Figure 6-5. A. Gene ontology (GO) analysis results from DAVID Bioinformatics Resources 6.8 for Max level mixture (N=3); **B.** The gene pathway enrichment analysis for differentially expressed genes (DEGs) of Max level mixture exposure using KOBAS 3.0 in three databases PANTHER, KEGG and REACTOME; **C.** The *in vitro* supervised pathway enrichment analysis for DEGs of Max level mixture exposure.

6.4.7 Supervised Pathway Analysis

A supervised pathway analysis was further conducted by mapping DEGs into a few xenobiotic response pathways (Xia et al. 2017) **(Figure 6-5C)**. Overall, the majority of responses were in the end points of genotoxicity, which was followed by adaptive stress response and endocrine disruption. For genotoxicity, 29 hits genes were found that accounted for 25% of total genes for this pathway. Important replication proteins were found all significantly upregulated such as minichromosome maintenance protein complex (MCM2:$\log_2$(FC) = 0.81; MCM5: 0.7; MCM7:0.76; MCM10: 0.98; and origin recognition complex (ORC6: 0.65; ORC1: 1.24). In regard to adaptive stress response, higher responses were found in nuclear factor erythroid 2-related factor 2 (Nrf2: 21 hits, 15%) and tumor protein p53 (TP53: 5 hits, 29%). For Nrf2 pathway, genes of solute carrier family (SLCA11: 1.17) and ATP-binding cassette transporter (ABC transporter: ABCC5 -0.73), functioning as drug metabolizing enzymes, were found significantly dysregulated. Lastly, the majority responses of hormone receptors were found in glucocorticoid receptor (GR: 10 hits, 13 %), thyroid hormone receptor alpha (THRα: 7 hits, 10%) and androgen receptor (AR: 8 hits, 9%).

6.4.8 Integration of Metabolome and Transcriptome through Joint Pathway Analysis

To integrate the metabolites and genes data of cells in response to Max exposure, we conducted a joint pathway analysis. Overall, we found some significantly dysregulated pathways with higher hits, namely "Pyrimidine metabolism", "Arginine and proline metabolism", "Purine metabolism" **(Figure 6-6A)**. Among these pathways, the genes and metabolome data could be well aligned and mapped into pyrimidine **(Figure 6-6B)** and purine metabolism **(Figure 6-6C)**, which is in line with abovementioned analysis.

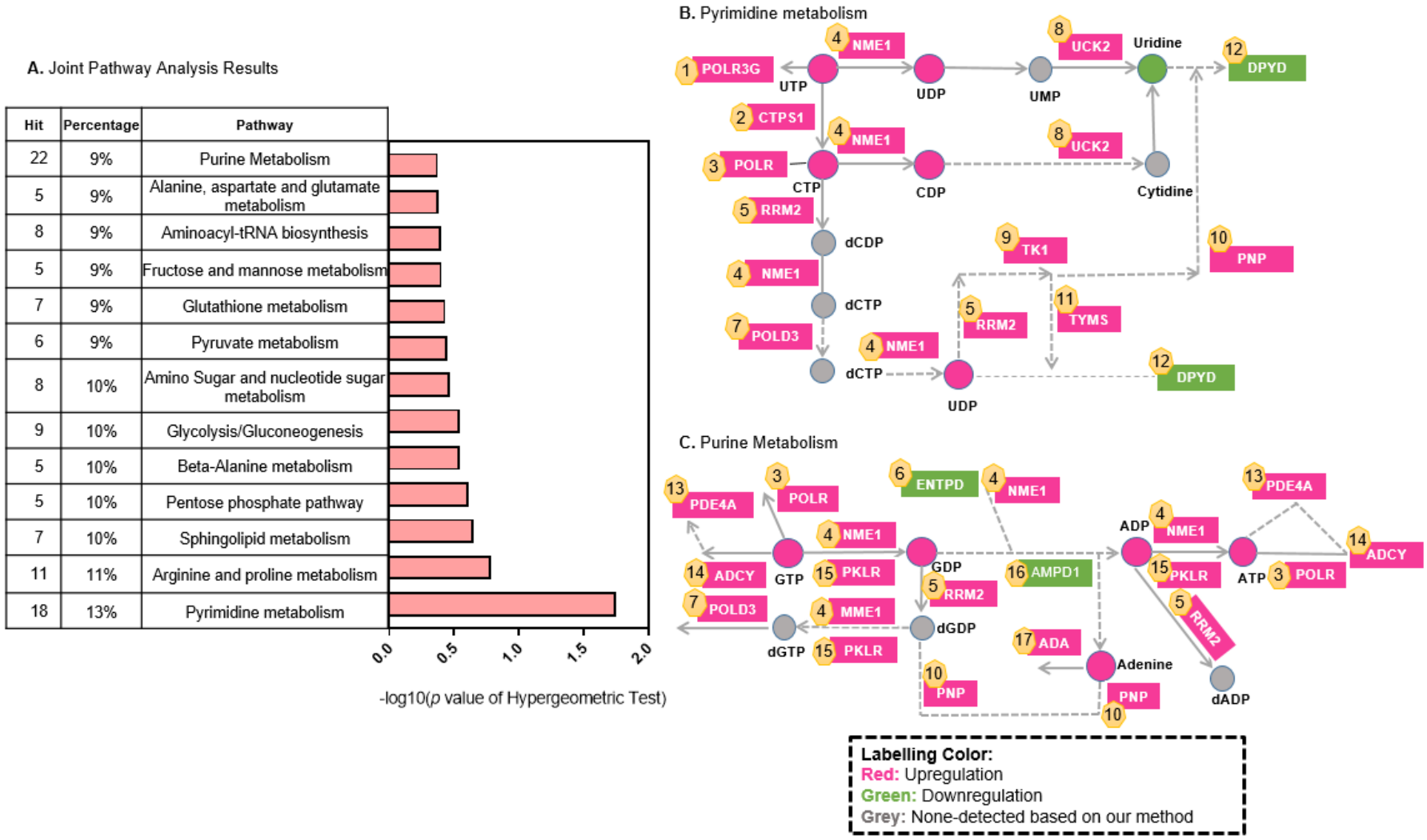

Figure 6-6. A. Significantly dysregulated pathways through integration of metabolites and genes data using joint pathway analysis in

Metaboanalyst; Dysregulated metabolites and genes in **B.** “Pyrimidine metabolism” and **C.** “Purine metabolism” in MCF-7 cells under the exposure of xenobiotic mixture at Max; Red and green indicate upregulation and downregulation (Gene name: 1. RNA Polymerase III Subunit G (POLR3G); 2. Adenosine Monophosphate Deaminase 1 (AMPD1); 17. Adenosine Deaminase (ADA)). CTP Synthase 1 (CTPS1); 3. RNA polymerase subunits (POLR); 4. Nucleoside diphosphate kinase A (NME1); 5. Ribonucleotide Reductase Regulatory Subunit M2 (RRM2); 6. Ectonucleoside Triphosphate Diphosphohydrolase (ENTPD); 7. Procollagen-Lysine, 2-Oxoglutarate 5-Dioxygenase 3 (PLOD3); 8. Uridine-Cytidine Kinase 2 (UCK2); 9. Thymidine Kinase 1 (TK1); 10. Purine Nucleoside Phosphorylase (PNP); 11. Thymidylate Synthetase (TYMS); 12. dihydropyrimidine dehydrogenase (DPYD); 13. Phosphodiesterase 4A (PDE4A); 14. Adenylate Cyclase 2 (ADCY); 15. Pyruvate Kinase L/R (PKLR); 16. Adenosine Monophosphate Deaminase 1 (AMPD1); 17. Adenosine Deaminase (ADA))

6.4.9 Relative Contribution of Each Chemical in the Mixture Effect

We performed the high-throughput metabolomics analysis for the cells using the counting-out method to prioritize the relative contribution of each chemical. The unsupervised hierarchical clustering analysis grouped similar objects among the targeted 19 metabolites across 25 treatment groups **(Figure 6-7A)**. Overall, the metabolome patterns from removing DHB or BPA showed great resemblance with the non-treated control (DMSO), suggesting their relatively higher contribution among the chemicals in this mixture. The metabolome patterns of removing some chemicals such as bisphenol A bis(2,3-dihydroxypropyl) ether (BADGE-H_2O) and bisphenol A diglycidyl ether (BADGE), showed great similarity with the All Compounds treatment, indicating their minimal contribution to the overall metabolome changes.

Several representative metabolites **(Figures 6-7B, 7C and 7D)** were selected to illustrate whether chemicals in the same category exhibit similar behavior. For example, removing chemicals from several categories such as PCPs, bisphenols (BPA, BPS) and most of the phthalates (DBP, dibutyl phthalate; MnBP, monobutyl phthalate; BzBP, benzylbutyl phthalate; MEHP, mono-(2-ethylhexyl)phthalate) showed a significant lower UDP level when compared with All Compounds treatment **(Figure 6-7B)**. This suggests that these chemicals are all likely to have an important contribution to UDP production. After the removal of MnBP, BzBP, genistein or BPA **(Figure 6-7C)**, the cellular lactate level was comparably lower than All Compounds though not reaching the level of control yet, implying that these chemicals are likely to be responsible for excess lactate production. After removing most of the chemicals **(Figure 6-7D)**, the cellular ATP levels were much lower but there was no statistical evidence to suggest that any of them is primarily responsible for ATP dysregulation. A large part of metabolites did not even exhibit significant dysregulation at 10 µM BPA (2.28 µg/mL), which is way much higher than the current dose of 12.9 ng/mL at Max, suggesting BPA alone was unlikely to initiate some metabolite dysregulation to the observed mixture effect **(see Figure S5)**.

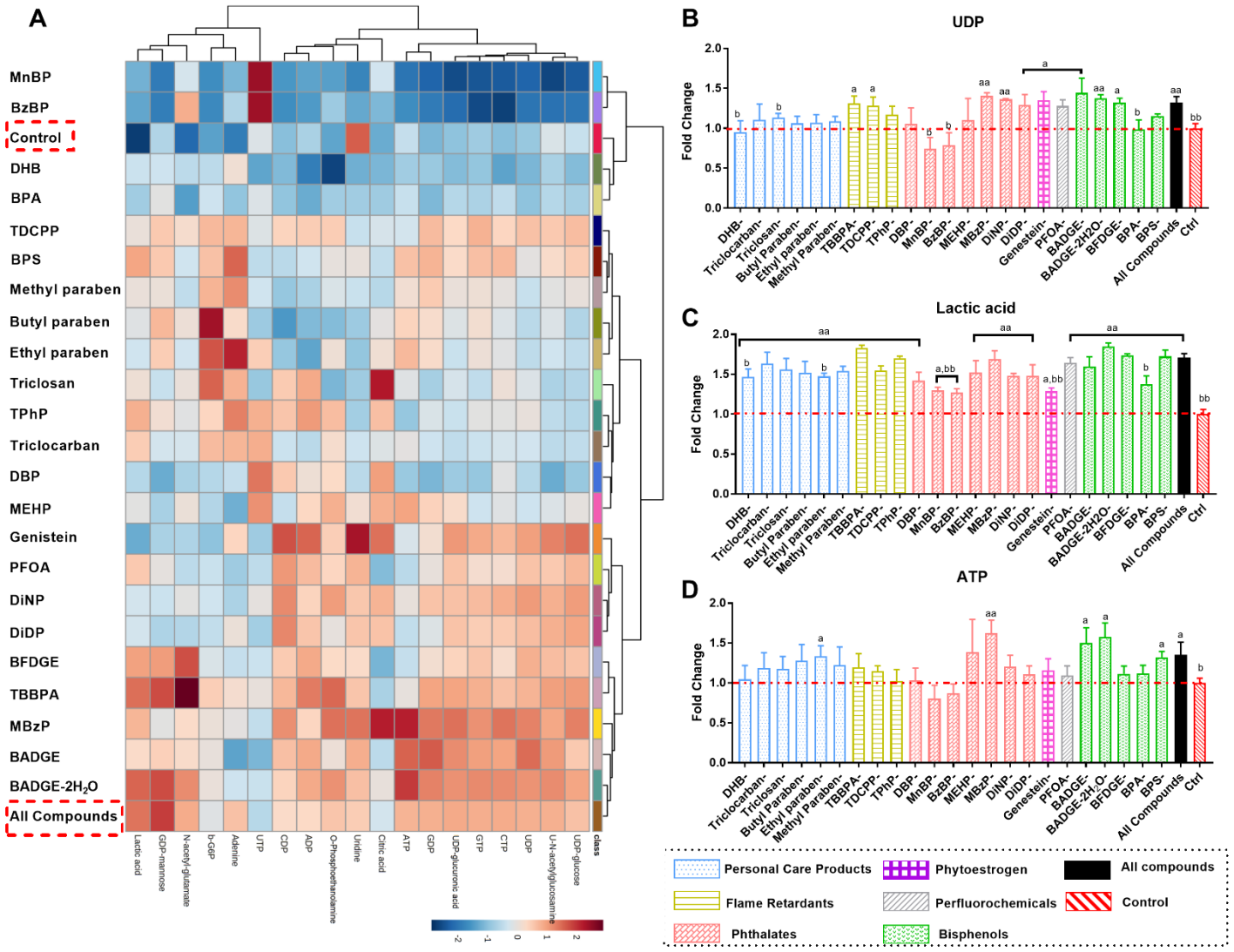
A
MnBP
BzBP
Control
DHB
BPA
TDCPP
BPS
Methyl paraben
Butyl paraben
Ethyl paraben
Triclosan
TPhP
Triclocarban
DBP
MEHP
Genistein
PFOA
DiNP
DiDP
BFDGE
TBBPA
MBzP
BADGE
BADGE-2H2O
All Compounds
Lactic acid
GDP-mannose
N-acetyl-glutamate
b-GBP
Adenine
UTP
CDP
ADP
O-Phosphoethanolamine
Uridine
Citric acid
ATP
GDP
UDP-glucuronic acid
GTP
CTP
UDP
U-N-acetylglucosamine
UDP-glucose
class
-2
-1
0
1
2
B
UDP
Fold Change
C
Lactic acid
D
ATP
Personal Care Products
Phytoestrogen
All compounds
Flame Retardants
Perfluorochemicals
Control
Phthalates
Bisphenols

Figure 6-7. Assessment on the relative contribution of each component to the observed effect using the high-throughput metabolomics-based "counting-out" method (N=3). Total 25 groups: including 23 treatment groups with one component removed with the others remaining at Max level, one 23 chemical mixture at Max level labeled as All Compounds and one DMSO control. **A.** Intuitive hierarchical clustering analysis for grouping similar objects among the targeted 19 metabolites across 25 groups; each colored cell on the map corresponds to a concentration value; clustering of metabolites was based on Ward's clustering method with the Euclidean distance. Bar graph of the fold change (mean ± SEM) of **B.** UDP; **C.** Lactic acid; **D.** ATP after the removal of each component; y-axis represents the fold change by comparing treated samples with control samples; each color/pattern represents a chemical category; symbol a indicates one treatment group is statistically different from the DMSO controls by One-way *ANOVA* and *Duncan* post-hoc analysis, "a" denotes $p \leq 0.05$ and "aa" denotes $p \leq 0.01$; symbol b indicates one treatment group is statistically different from the All Compounds group, "b" denotes $p \leq 0.05$ and "bb" denotes $p \leq 0.01$; Abbreviations: MnBP, mono-n-butyl phthalate; BzBP, benzylbutyl phthalate; DHB: 2,4-dihydroxybenzophenone; BPA, bisphenol A; TDCPP, tris (1,3-dichloroisopropyl) phosphate; BPS, bisphenol S; TPhP, triphenyl phosphate; DBP, dibutyl phthalate; MEHP, mono-ethylhexyl phthalate; PFOA, perfluorooctanoic acid; DiNP, di-iso-nonyl phthalate; DiDP, diisodecyl phthalate; BFDGE, bisphenol F-diglycidyl ether; TBBPA, tetrabromobisphenol A; MBzP, monobenzyl phthalate; BADGE, bisphenol A diglycidyl ether; BADGE-$2H_2O$, bisphenol A bis(2,3-dihydroxypropyl) ether; UDP-glucose, uridine diphosphate glucose; UDP, uridine diphosphate; CTP, cytidine triphosphate; GTP, guanosine triphosphate; UDP-glucuronic acid, uridine diphosphate glucuronic acid; GDP, guanosine diphosphate; ATP, adenosine triphosphate; ADP, adenosine diphosphate; CDP, cytidine 5'-diphosphate; UTP, uridine 5'triphosphate; b-G6P, beta-D-glucose-6-phosphate; GDP-mannose, guanosine diphosphate mannose.

6.5 Discussions

In the present study, we have employed metabolomics and transcriptomic profiling to reveal the impact of xenobiotic mixture exposure at a human-relevant level on the MCF7 cellular biological processes. The 23 chemicals selected are all those with great environmental concerns and have different or unknown MOA in toxicity. The data clearly showed that the xenobiotic cocktail has significantly altered the cellular biological process. Many of the dysregulated metabolites or genes were strongly associated with cell proliferation process and elevated oxidative stress levels. In addition, we have developed a "counting-out" method using high-throughput metabolomics to evaluate the relative contribution of a single chemical in the mixture. The data suggests DHB and BPA have a comparably higher contribution to these changes. These findings may provide insights regarding cell perturbations when exposed to xenobiotic mixtures at human-relevant levels and also a new "proof-of-concept" to decipher the low-dose mixture effect.

In metabolomics analysis, the changes for concentration below and including Max were associated with cell proliferation and elevated oxidative stress. Taking Max as an example, some key metabolites patterns such as generating ATP rapidly ($\log_2$ (FC) = 1.09 at Max) and lactate production (0.79) **(Figure B6)** agreed with prominent aspects of metabolism in proliferating cells (DeBerardinis et al. 2008). In addition, the dysregulation trend for pyrimidine and purine metabolism were quite similar with proliferating cells (Lee et al. 2017). In pyrimidine pathway **(Figure 6-4B)**, downstream metabolites (UDP: 0.52; UTP: 1.8; CDP: 1.27 and CTP: 1.51) are up-regulated over time while the upstream metabolites uridine is down-regulated (-0.45). The same trend was also found in purine metabolism **(Figure 6-4C)**. Pyrimidine and purine nucleotides are major energy carriers that play critical roles in DNA and RNA synthesis as well as membrane lipid biosynthesis and protein glycosylation (Moffatt et al. 2002). Their metabolisms are important in regulating cell cycle progression and maintaining the survival of the cells (Quéméneur et al. 2003, Wang et al. 2016). Regarding oxidative stress biomarkers, we observed a significant increase of oxidized glutathione ($\log_2$ (FC)>1.3 except 5Max) with depletion of glutathione for most doses, indicating the decrease of the GSH/GSSG ratios and elevated oxidative stress. Besides, some interrupted pathways were also related with anti-oxidation activities such as "Ascorbate and Aldarate metabolism" (Max) and "Glutathione metabolism" (5Max). The metabolome data showed that xenobiotic mixture exposure at human-relevant level altered the cellular activities through stimulating the proliferation and elevating oxidative stress.

Transcriptome alterations induced by xenobiotic mixture were in line with metabolome findings suggesting cell proliferation after mixture exposure. Above all, the maximally upregulated genes such as H19 and EGR3 were associated with cell proliferation process. H19 transcription has been found up-regulated during the S-phase of growth-simulated cells to promote cell cycle progression of breast cancer cells (Berteaux et al. 2005). While ERG3-deficient mice have reduced proliferation in response to pre-T cell receptor signals, revealing its role on promoting proliferation (Xi et al. 2004). In addition, the top GO terms of biological process "cell proliferation", "cell division" and "DNA replication process" were in substantial agreement with metabolome results. Besides, several chemicals in the mixture such as bisphenol diglycidyl ether (BADGE) and phthalates have been reported to have high affinity to the protein binding sites (Petersen et al. 2008, Yue et al. 2014) and environmental xenobiotics disrupt endocrine function by interfering with the binding of natural ligands to steroid receptors and binding proteins (Danzo 1997, Ishihara et al. 2003). Therefore, it is not surprising that molecular function "protein binding" was found with high gene percentage (48%), raising concerns that these xenobiotics may disrupt or alter some vital function through moving or transporting to the site of action. Lastly in pathway analysis, evidences have suggested that axon guidance molecules (AGMs) and SLIT2/ROBO1 signalling are important in regulating cancer cell proliferation (Dallol et al. 2002, Strickland et al. 2006, Marlow et al. 2008, Harburg et al. 2011). SLIT2 overexpression or treating with SLIT2 conditioned medium has reduced the proliferation of MCF-7 (Dallol et al. 2002, Marlow et al. 2008). In contrast, this gene was found downregulated (-1.03) in our study, which implies the proliferation of cells. In addition, we observed a consistent upregulation trend for E2F transcription factor family (E2F1:0.83; E2F2: 0.68; E2F6: 0.61; E2F7:0.83; E2F8: 0.65) in "Cell cycle" pathway. This family plays a crucial and well-established role in cell cycle progression that integrating with DNA repair and replication, chromatin assembly, condensation and segregation (Dyson 1998, Nahle et al. 2002, Ren et al. 2002).

Several biological activities were also enhanced after mixture exposure such as inducing genotoxicity and oxidative insults. In genotoxicity pathway, minichromosome maintenance protein (MCM) family implicate at the initiation step of DNA synthesis (Kearsey et al. 1998, Tye 1999) and origin recognition complex (ORC) is also essential for the initiation of DNA replication (Bell et al. 1992, Bell et al. 1993). The dysregulation of these families suggests mixture changed the DNA synthesis and replication process, resulting in the higher possibility of genetic mutations. In the Nrf2 pathway, the regulation of SLC and ABC transporter genes control the expression of proteins critical in detoxification and elimination of reactive oxygen

species (ROS) and electrophiles (Nguyen et al. 2009, Suzuki et al. 2013). The activation of the Nrf2 pathway suggests the mixture has produced chemical or oxidative insults, which is in compliance with the metabolome results of elevated oxidative stress. This genetic activation also raises concerns over the promotion on the development of *de novo* cancerous tumours by mixture exposure (DeNicola et al. 2011). Lastly, GR regulates genes controlling the development, metabolism and immune response. Its activation implies the mixture exposure may affect the anti-inflammatory and immunosuppressive actions of glucocorticoids resulting in failure to maintain homeostasis (Oakley et al. 2013).

Joint pathway analysis results have affirmed the findings that xenobiotic mixture at Max has activated pyrimidine and purine metabolism. The activation of pyrimidine may be initiated due the upregulation of thymidine kinases (e.g. TK1: 0.62) that were important in the activation of pyrimidine nucleoside analogues (Al-Madhoun et al. 2004). The reason of proliferation after mixture exposure can be explained by the fact that MCF-7 cell is a hormone-responsive breast cancer cell line and many components of the mixture are xenoestrogens (e.g. genistein, parabens, phthalates etc.). Previous studies have documented that xenoestrogens could promote cell proliferation (Brown et al. 1995, Blom et al. 1998). In addition, these xenobiotics can induce chemical insults/oxidative stress on cells through various mechanisms (Samet et al. 2018). Earlier studies have proposed that tumour cells enhanced glycolysis to provide adequate ATP for rapid proliferation as a protection from oxidative stress (Brand et al. 1997). Therefore, we assume that the cell stimulated the production of nucleotides to accommodate an increasing need in RNA and DNA synthesis after chemical insults and oxidative stress.

This study suggested that DHB and BPA have relatively higher contributions on overall metabolome changes while different chemicals may have a different effect on various metabolite regulation. The overall changing pattern of metabolites in purine and pyrimidine were generally quite similar among several chemicals. Taking UDP as an example, the concentration showed a significant decrease after removing ethyl paraben, MnBP, BzBP, BPA and DHB, indicating these chemicals have a substantial impact on the disruption of these pathways. These results could be explained that the dosing concentrations of these chemicals were considerably higher (all >100 ng/mL except BPA: 12.9 ng/mL) and studies have documented their ability to exert estrogenic effects or induce proliferation in human breast cancer cells (Suzuki et al. 2005, Chen et al. 2014, Arbuckle et al. 2016, Engeli et al. 2017, Le Fol et al. 2017). Overall, the counting-out concept along with high-throughput metabolomics provided a useful tool to screen causal chemicals in a low-dose mixture efficiently. Comparing with traditional methods (e.g. to examine the effect of each component first and then predict

the mixture effect), this approach is more suitable for a human or environmentally relevant level mixture for its observable molecular change during all experimental manipulations. In addition, considering the relative high cost of other omics tools such as sequencing and proteomics, the high-throughput analysis of metabolome has shown its superiority in the study of mixtures and their effects upon exposure at human-relevant levels.

6.6 Short Summary

In sum, we have evaluated the cellular metabolome and transcriptome changes upon exposure to the mixture of 23 organic contaminants at human-relevant levels. The relative contribution of each chemical on this mixture effect was also investigated. Both omics results revealed that the cellular activity after xenobiotic cocktail exposure was associated with cell proliferation and increased oxidative stress. In addition, with high-throughput metabolomics based "counting-out" method, we found that many chemicals in the mixture have different effects on metabolic pathway perturbation, while DHB and BPA comparably have higher contributions. Considering the fact that the current risk assessment usually focuses on the individual compound, it is of great significance to evaluate the mixture effect from exposure with higher complexity at human-relevant level. Besides, the "counting-out" method also provides a "proof-of-concept" approach to evaluate the relative contribution of each chemical, though the exact mechanism of how compounds interact with each other still remain unclear. Here, only 23 chemicals were selected in the present study and thus it is of great interest to study a more complex mixture covering both inorganics and organics that can mimic real-human exposome. In addition, in this study, cancer cell line was chosen as the experimental model and more human-relevant model such as *in vivo* animals and tissues can be considered in the future mixture study. As experimental studies cannot reasonably represent all possible exposure patterns for humans as they may be more or less sensitive to chemicals exposures, epidemiology studies are warranted to demonstrate the association of chemical mixture concentrations with adverse health outcomes in the future.

Chapter 7. Conclusions and Recommendations

7.1 Conclusions

This study developed a novel water-free method to analyze BADGEs in dust samples together with other two typical plasticizers bisphenol A (BPA) and bisphenol S (BPS). In order to investigate their levels in paired dust and urine samples, 33 paired samples were collected from Singapore. In both dust and urine samples, the predominant compounds were BPA, BADGE-$2H_2O$ and BPS. A significantly positive correlation of BPA levels in paired dust and urine samples was observed in this small-scale study. To tentatively explore the human health effect from exposure to these bisphenol plasticizers, we assessed the correlation between the urinary concentrations of these compounds and oxo-2'-deoxyguanosine (8-OHdG), an oxidative stress biomarker. The result showed that 8-OHdG level in urine samples was positively correlated with urinary BPA level and body mass index (BMI), suggesting that the elevated oxidative stress might be associated with BPA exposure and obesity.

Afterwards, this study developed a novel discovery platform to predict and identify the potential metabolites for emerging organic pollutants (EOCs) such as BADGE that often has scarce biotransformation information. In general, we adopted an 'empirical knowledge acquirement' strategy through amino acids' reaction with model compound. The results showed that incorporating experimental analysis with both *in silico* and knowledge-based prediction can greatly enhance the discovery potentials. We have also successfully identified BADGE's glucuronide, sulfate and glutathione conjugates and reaction products with thiol-containing metabolites in microsomes or HepG2 cell.

This study also compared the metabolic toxicity between BADGE and BPA using global metabolomics to elucidate their underlying mechanism. Both BADGE and BPA exposure affected the energy/sugar metabolism with upregulation of NADH and lactic acid. Although both chemicals triggered the dysregulation of arginine and proline metabolism, BPA exposure triggered higher perturbations and toxicity on this pathway which could be explained by its stronger estrogenic activity (100 times that of BADGE). Besides, accumulated evidence suggested that BADGE may also disturb the lipid metabolism.

Lastly, this study characterized the metabolome and transcriptome changes of breast cancer cell (MCF-7) by exposure to xenobiotic "cocktail" (including bisphenol plasticizers) at human-relevant levels calculated from previous large-scale biomonitoring data. Besides, it also proposed a novel high-throughput metabolomics-based "proof-of-concept" to figure out the

relative contribution of BADGE-related compounds by comparing the metabolome changes with and without it in the mixture (i.e., "counting-out" method). Both omics results revealed that the cellular activity after xenobiotic cocktail exposure was associated with cell proliferation and increased oxidative stress. In addition, with the "counting-out" method, we found that many chemicals in the mixture have different effects on metabolic pathway perturbation, while DHB and BPA comparably have higher contributions. Overall, the systems-biological results showed that xenobiotic mixture at human-relevant levels can significantly induce *in vitro* cellular changes. Furthermore, the "counting-out" method utilizing high-throughput metabolomics provides an effective way for the deconvolution of the mixture effect.
In sum, the major conclusions and contributions of this study were:
(i) revealing the actual contribution of BADGE and its derivatives in indoor dust samples for the first time through development of the water-free method; offering evidence that the indoor environment is of considerable importance to human exposure; revealing the elevated oxidative stress levels may be associated with BPA exposure and obesity.
(ii) developing an unbiased discovery platform for emerging organic contaminants; revealing the potential *in vitro* biotransformation products and metabolism pathways for BADGE for the first time;
(iii) elucidating the metabolic toxicity similarity and difference between BADGE and BPA; deepening the understanding on their underlying toxicity metabolism at system-biological level.
(iv) revealing the potential mixture effect through exposure to organic contaminants at human-relevant level; Evaluation of each component's contribution to the observed effect through development of a novel "counting-out" method.

7.2 Recommendations

There are a number of gaps in our knowledge around BADGEs in research follow from our findings and would benefit from further research:
Firstly, epidemiology study investigated the potential health effects from both short-term and long-term exposure to BADGEs has not been extensively investigated and further studies are needed. Due to the limited sample size (n=33) in this study, the further epidemiology study with large cohort samples is warranted to investigate the potential health effects from exposure to BADGEs. Our study as well as some earlier studies reported the potential association between bisphenol plasticizers exposure and the elevated oxidative stress level. However, this finding is yet to be validate through both large-scale epidemiology study and *in vitro* and *in*

vivo toxicological study.

Secondly, more validation and methodological work is needed on how to robustly identify the biotransformation products. For example, the identified metabolites with putative structure are warranted for further validation by the synthesis of metabolites. We also observed an explosion of filtered feature numbers were generated during the identification process and the function of peak decluttering /adduct grouping in XCMS is not quite ideal. For this limitation, more advanced method stable isotope-labelling can be applied to reduce the numbers of interested feature and efficiently identified potential metabolites. To better understand the biotransformation and toxicity of BADGE, it would be beneficial to incorporate the prediction of acute toxicity based on the structural formula using a web-application MetaTox tool (http://way2drug.com/mg2/).

Thirdly, in-depth exploration of the underlying toxicology mechanism of BADGE and BPA would be beneficial. For examples, few indicators suggested the lipid metabolism might be affected by exposure to both chemicals (e.g. the depletion of phospholipids precursor etc.). Since the extraction buffer used in this study is not adequate to extract the lipids and the results might of uncertainties. This study we only focus on the downstream metabolites, the information on upstream gene/protein regulation are yet unknown to us. Other omics approach (e.g. lipidomics, proteomics and transcriptomic) could be employed to elucidate the possible mechanism after exposure to BADGE. As BADGEs, BFDGEs and many other bisphenols usually coming from the same sources and human are very likely to be co-exposed to these chemicals together. These bisphenols have very similar structure and are likely to interact with each other. It would be interesting to investigate the possible interaction among the co-exposure of these bisphenols both *in vitro* and *in vivo*.

Lastly, research to carry out a more complex mixture covering both inorganics and organics that mimic real-human exposome would be beneficial. Since the primary aim of this study is to build a platform to characterize the mixture effect and also provide a "proof-of-concept" to prioritize the relative contribution of each component to the observed effect. Considering the heavy workload of the omics characterization and the "counting-out" method (N>90 in one batch experiment for 23 compounds), we did not try to include compounds as many as possible in this study. In addition, the cancer cell line was chosen as the experimental model in our study and more human-relevant models such as *in vivo* animals and tissues can be considered in future mixture studies.

References

Al-Madhoun, A. S., et al. (2004). "The role of thymidine kinases in the activation of pyrimidine nucleoside analogues." Mini reviews in medicinal chemistry **4**(4): 341-350.

Allen, F., et al. (2014). "CFM-ID: a web server for annotation, spectrum prediction and metabolite identification from tandem mass spectra." Nucleic acids research **42**(W1): W94-W99.

Anari, M. R., et al. (2004). "Integration of knowledge-based metabolic predictions with liquid chromatography data-dependent tandem mass spectrometry for drug metabolism studies: application to studies on the biotransformation of indinavir." Analytical chemistry **76**(3): 823-832.

Arbuckle, T. E., et al. (2016). "Maternal and early life exposure to phthalates: the Plastics and Personal-care Products use in Pregnancy (P4) study." Science of the Total Environment **551**: 344-356.

Asimakopoulos, A. G., et al. (2014). "Widespread occurrence of bisphenol A diglycidyl ethers, p-hydroxybenzoic acid esters (parabens), benzophenone type-UV filters, triclosan, and triclocarban in human urine from Athens, Greece." Science of the total environment **470**: 1243-1249.

Asimakopoulos, A. G., et al. (2016). "Urinary biomarkers of exposure to 57 xenobiotics and its association with oxidative stress in a population in Jeddah, Saudi Arabia." Environ. Res. **150**: 573-581.

Association, C. M. (1984). Comments in Response to Advance Notice of Proposed Rulemaking on Testing of Glycidol and its Derivatives. s. t. t. U. E. P. A. b. t. C. E. R. P. Panel. Washinton DC.

Ballesteros-Gómez, A., et al. (2007). "Determination of bisphenols A and F and their diglycidyl ethers in wastewater and river water by coacervative extraction and liquid chromatography–fluorimetry." Analytica chimica acta **603**(1): 51-59.

Bell, S. P., et al. (1993). "Yeast origin recognition complex functions in transcription silencing and DNA replication." science **262**(5141): 1844-1849.

Bell, S. P. and B. Stillman (1992). "ATP-dependent recognition of eukaryotic origins of DNA replication by a multiprotein complex." Nature **357**(6374): 128.

Berteaux, N., et al. (2005). "H19 mRNA-like noncoding RNA promotes breast cancer cell proliferation through positive control by E2F1." Journal of Biological Chemistry **280**(33): 29625-29636.

Beyer, B. A., et al. (2018). "Metabolomics-based discovery of a metabolite that enhances oligodendrocyte maturation." Nature Chemical Biology **14**(1): 22.

Bishop-Bailey, D., et al. (2000). "Bisphenol A diglycidyl ether (BADGE) is a PPAR gamma agonist in an ECV304 cell line." British Journal of Pharmacology **131**: 651-654.

Blom, A., et al. (1998). "Effects of xenoestrogenic environmental pollutants on the proliferation of a human breast cancer cell line (MCF-7)." Archives of environmental contamination and toxicology **34**(3): 306-310.

Boxall, A. B., et al. (2012). "Pharmaceuticals and personal care products in the environment: what are the big questions?" Environmental Health Perspectives **120**(9): 1221-1229.

Brand, K. A. and U. Hermfisse (1997). "Aerobic glycolysis by proliferating cells: a protective strategy against reactive oxygen species." The FASEB journal **11**(5): 388-395.

Brian, J. V., et al. (2007). "Evidence of estrogenic mixture effects on the reproductive performance of fish." Environmental Science & Technology **41**(1): 337-344.

Brown, N. M. and C. A. Lamartiniere (1995). "Xenoestrogens alter mammary gland differentiation and cell proliferation in the rat." Environmental Health Perspectives **103**(7-8): 708-713.

Cancer, I. A. f. R. o. (1989). Some organic solvents, resin monomers and related compounds, pigments and occupational exposures in paint manufacture and painting. Some Organic Solvents, Resin Monomers and Related Compounds, Pigments and Occupational Exposures in Paint Manufacture and Painting**:** 535-535.

Carpenter, D. O., et al. (2002). "Understanding the human health effects of chemical mixtures." Environmental Health Perspectives **110**(suppl 1): 25-42.

CDC (2018). Fourth National Report on Human Exposure to Environmental Chemicals. Department of Health and Human Services. Updated Tables, March 2018.

Chamorro-García, R., et al. (2012). "Bisphenol A diglycidyl ether induces adipogenic differentiation of multipotent stromal stem cells through a peroxisome proliferator–activated receptor gamma-independent mechanism." Environmental Health Perspectives **120**(7): 984-989.

Chen, F.-P. and M.-H. Chien (2014). "Lower concentrations of phthalates induce proliferation in human breast cancer cells." Climacteric **17**(4): 377-384.

Climie, I., et al. (1981). "Metabolism of the epoxy resin component 2, 2-bis [4-(2, 3-epoxypropoxy) phenyl] propane, the diglycidyl ether of bisphenol a (DGEBPA) in the mouse.; Part II. Identification of metabolites in urine and faeces following a single oral dose of 14C-DGEBPA." Xenobiotica **11**(6): 401-424.

Coulier, L., et al. (2010). "Analysis of reaction products of food contaminants and ingredients: bisphenol A diglycidyl ether (BADGE) in canned foods." Journal of Agricultural and Food Chemistry **58**(8): 4873-4882.

Dallol, A., et al. (2002). "SLIT2, a human homologue of the Drosophila Slit2 gene, has tumor suppressor activity and is frequently inactivated in lung and breast cancers." Cancer Research **62**(20): 5874-5880.

Danzo, B. J. (1997). "Environmental xenobiotics may disrupt normal endocrine function by interfering with the binding of physiological ligands to steroid receptors and binding proteins." Environmental Health Perspectives **105**(3): 294-301.

DeBerardinis, R. J., et al. (2008). "The biology of cancer: metabolic reprogramming fuels cell growth and proliferation." Cell Metabolism **7**(1): 11-20.

DeNicola, G. M., et al. (2011). "Oncogene-induced Nrf2 transcription promotes ROS detoxification and tumorigenesis." Nature **475**(7354): 106.

Dong, T., et al. (2019). "Human Indoor Exposome of Chemicals in Dust and Risk Prioritization Using EPA's ToxCast Database." Environmental Science & Technology.

Dyson, N. (1998). "The regulation of E2F by pRB-family proteins." Genes & Development **12**(15): 2245-2262.

Engeli, R., et al. (2017). "Interference of paraben compounds with estrogen metabolism by inhibition of 17β-hydroxysteroid dehydrogenases." International Journal of Molecular Sciences **18**(9): 2007.

Fang, M., et al. (2014). "Effect‐directed analysis of Elizabeth River porewater: Developmental toxicity in zebrafish (Danio rerio)." Environmental Toxicology and Chemistry **33**(12): 2767-2774.

Fang, M., et al. (2015). "Thermal degradation of small molecules: a global metabolomic investigation." Analytical chemistry **87**(21): 10935-10941.

Fang, M., et al. (2014). "Characterizing the Peroxisome Proliferator-Activated Receptor (PPAR γ) Ligand Binding Potential of Several Major Flame Retardants, Their Metabolites, and Chemical Mixtures in House Dust." Environmental Health Perspectives **123**(2): 166-172.

Fang, M., et al. (2013). "Investigating a novel flame retardant known as V6: measurements in baby products, house dust, and car dust." Environmental science & technology **47**(9): 4449-4454.

Fang, M., et al. (2015). "Activation of human peroxisome proliferator-activated nuclear receptors (PPARγ1) by semi-volatile compounds (SVOCs) and chemical mixtures in indoor dust." Environmental Science & Technology **49**(16): 10057-10064.

Fang, M., et al. (2015). "Effect-directed analysis of human peroxisome proliferator-activated nuclear receptors (PPARγ1) ligands in indoor dust." Environmental Science & Technology **49**(16): 10065-10073.

Fehlberg, S., et al. (2002). "Bisphenol A diglycidyl ether induces apoptosis in tumour cells independently of peroxisome proliferator-activated receptor-γ, in caspase-

dependent and-independent manners." Biochemical Journal **362**(3): 573-578.

Frederiksen, H., et al. (2010). "Correlations between phthalate metabolites in urine, serum, and seminal plasma from young Danish men determined by isotope dilution liquid chromatography tandem mass spectrometry." Journal of Analytical Toxicology **34**(7): 400-410.

Fülöp, N., et al. (2008). "Aging leads to increased levels of protein O-linked N-acetylglucosamine in heart, aorta, brain and skeletal muscle in Brown-Norway rats." Biogerontology **9**(3): 139.

Gallart-Ayala, H., et al. (2011). "Fast liquid chromatography-tandem mass spectrometry for the analysis of bisphenol A-diglycidyl ether, bisphenol F-diglycidyl ether and their derivatives in canned food and beverages." Journal of Chromatography A **1218**(12): 1603-1610.

Geens, T., et al. (2012). "A review of dietary and non-dietary exposure to bisphenol-A." Food and Chemical Toxicology **50**(10): 3725-3740.

Griffin, J. B., M. (2004). "Metabonomics: Its potential as a tool in toxicology for safety assessment and data integration. ." Current Drug Metabolism **5**(5): 389-398.

Guo, Y. and K. Kannan (2013). "A survey of phthalates and parabens in personal care products from the United States and its implications for human exposure." Environmental Science & Technology **47**(24): 14442-14449.

Harburg, G. C. and L. Hinck (2011). "Navigating breast cancer: axon guidance molecules as breast cancer tumor suppressors and oncogenes." Journal of Mammary Gland Biology and Neoplasia **16**(3): 257.

Harrad, S., et al. (2006). "Concentrations of polybrominated diphenyl ethers in indoor air and dust and polychlorinated biphenyls in indoor air in Birmingham, United Kingdom: Implications for human exposure." Environmental Science & Technology **40**: 4633-4638.

Hine, C., et al. (1958). "The toxicology of epoxy resins." A.M.A. Archives of Industrial Health **17**(2): 129-144.

Högberg, J., et al. (2007). "Phthalate diesters and their metabolites in human breast milk, blood or serum, and urine as biomarkers of exposure in vulnerable populations." Environmental Health Perspectives **116**(3): 334-339.

Huang, S. S., et al. (2017). "A multi-omic approach to elucidate low-dose effects of xenobiotics in zebrafish (Danio rerio) larvae." Aquatic toxicology **182**: 102-112.

Hyoung, U.-j., et al. (2007). "Developmental toxicity by exposure to bisphenol A diglycidyl ether during gestation and lactation period in Sprague-Dawley male rats." Journal of Preventive Medicine Public Health **40**(2): 155-161.

Ishihara, A., et al. (2003). "Endocrine disrupting chemicals: interference of thyroid

hormone binding to transthyretins and to thyroid hormone receptors." Molecular and Cellular Endocrinology **199**(1-2): 105-117.

Kasai, H. (1997). "Analysis of a form of oxidative DNA damage, 8-hydroxy-20-deoxyguanosine, as a marker of cellular oxidative stress during carcinogenesis." Mutattion Research **387**: 147-163.

Keaney, J. F. J., et al. (2003). "Framingham Study. Obesity and systemic oxidative stress: clinical correlates of oxidative stress in the Framingham Study." Arteriosclerosis Trombosis Vascular Biology. **23**: 434-439.

Kearsey, S. E. and K. Labib (1998). "MCM proteins: evolution, properties, and role in DNA replication." Biochimica et Biophysica Acta (BBA)-Gene Structure and Expression **1398**(2): 113-136.

Kim, S. I., et al. (2015). "Distribution of serum bisphenol A diglycidyl ether and its metabolite in Korean adult men and its association with reproductive hormone levels." Molecular & Cellular Toxicology **11**(1): 71-78.

Kirchmair, J., et al. (2013). "How do metabolites differ from their parent molecules and how are they excreted?" Journal of Chemical Information and Modeling **53**(2): 354-367.

Kluger, B., et al. (2013). "Stable isotopic labelling-assisted untargeted metabolic profiling reveals novel conjugates of the mycotoxin deoxynivalenol in wheat." Analytical and Bioanalytical Chemistry **405**(15): 5031-5036.

Ko, K.-P., et al. (2018). "Plasma phytoestrogens concentration and risk of colorectal cancer in two different Asian populations." Clinical Nutrition **37**(5): 1675-1682.

Kortenkamp, A. (2007). "Ten years of mixing cocktails: a review of combination effects of endocrine-disrupting chemicals." Environmental Health Perspectives **115**(Suppl 1): 98-105.

Laboratory, S. T. T. (1981). Toxicity studies with epoxy resins: in vitro genotoxicity studies with diglycidyl ether of Bisphenol A, EPITOKE 828, EPITOKE 1001, EPITOKE 1007. E. D. N. 878219937.

Lane, R., et al. (2015). "Bisphenol diglycidyl ethers and bisphenol A and their hydrolysis in drinking water." Water Research **72**: 331-339.

Lang, I. A., et al. (2008). "Association of urinary Bisphenol A concentration with medical disorder and laboratory abnormalities in adults." JAMA **300**(11): 1303-1310.

Le Fol, V., et al. (2017). "In vitro and in vivo estrogenic activity of BPA, BPF and BPS in zebrafish-specific assays." Ecotoxicology and Environmental Safety **142**: 150-156.

Lee, H.-J., et al. (2017). "Proteomic and metabolomic characterization of a mammalian cellular transition from quiescence to proliferation." Cell Reports **20**(3): 721-736.

Leon, Z. G.-C., J.C.; Donato, M. T.; Lahoz, A. (2013). "Mammalian cell metabolomics: Experimental design and sample preparation. ." Electrophoresis **34**(19): 2762-2775.

Levenson, A. S. and V. C. Jordan (1997). "MCF-7: the first hormone-responsive breast cancer cell line." Cancer Research **57**(15): 3071-3078.

Li, B. and C. N. Dewey (2011). "RSEM: accurate transcript quantification from RNA-Seq data with or without a reference genome." BMC bioinformatics **12**(1): 323.

Li, P., et al. (2017). "Concentrations of organophosphorus, polybromobenzene, and polybrominated diphenyl ether flame retardants in human serum, and relationships between concentrations and donor ages." Chemosphere **171**: 654-660.

Li, X., Sun, H., Yao, Y., Zhao, Z., Qin, X., Duan, Y., & Wang, L. (2018). "Distribution of Phthalate Metabolites between Paired Maternal–Fetal Samples." Environmental Science & Technology **52**(11): 6626-6635.

Liao, C., et al. (2012). "Occurrence of eight bisphenol analogues in indoor dust from the United States and several Asian countries: implications for human exposure." Environmental Science & Technology **46**(16): 9138-9145.

Lioy, P. J., et al. (2002). "Dust: a metric for use in residential and building exposure assessment and source characterization." Environmental Health Perspectives **110**(10): 969-983.

Liu, M., et al. (2019). "The occurrence of bisphenol plasticizers in paired dust and urine samples and its association with oxidative stress." Chemosphere **216**: 472-478.

Ma, B., et al. (2016). "Simultaneous determination of 8-oxo-2'-deoxyguanosine and 8-oxo-2'-deoxyadenosine in human retinal DNA by liquid chromatography nanoelectrospraytandem mass spectrometry." Scientific Reports **6**: 22375.

Marlow, R., et al. (2008). "SLITs suppress tumor growth in vivo by silencing Sdf1/Cxcr4 within breast epithelium." Cancer Research **68**(19): 7819-7827.

Marqueño, A., et al. (2019). "Toxic effects of bisphenol A diglycidyl ether and derivatives in human placental cells." Environmental Pollution **244**: 513-521.

Meeker, J. D., et al. (2013). "Urinary metabolites of organophosphate flame retardants: temporal variability and correlations with house dust concentrations." Environmental Health Perspectives **121**(5): 580-585.

Moffatt, B. A. and H. Ashihara (2002). "Purine and pyrimidine nucleotide synthesis and metabolism." The Arabidopsis Book/American Society of Plant Biologists **1**.

Møller, L., et al. (2012). Survey of Bisphenol A and Bisphenol-A-diglycidyl Ether Polymer, The Danish Environmental Protection Agency.

Nagayama, J., et al. (2000). "Comparison between brominated flame retardants and dioxins or organochlorine compounds in blood levels of Japanese adults."

Organohalogen compounds **48**: 27-30.

Nahle, Z., et al. (2002). "Direct coupling of the cell cycle and cell death machinery by E2F." Nature Cell Biology **4**(11): 859.

Nakazawa, H., et al. (2002). "In vitro assay of hydrolysis and chlorohydroxy derivatives of bisphenol A diglycidyl ether for estrogenic activity." Food and Chemical Toxicology **40**(12): 1827-1832.

Nerin, C., et al. (2014). "Compounds from multilayer plastic bags cause reproductive failures in artificial insemination." Scientific Reports **4**: 4913.

Nguyen, T., et al. (2009). "The Nrf2-antioxidant response element signaling pathway and its activation by oxidative stress." Journal of Biological Chemistry **284**(20): 13291-13295.

Nolan, R., et al. (1981). Diglyciyl Ether of Bisphenol A (DGEBPA): Fate in Male Fischer 344 Rats (Probe), Dow Chemical Company.

Oakley, R. H. and J. A. Cidlowski (2013). "The biology of the glucocorticoid receptor: new signaling mechanisms in health and disease." Journal of Allergy and Clinical Immunology **132**(5): 1033-1044.

Ortiz-Villanueva, E., et al. (2017). "Metabolic disruption of zebrafish (Danio rerio) embryos by bisphenol A. An integrated metabolomic and transcriptomic approach." Environmental Pollution **231**: 22-36.

Park, H.-G. and M.-K. Yeo (2012). "The toxicity of triclosan, bisphenol A, bisphenol A diglycidyl ether to the regeneration of cnidarian, Hydra magnipapillata." Molecular & Cellular Toxicology **8**(3): 209-216.

Peng, B., et al. (2019). "Competitive Biotransformation among Phenolic Xenobiotic Mixtures: Underestimated Risks for Toxicity Assessment." Environmental Science & Technology **53**(20): 12081-12090.

Peng, L., et al. (2015). "Determination of organophosphate esters in human serum using gel permeation chromatograph and solid phase extraction coupled with gas chromatography-mass spectrometry." Chinese Journal of Analytical Chemistry **43**(7): 1033-1039.

Petersen, H., et al. (2008). "Bisphenol A diglycidyl ether (BADGE) migrating from packaging material 'disappears' in food: reaction with food components." Food Additives and Contaminants **25**(7): 911-920.

Potratz, S., et al. (2016). "Combination of metabolomics with cellular assays reveals new biomarkers and mechanistic insights on xenoestrogenic exposures in MCF-7 cells." Chemical Research in Toxicology **30**(4): 883-892.

Quéméneur, L., et al. (2003). "Differential control of cell cycle, proliferation, and survival of primary T lymphocytes by purine and pyrimidine nucleotides." The Journal

of Immunology **170**(10): 4986-4995.

Ramilo, G., et al. (2006). "Cytotoxic effects of BADGE (bisphenol A diglycidyl ether) and BFDGE (bisphenol F diglycidyl ether) on Caco-2 cells in vitro." Archives of Toxicology **80**(11): 748-755.

Rappaport, S. M., et al. (2014). "The blood exposome and its role in discovering causes of disease." Environmental Health Perspectives **122**(8): 769-774.

Ren, B., et al. (2002). "E2F integrates cell cycle progression with DNA repair, replication, and G2/M checkpoints." Genes & development **16**(2): 245-256.

Repouskou, A., et al. (2019). "Gestational exposure to an epidemiologically defined mixture of phthalates leads to gonadal dysfunction in mouse offspring of both sexes." Scientific Reports **9**(1): 6424.

Ridder, L. and M. Wagener (2008). "SyGMa: combining expert knowledge and empirical scoring in the prediction of metabolites." ChemMedChem: Chemistry Enabling Drug Discovery **3**(5): 821-832.

Robinson, M. D., et al. (2010). "edgeR: a Bioconductor package for differential expression analysis of digital gene expression data." Bioinformatics **26**(1): 139-140.

Rosso, G., et al. (2018). "Cytotoxicity of seven bisphenol analogues compared to bisphenol A and relationships with membrane affinity data." Chemosphere **201**: 432-440.

Rudik, A. V., et al. (2017). "MetaTox: web application for predicting structure and toxicity of xenobiotics' metabolites." Journal of Chemical Information and Modeling **57**(4): 638-642.

Russo, G., et al. (2018). "Cytotoxicity of seven bisphenol analogues compared to bisphenol A and relationships with membrane affinity data." Chemosphere **201**: 432-440.

Samet, J. M. and P. A. Wages (2018). "Oxidative stress from environmental exposures." Current Opinion in Toxicology **7**: 60-66.

Satoh, K., et al. (2004). "Study on anti-androgenic effects of bisphenol a diglycidyl ether (BADGE), bisphenol F diglycidyl ether (BFDGE) and their derivatives using cells stably transfected with human androgen receptor, AR-EcoScreen." Food and Chemical Toxicology **42**(6): 983-993.

Schmalz, G., et al. (1999). "Bisphenol-A content of resin monomers and related degradation products." Clinical Oral Investigations **3**: 114-119.

Schmidt, J., et al. (2013). "Bioactivation of bisphenol A and its analogs (BPF, BPAF, BPZ and DMBPA) in human liver microsomes." Toxicology in vitro **27**(4): 1267-1276.

Silva, E., et al. (2002). "Something from "nothing"− eight weak estrogenic chemicals

combined at concentrations below NOECs produce significant mixture effects." Environmental Science & Technology **36**(8): 1751-1756.

Souza, T., et al. (2016). "New insights into BaP-induced toxicity: role of major metabolites in transcriptomics and contribution to hepatocarcinogenesis." Archives of Toxicology **90**(6): 1449-1458.

Stapleton, H. M., et al. (2005). "Polybrominated diphenyl ethers in house dust and clothes dryer lint." Environmental Science & Technology **39**: 925-931.

Strickland, P., et al. (2006). "Slit2 and netrin 1 act synergistically as adhesive cues to generate tubular bi-layers during ductal morphogenesis." Development **133**(5): 823-832.

Suárez, S., et al. (2000). "Genotoxicity of the coating lacquer on food cans, bisphenol A diglycidyl ether (BADGE), its hydrolysis products and a chlorohydrin of BADGE." Mutation Research/Genetic Toxicology and Environmental Mutagenesis **470**(2): 221-228.

Sueiro, R. A., et al. (2006). "Study on mutagenic effects of bisphenol A diglycidyl ether (BADGE) and its derivatives in the Escherichia coli tryptophan reverse mutation assay." Mutation Research/Genetic Toxicology and Environmental Mutagenesis **609**(1): 11-16.

Suzuki, T., et al. (2005). "Estrogenic and antiandrogenic activities of 17 benzophenone derivatives used as UV stabilizers and sunscreens." Toxicology and Applied Pharmacology **203**(1): 9-17.

Suzuki, T., et al. (2013). "Toward clinical application of the Keap1–Nrf2 pathway." Trends in Pharmacological Sciences **34**(6): 340-346.

Thomsen, C., et al. (2002). "Brominated flame retardants in archived serum samples from Norway: a study on temporal trends and the role of age. ." Environmental Science & Technology **36**(7): 1414-1418.

Tran, T. M., et al. (2016). "Occurrence of phthalate diesters (phthalates), p-hydroxybenzoic acid esters (parabens), bisphenol A diglycidyl ether (BADGE) and their derivatives in indoor dust from Vietnam: implications for exposure." Chemosphere **144**: 1553-1559.

Trapnell, C., et al. (2009). "TopHat: discovering splice junctions with RNA-Seq." Bioinformatics **25**(9): 1105-1111.

Tye, B. K. (1999). "MCM proteins in DNA replication." Annual Review of Biochemistry **68**(1): 649-686.

Vandenberg, L. N., et al. (2007). "Human exposure to bisphenol A (BPA)." Reproductive Toxicology **24**(2): 139-177.

Vander Heiden, M. G., et al. (2009). "Understanding the Warburg effect: the metabolic

requirements of cell proliferation." Science **324**(5930): 1029-1033.

Vemuri, G., et al. (2007). "Increasing NADH oxidation reduces overflow metabolism in Saccharomyces cerevisiae." Proceedings of the National Academy of Sciences **104**(7): 2402-2407.

Vincent, H. K., et al. (2007). "Oxidative stress and potential interventions to reduce oxidative stress in overweight and obesity." Diabetes, Obesity Metabolism. **9**: 813-839.

Von Goetz, N., et al. (2010). "Bisphenol a: how the most relevant exposure sources contribute to total consumer exposure." Risk Analysis **30**(3): 473-487.

Wang, L., et al. (2012). "Occurrence and human exposure of p-hydroxybenzoic acid esters (parabens), bisphenol A diglycidyl ether (BADGE), and their hydrolysis products in indoor dust from the United States and three East Asian countries." Environmental Science & Technology **46**(21): 11584-11593.

Wang, L., et al. (2012). "Widespread occurrence and distribution of bisphenol A diglycidyl ether (BADGE) and its derivatives in human urine from the United States and China." Environmental Science & Technology **46**(23): 12968-12976.

Wang, L., et al. (2015). "Widespread occurrence and accumulation of bisphenol A diglycidyl ether (BADGE), bisphenol F diglycidyl ether (BFDGE) and their derivatives in human blood and adipose fat." Environmental Science & Technology **49**(5): 3150-3157.

Wang, W., et al. (2015). "A comparative assessment of human exposure to tetrabromobisphenol A and eight bisphenols including bisphenol A via indoor dust ingestion in twelve countries." Environment International **83**: 183-191.

Wang, Y., et al. (2016). "Cross talk between nucleotide synthesis pathways with cellular immunity in constraining hepatitis E virus replication." Antimicrobial Agents and Chemotherapy **60**(5): 2834-2848.

Wang, Z., et al. (2018). "Development of a Correlative Strategy To Discover Colorectal Tumor Tissue Derived Metabolite Biomarkers in Plasma Using Untargeted Metabolomics." Analytical Chemistry **91**(3): 2401-2408.

West, P. R., et al. (2010). "Predicting human developmental toxicity of pharmaceuticals using human embryonic stem cells and metabolomics." Toxicology and Applied Pharmacology **247**(1): 18-27.

Wilford, B. H., et al. (2005). "Polybrominated diphenyl ethers in indoor dust in Ottawa, Canada: Implications for sources and exposure." Environmental Science & Technology **39**: 7027-7035.

Wolkowicz, I. H., et al. (2016). "Developmental toxicity of bisphenol A diglycidyl ether (Epoxinde Resin BADGE) during the early life cycle of a native amphibian species." Environmental Toxicology and Chemistry **35**(12): 3031-3038.

Wonisch, W., et al. (2012). "Oxidative stress increases continuously with BMI and age with unfavourable profiles in males." The Aging Male **15**(3): 159-165.

Wright, H. M., et al. (2000). "A synthetic antagonist for the peroxisome proliferator-activated receptor γ inhibits adipocyte differentiation." Journal of Biological Chemistry **275**(3): 1873-1877.

Xi, H. and G. J. Kersh (2004). "Early growth response gene 3 regulates thymocyte proliferation during the transition from CD4− CD8− to CD4+ CD8+ 1." The Journal of Immunology **172**(2): 964-971.

Xia, P., et al. (2017). "Benchmarking water quality from wastewater to drinking waters using reduced transcriptome of human cells." Environmental Science & Technology **51**(16): 9318-9326.

Xiao, Z., et al. (2011). "Determination of three brominated flame retardants in human serum using solid-phase extraction coupled with ultra-performance liquid chromatography-tandem mass spectrometry and gas chromatography-mass spectrometry." Chinese Journal of Chromatography **29**(12): 1165-1172.

Xue, J. and K. Kannan (2016). "Novel finding of widespread occurrence and accumulation of bisphenol A diglycidyl ethers (BADGEs) and novolac glycidyl ethers (NOGEs) in marine mammals from the United States coastal waters." Environmental Science & Technology **50**(4): 1703-1710.

Xue, J. and K. Kannan (2019). "Mass flows and removal of eight bisphenol analogs, bisphenol A diglycidyl ether and its derivatives in two wastewater treatment plants in New York State, USA." Science of the Total Environment **648**: 442-449.

Xue, J., et al. (2018). "Resin-based dental sealants as a source of human exposure to bisphenol analogues, bisphenol A diglycidyl ether, and its derivatives." Environmental Research **162**: 35-40.

Xue, J., et al. (2017). "Bisphenols, benzophenones, and bisphenol A diglycidyl ethers in textiles and infant clothing." Environmental Science & Technology **51**(9): 5279-5286.

Xue, J., et al. (2015). "Occurrence of bisphenol A diglycidyl ethers (BADGEs) and novolac glycidyl ethers (NOGEs) in archived biosolids from the U.S. EPA's targeted national sewage sludge survey." Environmental Science & Technology **49**(11): 6538-6544.

Xue, J., et al. (2016). "Occurrence of bisphenols, bisphenol A diglycidyl ethers (BADGEs), and novolac glycidyl ethers (NOGEs) in indoor air from Albany, New York, USA, and its implications for inhalation exposure." Chemosphere **151**: 1-8.

Xue, J., et al. (2015). "Urinary levels of endocrine-disrupting chemicals, including bisphenols, bisphenol A diglycidyl ethers, benzophenones, parabens, and triclosan in obese and non-obese Indian children." Environmental research **137**: 120-128.

Yang, Y., et al. (2014). "Urinary levels of bisphenol analogues in residents living near

a manufacturing plant in south China." Chemosphere **112**: 481-486.

Yang, Y. J., et al. (2009). "Bisphenol A exposure is associated with oxidative stress and inflammation in postmenopausal women." Environmental Research **109**(6): 797-801.

Yang, Y. J., et al. (2010). "Acute testis toxicity of bisphenol A diglycidyl ether in Sprague-Dawley rats." Journal of Preventive Medicine and Public Health **43**(2): 131-137.

Ye, X., et al. (2015). "Urinary concentrations of bisphenol A and three other bisphenols in convenience samples of US adults during 2000−2014." Environmental Science & Technology **49**: 11834−11839.

Yousofshahi, M., et al. (2015). "PROXIMAL: a method for Prediction of Xenobiotic Metabolism." BMC Systems Biology **9**(1): 94.

Yue, Y., et al. (2014). "The binding affinity of phthalate plasticizers-protein revealed by spectroscopic techniques and molecular modeling." Food and Chemical Toxicology **71**: 244-253.

Zhang, T., et al. (2016). "Urinary concentrations of Bisphenols and their association with biomarkers of oxidative stress in people living near E-Waste recycling facilities in China." Environmental Science & Technology **50**(7): 4045-4053.

Zhang, Y., et al. (2018). ""“Cocktail” of Xenobiotics at Human Relevant Levels Reshapes the Gut Bacterial Metabolome in a Species-Specific Manner." Environmental Science & Technology **52**(19): 11402-11410.

Zhang, Z., et al. (2011). "Urinary bisphenol A concentrations and their implications for human exposure in several Asian countries." Environmental Science & Technology **45**: 7044-7050.

Zhao, F., et al. (2017). "Organophosphorus flame retardants in pregnant women and their transfer to chorionic villi." Environmental Science & Technology **51**(11): 6489-6497.

Appendix A

Table A1. Information of recruited participants from Singapore

ID	Gender	Age	Weight (kg)	Height (cm)	Body Mass Index
1	F	25	51	157	20.69
2	M	25	60	170	20.76
3	M	37	69	163	25.97
4	M	25	55	165	20.20
5	M	23	66	177	21.07
6	F	27	48	158	19.23
7	F	25	57	163	21.45
8	M	22	68	180	20.99
9	M	23	57	173	19.05
10	M	23	78	178	24.62
11	F	28	55	160	21.48
12	M	30	73	168	25.86
13	F	23	50	152	21.64
14	F	30	54	163	20.32
15	M	29	60	165	22.04
16	F	22	53	163	19.95
17	F	27	55	170	19.03
18	F	31	54	162	20.58
19	M	34	69	169	24.16
20	M	27	70	172	23.66
21	M	26	63	172	21.30
22	M	32	74	176	23.89
23	F	27	48	163	18.07
24	M	23	70	180	21.60
25	M	29	75	173	25.06
26	M	28	85	178	26.83
27	M	24	57	174	18.83
28	M	23	61	170	21.11

29	F	22	57	168	20.20
30	F	28	60	165	22.04
31	F	26	47	163	17.69
32	M	29	84	178	26.51
33	M	26	67	171	22.91

Notes:

The dust samples for participants No.8 lost during transport.

Table A2. Parameters of MS/MS analysis for target analytes [a]

Analytes	Precursor	Product Ion	Fragmentor (volts)	Collision Energy (volts)
BPS	249	108	140	25
		92	140	37
BFDGE-2H_2O	366	181	72	9
		107	72	29
BADGE-2H_2O	394	209	67	9
		135	67	29
$^{13}C_{12}$-BPA	239	224	101	13
BPA	227	212	101	13
		133	101	21
BADGE-H_2O	376	209	64	9
		135	64	29
BFDGE	330	163	62	21
		133	62	21
BADGE-H_2O-HCl	412	227	69	9
		135	69	33
BFDGE-2HCl	402	199	79	9
BADGE-d_6	364	197	65	9
BADGE	358	191	65	9
		135	65	29
BADGE-HCl	394	227	72	9
BADGE- 2HCl	430	227	90	10
8-OHdG	282	192	105	13
		150	105	21
8-OHdG- ^{13}C,$^{15}N_2$	285	195	105	21
		151	105	20

Notes:

[a] Gas Temperature: 300°C, Gas Flow: 10 l/min, Nebulizer: 25 psi, Sheath Gas Temp: 350°C, Sheath Gas Flow 10 l/min; Capillary 3500 V; Positive mode was used for all BADGEs and BFDGEs; Negative mode was used for BPA, BPS and 8-OHdG

Table A3. Concentrations of BADGE-related compounds detected in SRM2585 (ng/g dust) and the intra- and inter-day variability (n=5)

Analytes	**Mean**	**S.D.** [a]	**%RSD (Intra-day)**[b]	**%RSD (Inter-day)**
BPA	57,809	13,851	9	23
BPS	4,486	1,201	12	27
BADGE	35	10	22	29
BADGE-H_2O	345	89	2	25
BADGE-$2H_2O$	486	105	23	21
BADGE-H_2O-HCl	229	42	15	18
BADGE-HCl	44	24	19	25
BADGE-2HCl	150	44	14	29
BFDGE	367	74	1	25

[a] S.D. =standard deviation

[b] %RSD= relative standard deviation

Table A4. Spearman Correlations of bisphenol plasticizers in dust samples from Singapore

Analytes	**BPA**	**BPS**	**BADGE**	**BADGE-H_2O**	**BADGE-$2H_2O$**	**BADGE-HCl-H_2O**	**BADGE-HCl**	**BADGE-2HCl**	**BFDGE**	**BFDGE-$2H_2O$**	**BFDGE-2HCl**
BPA	1.000										
BPS	-0.003	1.000									
BADGE	0.265	0.354*	1.000								
BADGE-H_2O	0.489 **	0.283	0.254	1.000							
BADGE-$2H_2O$	0.378*	0.362*	0.450**	0.605**	1.000						
BADGE-HCl-H_2O	0.453 **	0.280	0.396*	0.632**	0.745**	1.000					
BADGE-HCl	-0.042	0.469 **	0.237	0.582**	0.312	0.418*	1.000				
BADGE-2HCl	0.165	0.373*	0.303	0.365*	0.316	0.726**	0.396*	1.000			
BFDGE	0.158	0.407*	-0.020	0.282	0.189	0.333	0.430*	0.365*	1.000		
BFDGE-$2H_2O$	0.008	0.032	-0.159	-0.076	-0.090	-0.277	0.016	-0.328	0.363*	1.000	
BFDGE-2HCl	0.146	0.068	0.069	0.068	-0.068	0.029	-0.208	0.010	0.054	-0.118	1.000

*. Correlation is significant with $p<0.05$

**. Correlation is very significant with $p<0.01$

Figure A1. Recovery of analytes through silica gel cartridge by different combination of solvents [a]

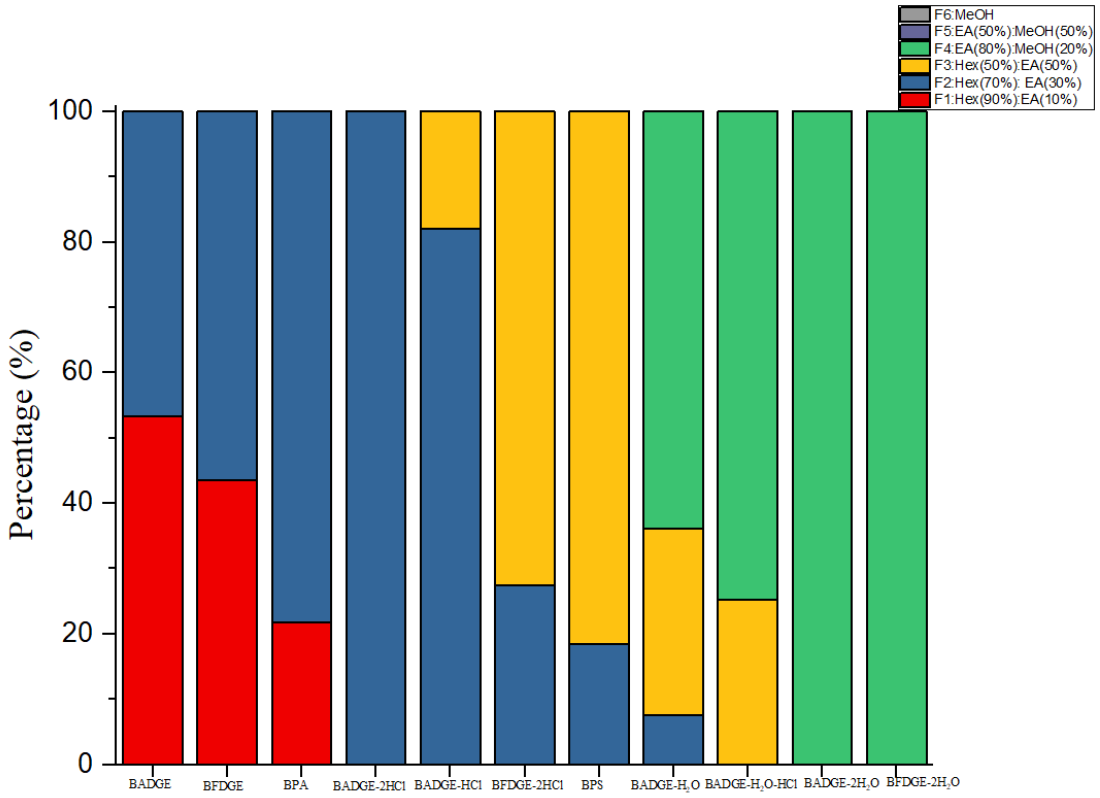

[a]Hex: Hexane; EA: Ethyl Acetate; MeOH: Methanol.

Figure A2. Measured recovery of BADGE in dust matrix spikes [a]

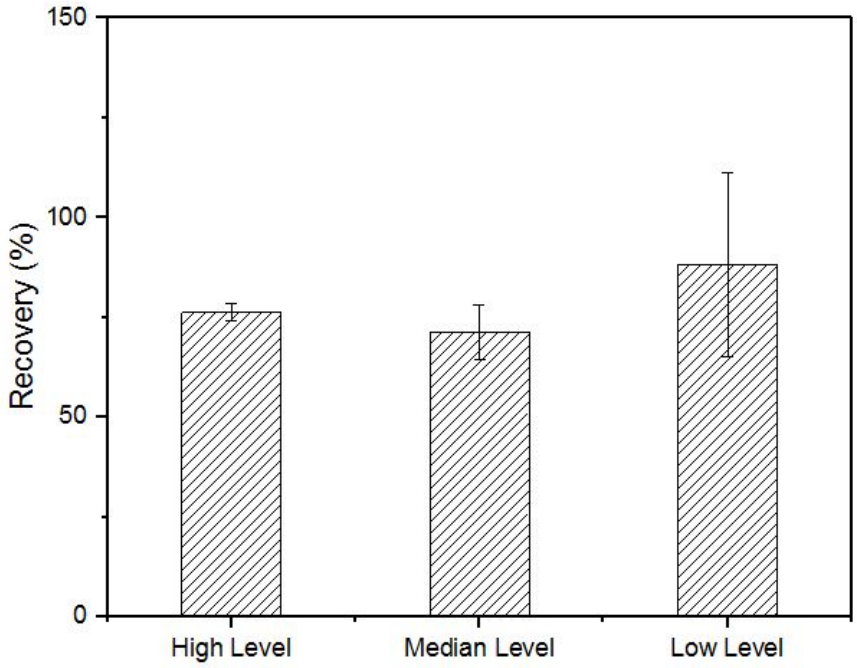

[a] High Level: 200 ng spikes into SRM2585; Median Level: 20 ng spikes into SRM2585; Low Level: 1 ng spikes into SRM 2585.

Appendix B

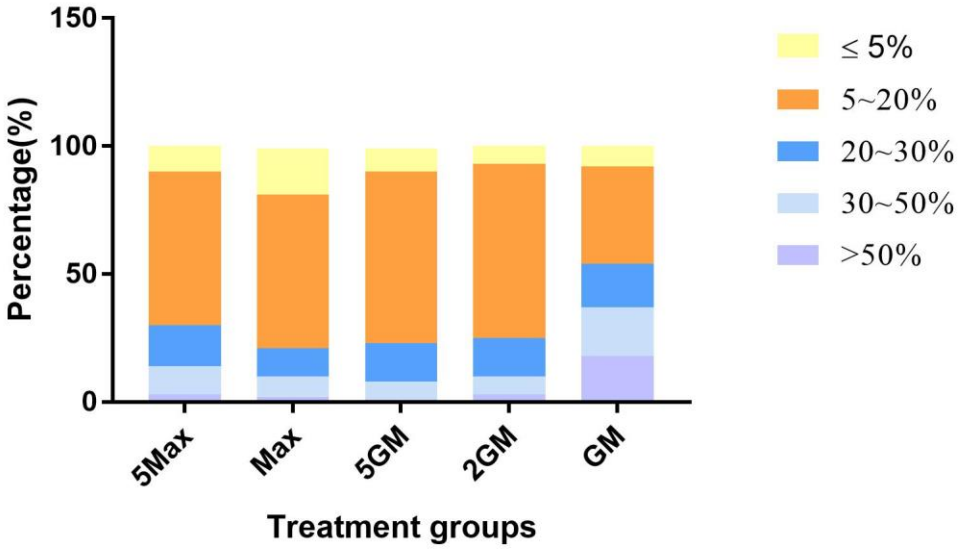

Figure B1. The distribution of relative standard error (%) for each treatment groups' features (*p*-value ⩽0.05, maximal intensity >10,000, and |fold change| >1.3)

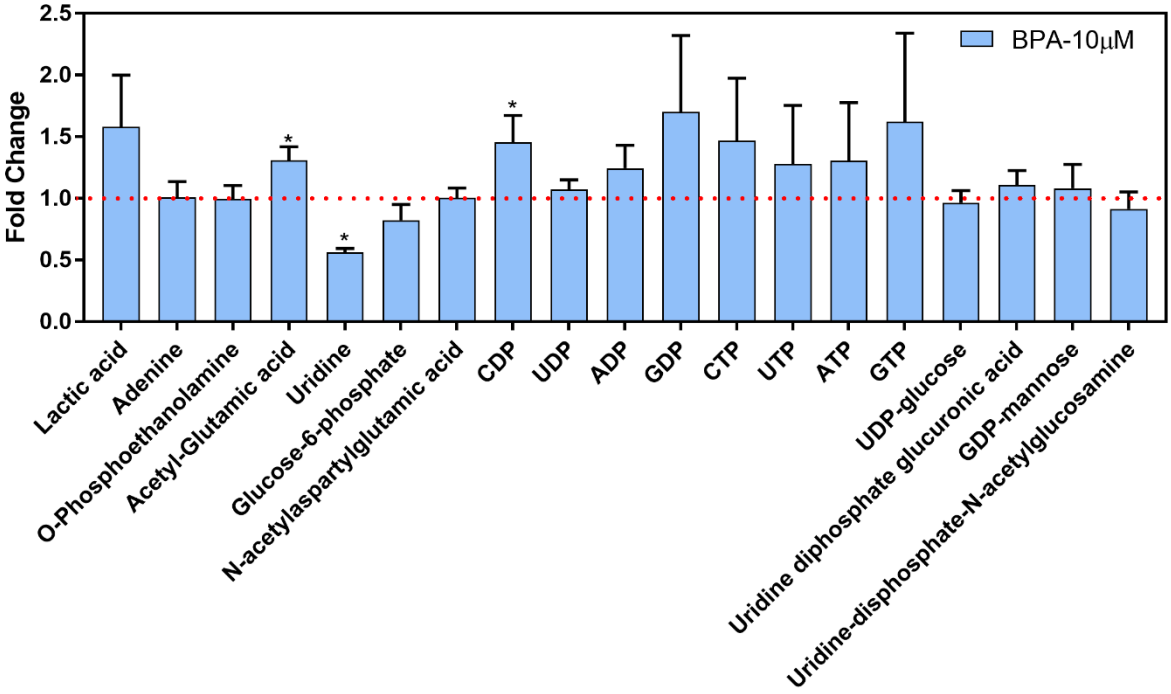

Figure B2. The fold change (N=4; Mean ± S.D.) of the metabolic responses of MCF-7 after exposure to bisphenol A (BPA) at 10μM (2.28 μg/mL)

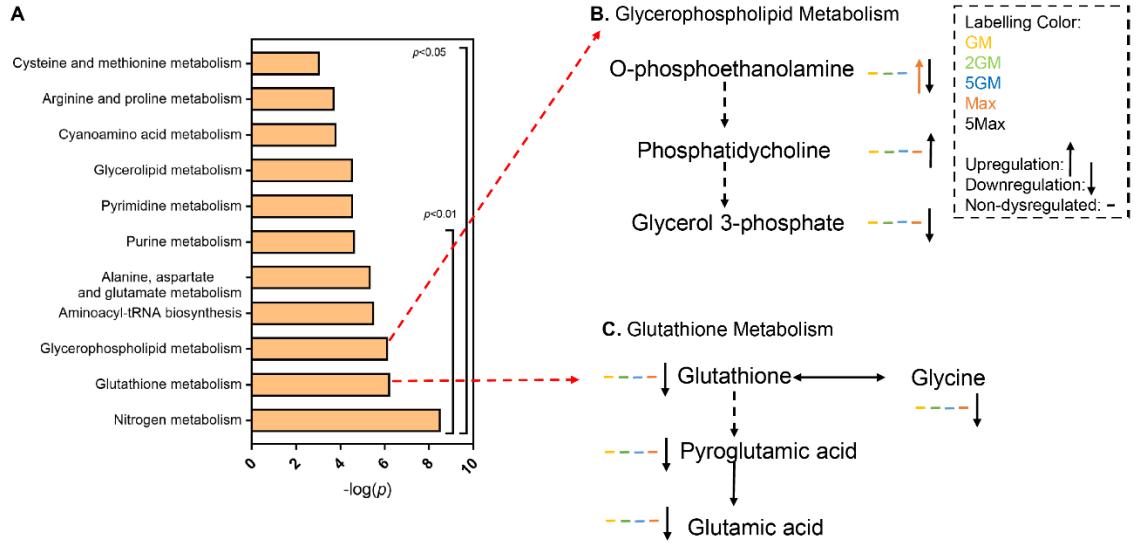

Figure B3. Significant dysregulated pathways of the xenobiotic mixture exposure at 5-fold Max. A. Metabolic pathway analysis for xenobiotic mixture at 5-fold Max using Metaboanalyst (p <0.05); Up and down regulation of metabolites at different concentration (GM, 2GM, 5GM, Max and 5Max) in B. Glycerophospholipid metabolism; C. Glutathione metabolism.

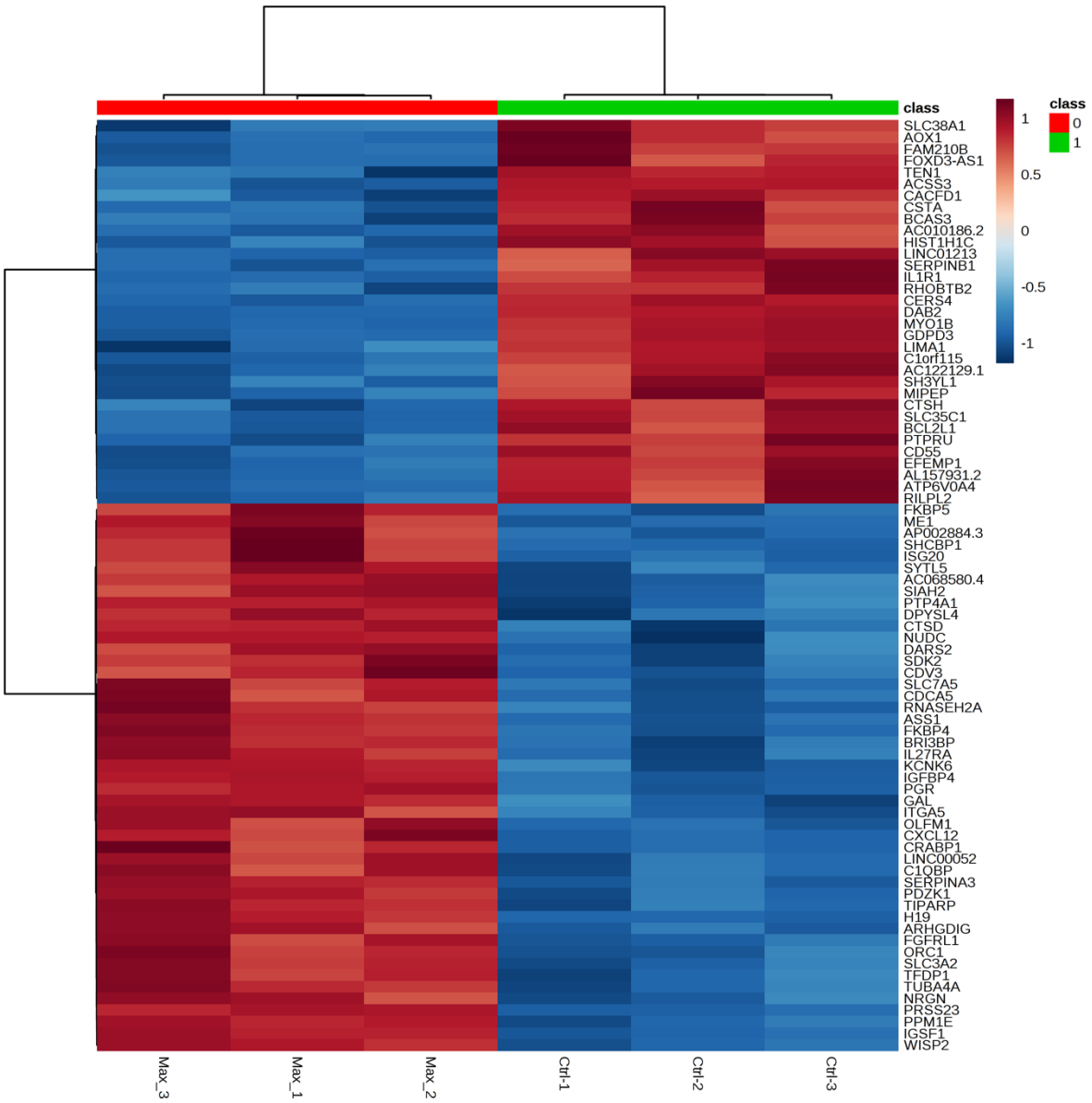

Figure B4. Heat map showing fold change of significantly dysregulated genes (Top 80) significantly dysregulated genes (adjusted p <0.05, $|\log_2$ (fold change)| >0.68) in MCF-7 cells exposed to maximum human-relevant levels of mixtures for 40 hours.

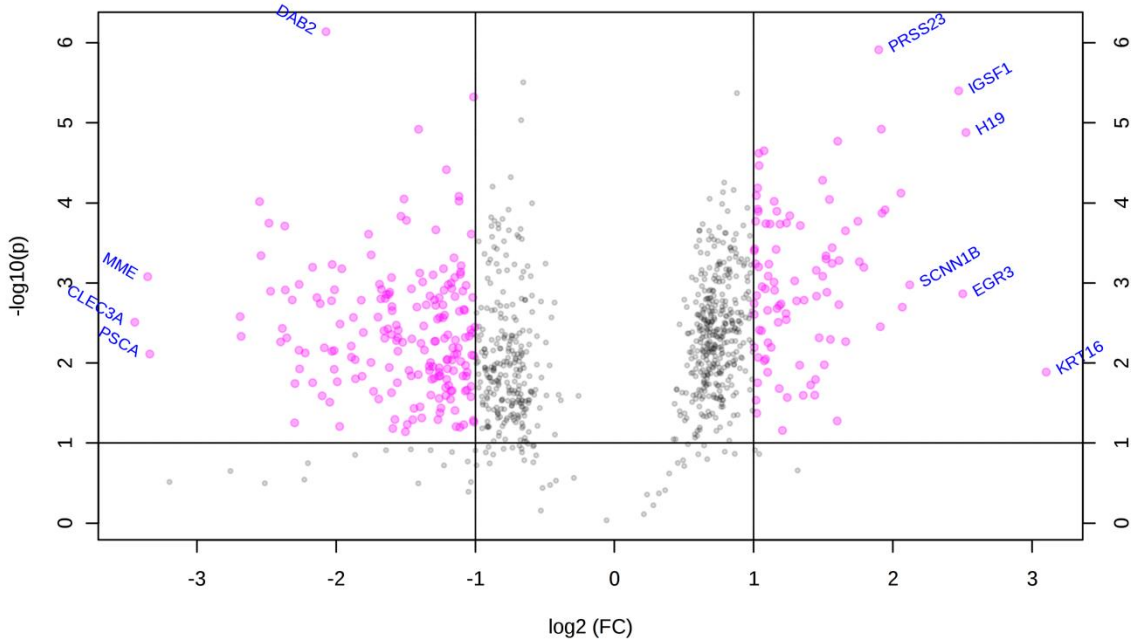

Figure B5. Volcano plot for all dysregulated genes for the mixture at Max comparing with control.

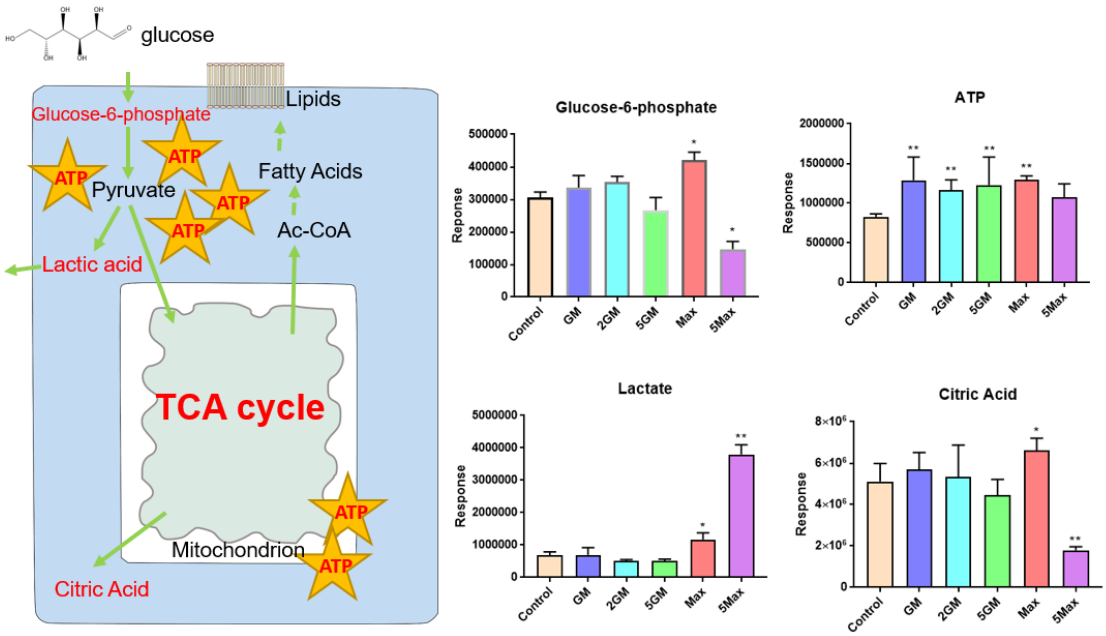

Figure B6. General mechanism for cell proliferation caused by the xenobiotic cocktail from GM to Max level

Table B1. Quantified protein concentrations for different treatment groups using micro BCA assay (N=3).

Groups	Concentrations (µg/mL)	S.D.
GM	35.7	3.1
2GM	35.0	2.2
5GM	31.6	3.3
Max	33.6	2.7
5Max	27.5	0.9
Ctrl	32.0	4.2

Notes: Samples were reconstituted in the normalized volume of Acetonitrile: water (1:1, v/v) (e.g. the lowest protein content samples were reconstituted in 40 µL and other samples were reconstitute based on the same protein content/volume ratio accordingly.

Table B2. Detailed information of identified 54 dysregulated metabolites (Significance criteria: Fold Change (FC)⩾1.3, p-value⩽0.05 and maximal intensity > 10,000)

Compounds	HMDB	KEGG	Mode	GM			2GM			5GM			Max			5Max		
				log2 (FC)	*p*	*RSD (%)*	log2 (FC)	*p*	*RSD (%)*	log2 (FC)	*p*	*RSD (%)*	log2 (FC)	*p*	*RSD (%)*	log2 (FC)	*p*	*RSD (%)*
LysoPE(18:1(9Z)/0:0)	HMDB0011506	-	Positive	-0.07	0.755	16	-0.09	0.671	8	-0.06	0.756	12.1	-0.19	0.330	12	-0.52	0.069	20
PC(O-15:0/2:0)	HMDB0007940	-	Negative	0.43	0.189	12	0.19	0.549	17	0.72	0.031	34.1	0.26	0.418	10	1.01	0.014	22
LysoPA(18:0/0:0)	HMDB0007854	C00416	Negative	0.29	0.188	18	0.18	0.460	12	0.58	0.134	22.7	0.30	0.160	6	1.03	0.007	16
b-G6P	HMDB0003498	C01172	Negative	0.37	0.088	20	0.25	0.145	17	0.07	0.741	9.0	0.57	0.002	12	-0.94	0.002	16
Oxidized Glutathione	HMDB0003337	C00127	Negative	0.92	0.022	9	0.58	0.079	12	0.44	0.180	8.3	0.89	0.100	4	-0.59	0.092	51
Butyrylcarnitine	HMDB0002013	C02862	Positive	-0.06	0.732	23	0.31	0.118	11	0.29	0.055	28.6	0.52	0.009	4	-0.53	0.017	16
Butyryl-L-carnitine	HMDB0002013		Positive	0.37	0.094	15	0.36	0.051	7	0.59	0.010	3.9	-0.47	0.053	13	0.06	0.732	27
CDP	HMDB0001546	C00112	Negative	0.88	0.002	9	1.01	0.000	15	0.95	0.017	7.0	1.27	0.000	8	-0.30	0.168	7
Phosphocreatine	HMDB0001511	C02305	Negative	0.00	0.976	16	-0.08	0.564	7	0.00	0.974	12.9	-0.16	0.177	20	-5.12	0.000	17
ADP	HMDB0001341	C00008	Negative	0.64	0.020	16	0.49	0.003	17	0.57	0.064	14.0	0.64	0.000	21	0.38	0.029	27
GTP	HMDB0001273	C00044	Negative	1.31	0.002	11	0.93	0.038	24	0.86	0.153	14.0	1.32	0.004	9	-0.79	0.200	6
GDP	HMDB0001201	C00035	Negative	1.00	0.008	13	0.70	0.056	24	0.70	0.154	14.2	0.97	0.007	8	0.25	0.529	9
MTA	HMDB0001173	C00170	Positive	-0.14	0.655	22	0.12	0.672	14	0.08	0.765	28.0	0.60	0.050	29	-1.49	0.015	11

GDP-mannose	HMDB0001163	C00096	Negative	-0.45	0.142	24	-0.97	0.026	13	-0.92	0.024	10.7	-1.11	0.014	9	0.73	0.412	6
NAcGlu	HMDB0001138	C00624	Negative	0.19	0.483	29	0.15	0.568	28	0.26	0.275	23.2	0.48	0.008	8	-0.09	0.526	6
UDP-D-glucuronic acid	HMDB0000935	C00167	Negative	0.42	0.005	7	0.35	0.078	15	0.13	0.347	45.0	0.64	0.000	14	-0.15	0.086	24
L-Tryptophan	HMDB0000929	C00078	Negative	-0.09	0.630	16	-0.26	0.188	11	-0.04	0.832	17.7	0.37	0.094	17	0.24	0.271	19
NAD	HMDB0000902	C00003	Negative	0.13	0.160	7	0.15	0.255	16	0.13	0.113	2.6	0.12	0.178	13	-0.68	0.000	16
Stearic acid	HMDB0000827	C01530	Negative	0.38	0.076	20	0.24	0.131	17	0.22	0.221	9.0	0.42	0.087	12	0.61	0.017	16
Propionylcarnitine	HMDB0000824	C03017	Positive	-0.70	0.033	8	-0.13	0.581	19	-0.15	0.527	7.7	-0.06	0.806	7	-4.55	0.000	4
N-Acetyl-L-aspartic acid	HMDB0000812	C01042	Negative	0.08	0.583	13	0.12	0.596	18	0.15	0.374	8.7	0.33	0.044	16	-3.35	0.000	12
Octanoylcarnitine	HMDB0000791	C02838	Positive	-0.46	0.289	12	-1.04	0.015	100	-1.41	0.002	9.0	-0.80	0.014	17	-0.23	0.376	20
Malic acid	HMDB0000744	C00711	Negative	0.19	0.233	7	0.18	0.423	18	0.19	0.250	8.2	0.20	0.137	5	-1.75	0.000	3
Leucine	HMDB0000687	C00123	Negative	0.03	0.896	46	-0.14	0.414	100	-0.02	0.922	77.5	0.43	0.151	56	0.64	0.003	68
Decanoylcarnitine	HMDB0000651	C03299	Positive	-0.87	0.018	10	-1.08	0.011	18	-1.35	0.001	11.4	-0.93	0.005	9	0.22	0.378	16
PC(16:0/0:0)	HMDB0000564	-	Positive	-0.12	0.574	9	-0.22	0.170	16	0.16	0.266	37.7	-0.22	0.143	15	0.64	0.001	23
ATP	HMDB0000538	C00002	Negative	1.18	0.000	14	0.79	0.010	14	0.74	0.147	9.2	1.09	0.002	11	-0.81	0.039	5
2-Methylbutyroylcarnitine	HMDB0000378	-	Positive	-0.19	0.256	4	0.11	0.550	4	0.15	0.289	8.7	0.01	0.952	6	-3.74	0.000	3
Uridine	HMDB0000296	C00299	Negative	-0.75	0.007	30	-1.05	0.003	13	-1.13	0.002	14.4	-0.45	0.040	30	-0.15	0.445	28

UDP	HMDB0000295	C00015	Negative	-0.06	0.732	6	0.31	0.118	12	0.29	0.055	22.4	0.52	0.009	5	-0.53	0.017	7
UDP-Glc-NAc	HMDB0000290	C00043	Negative	0.26	0.058	57	0.36	0.087	40	0.32	0.027	4.6	0.48	0.003	13	-0.29	0.045	23
UDP-glucose	HMDB0000286	C00029	Negative	0.26	0.038	18	0.33	0.088	29	0.26	0.040	5.6	0.49	0.001	10	-2.11	0.000	48
UTP	HMDB0000285	C00075	Negative	1.53	0.000	11	1.30	0.001	7	1.15	0.034	9.8	1.83	0.000	13	-1.88	0.004	14
Thymidine	HMDB0000273	C00214	Negative	-0.46	0.227	32	-1.22	0.058	41	-0.99	0.069	3.0	-0.57	0.191	10	-0.80	0.109	23
Pyroglutamic acid	HMDB0000267	C01879	Negative	-0.04	0.794	7	-0.03	0.832	8	-0.03	0.806	1.5	0.14	0.348	5	-1.93	0.000	5
Taurine	HMDB0000251	C00245	Negative	-0.16	0.293	5	-0.15	0.314	18	0.01	0.946	10.4	0.03	0.813	4	-1.83	0.000	13
O-Phosphoethanolamine	HMDB0000224	C00346	Negative	0.04	0.735	16	-0.05	0.723	10	0.03	0.867	28.7	0.48	0.003	5	-1.13	0.000	25
L-Palmitoylcarnitine	HMDB0000222	C02990	Positive	-0.57	0.015	32	-0.72	0.016	8	-0.73	0.002	12.3	-0.60	0.007	18	1.35	0.044	8
Palmitic acid	HMDB0000220	C00249	Negative	0.13	0.367	10	0.08	0.481	5	0.21	0.139	4.9	0.29	0.082	10	0.47	0.020	7
Pantothenic acid	HMDB0000210	C00864	Positive	-0.38	0.241	14	-0.27	0.387	19	-0.28	0.339	39.2	0.08	0.763	12	0.55	0.052	31
Acetylcarnitine	HMDB0000201	C02571	Positive	-0.22	0.058	20	-0.11	0.307	14	-0.15	0.121	9.0	0.00	0.959	8	-0.43	0.004	23
Aspartic acid	HMDB0000191	C00049	Negative	0.24	0.051	15	0.34	0.089	14	0.34	0.030	11.0	0.29	0.020	8	-4.35	0.000	5
Lactate	HMDB0000190	C00186	Negative	0.04	0.891	27	-0.40	0.034	30	-0.42	0.036	22.8	0.79	0.006	21	2.49	0.000	36
Proline	HMDB0000162	C00148	Negative	0.02	0.844	86	0.08	0.451	46	0.15	0.196	24.1	0.33	0.034	65	-1.14	0.000	55
Glutamate	HMDB0000148	C00025	Negative	-0.03	0.862	18	-0.03	0.855	28	-0.04	0.785	27.9	0.17	0.292	14	-2.05	0.000	14
Glycerol 3-phosphate	HMDB0000126	C00093	Negative	0.05	0.851	15	0.03	0.89	29	0.09	0.68	17.1	-0.06	0.78	9	-2.63	0.00	9

								3			3			1			0	
Glutathione	HMDB0000125	C00051	Negative	-1.04	0.132	5	-0.24	0.617	12	0.00	0.993	41.5	-0.16	0.776	15	-2.76	0.007	32
Glycine	HMDB0000123	C00037	Negative	0.07	0.769	8	-0.08	0.778	22	0.07	0.809	46.8	0.21	0.338	15	-0.57	0.049	43
Citric acid	HMDB0000094	C00158	Negative	0.15	0.377	3	0.06	0.812	5	-0.20	0.301	6.7	0.37	0.027	8	-1.51	0.000	7
CTP	HMDB0000082	C00063	Negative	1.35	0.000	10	1.08	0.002	20	0.91	0.085	14.9	1.51	0.001	8	-1.50	0.012	7
L-Carnitine	HMDB0000062	C00318	Positive	0.00	0.968	14	0.16	0.037	28	0.21	0.025	17.2	0.38	0.002	18	-0.44	0.001	89
Adenosine	HMDB0000050	C00212	Negative	-0.75	0.054	34	-1.21	0.009	26	-0.83	0.027	16.1	-0.66	0.080	17	-0.08	0.801	7
AMP	HMDB0000045	C00020	Negative	-0.18	0.548	26	-0.11	0.676	23	-0.17	0.431	24.9	-0.23	0.325	44	0.76	0.002	12
Adenine	HMDB0000034	C00147	Negative	-0.11	0.683	17	-0.19	0.531	20	0.20	0.410	9.9	0.65	0.031	16	-1.48	0.011	43

Table B3. Detailed information of significantly dysregulated genes (Significance criteria: Fold Change ⩾ 1.5, adjust p-value ⩽ 0.05)

Ensemble_Gene ID	Official Gene Symbol	log2(FC)	*p*-value	*p*-adjusted	regulate
ENSG00000166509	CLEC3A	-3.1938494	2.57E-105	4.31E-101	down
ENSG00000115594	IL1R1	-2.4417735	1.23E-78	1.03E-74	down
ENSG00000167653	PSCA	-2.925155	4.68E-54	1.57E-50	down
ENSG00000146674	IGFBP3	-2.2171159	4.71E-53	1.32E-49	down
ENSG00000196549	MME	-3.0570119	1.25E-43	1.90E-40	down
ENSG00000135318	NT5E	-2.1174147	2.59E-42	3.63E-39	down
ENSG00000064787	BCAS1	-1.8083909	1.39E-39	1.80E-36	down
ENSG00000115461	IGFBP5	-1.5961718	9.23E-37	9.13E-34	down
ENSG00000178372	CALML5	-1.5518823	8.50E-35	7.52E-32	down
ENSG00000172478	C2orf54	-2.1538713	6.11E-33	5.14E-30	down
ENSG00000153071	DAB2	-1.8329273	3.56E-32	2.85E-29	down
ENSG00000283526	AL160276.1	-1.3779824	1.42E-29	9.92E-27	down
ENSG00000283075	AL157931.2	-1.4306447	2.90E-29	1.95E-26	down
ENSG00000121552	CSTA	-2.1841436	3.20E-29	2.07E-26	down
ENSG00000136048	DRAM1	-1.256098	1.26E-28	7.84E-26	down
ENSG00000168899	VAMP5	-1.8447724	4.92E-28	2.85E-25	down
ENSG00000168743	NPNT	-1.3159993	1.57E-27	8.77E-25	down
ENSG00000117472	TSPAN1	-1.5372549	4.88E-27	2.64E-24	down
ENSG00000102886	GDPD3	-1.34105	2.19E-26	1.12E-23	down
ENSG00000147883	CDKN2B	-1.6362291	1.80E-25	8.62E-23	down
ENSG00000183569	SERHL2	-1.495579	4.36E-25	2.04E-22	down
ENSG00000145569	FAM105A	-1.3702203	6.92E-25	3.14E-22	down
ENSG00000131171	SH3BGRL	-1.0573169	1.18E-24	5.20E-22	down
ENSG00000124406	ATP8A1	-1.7524392	1.54E-24	6.65E-22	down
ENSG00000138356	AOX1	-1.9706735	1.85E-24	7.78E-22	down
ENSG00000158055	GRHL3	-1.9708416	3.40E-24	1.39E-21	down
ENSG00000164761	TNFRSF11B	-1.5444578	5.00E-24	2.00E-21	down
ENSG00000170442	KRT86	-1.7844424	1.18E-23	4.60E-21	down
ENSG00000205426	KRT81	-1.5504297	3.64E-23	1.30E-20	down
ENSG00000272196	HIST2H2AA4	-1.2955569	3.86E-23	1.35E-20	down
ENSG00000154330	PGM5	-1.9127934	5.16E-23	1.77E-20	down
ENSG00000244468	AC093001.1	-1.9283164	7.40E-23	2.49E-20	down
ENSG00000181830	SLC35C1	-1.1419422	8.01E-23	2.64E-20	down
ENSG00000168675	LDLRAD4	-1.5044323	1.61E-22	5.20E-20	down
ENSG00000079257	LXN	-1.262283	1.85E-22	5.86E-20	down
ENSG00000121671	CRY2	-1.2419654	4.19E-22	1.28E-19	down
ENSG00000165272	AQP3	-1.4729834	4.29E-22	1.29E-19	down

ENSG00000095321	CRAT	-1.5576143	5.90E-22	1.74E-19	down
ENSG00000163629	PTPN13	-1.1062436	9.37E-22	2.71E-19	down
ENSG00000136928	GABBR2	-1.8435217	4.11E-21	1.13E-18	down
ENSG00000128641	MYO1B	-0.9759229	9.60E-21	2.60E-18	down
ENSG00000196126	HLA-DRB1	-1.3711221	1.98E-20	5.05E-18	down
ENSG00000218416	PP14571	-1.5262959	2.16E-20	5.41E-18	down
ENSG00000086548	CEACAM6	-1.4543045	2.90E-20	6.92E-18	down
ENSG00000094755	GABRP	-2.067175	2.93E-20	6.92E-18	down
ENSG00000173890	GPR160	-1.2155989	3.25E-20	7.57E-18	down
ENSG00000137501	SYTL2	-0.9199505	4.25E-20	9.78E-18	down
ENSG00000162981	FAM84A	-1.2226537	1.17E-19	2.60E-17	down
ENSG00000170477	KRT4	-2.523015	1.30E-19	2.83E-17	down
ENSG00000169239	CA5B	-1.2849164	1.70E-19	3.66E-17	down
ENSG00000232938	RPL23AP87	-1.3190461	2.10E-19	4.41E-17	down
ENSG00000198125	MB	-1.2333997	5.76E-19	1.18E-16	down
ENSG00000050405	LIMA1	-1.194746	7.98E-19	1.61E-16	down
ENSG00000137393	RNF144B	-1.8300437	9.27E-19	1.83E-16	down
ENSG00000262094	AC139099.1	-1.7649759	1.55E-18	3.03E-16	down
ENSG00000196917	HCAR1	-1.4134381	1.95E-18	3.77E-16	down
ENSG00000170044	ZPLD1	-2.3803441	3.65E-18	6.97E-16	down
ENSG00000198189	HSD17B11	-1.8378013	3.70E-18	6.99E-16	down
ENSG00000164938	TP53INP1	-1.4213067	5.04E-18	9.21E-16	down
ENSG00000112697	TMEM30A	-0.8826569	7.59E-18	1.36E-15	down
ENSG00000163993	S100P	-1.599179	9.13E-18	1.60E-15	down
ENSG00000111052	LIN7A	-1.0886751	1.52E-17	2.61E-15	down
ENSG00000035115	SH3YL1	-0.9768889	1.81E-17	3.07E-15	down
ENSG00000253882	AC099548.2	-1.8190928	1.83E-17	3.07E-15	down
ENSG00000130066	SAT1	-1.1999019	2.00E-17	3.29E-15	down
ENSG00000112531	QKI	-0.9893677	2.35E-17	3.80E-15	down
ENSG00000119938	PPP1R3C	-1.2065672	4.43E-17	7.09E-15	down
ENSG00000256594	AC010186.2	-1.1732408	5.80E-17	9.20E-15	down
ENSG00000146038	DCDC2	-1.003629	6.34E-17	9.96E-15	down
ENSG00000158406	HIST1H4H	-1.172394	6.87E-17	1.07E-14	down
ENSG00000109099	PMP22	-1.139431	9.90E-17	1.53E-14	down
ENSG00000110375	UPK2	-1.1880727	1.20E-16	1.80E-14	down
ENSG00000170379	TCAF2	-1.5538611	1.43E-16	2.09E-14	down
ENSG00000065809	FAM107B	-0.9970453	3.13E-16	4.42E-14	down
ENSG00000250722	SELENOP	-2.0268804	3.49E-16	4.84E-14	down
ENSG00000105929	ATP6V0A4	-1.3337664	3.88E-16	5.35E-14	down
ENSG00000074527	NTN4	-1.5067475	6.26E-16	8.49E-14	down
ENSG00000147526	TACC1	-0.9987861	2.15E-15	2.80E-13	down

ENSG00000105974	CAV1	-1.039077	2.19E-15	2.83E-13	down
ENSG00000134258	VTCN1	-1.8219866	2.33E-15	2.99E-13	down
ENSG00000113532	ST8SIA4	-1.0222514	3.18E-15	4.02E-13	down
ENSG00000140859	KIFC3	-1.1444865	4.60E-15	5.77E-13	down
ENSG00000243244	STON1	-1.5531036	7.62E-15	9.42E-13	down
ENSG00000136205	TNS3	-1.2964674	8.35E-15	1.02E-12	down
ENSG00000273184	AC010655.4	-0.9541981	1.31E-14	1.56E-12	down
ENSG00000169242	EFNA1	-1.1424173	1.34E-14	1.59E-12	down
ENSG00000109339	MAPK10	-1.8511213	1.46E-14	1.71E-12	down
ENSG00000104081	BMF	-1.4402083	1.53E-14	1.79E-12	down
ENSG00000129682	FGF13	-1.3658756	1.99E-14	2.25E-12	down
ENSG00000115380	EFEMP1	-0.9907858	2.52E-14	2.83E-12	down
ENSG00000102547	CAB39L	-1.375036	4.12E-14	4.56E-12	down
ENSG00000183111	ARHGEF37	-1.2027353	4.18E-14	4.59E-12	down
ENSG00000164463	CREBRF	-1.5024667	4.83E-14	5.27E-12	down
ENSG00000071073	MGAT4A	-0.9269792	5.50E-14	5.89E-12	down
ENSG00000105856	HBP1	-1.0611958	8.91E-14	9.30E-12	down
ENSG00000165959	CLMN	-0.9974189	9.64E-14	1.00E-11	down
ENSG00000111961	SASH1	-1.1491655	1.14E-13	1.16E-11	down
ENSG00000106025	TSPAN12	-1.3954873	1.56E-13	1.55E-11	down
ENSG00000171724	VAT1L	-1.6652143	1.78E-13	1.76E-11	down
ENSG00000101115	SALL4	-0.9779078	1.88E-13	1.85E-11	down
ENSG00000143341	HMCN1	-1.0986889	1.91E-13	1.87E-11	down
ENSG00000221866	PLXNA4	-1.098346	2.27E-13	2.19E-11	down
ENSG00000119801	YPEL5	-0.8683228	2.50E-13	2.40E-11	down
ENSG00000186197	EDARADD	-1.6818328	2.86E-13	2.70E-11	down
ENSG00000180596	HIST1H2BC	-1.1738414	3.95E-13	3.65E-11	down
ENSG00000228613	AC141930.1	-1.3215983	4.89E-13	4.44E-11	down
ENSG00000115919	KYNU	-0.887237	6.28E-13	5.61E-11	down
ENSG00000164684	ZNF704	-1.0619327	7.20E-13	6.37E-11	down
ENSG00000185664	PMEL	-1.1122409	7.99E-13	7.03E-11	down
ENSG00000274180	NATD1	-1.3103984	8.16E-13	7.14E-11	down
ENSG00000132669	RIN2	-1.2924163	8.90E-13	7.75E-11	down
ENSG00000127084	FGD3	-1.1464213	1.23E-12	1.06E-10	down
ENSG00000170017	ALCAM	-0.8109977	1.45E-12	1.24E-10	down
ENSG00000147251	DOCK11	-1.4237082	1.89E-12	1.58E-10	down
ENSG00000089820	ARHGAP4	-0.9143559	1.89E-12	1.58E-10	down
ENSG00000242498	ARPIN	-1.0295983	2.56E-12	2.07E-10	down
ENSG00000196352	CD55	-0.7979445	2.55E-12	2.07E-10	down
ENSG00000131238	PPT1	-0.8241489	3.41E-12	2.72E-10	down
ENSG00000235584	AC008268.1	-1.8427264	3.47E-12	2.75E-10	down

ENSG00000143578	CREB3L4	-0.8544637	3.79E-12	2.98E-10	down
ENSG00000187848	P2RX2	-1.5255927	4.16E-12	3.25E-10	down
ENSG00000116667	C1orf21	-0.7647736	4.25E-12	3.31E-10	down
ENSG00000114626	ABTB1	-1.0066329	4.31E-12	3.34E-10	down
ENSG00000197815	AC122129.1	-1.4746033	4.71E-12	3.60E-10	down
ENSG00000041353	RAB27B	-1.0268098	4.82E-12	3.66E-10	down
ENSG00000135374	ELF5	-1.291271	5.61E-12	4.23E-10	down
ENSG00000257379	AC023509.1	-0.9222862	6.15E-12	4.62E-10	down
ENSG00000236601	AL732372.1	-1.6679626	6.81E-12	5.09E-10	down
ENSG00000224984	AL512363.1	-0.8993202	6.87E-12	5.11E-10	down
ENSG00000162078	ZG16B	-0.8401396	6.99E-12	5.18E-10	down
ENSG00000204323	SMIM5	-1.1066917	7.10E-12	5.24E-10	down
ENSG00000092969	TGFB2	-1.673117	7.53E-12	5.53E-10	down
ENSG00000164309	CMYA5	-0.9803063	8.27E-12	6.04E-10	down
ENSG00000131378	RFTN1	-1.2152899	8.42E-12	6.12E-10	down
ENSG00000167608	TMC4	-0.8373854	8.90E-12	6.45E-10	down
ENSG00000013588	GPRC5A	-0.8618046	9.59E-12	6.92E-10	down
ENSG00000124098	FAM210B	-0.8242203	9.66E-12	6.94E-10	down
ENSG00000248405	PRR5-ARHGAP8	-0.9639716	9.77E-12	6.99E-10	down
ENSG00000090238	YPEL3	-1.1771106	9.81E-12	6.99E-10	down
ENSG00000114796	KLHL24	-1.3022726	1.48E-11	1.02E-09	down
ENSG00000124493	GRM4	-1.5769658	1.53E-11	1.06E-09	down
ENSG00000279117	AP001972.5	-0.9289024	1.70E-11	1.16E-09	down
ENSG00000236743	AL732372.2	-1.840187	1.85E-11	1.26E-09	down
ENSG00000184613	NELL2	-0.751336	1.95E-11	1.32E-09	down
ENSG00000115290	GRB14	-1.0600252	2.14E-11	1.44E-09	down
ENSG00000145808	ADAMTS19	-0.7933903	2.14E-11	1.44E-09	down
ENSG00000205488	CALML3-AS1	-1.5946104	2.16E-11	1.44E-09	down
ENSG00000102934	PLLP	-1.0315957	2.26E-11	1.51E-09	down
ENSG00000277075	HIST1H2AE	-1.1177113	2.38E-11	1.57E-09	down
ENSG00000196950	SLC39A10	-0.8588778	2.47E-11	1.62E-09	down
ENSG00000141376	BCAS3	-0.6853508	2.81E-11	1.83E-09	down
ENSG00000197308	GATA3-AS1	-0.8673386	2.86E-11	1.86E-09	down
ENSG00000187672	ERC2	-1.310433	2.95E-11	1.90E-09	down
ENSG00000105219	CNTD2	-0.9114502	3.12E-11	2.00E-09	down
ENSG00000162496	DHRS3	-1.5172539	3.44E-11	2.19E-09	down
ENSG00000197872	FAM49A	-1.4407889	3.55E-11	2.25E-09	down
ENSG00000007306	CEACAM7	-1.6849169	4.03E-11	2.51E-09	down
ENSG00000187837	HIST1H1C	-0.8801196	4.12E-11	2.56E-09	down
ENSG00000145911	N4BP3	-0.674453	4.77E-11	2.95E-09	down

ENSG00000108840	HDAC5	-1.0075364	5.51E-11	3.38E-09	down
ENSG00000163083	INHBB	-0.8796312	8.49E-11	5.13E-09	down
ENSG00000183323	CCDC125	-0.9591041	1.00E-10	5.97E-09	down
ENSG00000181218	HIST3H2A	-0.8621619	1.05E-10	6.24E-09	down
ENSG00000237807	AC022034.2	-1.6536507	1.06E-10	6.29E-09	down
ENSG00000140479	PCSK6	-0.7766523	1.19E-10	6.96E-09	down
ENSG00000159423	ALDH4A1	-0.8113015	1.30E-10	7.58E-09	down
ENSG00000102683	SGCG	-0.8526967	1.40E-10	8.08E-09	down
ENSG00000100100	PIK3IP1	-1.1160438	1.42E-10	8.18E-09	down
ENSG00000071967	CYBRD1	-1.209192	1.43E-10	8.19E-09	down
ENSG00000203812	HIST2H2AA3	-0.8312307	1.45E-10	8.31E-09	down
ENSG00000105668	UPK1A	-1.5938151	1.81E-10	1.02E-08	down
ENSG00000277159	AL139384.2	-1.1938965	1.94E-10	1.09E-08	down
ENSG00000225663	MCRIP1	-0.8770579	1.98E-10	1.11E-08	down
ENSG00000171940	ZNF217	-0.6960785	2.06E-10	1.15E-08	down
ENSG00000187244	BCAM	-0.6935946	2.36E-10	1.31E-08	down
ENSG00000081307	UBA5	-0.676136	2.43E-10	1.34E-08	down
ENSG00000118640	VAMP8	-0.6601636	2.45E-10	1.34E-08	down
ENSG00000048540	LMO3	-1.6057419	2.48E-10	1.35E-08	down
ENSG00000181449	SOX2	-0.9056564	2.54E-10	1.38E-08	down
ENSG00000164751	PEX2	-0.826218	2.69E-10	1.45E-08	down
ENSG00000109436	TBC1D9	-0.7126744	3.06E-10	1.63E-08	down
ENSG00000162545	CAMK2N1	-0.8020377	3.22E-10	1.69E-08	down
ENSG00000042062	RIPOR3	-1.1169704	3.44E-10	1.80E-08	down
ENSG00000123933	MXD4	-0.6983209	3.90E-10	2.03E-08	down
ENSG00000065361	ERBB3	-0.7948729	3.95E-10	2.04E-08	down
ENSG00000136888	ATP6V1G1	-0.7303951	4.44E-10	2.28E-08	down
ENSG00000103811	CTSH	-0.797544	5.01E-10	2.55E-08	down
ENSG00000198502	HLA-DRB5	-0.9439412	5.28E-10	2.68E-08	down
ENSG00000182732	RGS6	-0.9430768	5.53E-10	2.80E-08	down
ENSG00000150977	RILPL2	-0.8137573	6.46E-10	3.24E-08	down
ENSG00000166046	TCP11L2	-1.1146261	6.81E-10	3.41E-08	down
ENSG00000165899	OTOGL	-1.2638479	7.25E-10	3.60E-08	down
ENSG00000251562	MALAT1	-0.8083052	7.50E-10	3.69E-08	down
ENSG00000008086	CDKL5	-0.9925966	8.90E-10	4.34E-08	down
ENSG00000134202	GSTM3	-0.7533533	8.98E-10	4.36E-08	down
ENSG00000188641	DPYD	-1.1006453	9.63E-10	4.65E-08	down
ENSG00000180730	SHISA2	-1.0087525	9.77E-10	4.69E-08	down
ENSG00000149573	MPZL2	-0.7016711	1.21E-09	5.72E-08	down
ENSG00000116209	TMEM59	-0.7590453	1.24E-09	5.82E-08	down
ENSG00000101417	PXMP4	-0.7610276	1.25E-09	5.85E-08	down

ENSG00000245750	DRAIC	-1.3955821	1.26E-09	5.87E-08	down
ENSG00000249242	TMEM150C	-0.6734153	1.31E-09	6.10E-08	down
ENSG00000104763	ASAH1	-0.6947472	1.32E-09	6.10E-08	down
ENSG00000178826	TMEM139	-1.1691149	1.33E-09	6.13E-08	down
ENSG00000012822	CALCOCO1	-0.9785741	1.34E-09	6.18E-08	down
ENSG00000174498	IGDCC3	-1.1893999	1.54E-09	6.98E-08	down
ENSG00000049089	COL9A2	-0.9675142	1.56E-09	7.09E-08	down
ENSG00000163435	ELF3	-0.8226798	1.64E-09	7.37E-08	down
ENSG00000155966	AFF2	-1.7471147	1.67E-09	7.46E-08	down
ENSG00000205133	TRIQK	-0.7719034	1.67E-09	7.46E-08	down
ENSG00000186212	SOWAHB	-0.9950261	1.94E-09	8.53E-08	down
ENSG00000154930	ACSS1	-0.7897617	2.08E-09	9.07E-08	down
ENSG00000163898	LIPH	-1.1721915	2.17E-09	9.42E-08	down
ENSG00000042317	SPATA7	-0.855041	2.32E-09	9.99E-08	down
ENSG00000168143	FAM83B	-0.7816592	2.32E-09	9.99E-08	down
ENSG00000172461	FUT9	-1.0968943	2.33E-09	1.00E-07	down
ENSG00000267131	AC005746.2	-0.8785972	2.33E-09	1.00E-07	down
ENSG00000151715	TMEM45B	-1.0622286	2.38E-09	1.02E-07	down
ENSG00000249348	UGDH-AS1	-0.7993093	2.41E-09	1.03E-07	down
ENSG00000171992	SYNPO	-1.0622595	2.71E-09	1.15E-07	down
ENSG00000240303	ACAD11	-0.9675218	2.77E-09	1.17E-07	down
ENSG00000172915	NBEA	-0.9248845	2.85E-09	1.20E-07	down
ENSG00000271385	AL161798.1	-1.4366942	3.13E-09	1.30E-07	down
ENSG00000139219	COL2A1	-1.4937238	3.16E-09	1.31E-07	down
ENSG00000266714	MYO15B	-1.1176954	3.47E-09	1.43E-07	down
ENSG00000215018	COL28A1	-1.6896324	3.58E-09	1.47E-07	down
ENSG00000274810	NPHP3-ACAD11	-0.9786503	3.71E-09	1.51E-07	down
ENSG00000187122	SLIT1	-1.3752143	3.79E-09	1.54E-07	down
ENSG00000027001	MIPEP	-0.6312975	4.18E-09	1.68E-07	down
ENSG00000103479	RBL2	-0.7796902	4.20E-09	1.69E-07	down
ENSG00000114166	KAT2B	-0.8797942	4.27E-09	1.71E-07	down
ENSG00000223764	AL645608.1	-0.7232745	4.35E-09	1.73E-07	down
ENSG00000160325	CACFD1	-0.7484769	4.85E-09	1.91E-07	down
ENSG00000197558	SSPO	-0.8385167	4.87E-09	1.92E-07	down
ENSG00000278828	HIST1H3H	-0.8371121	4.96E-09	1.95E-07	down
ENSG00000166821	PEX11A	-0.7845808	5.14E-09	2.01E-07	down
ENSG00000175662	TOM1L2	-0.7379929	5.26E-09	2.06E-07	down
ENSG00000058799	YIPF1	-0.7555891	5.46E-09	2.12E-07	down
ENSG00000270342	AL499605.1	-0.6640946	6.18E-09	2.38E-07	down
ENSG00000215845	TSTD1	-0.6883192	7.37E-09	2.81E-07	down

ENSG00000131981	LGALS3	-0.6891677	7.56E-09	2.87E-07	down
ENSG00000196747	HIST1H2AI	-0.9904261	7.65E-09	2.90E-07	down
ENSG00000111371	SLC38A1	-0.6388889	8.25E-09	3.10E-07	down
ENSG00000204054	LINC00963	-0.6982054	8.39E-09	3.15E-07	down
ENSG00000166946	CCNDBP1	-0.7284054	8.79E-09	3.29E-07	down
ENSG00000054983	GALC	-0.6836437	9.49E-09	3.53E-07	down
ENSG00000102409	BEX4	-0.8087403	9.48E-09	3.53E-07	down
ENSG00000204740	MALRD1	-0.6909696	9.57E-09	3.55E-07	down
ENSG00000155093	PTPRN2	-1.1422076	9.85E-09	3.64E-07	down
ENSG00000135407	AVIL	-1.3436433	1.14E-08	4.16E-07	down
ENSG00000277224	HIST1H2BF	-1.2991464	1.15E-08	4.21E-07	down
ENSG00000175895	PLEKHF2	-0.6261135	1.18E-08	4.32E-07	down
ENSG00000111319	SCNN1A	-1.0183922	1.36E-08	4.92E-07	down
ENSG00000167740	CYB5D2	-0.7548536	1.48E-08	5.29E-07	down
ENSG00000144369	FAM171B	-1.0990019	1.49E-08	5.32E-07	down
ENSG00000114405	C3orf14	-0.6853855	1.53E-08	5.44E-07	down
ENSG00000156011	PSD3	-0.8401794	1.56E-08	5.51E-07	down
ENSG00000249846	LINC02021	-1.3511578	1.56E-08	5.51E-07	down
ENSG00000162976	PQLC3	-0.710859	1.61E-08	5.67E-07	down
ENSG00000120885	CLU	-0.6736167	1.63E-08	5.72E-07	down
ENSG00000111058	ACSS3	-0.637651	1.68E-08	5.88E-07	down
ENSG00000261888	AC144831.1	-0.9949004	1.71E-08	5.96E-07	down
ENSG00000156103	MMP16	-0.8800743	1.89E-08	6.56E-07	down
ENSG00000015520	NPC1L1	-0.9550795	1.90E-08	6.58E-07	down
ENSG00000105810	CDK6	-0.8697225	1.94E-08	6.70E-07	down
ENSG00000006459	KDM7A	-0.7288948	2.03E-08	6.95E-07	down
ENSG00000151150	ANK3	-0.786061	2.17E-08	7.40E-07	down
ENSG00000021355	SERPINB1	-0.6703869	2.37E-08	8.03E-07	down
ENSG00000180573	HIST1H2AC	-0.7814394	2.39E-08	8.04E-07	down
ENSG00000125637	PSD4	-0.6486956	2.39E-08	8.04E-07	down
ENSG00000196693	ZNF33B	-0.9192151	2.39E-08	8.04E-07	down
ENSG00000184292	TACSTD2	-0.6326839	2.44E-08	8.18E-07	down
ENSG00000260342	AC138811.2	-1.0725182	2.68E-08	8.94E-07	down
ENSG00000116977	LGALS8	-0.6209035	3.05E-08	1.01E-06	down
ENSG00000152518	ZFP36L2	-0.6438432	3.10E-08	1.02E-06	down
ENSG00000171552	BCL2L1	-0.6168041	3.39E-08	1.11E-06	down
ENSG00000090661	CERS4	-0.6754271	3.47E-08	1.13E-06	down
ENSG00000136153	LMO7	-0.8225258	3.52E-08	1.14E-06	down
ENSG00000243566	UPK3B	-0.8322103	3.65E-08	1.18E-06	down
ENSG00000162817	C1orf115	-0.7007051	3.68E-08	1.19E-06	down
ENSG00000074696	HACD3	-0.6262153	4.05E-08	1.29E-06	down

ENSG00000121966	CXCR4	-1.0369135	4.24E-08	1.35E-06	down
ENSG00000003436	TFPI	-0.9313969	4.37E-08	1.38E-06	down
ENSG00000157514	TSC22D3	-0.753114	4.41E-08	1.39E-06	down
ENSG00000135480	KRT7	-0.8410477	4.50E-08	1.41E-06	down
ENSG00000107984	DKK1	-0.7237085	4.58E-08	1.43E-06	down
ENSG00000213204	AL049697.1	-1.3268027	4.60E-08	1.44E-06	down
ENSG00000144785	AC073896.1	-1.0201297	4.67E-08	1.46E-06	down
ENSG00000142606	MMEL1	-1.1728608	4.75E-08	1.48E-06	down
ENSG00000132932	ATP8A2	-1.2208482	4.82E-08	1.49E-06	down
ENSG00000151322	NPAS3	-0.8837007	4.91E-08	1.52E-06	down
ENSG00000271533	Z83843.1	-1.057297	5.00E-08	1.54E-06	down
ENSG00000168300	PCMTD1	-0.894962	5.10E-08	1.57E-06	down
ENSG00000140470	ADAMTS17	-1.0632519	5.35E-08	1.64E-06	down
ENSG00000127863	TNFRSF19	-0.8782883	5.61E-08	1.71E-06	down
ENSG00000137486	ARRB1	-0.7079039	5.62E-08	1.71E-06	down
ENSG00000112902	SEMA5A	-1.2166966	6.03E-08	1.82E-06	down
ENSG00000163346	PBXIP1	-0.7832983	6.48E-08	1.94E-06	down
ENSG00000163683	SMIM14	-0.5956826	6.50E-08	1.94E-06	down
ENSG00000273472	AC096733.2	-0.789224	7.23E-08	2.15E-06	down
ENSG00000196776	CD47	-0.5892016	7.51E-08	2.22E-06	down
ENSG00000197892	KIF13B	-0.8744789	7.65E-08	2.25E-06	down
ENSG00000141736	ERBB2	-0.6489883	7.94E-08	2.32E-06	down
ENSG00000134531	EMP1	-1.3539888	8.36E-08	2.44E-06	down
ENSG00000113916	BCL6	-0.951159	8.84E-08	2.58E-06	down
ENSG00000211689	TRGC1	-1.3607705	8.88E-08	2.58E-06	down
ENSG00000189171	S100A13	-0.6817842	9.31E-08	2.70E-06	down
ENSG00000213937	CLDN9	-0.6931175	9.58E-08	2.77E-06	down
ENSG00000106789	CORO2A	-0.8392979	1.27E-07	3.57E-06	down
ENSG00000177337	DLGAP1-AS1	-1.1835648	1.31E-07	3.69E-06	down
ENSG00000261116	AL049555.1	-0.7356041	1.33E-07	3.74E-06	down
ENSG00000135124	P2RX4	-0.5851702	1.35E-07	3.79E-06	down
ENSG00000202522	Y_RNA	-0.8539026	1.39E-07	3.88E-06	down
ENSG00000244541	LINC01213	-1.2496192	1.41E-07	3.94E-06	down
ENSG00000197670	AL157838.1	-1.0978262	1.48E-07	4.11E-06	down
ENSG00000168216	LMBRD1	-0.732635	1.52E-07	4.19E-06	down
ENSG00000089351	GRAMD1A	-0.6226064	1.55E-07	4.28E-06	down
ENSG00000117614	SYF2	-0.664933	1.57E-07	4.32E-06	down
ENSG00000153404	PLEKHG4B	-1.202861	1.57E-07	4.32E-06	down
ENSG00000214894	LINC00243	-1.3579433	1.64E-07	4.49E-06	down
ENSG00000154654	NCAM2	-0.687849	1.67E-07	4.57E-06	down
ENSG00000182782	HCAR2	-1.4825505	1.69E-07	4.60E-06	down

ENSG00000231419	LINC00689	-1.2680064	1.74E-07	4.71E-06	down
ENSG00000224032	EPB41L4A-AS1	-0.8288621	1.77E-07	4.77E-06	down
ENSG00000054793	ATP9A	-0.6958804	1.87E-07	5.02E-06	down
ENSG00000162949	CAPN13	-1.0559561	1.90E-07	5.09E-06	down
ENSG00000172602	RND1	-0.8755441	1.91E-07	5.11E-06	down
ENSG00000204991	SPIRE2	-0.6911718	1.91E-07	5.11E-06	down
ENSG00000153113	CAST	-0.6047588	1.94E-07	5.18E-06	down
ENSG00000105784	RUNDC3B	-0.9330043	1.99E-07	5.30E-06	down
ENSG00000198478	SH3BGRL2	-0.6969815	2.00E-07	5.32E-06	down
ENSG00000177519	RPRM	-0.8855382	2.38E-07	6.27E-06	down
ENSG00000175611	LINC00476	-0.8019648	2.42E-07	6.35E-06	down
ENSG00000163322	FAM175A	-0.8759734	2.66E-07	6.92E-06	down
ENSG00000185442	FAM174B	-0.6134658	2.75E-07	7.14E-06	down
ENSG00000265246	AC129926.1	-1.3552874	2.91E-07	7.50E-06	down
ENSG00000268790	AC008764.4	-0.9029814	2.92E-07	7.52E-06	down
ENSG00000184012	TMPRSS2	-0.7843442	3.16E-07	8.08E-06	down
ENSG00000138764	CCNG2	-0.6936907	3.23E-07	8.25E-06	down
ENSG00000115221	ITGB6	-1.0875309	3.94E-07	9.92E-06	down
ENSG00000119878	CRIPT	-0.7262722	3.96E-07	9.96E-06	down
ENSG00000174080	CTSF	-0.7360156	4.16E-07	1.04E-05	down
ENSG00000277758	FO681492.1	-0.7729724	4.21E-07	1.05E-05	down
ENSG00000129422	MTUS1	-0.7297564	4.24E-07	1.06E-05	down
ENSG00000069493	CLEC2D	-0.9920658	4.42E-07	1.10E-05	down
ENSG00000155957	TMBIM4	-0.6339344	4.94E-07	1.22E-05	down
ENSG00000197603	C5orf42	-0.7211096	4.93E-07	1.22E-05	down
ENSG00000265972	TXNIP	-0.649604	5.27E-07	1.29E-05	down
ENSG00000105373	NOP53	-0.6550622	5.41E-07	1.32E-05	down
ENSG00000141337	ARSG	-0.6621606	5.55E-07	1.35E-05	down
ENSG00000140873	ADAMTS18	-1.4451627	5.62E-07	1.36E-05	down
ENSG00000154153	RETREG1	-0.7071764	5.69E-07	1.37E-05	down
ENSG00000001461	NIPAL3	-0.7805535	5.95E-07	1.43E-05	down
ENSG00000203865	ATP1A1-AS1	-0.9674178	6.13E-07	1.47E-05	down
ENSG00000229391	HLA-DRB6	-1.3779777	6.24E-07	1.49E-05	down
ENSG00000166173	LARP6	-0.8566805	6.64E-07	1.57E-05	down
ENSG00000080200	CRYBG3	-0.9438313	6.75E-07	1.59E-05	down
ENSG00000100290	BIK	-0.9874459	6.86E-07	1.61E-05	down
ENSG00000146376	ARHGAP18	-0.8039992	7.10E-07	1.66E-05	down
ENSG00000258072	AC126177.7	-0.9288864	7.19E-07	1.68E-05	down
ENSG00000184924	PTRHD1	-0.6736882	8.15E-07	1.88E-05	down
ENSG00000267368	UPK3BL1	-0.6411482	8.29E-07	1.91E-05	down

ENSG00000076513	ANKRD13A	-0.6286679	8.48E-07	1.95E-05	down
ENSG00000183401	CCDC159	-0.9323947	9.32E-07	2.11E-05	down
ENSG00000177685	CRACR2B	-0.7392495	9.35E-07	2.12E-05	down
ENSG00000156127	BATF	-0.633081	9.68E-07	2.18E-05	down
ENSG00000109083	IFT20	-0.7584815	9.82E-07	2.21E-05	down
ENSG00000182165	TP53TG1	-0.6622303	1.01E-06	2.26E-05	down
ENSG00000114670	NEK11	-0.802003	1.03E-06	2.30E-05	down
ENSG00000179627	ZBTB42	-0.6119201	1.05E-06	2.34E-05	down
ENSG00000154265	ABCA5	-0.7210413	1.11E-06	2.47E-05	down
ENSG00000184730	APOBR	-1.0571594	1.15E-06	2.55E-05	down
ENSG00000060656	PTPRU	-0.632122	1.21E-06	2.67E-05	down
ENSG00000166432	ZMAT1	-0.9388115	1.29E-06	2.83E-05	down
ENSG00000175309	PHYKPL	-0.6260494	1.32E-06	2.90E-05	down
ENSG00000175155	YPEL2	-0.8005066	1.34E-06	2.93E-05	down
ENSG00000111790	FGFR1OP2	-0.6294522	1.39E-06	3.04E-05	down
ENSG00000176155	CCDC57	-0.5922145	1.40E-06	3.05E-05	down
ENSG00000116117	PARD3B	-0.8098286	1.42E-06	3.08E-05	down
ENSG00000169231	THBS3	-0.725818	1.44E-06	3.11E-05	down
ENSG00000136867	SLC31A2	-0.7832484	1.46E-06	3.14E-05	down
ENSG00000126775	ATG14	-0.6613949	1.46E-06	3.14E-05	down
ENSG00000044524	EPHA3	-1.2420698	1.46E-06	3.15E-05	down
ENSG00000266934	AC005746.1	-1.2257664	1.47E-06	3.16E-05	down
ENSG00000163762	TM4SF18	-1.3684306	1.61E-06	3.42E-05	down
ENSG00000274173	AL035661.1	-0.6493492	1.66E-06	3.52E-05	down
ENSG00000133639	BTG1	-0.6669044	1.75E-06	3.68E-05	down
ENSG00000169862	CTNND2	-0.6249882	1.82E-06	3.79E-05	down
ENSG00000124257	NEURL2	-1.2137851	1.83E-06	3.80E-05	down
ENSG00000156453	PCDH1	-0.7541344	1.87E-06	3.88E-05	down
ENSG00000203814	HIST2H2BF	-0.8420211	2.05E-06	4.24E-05	down
ENSG00000102554	KLF5	-0.6728578	2.07E-06	4.27E-05	down
ENSG00000173193	PARP14	-0.6605671	2.09E-06	4.31E-05	down
ENSG00000163840	DTX3L	-0.6406502	2.19E-06	4.49E-05	down
ENSG00000279930	AL032819.2	-1.3265049	2.36E-06	4.80E-05	down
ENSG00000001460	STPG1	-0.9206381	2.41E-06	4.89E-05	down
ENSG00000223478	AL441992.1	-0.8401367	2.48E-06	5.02E-05	down
ENSG00000177410	ZFAS1	-0.6434576	2.50E-06	5.04E-05	down
ENSG00000240216	CPHL1P	-1.2170336	2.60E-06	5.20E-05	down
ENSG00000215386	MIR99AHG	-1.1525921	2.62E-06	5.23E-05	down
ENSG00000112419	PHACTR2	-0.709516	2.74E-06	5.43E-05	down
ENSG00000182912	TSPEAR-AS2	-1.2703333	2.73E-06	5.43E-05	down
ENSG00000108786	HSD17B1	-0.879025	2.74E-06	5.43E-05	down

ENSG00000273802	HIST1H2BG	-0.8121484	2.81E-06	5.55E-05	down
ENSG00000168702	LRP1B	-0.7308122	2.90E-06	5.70E-05	down
ENSG00000185532	PRKG1	-1.0048147	2.92E-06	5.73E-05	down
ENSG00000007255	TRAPPC6A	-0.6158353	2.97E-06	5.80E-05	down
ENSG00000176834	VSIG10	-0.631264	3.04E-06	5.91E-05	down
ENSG00000155158	TTC39B	-0.7179237	3.09E-06	5.98E-05	down
ENSG00000197191	CYSRT1	-0.7572729	3.08E-06	5.98E-05	down
ENSG00000269386	RAB11B-AS1	-1.0398917	3.15E-06	6.08E-05	down
ENSG00000101850	GPR143	-0.7157681	3.23E-06	6.22E-05	down
ENSG00000111859	NEDD9	-0.6899818	3.31E-06	6.36E-05	down
ENSG00000105327	BBC3	-0.704241	3.32E-06	6.37E-05	down
ENSG00000135709	KIAA0513	-0.6659096	3.42E-06	6.53E-05	down
ENSG00000106479	ZNF862	-0.6177872	3.47E-06	6.61E-05	down
ENSG00000132561	MATN2	-0.5892807	3.56E-06	6.76E-05	down
ENSG00000215472	RPL17-C18orf32	-1.2739409	3.58E-06	6.79E-05	down
ENSG00000125999	BPIFB1	-1.3361264	3.61E-06	6.83E-05	down
ENSG00000100784	RPS6KA5	-0.6878775	3.79E-06	7.15E-05	down
ENSG00000249319	AC068533.4	-0.7731801	3.90E-06	7.33E-05	down
ENSG00000066468	FGFR2	-0.726539	3.98E-06	7.45E-05	down
ENSG00000159388	BTG2	-0.6155069	4.08E-06	7.62E-05	down
ENSG00000179163	FUCA1	-0.5903768	4.25E-06	7.91E-05	down
ENSG00000134291	TMEM106C	-0.5956511	4.56E-06	8.44E-05	down
ENSG00000167964	RAB26	-0.7274245	4.72E-06	8.69E-05	down
ENSG00000263155	MYZAP	-1.2082255	4.77E-06	8.77E-05	down
ENSG00000141738	GRB7	-0.8687531	4.89E-06	8.97E-05	down
ENSG00000243749	TMEM35B	-0.7111741	4.90E-06	8.97E-05	down
ENSG00000176209	SMIM19	-0.6481743	4.98E-06	9.10E-05	down
ENSG00000030419	IKZF2	-0.7997313	5.05E-06	9.19E-05	down
ENSG00000273151	AC073957.3	-0.8143501	5.04E-06	9.19E-05	down
ENSG00000127540	UQCR11	-0.6011875	5.08E-06	9.22E-05	down
ENSG00000105519	CAPS	-0.619165	5.24E-06	9.50E-05	down
ENSG00000255398	HCAR3	-1.3151974	5.42E-06	9.78E-05	down
ENSG00000234616	JRK	-0.6545443	5.49E-06	9.89E-05	down
ENSG00000157399	ARSE	-0.7608408	5.55E-06	9.94E-05	down
ENSG00000258334	AC125611.4	-1.0990885	5.82E-06	0.00010332	down
ENSG00000113580	NR3C1	-0.6390771	5.95E-06	0.00010545	down
ENSG00000211452	DIO1	-1.278734	6.01E-06	0.00010623	down
ENSG00000185518	SV2B	-1.1161172	6.03E-06	0.00010637	down
ENSG00000069812	HES2	-0.6309467	6.06E-06	0.00010682	down
ENSG00000149809	TM7SF2	-0.6019462	6.15E-06	0.00010811	down

ENSG00000241720	AL158847.1	-1.0729146	6.22E-06	0.0001093	down
ENSG00000158828	PINK1	-0.6838293	6.30E-06	0.00011043	down
ENSG00000226200	SGMS1-AS1	-1.0117529	6.40E-06	0.00011215	down
ENSG00000284540	AC066615.1	-1.2905311	6.70E-06	0.0001168	down
ENSG00000089289	IGBP1	-0.6144352	6.80E-06	0.00011819	down
ENSG00000267750	RUNDC3A-AS1	-0.6907987	6.93E-06	0.00012008	down
ENSG00000279692	AC110285.7	-1.020801	7.18E-06	0.00012381	down
ENSG00000156804	FBXO32	-0.8715064	7.51E-06	0.00012887	down
ENSG00000120708	TGFBI	-0.840539	7.66E-06	0.00013055	down
ENSG00000229312	AL353693.1	-1.1446429	8.06E-06	0.00013731	down
ENSG00000114770	ABCC5	-0.7259819	8.09E-06	0.00013761	down
ENSG00000256683	ZNF350	-0.7786163	9.13E-06	0.00015359	down
ENSG00000158286	RNF207	-1.0276857	9.18E-06	0.00015431	down
ENSG00000008853	RHOBTB2	-0.6090102	9.45E-06	0.00015855	down
ENSG00000162927	PUS10	-0.81441	9.77E-06	0.00016323	down
ENSG00000244270	AL139099.1	-1.1626107	9.76E-06	0.00016323	down
ENSG00000175938	ORAI3	-0.6136374	9.79E-06	0.0001634	down
ENSG00000074370	ATP2A3	-0.6388534	9.81E-06	0.0001635	down
ENSG00000278677	HIST1H2AM	-0.9888646	1.00E-05	0.00016695	down
ENSG00000143952	VPS54	-0.5933911	1.01E-05	0.000167	down
ENSG00000125356	NDUFA1	-0.6011949	1.01E-05	0.00016786	down
ENSG00000171105	INSR	-0.82842	1.03E-05	0.00017052	down
ENSG00000101846	STS	-0.8340738	1.05E-05	0.00017298	down
ENSG00000205890	AC108134.1	-0.74176	1.05E-05	0.0001731	down
ENSG00000196730	DAPK1	-1.2449842	1.07E-05	0.00017663	down
ENSG00000116574	RHOU	-0.6701351	1.13E-05	0.0001853	down
ENSG00000121858	TNFSF10	-1.2287129	1.21E-05	0.00019663	down
ENSG00000223891	OSER1-AS1	-0.7620456	1.27E-05	0.00020541	down
ENSG00000272079	AC004233.3	-0.7374256	1.28E-05	0.00020601	down
ENSG00000171443	ZNF524	-0.6550097	1.31E-05	0.00021004	down
ENSG00000178568	ERBB4	-0.8359857	1.30E-05	0.00021004	down
ENSG00000205189	ZBTB10	-0.5891007	1.34E-05	0.00021514	down
ENSG00000004799	PDK4	-1.0279084	1.36E-05	0.00021731	down
ENSG00000148671	ADIRF	-0.6805153	1.52E-05	0.00024006	down
ENSG00000153246	PLA2R1	-0.7799167	1.62E-05	0.00025302	down
ENSG00000149212	SESN3	-0.6480947	1.65E-05	0.0002565	down
ENSG00000105518	TMEM205	-0.5920443	1.65E-05	0.0002565	down
ENSG00000135926	TMBIM1	-0.705956	1.67E-05	0.00025871	down
ENSG00000235277	AF127577.3	-0.8958075	1.68E-05	0.00025963	down
ENSG00000246985	SOCS2-AS1	-1.1718832	1.68E-05	0.00025963	down

ENSG00000134201	GSTM5	-1.0777498	1.69E-05	0.00026113	down
ENSG00000171476	HOPX	-1.1914021	1.70E-05	0.00026254	down
ENSG00000253958	CLDN23	-0.70767	1.77E-05	0.00027258	down
ENSG00000095585	BLNK	-1.0048112	1.82E-05	0.00027998	down
ENSG00000168026	TTC21A	-0.9902836	1.83E-05	0.00028069	down
ENSG00000184154	LRTOMT	-0.6238123	1.87E-05	0.00028532	down
ENSG00000168928	CTRB2	-1.1632503	1.88E-05	0.0002871	down
ENSG00000279924	AL356585.4	-0.7648582	1.90E-05	0.00028876	down
ENSG00000146278	PNRC1	-0.6228907	1.92E-05	0.00029197	down
ENSG00000166750	SLFN5	-0.816826	1.93E-05	0.00029219	down
ENSG00000104883	PEX11G	-0.9508547	1.94E-05	0.00029416	down
ENSG00000132141	CCT6B	-0.964884	1.99E-05	0.0002998	down
ENSG00000104419	NDRG1	-0.6517701	2.03E-05	0.00030433	down
ENSG00000130005	GAMT	-0.6997229	2.05E-05	0.00030633	down
ENSG00000119899	SLC17A5	-0.65798	2.04E-05	0.00030633	down
ENSG00000120725	SIL1	-0.6071205	2.05E-05	0.00030644	down
ENSG00000078142	PIK3C3	-0.7230095	2.09E-05	0.00031127	down
ENSG00000110080	ST3GAL4	-0.6325263	2.13E-05	0.0003164	down
ENSG00000179818	PCBP1-AS1	-0.6507529	2.18E-05	0.0003241	down
ENSG00000196139	AKR1C3	-1.1340898	2.21E-05	0.00032781	down
ENSG00000149260	CAPN5	-0.6966467	2.35E-05	0.00034444	down
ENSG00000111653	ING4	-0.7993052	2.38E-05	0.00034887	down
ENSG00000196159	FAT4	-1.1489654	2.43E-05	0.00035627	down
ENSG00000223564	CYP4F32P	-0.9881232	2.46E-05	0.00035938	down
ENSG00000230590	FTX	-0.6830851	2.55E-05	0.00037031	down
ENSG00000120833	SOCS2	-0.7067212	2.58E-05	0.00037318	down
ENSG00000233198	RNF224	-0.9273069	2.59E-05	0.00037367	down
ENSG00000261235	AC092142.1	-1.0229042	2.59E-05	0.00037367	down
ENSG00000150347	ARID5B	-0.7177361	2.61E-05	0.00037688	down
ENSG00000131781	FMO5	-0.7215851	2.76E-05	0.00039406	down
ENSG00000143365	RORC	-0.7156291	2.76E-05	0.00039441	down
ENSG00000267795	SMIM22	-0.7664732	2.93E-05	0.00041583	down
ENSG00000055163	CYFIP2	-0.6293979	2.95E-05	0.00041828	down
ENSG00000166920	C15orf48	-0.8608673	3.09E-05	0.00043403	down
ENSG00000251615	AC104825.3	-1.2068537	3.16E-05	0.00044144	down
ENSG00000101384	JAG1	-0.6634344	3.15E-05	0.00044144	down
ENSG00000165240	ATP7A	-0.6006228	3.23E-05	0.00044975	down
ENSG00000006756	ARSD	-0.5895764	3.36E-05	0.00046545	down
ENSG00000256073	URB1-AS1	-0.5876925	3.38E-05	0.00046723	down
ENSG00000137936	BCAR3	-0.6535094	3.64E-05	0.00049942	down
ENSG00000103056	SMPD3	-1.0586499	3.70E-05	0.0005061	down

ENSG00000120925	RNF170	-0.6586485	3.80E-05	0.00051746	down
ENSG00000100300	TSPO	-0.6662624	3.82E-05	0.00051946	down
ENSG00000080224	EPHA6	-0.8796221	3.94E-05	0.00053207	down
ENSG00000095383	TBC1D2	-0.6490993	3.99E-05	0.00053718	down
ENSG00000171522	PTGER4	-0.730211	3.99E-05	0.00053792	down
ENSG00000260285	AL133367.1	-0.6874418	4.00E-05	0.00053849	down
ENSG00000260025	AC009414.2	-0.9557009	4.02E-05	0.0005406	down
ENSG00000264920	AC018521.5	-0.7507465	4.16E-05	0.00055787	down
ENSG00000236830	CBR3-AS1	-0.7257713	4.18E-05	0.00056067	down
ENSG00000168890	TMEM150A	-0.6998336	4.23E-05	0.0005654	down
ENSG00000110436	SLC1A2	-0.7986793	4.32E-05	0.00057439	down
ENSG00000091136	LAMB1	-0.6335281	4.35E-05	0.00057892	down
ENSG00000260337	AC091544.5	-1.1858262	4.39E-05	0.00058375	down
ENSG00000143416	SELENBP1	-0.5900511	4.65E-05	0.00061333	down
ENSG00000228492	RAB11FIP1P1	-0.9882775	4.86E-05	0.00063809	down
ENSG00000169908	TM4SF1	-0.9685667	4.95E-05	0.00064805	down
ENSG00000170367	CST5	-1.1749318	4.96E-05	0.0006498	down
ENSG00000166387	PPFIBP2	-0.7686778	4.97E-05	0.00064985	down
ENSG00000261776	AC079414.2	-1.1485563	5.03E-05	0.00065625	down
ENSG00000139112	GABARAPL1	-0.9190855	5.08E-05	0.00065961	down
ENSG00000235863	B3GALT4	-0.7444506	5.20E-05	0.00067225	down
ENSG00000162069	BICDL2	-0.6164874	5.25E-05	0.00067759	down
ENSG00000108187	PBLD	-0.6650136	5.31E-05	0.00068412	down
ENSG00000138640	FAM13A	-1.0208578	5.43E-05	0.00069598	down
ENSG00000142973	CYP4B1	-0.9560003	5.53E-05	0.00070775	down
ENSG00000154856	APCDD1	-0.7901031	5.68E-05	0.00072549	down
ENSG00000137648	TMPRSS4	-0.7092108	5.96E-05	0.0007559	down
ENSG00000218227	AC136632.1	-1.1639341	6.02E-05	0.00076226	down
ENSG00000278864	AC055811.4	-0.9061737	6.08E-05	0.000769	down
ENSG00000174500	GCSAM	-1.1283452	6.09E-05	0.0007699	down
ENSG00000231312	AC007388.1	-0.7592873	6.14E-05	0.0007756	down
ENSG00000182919	C11orf54	-0.6460556	6.26E-05	0.00078742	down
ENSG00000174456	C12orf76	-0.635918	6.31E-05	0.00079338	down
ENSG00000279759	AC118344.2	-0.8069914	6.36E-05	0.00079696	down
ENSG00000169247	SH3TC2	-1.103236	6.48E-05	0.00081064	down
ENSG00000179841	AKAP5	-0.6489415	6.53E-05	0.00081429	down
ENSG00000142279	WTIP	-0.7635797	6.70E-05	0.00083403	down
ENSG00000106018	VIPR2	-0.6282852	6.72E-05	0.00083568	down
ENSG00000087085	ACHE	-0.9081425	6.75E-05	0.00083786	down
ENSG00000174628	IQCK	-0.8001263	7.16E-05	0.00088225	down
ENSG00000140937	CDH11	-0.8472506	7.33E-05	0.00090015	down

ENSG00000166262	FAM227B	-0.7739259	7.42E-05	0.00090829	down
ENSG00000113971	NPHP3	-0.7227816	8.08E-05	0.00097959	down
ENSG00000224940	PRRT4	-0.866859	8.24E-05	0.00099605	down
ENSG00000013392	RWDD2A	-0.7467408	8.31E-05	0.00100288	down
ENSG00000239521	GATS	-0.6617794	8.76E-05	0.0010527	down
ENSG00000257261	AC008014.1	-0.6572118	9.13E-05	0.00108906	down
ENSG00000164010	ERMAP	-0.6442074	9.13E-05	0.00108906	down
ENSG00000263004	AC007114.1	-0.8426602	9.36E-05	0.00111437	down
ENSG00000185386	MAPK11	-0.6060594	9.48E-05	0.00112637	down
ENSG00000258539	AC068896.1	-0.7492296	9.53E-05	0.00113004	down
ENSG00000280156	AC006548.3	-0.6494641	9.56E-05	0.00113056	down
ENSG00000135773	CAPN9	-0.9100672	9.73E-05	0.00114594	down
ENSG00000130518	KIAA1683	-0.7505597	9.87E-05	0.00116084	down
ENSG00000183049	CAMK1D	-0.6155721	9.94E-05	0.00116711	down
ENSG00000145147	SLIT2	-1.0292122	0.00010001	0.00117288	down
ENSG00000230798	FOXD3-AS1	-0.7554329	0.00010195	0.00119154	down
ENSG00000165716	FAM69B	-0.6696659	0.00010706	0.00124258	down
ENSG00000135373	EHF	-1.0993107	0.00010719	0.00124323	down
ENSG00000224660	SH3BP5-AS1	-0.8025312	0.00011281	0.00129651	down
ENSG00000203709	C1orf132	-0.8083853	0.00011327	0.00130032	down
ENSG00000262772	LINC01977	-0.5870805	0.00011664	0.00133442	down
ENSG00000182568	SATB1	-1.0727565	0.00012125	0.00138061	down
ENSG00000259673	IQCH-AS1	-0.6250395	0.00012526	0.00142137	down
ENSG00000172197	MBOAT1	-0.5934729	0.0001262	0.00142629	down
ENSG00000163141	BNIPL	-0.7222085	0.00012618	0.00142629	down
ENSG00000203635	AC144450.1	-0.8608623	0.00013056	0.00146966	down
ENSG00000230021	AL669831.3	-0.9359376	0.00013192	0.00148393	down
ENSG00000196074	SYCP2	-0.6241752	0.00013459	0.0015049	down
ENSG00000247011	AC005920.1	-1.1076686	0.00013496	0.00150603	down
ENSG00000154342	WNT3A	-0.9752736	0.00013509	0.00150603	down
ENSG00000143224	PPOX	-0.6301418	0.00013907	0.00154166	down
ENSG00000225791	TRAM2-AS1	-0.7168695	0.00014692	0.00161491	down
ENSG00000257949	TEN1	-0.6161777	0.00015281	0.00167193	down
ENSG00000243926	TIPARP-AS1	-0.8932326	0.00015489	0.00168811	down
ENSG00000164117	FBXO8	-0.633465	0.0001553	0.00169038	down
ENSG00000187240	DYNC2H1	-0.6562309	0.00015924	0.00172769	down
ENSG00000127249	ATP13A4	-1.0947757	0.00016197	0.0017502	down
ENSG00000233822	HIST1H2BN	-0.746174	0.00016677	0.00179318	down
ENSG00000018280	SLC11A1	-0.9013889	0.00017058	0.0018306	down
ENSG00000187689	AMTN	-1.0882602	0.00017689	0.00188514	down
ENSG00000070526	ST6GALNAC1	-1.076645	0.00017924	0.00190649	down

ENSG00000072818	ACAP1	-0.594644	0.00017945	0.00190755	down
ENSG00000196511	TPK1	-0.7496356	0.00018019	0.00191299	down
ENSG00000139714	MORN3	-0.9085526	0.00018042	0.00191426	down
ENSG00000124370	MCEE	-0.7243074	0.00018515	0.00195327	down
ENSG00000274928	KRT89P	-1.0571152	0.00018578	0.00195876	down
ENSG00000168016	TRANK1	-0.6851196	0.0001887	0.00198329	down
ENSG00000175894	TSPEAR	-0.8729647	0.00019325	0.00202355	down
ENSG00000281005	LINC00921	-0.9971849	0.00019501	0.00204071	down
ENSG00000177822	AC098864.1	-0.7501514	0.00020354	0.00211281	down
ENSG00000102796	DHRS12	-0.7852254	0.0002038	0.00211425	down
ENSG00000165434	PGM2L1	-0.755186	0.00020499	0.00212131	down
ENSG00000185291	IL3RA	-0.7322778	0.0002064	0.00213459	down
ENSG00000280254	AC233723.2	-0.6625102	0.0002068	0.00213739	down
ENSG00000127720	METTL25	-0.6380917	0.00020775	0.00214493	down
ENSG00000233223	AC016876.1	-0.6807472	0.00020791	0.00214493	down
ENSG00000180251	SLC9A4	-1.0127074	0.00020965	0.00215894	down
ENSG00000217442	SYCE3	-1.014585	0.0002108	0.00216807	down
ENSG00000119636	BBOF1	-0.7824405	0.00021397	0.00219664	down
ENSG00000198157	HMGN5	-0.7760704	0.00022261	0.00227288	down
ENSG00000257084	MIR200CHG	-0.8087362	0.00023022	0.00233582	down
ENSG00000250786	SNHG18	-0.8379475	0.00023275	0.00235493	down
ENSG00000152582	SPEF2	-0.8394021	0.00024792	0.00249342	down
ENSG00000203288	TDRKH-AS1	-0.6204647	0.00025779	0.00257886	down
ENSG00000186496	ZNF396	-0.8429749	0.00026457	0.00263709	down
ENSG00000185112	FAM43A	-0.6682746	0.00028042	0.00277496	down
ENSG00000164056	SPRY1	-0.9884205	0.00028111	0.00277737	down
ENSG00000169122	FAM110B	-0.8856054	0.00028169	0.00277985	down
ENSG00000115705	TPO	-0.8564093	0.00028892	0.00284326	down
ENSG00000053108	FSTL4	-0.7041789	0.00028929	0.00284468	down
ENSG00000185168	LINC00482	-0.9046836	0.00029103	0.00285528	down
ENSG00000240065	PSMB9	-0.8693949	0.00029147	0.00285541	down
ENSG00000184254	ALDH1A3	-0.729869	0.00029746	0.00290473	down
ENSG00000172296	SPTLC3	-1.0279272	0.00029978	0.00292575	down
ENSG00000167131	CCDC103	-0.9737949	0.0003052	0.00296656	down
ENSG00000139364	TMEM132B	-0.9019076	0.00030574	0.00296837	down
ENSG00000240338	AC009078.2	-1.0003677	0.00030754	0.00298241	down
ENSG00000213355	CNN2P8	-1.0319602	0.00030994	0.00300225	down
ENSG00000157703	SVOPL	-0.9950239	0.00031329	0.00302596	down
ENSG00000130653	PNPLA7	-0.6388809	0.00031892	0.00306446	down
ENSG00000176920	FUT2	-0.9511098	0.00033231	0.00316954	down
ENSG00000186132	C2orf76	-0.5851912	0.00033376	0.00318162	down

ENSG00000234949	AC104667.2	-0.7509585	0.00033433	0.00318502	down
ENSG00000197766	CFD	-0.725146	0.00033847	0.0032137	down
ENSG00000281501	AC104662.3	-0.7765008	0.00034279	0.00324374	down
ENSG00000140876	NUDT7	-0.6674463	0.00034484	0.00326132	down
ENSG00000114656	KIAA1257	-0.7395821	0.0003593	0.00337342	down
ENSG00000272732	AC004982.1	-0.9994655	0.00037252	0.00347231	down
ENSG00000266903	AC243964.2	-1.0320637	0.00037653	0.00350583	down
ENSG00000170369	CST2	-1.0257321	0.00038301	0.00355352	down
ENSG00000266970	AC061992.1	-0.9482687	0.00039447	0.00362263	down
ENSG00000168032	ENTPD3	-1.0042685	0.0003959	0.00363377	down
ENSG00000116016	EPAS1	-0.6139565	0.00040201	0.00367987	down
ENSG00000135842	FAM129A	-0.7140518	0.00042336	0.00384176	down
ENSG00000258701	LINC00638	-0.6980464	0.00042731	0.00387138	down
ENSG00000179082	C9orf106	-0.8025581	0.00042838	0.00387899	down
ENSG00000151303	AL136982.1	-0.9652015	0.00043013	0.00389064	down
ENSG00000086619	ERO1B	-0.7173405	0.00043058	0.00389255	down
ENSG00000121361	KCNJ8	-1.017415	0.00043529	0.00392674	down
ENSG00000126016	AMOT	-0.6583964	0.00045567	0.00408648	down
ENSG00000198691	ABCA4	-1.0105042	0.00047971	0.00425548	down
ENSG00000243069	ARHGEF26-AS1	-0.9253135	0.00048456	0.00429056	down
ENSG00000236699	ARHGEF38	-0.9171874	0.00049171	0.00433558	down
ENSG00000280776	AC021079.1	-0.712299	0.00050253	0.00441021	down
ENSG00000197647	ZNF433	-0.5920612	0.00051393	0.00449614	down
ENSG00000173467	AGR3	-0.5875368	0.00051551	0.00450125	down
ENSG00000189058	APOD	-0.7500056	0.00054657	0.00473243	down
ENSG00000090539	CHRD	-0.9048549	0.00054818	0.00474395	down
ENSG00000256043	CTSO	-0.9995602	0.00055538	0.00479147	down
ENSG00000258830	AC137834.1	-0.775214	0.00055999	0.00482871	down
ENSG00000184374	COLEC10	-0.9743454	0.00056814	0.00489399	down
ENSG00000130433	CACNG6	-0.9911802	0.00057348	0.00492987	down
ENSG00000103888	CEMIP	-0.7343352	0.00057592	0.00494834	down
ENSG00000163818	LZTFL1	-0.648774	0.00057634	0.00494943	down
ENSG00000269893	SNHG8	-0.6046634	0.00059438	0.0050835	down
ENSG00000274750	HIST1H3E	-0.6328105	0.00060808	0.00517963	down
ENSG00000156050	FAM161B	-0.6123517	0.0006243	0.00530975	down
ENSG00000189127	ANKRD34B	-0.7804546	0.00062801	0.00533856	down
ENSG00000096006	CRISP3	-0.9480829	0.00062851	0.0053401	down
ENSG00000197050	ZNF420	-0.6930109	0.00067467	0.00565226	down
ENSG00000231133	HAR1B	-0.8044802	0.00068374	0.00571654	down
ENSG00000116885	OSCP1	-0.6955758	0.0006879	0.00573743	down

ENSG00000165078	CPA6	-0.9814142	0.00068882	0.00574218	down
ENSG00000176399	DMRTA1	-0.7634748	0.00069965	0.00581369	down
ENSG00000186088	GSAP	-0.7554913	0.00069997	0.00581369	down
ENSG00000170222	ADPRM	-0.8564155	0.00071395	0.0059048	down
ENSG00000183844	FAM3B	-0.978386	0.00071816	0.00593675	down
ENSG00000088881	EBF4	-0.715028	0.00072303	0.00596822	down
ENSG00000272288	AL451165.2	-0.7952328	0.00072587	0.00598278	down
ENSG00000166275	BORCS7	-0.6088643	0.0007349	0.00604239	down
ENSG00000181634	TNFSF15	-0.9508148	0.00074905	0.00613891	down
ENSG00000255346	NOX5	-0.7213221	0.00075103	0.00615099	down
ENSG00000137628	DDX60	-0.9379133	0.00075404	0.00617264	down
ENSG00000100373	UPK3A	-0.9686157	0.00076065	0.00621749	down
ENSG00000088538	DOCK3	-0.6798946	0.00078495	0.0063575	down
ENSG00000143036	SLC44A3	-0.9499018	0.0008029	0.0064745	down
ENSG00000217576	AL158066.1	-0.7629216	0.00080377	0.0064756	down
ENSG00000135363	LMO2	-0.7394998	0.00084443	0.00677399	down
ENSG00000224008	LINC01441	-0.9420494	0.00087308	0.0069619	down
ENSG00000158423	RIBC1	-0.6943225	0.00087799	0.00698981	down
ENSG00000172264	MACROD2	-0.6017415	0.00088577	0.00704172	down
ENSG00000271614	ATP2B1-AS1	-0.6550538	0.00096496	0.00754286	down
ENSG00000239665	AL157392.3	-0.6434737	0.00096544	0.00754307	down
ENSG00000254531	FLJ20021	-0.6349954	0.00097067	0.00756989	down
ENSG00000100027	YPEL1	-0.8447373	0.00097165	0.00757402	down
ENSG00000115257	PCSK4	-0.841557	0.00097559	0.00759765	down
ENSG00000278817	AC007325.4	-0.6110949	0.0010015	0.00776707	down
ENSG00000085741	WNT11	-0.7819887	0.00101149	0.00781927	down
ENSG00000172824	CES4A	-0.6456583	0.00103046	0.00793935	down
ENSG00000254231	AC103760.1	-0.9465357	0.00103175	0.00793935	down
ENSG00000069667	RORA	-0.6349752	0.00103626	0.00796523	down
ENSG00000014257	ACPP	-0.6843039	0.00103653	0.00796523	down
ENSG00000271853	AL162258.1	-0.680166	0.00104603	0.00801705	down
ENSG00000280424	BX537318.2	-0.9164897	0.00105828	0.00808795	down
ENSG00000167614	TTYH1	-0.919269	0.00108294	0.00823896	down
ENSG00000225978	HAR1A	-0.887646	0.00113302	0.00855801	down
ENSG00000169347	GP2	-0.9292888	0.00113721	0.00858195	down
ENSG00000066923	STAG3	-0.6383446	0.00114996	0.00866259	down
ENSG00000104755	ADAM2	-0.8552606	0.00115424	0.00868065	down
ENSG00000258938	AL162311.3	-0.7920189	0.00116573	0.00875001	down
ENSG00000161328	LRRC56	-0.6122328	0.00119621	0.00892827	down
ENSG00000050628	PTGER3	-0.9370515	0.00121663	0.00904719	down
ENSG00000271474	AC106881.1	-0.905599	0.00122889	0.00911938	down

ENSG00000172164	SNTB1	-0.7796544	0.00123752	0.00916899	down
ENSG00000178385	PLEKHM3	-0.6919327	0.00127563	0.00941925	down
ENSG00000241484	ARHGAP8	-0.5872253	0.00130741	0.00959075	down
ENSG00000282988	HIST1H3D	-0.6477031	0.00132406	0.00969169	down
ENSG00000185522	LMNTD2	-0.6334612	0.00141198	0.01020192	down
ENSG00000267666	AC004156.1	-0.8781377	0.00143898	0.0103614	down
ENSG00000099338	CATSPERG	-0.6624555	0.00145695	0.01046996	down
ENSG00000277496	AL357033.4	-0.8962816	0.00146563	0.01050381	down
ENSG00000165171	METTL27	-0.7433124	0.00148947	0.01064412	down
ENSG00000249684	AC106795.2	-0.8786547	0.0015071	0.01073691	down
ENSG00000170396	ZNF804A	-0.8946656	0.00151748	0.01078342	down
ENSG00000136059	VILL	-0.8307773	0.00164245	0.01152525	down
ENSG00000240423	LINC00636	-0.7134557	0.00165349	0.01158824	down
ENSG00000120915	EPHX2	-0.6550454	0.00166972	0.01168737	down
ENSG00000181513	ACBD4	-0.6237827	0.00167318	0.0117018	down
ENSG00000272894	AC004982.2	-0.8505567	0.00167648	0.01171514	down
ENSG00000280152	AC009078.3	-0.6559822	0.00168323	0.01175745	down
ENSG00000171174	RBKS	-0.7279799	0.00168856	0.01177644	down
ENSG00000274985	PTCHD3P1	-0.8968627	0.00170808	0.0118964	down
ENSG00000130751	NPAS1	-0.840463	0.00173582	0.01204034	down
ENSG00000172551	MUCL1	-0.6509073	0.00174594	0.01209493	down
ENSG00000164683	HEY1	-0.8085494	0.00176063	0.01218161	down
ENSG00000256443	AP003559.1	-0.7912525	0.00182369	0.01255077	down
ENSG00000232859	LYRM9	-0.6429872	0.00183588	0.01261911	down
ENSG00000255471	AP001528.2	-0.8277604	0.00184558	0.01266507	down
ENSG00000225968	ELFN1	-0.643955	0.00184422	0.01266507	down
ENSG00000220793	AC087190.1	-0.8649348	0.00185462	0.01271678	down
ENSG00000109794	FAM149A	-0.7079147	0.00188001	0.01285935	down
ENSG00000270177	AC104109.2	-0.8488591	0.00193007	0.01312695	down
ENSG00000154721	JAM2	-0.8471982	0.00193967	0.01317627	down
ENSG00000185666	SYN3	-0.8765529	0.00196903	0.01333259	down
ENSG00000278921	EPB41L4A-AS2	-0.7914254	0.00197526	0.0133479	down
ENSG00000268416	AC010329.1	-0.6978672	0.00197671	0.01335232	down
ENSG00000237489	LINC00959	-0.6028185	0.00197757	0.01335275	down
ENSG00000277701	AC159540.2	-0.8737653	0.0020156	0.01356781	down
ENSG00000154099	DNAAF1	-0.7505879	0.00201836	0.01357441	down
ENSG00000250986	AC141928.1	-0.649645	0.00202078	0.01358449	down
ENSG00000256618	MTRNR2L1	-0.8910221	0.00209006	0.01394422	down
ENSG00000255498	AC068385.1	-0.8806819	0.00209911	0.01398795	down
ENSG00000130813	C19orf66	-0.6005518	0.00214944	0.01426115	down

ENSG00000234678	ELF3-AS1	-0.8451108	0.0021553	0.01427746	down
ENSG00000273361	AC021016.3	-0.8759737	0.00216472	0.01432292	down
ENSG00000282851	BISPR	-0.6515654	0.0022198	0.01462981	down
ENSG00000124343	XG	-0.6983967	0.00223688	0.0147308	down
ENSG00000186326	RGS9BP	-0.7425172	0.00228904	0.01497452	down
ENSG00000249661	TNRC18P1	-0.8100959	0.00232908	0.01515391	down
ENSG00000149922	TBX6	-0.6775304	0.00240933	0.01556758	down
ENSG00000101203	COL20A1	-0.8538829	0.00242102	0.01563709	down
ENSG00000104059	FAM189A1	-0.7591995	0.00256983	0.0164465	down
ENSG00000168589	DYNLRB2	-0.8507146	0.00260672	0.01663825	down
ENSG00000004848	ARX	-0.7469472	0.00260883	0.0166454	down
ENSG00000261812	TUBB8P7	-0.7097926	0.00262764	0.01673367	down
ENSG00000281453	TGFB2-OT1	-0.8536511	0.00263697	0.01678037	down
ENSG00000172748	ZNF596	-0.6862705	0.00264252	0.0168093	down
ENSG00000046653	GPM6B	-0.8095498	0.00264403	0.01681255	down
ENSG00000213443	AC007068.1	-0.8602856	0.00269274	0.01704491	down
ENSG00000175463	TBC1D10C	-0.7500829	0.00272543	0.0172194	down
ENSG00000230836	LINC01293	-0.8631803	0.00278884	0.017554	down
ENSG00000226754	AL606760.1	-0.7168788	0.00281115	0.01765501	down
ENSG00000272514	CFAP206	-0.7121388	0.00282657	0.01772656	down
ENSG00000175318	GRAMD2	-0.8176076	0.00292289	0.01822198	down
ENSG00000130544	ZNF557	-0.5894073	0.00294811	0.01835033	down
ENSG00000179071	CCDC89	-0.8595313	0.00304922	0.01884707	down
ENSG00000137819	PAQR5	-0.6564489	0.00311855	0.0192261	down
ENSG00000270571	AC007681.1	-0.8116597	0.00312319	0.01924766	down
ENSG00000276075	AC027682.6	-0.8485033	0.00317937	0.01953189	down
ENSG00000157654	PALM2-AKAP2	-0.8272991	0.00320613	0.01967222	down
ENSG00000268628	AL121761.2	-0.8217304	0.00323714	0.01983351	down
ENSG00000104870	FCGRT	-0.8112544	0.00325044	0.01989958	down
ENSG00000231107	LINC01508	-0.8256548	0.00325908	0.01992435	down
ENSG00000169894	MUC3A	-0.5936013	0.00332847	0.02028954	down
ENSG00000233750	CICP27	-0.6218258	0.00341685	0.02065594	down
ENSG00000158270	COLEC12	-0.7327908	0.00346038	0.0208591	down
ENSG00000167733	HSD11B1L	-0.748487	0.00348455	0.02098975	down
ENSG00000159184	HOXB13	-0.7421685	0.00350187	0.02105629	down
ENSG00000225969	ABHD11-AS1	-0.8089714	0.00354501	0.02127006	down
ENSG00000278995	Z69720.2	-0.7559282	0.0035738	0.02141987	down
ENSG00000244486	SCARF2	-0.8127109	0.00361481	0.02156566	down
ENSG00000008311	AASS	-0.8321891	0.00362932	0.02162919	down
ENSG00000129946	SHC2	-0.7438289	0.00379476	0.02240068	down

ENSG00000244968	LIFR-AS1	-0.6317424	0.00388869	0.02285079	down
ENSG00000282933	RHOXF1P3	-0.6549272	0.00392439	0.0229509	down
ENSG00000166183	ASPG	-0.7312739	0.00398109	0.02318301	down
ENSG00000172159	FRMD3	-0.7576349	0.00400184	0.02328773	down
ENSG00000135338	LCA5	-0.6788053	0.00406299	0.02357827	down
ENSG00000116678	LEPR	-0.6273068	0.00411084	0.02380659	down
ENSG00000166823	MESP1	-0.7356346	0.0041568	0.02402312	down
ENSG00000109819	PPARGC1A	-0.6363927	0.00420816	0.02426151	down
ENSG00000133943	C14orf159	-0.6328454	0.00426223	0.02450559	down
ENSG00000139946	PELI2	-0.782214	0.00427563	0.02454108	down
ENSG00000269516	CYP4F23P	-0.8141908	0.00436258	0.02493794	down
ENSG00000133116	KL	-0.784237	0.00440261	0.02513258	down
ENSG00000214447	FAM187A	-0.6279586	0.00447532	0.02545392	down
ENSG00000169184	MN1	-0.8120545	0.00468525	0.02645844	down
ENSG00000260081	AF274858.3	-0.6577541	0.00477582	0.02683462	down
ENSG00000147576	ADHFE1	-0.7854558	0.00494499	0.02760063	down
ENSG00000173546	CSPG4	-0.7839189	0.00500025	0.0278628	down
ENSG00000178460	MCMDC2	-0.7967791	0.00502908	0.02801414	down
ENSG00000254718	AL157756.1	-0.8057417	0.00510668	0.02833374	down
ENSG00000172482	AGXT	-0.8042287	0.00511107	0.02834873	down
ENSG00000073605	GSDMB	-0.6517787	0.00511763	0.02836638	down
ENSG00000102313	ITIH6	-0.79425	0.00516789	0.02857975	down
ENSG00000079337	RAPGEF3	-0.6473827	0.00524296	0.02888011	down
ENSG00000225385	AL353572.1	-0.7489985	0.00527054	0.02899403	down
ENSG00000213145	CRIP1	-0.715953	0.00528547	0.02905712	down
ENSG00000231119	AL031666.1	-0.807616	0.00534947	0.02936093	down
ENSG00000128284	APOL3	-0.8004088	0.00539698	0.02950604	down
ENSG00000251143	AP002490.1	-0.7346301	0.00541744	0.02956021	down
ENSG00000151117	TMEM86A	-0.6284935	0.00544629	0.02970798	down
ENSG00000088340	FER1L4	-0.6514477	0.00554405	0.03015316	down
ENSG00000258279	LINC00592	-0.7977549	0.00557774	0.0302776	down
ENSG00000183023	SLC8A1	-0.626957	0.0056524	0.03059394	down
ENSG00000182612	TSPAN10	-0.7853633	0.0056993	0.03081803	down
ENSG00000279908	AC026748.1	-0.7903234	0.00593091	0.03181453	down
ENSG00000271780	AL118558.3	-0.6305881	0.00594363	0.03184207	down
ENSG00000274349	ZNF658	-0.7958345	0.0059783	0.03199723	down
ENSG00000251495	PPIAP11	-0.7227202	0.00603435	0.03221516	down
ENSG00000231672	DIRC3	-0.7964869	0.00606493	0.03234759	down
ENSG00000259583	AC015712.2	-0.7536242	0.00608861	0.03246359	down
ENSG00000226091	LINC00937	-0.7400313	0.00614844	0.0326996	down
ENSG00000244239	AC007009.1	-0.6171248	0.00628118	0.03322178	down

ENSG00000176896	TCEANC	-0.682251	0.00630346	0.0333027	down
ENSG00000158164	TMSB15A	-0.7877816	0.00639232	0.03364527	down
ENSG00000113448	PDE4D	-0.6796945	0.00664626	0.03463475	down
ENSG00000066185	ZMYND12	-0.7788779	0.00670007	0.03485031	down
ENSG00000171385	KCND3	-0.6210844	0.00677282	0.03516178	down
ENSG00000171116	HSFX1	-0.7653515	0.006795	0.03521332	down
ENSG00000235138	AL445931.1	-0.725683	0.00689621	0.03568277	down
ENSG00000198569	SLC34A3	-0.7206006	0.0070169	0.03620694	down
ENSG00000148655	LRMDA	-0.7736295	0.00702889	0.03625769	down
ENSG00000241288	AC092902.2	-0.6538693	0.0070597	0.03636083	down
ENSG00000011201	ANOS1	-0.6080795	0.00707898	0.03642999	down
ENSG00000187695	AC112484.1	-0.7770126	0.00730238	0.03729071	down
ENSG00000138670	RASGEF1B	-0.6796719	0.00730508	0.03729187	down
ENSG00000235890	TSPEAR-AS1	-0.7766216	0.00743959	0.03781211	down
ENSG00000169758	TMEM266	-0.765713	0.00775282	0.03910518	down
ENSG00000184845	DRD1	-0.7484012	0.00775309	0.03910518	down
ENSG00000139626	ITGB7	-0.710892	0.00775577	0.03910697	down
ENSG00000150676	CCDC83	-0.7636123	0.00839774	0.04173048	down
ENSG00000280300	AC117503.5	-0.7232837	0.00854867	0.04226801	down
ENSG00000196167	COLCA1	-0.7301589	0.00879622	0.04321231	down
ENSG00000162620	LRRIQ3	-0.7478903	0.00881472	0.0432779	down
ENSG00000121075	TBX4	-0.7330277	0.00882671	0.04331146	down
ENSG00000184384	MAML2	-0.7321888	0.00884398	0.04338349	down
ENSG00000255277	ABCC6P2	-0.7533033	0.00895679	0.04380902	down
ENSG00000246763	RGMB-AS1	-0.7469552	0.00905858	0.04417169	down
ENSG00000266820	KPNA2P3	-0.7073876	0.00916596	0.04462429	down
ENSG00000223865	HLA-DPB1	-0.7338358	0.00917485	0.04465464	down
ENSG00000188199	NUTM2B	-0.6120983	0.00919435	0.04473658	down
ENSG00000109680	TBC1D19	-0.6041969	0.00947397	0.04584495	down
ENSG00000189431	RASSF10	-0.6881077	0.00948251	0.04584741	down
ENSG00000085276	MECOM	-0.7227511	0.00949418	0.04587669	down
ENSG00000146411	SLC2A12	-0.7515403	0.00951274	0.0459439	down
ENSG00000116748	AMPD1	-0.7522398	0.00952686	0.04598175	down
ENSG00000214708	AC116407.1	-0.7318427	0.00954436	0.04605295	down
ENSG00000240567	LINC02067	-0.7408259	0.009557	0.04609316	down
ENSG00000279595	AC126335.2	-0.7470391	0.00955817	0.04609316	down
ENSG00000276966	HIST1H4E	-0.7193954	0.00957149	0.04613089	down
ENSG00000151067	CACNA1C	-0.7193428	0.00966244	0.04643945	down
ENSG00000276850	AC245041.3	-0.7490202	0.00985778	0.04711882	down
ENSG00000270547	LINC01235	-0.737227	0.0101173	0.04810841	down
ENSG00000260774	AC021087.3	-0.6893087	0.0101192	0.04810841	down

ENSG00000095637	SORBS1	-0.686284	0.01015006	0.04822786	down
ENSG00000104953	TLE6	-0.726698	0.01017488	0.04829118	down
ENSG00000169618	PROKR1	-0.727952	0.01035026	0.04897139	down
ENSG00000182795	C1orf116	-0.7169818	0.01042515	0.04920109	down
ENSG00000239704	CDRT4	-0.7390167	0.01044303	0.04922604	down
ENSG00000258102	MAP1LC3B2	-0.7223476	0.01045094	0.04922604	down
ENSG00000130600	H19	2.38588534	1.36E-77	7.60E-74	up
ENSG00000150687	PRSS23	1.86013685	2.47E-69	1.04E-65	up
ENSG00000107562	CXCL12	2.0655876	2.28E-52	5.48E-49	up
ENSG00000179388	EGR3	2.32293444	8.52E-47	1.79E-43	up
ENSG00000147255	IGSF1	2.20895076	3.05E-45	5.70E-42	up
ENSG00000082175	PGR	1.76038633	7.08E-44	1.19E-40	up
ENSG00000108352	RAPGEFL1	1.68677517	1.50E-38	1.80E-35	up
ENSG00000135454	B4GALNT1	1.63700979	3.47E-38	3.89E-35	up
ENSG00000196208	GREB1	1.49999775	6.89E-37	7.23E-34	up
ENSG00000111341	MGP	1.64337431	3.07E-35	2.87E-32	up
ENSG00000103257	SLC7A5	1.78990195	4.26E-32	3.25E-29	up
ENSG00000168003	SLC3A2	1.22538752	1.25E-30	9.12E-28	up
ENSG00000174827	PDZK1	1.40630798	3.15E-28	1.89E-25	up
ENSG00000250644	AC068580.4	1.18903333	6.21E-27	3.26E-24	up
ENSG00000182575	NXPH3	1.47620328	8.36E-26	4.13E-23	up
ENSG00000185697	MYBL1	1.31901962	1.26E-23	4.81E-21	up
ENSG00000109321	AREG	1.73602078	1.94E-23	7.24E-21	up
ENSG00000160182	TFF1	1.07344956	3.15E-23	1.15E-20	up
ENSG00000134830	C5AR2	1.31547139	3.82E-22	1.19E-19	up
ENSG00000147041	SYTL5	0.9820599	2.83E-21	8.05E-19	up
ENSG00000064205	WISP2	1.47385273	3.67E-21	1.03E-18	up
ENSG00000196136	SERPINA3	1.00180514	1.12E-20	2.98E-18	up
ENSG00000143126	CELSR2	1.12709609	1.32E-20	3.47E-18	up
ENSG00000112245	PTP4A1	0.95543898	1.45E-20	3.75E-18	up
ENSG00000130707	ASS1	1.02485922	2.19E-20	5.42E-18	up
ENSG00000186832	KRT16	2.32190127	2.61E-20	6.36E-18	up
ENSG00000069188	SDK2	1.4636282	4.99E-20	1.13E-17	up
ENSG00000166833	NAV2	1.73701223	1.17E-19	2.60E-17	up
ENSG00000163873	GRIK3	1.35653848	2.08E-19	4.41E-17	up
ENSG00000111816	FRK	1.32559618	3.93E-19	8.15E-17	up
ENSG00000130558	OLFM1	0.9751884	8.03E-19	1.61E-16	up
ENSG00000154553	PDLIM3	1.79340972	4.44E-18	8.29E-16	up
ENSG00000256870	SLC5A8	1.89728214	4.91E-18	9.07E-16	up
ENSG00000012171	SEMA3B	1.23455057	5.65E-18	1.02E-15	up
ENSG00000123416	TUBA1B	0.91781682	8.79E-18	1.55E-15	up

ENSG00000127418	FGFRL1	0.99939943	1.38E-17	2.40E-15	up
ENSG00000137267	TUBB2A	1.43172658	1.95E-17	3.24E-15	up
ENSG00000261373	VPS9D1-AS1	1.03281356	2.07E-17	3.38E-15	up
ENSG00000116649	SRM	0.96555488	1.08E-16	1.64E-14	up
ENSG00000065328	MCM10	0.98007211	1.08E-16	1.64E-14	up
ENSG00000188176	SMTNL2	1.72693951	1.21E-16	1.80E-14	up
ENSG00000176014	TUBB6	0.93709836	1.38E-16	2.04E-14	up
ENSG00000175175	PPM1E	1.03363987	1.51E-16	2.19E-14	up
ENSG00000171793	CTPS1	1.13972745	2.15E-16	3.09E-14	up
ENSG00000127564	PKMYT1	0.98296454	3.04E-16	4.33E-14	up
ENSG00000085840	ORC1	1.24507354	3.16E-16	4.42E-14	up
ENSG00000258947	TUBB3	1.07702466	4.68E-16	6.39E-14	up
ENSG00000170500	LONRF2	0.88599016	7.84E-16	1.05E-13	up
ENSG00000004478	FKBP4	0.9945451	8.53E-16	1.14E-13	up
ENSG00000181788	SIAH2	0.83130933	1.46E-15	1.93E-13	up
ENSG00000259527	LINC00052	1.39209766	1.92E-15	2.52E-13	up
ENSG00000197249	SERPINA1	1.12033674	2.62E-15	3.33E-13	up
ENSG00000164687	FABP5	1.23587625	6.99E-15	8.71E-13	up
ENSG00000244242	IFITM10	1.11726272	1.03E-14	1.25E-12	up
ENSG00000258017	AC011603.3	0.92786287	1.18E-14	1.43E-12	up
ENSG00000135502	SLC26A10	1.69207039	1.27E-14	1.52E-12	up
ENSG00000117593	DARS2	0.95556561	1.58E-14	1.83E-12	up
ENSG00000175920	DOK7	0.81608077	1.62E-14	1.87E-12	up
ENSG00000242173	ARHGDIG	1.05495317	1.72E-14	1.97E-12	up
ENSG00000088826	SMOX	1.44276238	1.99E-14	2.25E-12	up
ENSG00000146670	CDCA5	0.89451906	3.50E-14	3.90E-12	up
ENSG00000074211	PPP2R2C	0.85515004	4.90E-14	5.31E-12	up
ENSG00000196230	TUBB	0.87868569	5.44E-14	5.86E-12	up
ENSG00000107819	SFXN3	1.07927545	6.10E-14	6.49E-12	up
ENSG00000128268	MGAT3	1.84926051	6.59E-14	6.97E-12	up
ENSG00000141753	IGFBP4	0.84302593	8.35E-14	8.77E-12	up
ENSG00000075702	WDR62	0.91389944	9.71E-14	1.00E-11	up
ENSG00000100591	AHSA1	0.80091931	1.00E-13	1.03E-11	up
ENSG00000188488	SERPINA5	0.93856679	1.17E-13	1.18E-11	up
ENSG00000157193	LRP8	1.05556381	1.21E-13	1.21E-11	up
ENSG00000184702	Sep-05	1.17762785	1.47E-13	1.47E-11	up
ENSG00000128567	PODXL	0.85445093	2.06E-13	2.00E-11	up
ENSG00000134107	BHLHE40	1.26601318	2.53E-13	2.40E-11	up
ENSG00000117984	CTSD	0.94470411	2.53E-13	2.40E-11	up
ENSG00000166881	NEMP1	0.79767699	2.93E-13	2.75E-11	up
ENSG00000117399	CDC20	0.88324758	3.33E-13	3.11E-11	up

ENSG00000091527	CDV3	0.73039684	3.89E-13	3.61E-11	up
ENSG00000120694	HSPH1	0.80871871	4.04E-13	3.71E-11	up
ENSG00000171067	C11orf24	0.99360878	4.67E-13	4.26E-11	up
ENSG00000131462	TUBG1	0.93386191	5.60E-13	5.04E-11	up
ENSG00000171848	RRM2	0.80914214	5.61E-13	5.04E-11	up
ENSG00000014138	POLA2	0.82602196	7.16E-13	6.36E-11	up
ENSG00000069482	GAL	1.55799116	1.11E-12	9.62E-11	up
ENSG00000166508	MCM7	0.75934326	1.24E-12	1.06E-10	up
ENSG00000143476	DTL	1.04845652	1.50E-12	1.27E-10	up
ENSG00000167552	TUBA1A	0.73337719	1.71E-12	1.44E-10	up
ENSG00000168447	SCNN1B	1.59175888	1.95E-12	1.62E-10	up
ENSG00000101412	E2F1	0.83221623	2.03E-12	1.68E-10	up
ENSG00000170873	MTSS1	1.01858069	2.05E-12	1.69E-10	up
ENSG00000164619	BMPER	1.44417674	2.53E-12	2.07E-10	up
ENSG00000166426	CRABP1	1.01906104	2.75E-12	2.22E-10	up
ENSG00000146918	NCAPG2	0.79609714	2.83E-12	2.28E-10	up
ENSG00000131650	KREMEN2	0.94285087	3.02E-12	2.42E-10	up
ENSG00000157303	SUSD3	1.31145742	3.72E-12	2.94E-10	up
ENSG00000108179	PPIF	0.8559625	4.45E-12	3.43E-10	up
ENSG00000157600	TMEM164	0.82864093	4.48E-12	3.44E-10	up
ENSG00000167553	TUBA1C	0.88548786	4.89E-12	3.70E-10	up
ENSG00000177192	PUS1	0.93461361	1.10E-11	7.83E-10	up
ENSG00000112183	RBM24	1.27102984	1.16E-11	8.22E-10	up
ENSG00000172216	CEBPB	0.81659452	1.24E-11	8.69E-10	up
ENSG00000172137	CALB2	1.34058332	1.28E-11	8.95E-10	up
ENSG00000013810	TACC3	0.76247224	1.28E-11	8.96E-10	up
ENSG00000126067	PSMB2	0.77609975	1.43E-11	9.90E-10	up
ENSG00000166986	MARS	0.82258746	1.69E-11	1.16E-09	up
ENSG00000166886	NAB2	0.86686417	2.37E-11	1.57E-09	up
ENSG00000101003	GINS1	0.70506934	2.45E-11	1.61E-09	up
ENSG00000108561	C1QBP	0.7233785	2.50E-11	1.64E-09	up
ENSG00000120800	UTP20	0.88731535	3.10E-11	2.00E-09	up
ENSG00000166851	PLK1	0.85879489	3.32E-11	2.12E-09	up
ENSG00000127824	TUBA4A	1.30615063	3.63E-11	2.29E-09	up
ENSG00000115641	FHL2	1.05379636	3.80E-11	2.39E-09	up
ENSG00000197451	HNRNPAB	0.72356668	3.83E-11	2.40E-09	up
ENSG00000071539	TRIP13	0.84922708	3.99E-11	2.49E-09	up
ENSG00000178999	AURKB	0.88785777	4.93E-11	3.04E-09	up
ENSG00000165304	MELK	0.80828533	5.57E-11	3.40E-09	up
ENSG00000103126	AXIN1	0.81241661	6.37E-11	3.88E-09	up
ENSG00000174871	CNIH2	1.00971586	8.23E-11	4.99E-09	up

ENSG00000188976	NOC2L	0.72321609	9.02E-11	5.43E-09	up
ENSG00000164128	NPY1R	0.87549579	9.45E-11	5.67E-09	up
ENSG00000073111	MCM2	0.81254867	9.93E-11	5.94E-09	up
ENSG00000184992	BRI3BP	0.74796171	1.12E-10	6.63E-09	up
ENSG00000094804	CDC6	0.77205835	1.24E-10	7.24E-09	up
ENSG00000174945	AMZ1	0.96587863	1.30E-10	7.58E-09	up
ENSG00000100714	MTHFD1	0.75289803	1.36E-10	7.90E-09	up
ENSG00000135549	PKIB	0.8246436	1.59E-10	9.03E-09	up
ENSG00000250303	AP002884.3	1.08829311	1.63E-10	9.27E-09	up
ENSG00000087586	AURKA	0.66023503	1.66E-10	9.41E-09	up
ENSG00000128564	VGF	0.86751734	2.33E-10	1.29E-08	up
ENSG00000100092	SH3BP1	1.00431601	2.33E-10	1.29E-08	up
ENSG00000105245	NUMBL	0.93894761	2.43E-10	1.34E-08	up
ENSG00000155660	PDIA4	0.6941542	2.49E-10	1.35E-08	up
ENSG00000196924	FLNA	1.04897955	2.59E-10	1.40E-08	up
ENSG00000116455	WDR77	0.79592197	2.82E-10	1.52E-08	up
ENSG00000110104	CCDC86	0.92645447	2.86E-10	1.53E-08	up
ENSG00000096384	HSP90AB1	0.76442606	2.89E-10	1.54E-08	up
ENSG00000092853	CLSPN	0.8339215	3.07E-10	1.63E-08	up
ENSG00000159259	CHAF1B	0.8923294	3.11E-10	1.65E-08	up
ENSG00000276043	UHRF1	0.88572792	3.18E-10	1.68E-08	up
ENSG00000235027	AC068580.3	1.07541517	3.58E-10	1.87E-08	up
ENSG00000166197	NOLC1	0.74576783	3.92E-10	2.03E-08	up
ENSG00000130706	ADRM1	0.68910905	4.40E-10	2.27E-08	up
ENSG00000037897	METTL1	0.91932453	4.46E-10	2.28E-08	up
ENSG00000175792	RUVBL1	0.73304858	4.95E-10	2.53E-08	up
ENSG00000140961	OSGIN1	1.06183421	5.82E-10	2.94E-08	up
ENSG00000074410	CA12	0.67694686	6.41E-10	3.23E-08	up
ENSG00000113368	LMNB1	0.71988368	6.93E-10	3.46E-08	up
ENSG00000105011	ASF1B	0.72905798	7.28E-10	3.61E-08	up
ENSG00000100605	ITPK1	0.68454342	7.30E-10	3.61E-08	up
ENSG00000138166	DUSP5	1.24465839	7.45E-10	3.67E-08	up
ENSG00000196923	PDLIM7	0.99565512	8.04E-10	3.94E-08	up
ENSG00000258232	AC125611.3	0.76729536	8.31E-10	4.06E-08	up
ENSG00000085999	RAD54L	0.90368895	9.40E-10	4.55E-08	up
ENSG00000147536	GINS4	0.87719069	9.67E-10	4.65E-08	up
ENSG00000092621	PHGDH	0.80239225	1.03E-09	4.92E-08	up
ENSG00000051180	RAD51	0.88294635	1.04E-09	4.96E-08	up
ENSG00000115657	ABCB6	0.77484297	1.12E-09	5.31E-08	up
ENSG00000115310	RTN4	0.68050023	1.14E-09	5.39E-08	up
ENSG00000116120	FARSB	0.72544352	1.23E-09	5.82E-08	up

ENSG00000090273	NUDC	0.75281845	1.26E-09	5.87E-08	up
ENSG00000065833	ME1	0.75651121	1.30E-09	6.07E-08	up
ENSG00000125148	MT2A	0.84632421	1.40E-09	6.41E-08	up
ENSG00000135547	HEY2	1.42613047	1.44E-09	6.58E-08	up
ENSG00000188229	TUBB4B	0.69064874	1.49E-09	6.80E-08	up
ENSG00000067057	PFKP	0.76425712	1.54E-09	6.98E-08	up
ENSG00000111696	NT5DC3	1.01180407	1.57E-09	7.09E-08	up
ENSG00000066044	ELAVL1	0.73241256	1.58E-09	7.11E-08	up
ENSG00000022267	FHL1	0.83580293	1.66E-09	7.43E-08	up
ENSG00000197170	PSMD12	0.62422737	1.78E-09	7.94E-08	up
ENSG00000107833	NPM3	0.87561556	1.82E-09	8.07E-08	up
ENSG00000097021	ACOT7	0.76334252	1.82E-09	8.07E-08	up
ENSG00000165891	E2F7	0.8365714	1.84E-09	8.14E-08	up
ENSG00000103653	CSK	0.73141117	1.88E-09	8.28E-08	up
ENSG00000096060	FKBP5	0.76874817	1.99E-09	8.71E-08	up
ENSG00000101447	FAM83D	0.77121651	2.00E-09	8.75E-08	up
ENSG00000100462	PRMT5	0.6398109	2.28E-09	9.87E-08	up
ENSG00000101361	NOP56	0.75983745	2.47E-09	1.05E-07	up
ENSG00000204394	VARS	0.75686673	2.60E-09	1.10E-07	up
ENSG00000126602	TRAP1	0.65302174	2.77E-09	1.17E-07	up
ENSG00000158292	GPR153	0.74663142	2.98E-09	1.25E-07	up
ENSG00000153094	BCL2L11	0.78322404	3.04E-09	1.27E-07	up
ENSG00000051128	HOMER3	0.75266768	3.07E-09	1.28E-07	up
ENSG00000110719	TCIRG1	0.78425617	3.10E-09	1.29E-07	up
ENSG00000176890	TYMS	0.65945653	3.44E-09	1.42E-07	up
ENSG00000154328	NEIL2	0.95148548	3.45E-09	1.42E-07	up
ENSG00000138031	ADCY3	0.76216212	3.50E-09	1.43E-07	up
ENSG00000006047	YBX2	0.74838581	3.75E-09	1.53E-07	up
ENSG00000188486	H2AFX	0.68839367	4.00E-09	1.62E-07	up
ENSG00000106305	AIMP2	0.73371561	4.13E-09	1.67E-07	up
ENSG00000123136	DDX39A	0.64363521	4.24E-09	1.70E-07	up
ENSG00000093009	CDC45	0.80280562	4.30E-09	1.71E-07	up
ENSG00000118513	MYB	0.71147559	4.54E-09	1.81E-07	up
ENSG00000111641	NOP2	0.83670475	4.65E-09	1.84E-07	up
ENSG00000131876	SNRPA1	0.6681672	4.77E-09	1.89E-07	up
ENSG00000118707	TGIF2	0.74801024	5.41E-09	2.11E-07	up
ENSG00000145220	LYAR	0.80332916	5.50E-09	2.13E-07	up
ENSG00000177614	PGBD5	1.01845199	5.73E-09	2.22E-07	up
ENSG00000123213	NLN	0.65923275	5.74E-09	2.22E-07	up
ENSG00000134533	RERG	0.6834131	6.19E-09	2.38E-07	up
ENSG00000125459	MSTO1	0.83383108	6.97E-09	2.68E-07	up

ENSG00000165731	RET	0.65613846	6.99E-09	2.68E-07	up
ENSG00000070814	TCOF1	0.81455358	7.46E-09	2.84E-07	up
ENSG00000169085	C8orf46	1.41573681	7.55E-09	2.87E-07	up
ENSG00000113810	SMC4	0.63066287	7.92E-09	2.99E-07	up
ENSG00000113763	UNC5A	0.99135183	8.05E-09	3.03E-07	up
ENSG00000134690	CDCA8	0.69189879	9.41E-09	3.51E-07	up
ENSG00000100297	MCM5	0.73222165	9.77E-09	3.62E-07	up
ENSG00000148840	PPRC1	0.73407561	1.06E-08	3.92E-07	up
ENSG00000124215	CDH26	1.41950832	1.08E-08	3.96E-07	up
ENSG00000113649	TCERG1	0.76609619	1.13E-08	4.15E-07	up
ENSG00000130695	CEP85	0.74393961	1.19E-08	4.32E-07	up
ENSG00000112759	SLC29A1	0.66588237	1.21E-08	4.39E-07	up
ENSG00000064652	SNX24	0.72362235	1.26E-08	4.55E-07	up
ENSG00000172183	ISG20	0.79151101	1.30E-08	4.71E-07	up
ENSG00000154217	PITPNC1	0.75115585	1.37E-08	4.94E-07	up
ENSG00000108829	LRRC59	0.77905989	1.39E-08	5.01E-07	up
ENSG00000099337	KCNK6	0.72632639	1.41E-08	5.04E-07	up
ENSG00000156398	SFXN2	0.69590543	1.50E-08	5.33E-07	up
ENSG00000075624	ACTB	0.82281726	1.58E-08	5.56E-07	up
ENSG00000062822	POLD1	0.65248435	1.65E-08	5.77E-07	up
ENSG00000143502	SUSD4	0.71915794	1.77E-08	6.16E-07	up
ENSG00000013275	PSMC4	0.60755522	1.78E-08	6.19E-07	up
ENSG00000188735	TMEM120B	0.72153806	1.99E-08	6.86E-07	up
ENSG00000203618	GP1BB	1.26978933	1.99E-08	6.86E-07	up
ENSG00000138092	CENPO	0.71111258	2.00E-08	6.88E-07	up
ENSG00000108424	KPNB1	0.61541898	2.00E-08	6.88E-07	up
ENSG00000117308	GALE	0.71887677	2.07E-08	7.06E-07	up
ENSG00000102900	NUP93	0.824439	2.25E-08	7.65E-07	up
ENSG00000131153	GINS2	0.64908444	2.37E-08	8.03E-07	up
ENSG00000136982	DSCC1	0.71633566	2.58E-08	8.64E-07	up
ENSG00000183779	ZNF703	0.61215387	2.60E-08	8.70E-07	up
ENSG00000077312	SNRPA	0.64978569	2.64E-08	8.81E-07	up
ENSG00000005189	REXO5	0.79256805	2.82E-08	9.38E-07	up
ENSG00000151012	SLC7A11	1.17455283	3.01E-08	1.00E-06	up
ENSG00000092470	WDR76	0.76622728	3.04E-08	1.01E-06	up
ENSG00000019144	PHLDB1	0.72333725	3.16E-08	1.04E-06	up
ENSG00000149428	HYOU1	0.68641824	3.23E-08	1.06E-06	up
ENSG00000104998	IL27RA	0.88270765	3.28E-08	1.07E-06	up
ENSG00000165868	HSPA12A	0.93618122	3.27E-08	1.07E-06	up
ENSG00000153044	CENPH	0.67995577	3.30E-08	1.08E-06	up
ENSG00000181649	PHLDA2	0.92780791	3.35E-08	1.09E-06	up

ENSG00000072682	P4HA2	0.77054839	3.49E-08	1.13E-06	up
ENSG00000239672	NME1	0.68343213	3.51E-08	1.14E-06	up
ENSG00000095319	NUP188	0.73440575	3.77E-08	1.21E-06	up
ENSG00000161638	ITGA5	1.0788282	3.76E-08	1.21E-06	up
ENSG00000164970	FAM219A	0.86622089	3.85E-08	1.23E-06	up
ENSG00000239887	C1orf226	0.83412469	3.86E-08	1.23E-06	up
ENSG00000198947	DMD	0.91621515	4.31E-08	1.37E-06	up
ENSG00000136574	GATA4	1.5821872	4.37E-08	1.38E-06	up
ENSG00000093167	LRRFIP2	0.62061051	4.48E-08	1.41E-06	up
ENSG00000162729	IGSF8	0.7285458	4.53E-08	1.42E-06	up
ENSG00000163659	TIPARP	0.68782351	4.75E-08	1.48E-06	up
ENSG00000116830	TTF2	0.67334593	4.81E-08	1.49E-06	up
ENSG00000170439	METTL7B	0.83095475	5.04E-08	1.55E-06	up
ENSG00000147256	ARHGAP36	1.52878011	5.44E-08	1.67E-06	up
ENSG00000130204	TOMM40	0.73213094	5.52E-08	1.69E-06	up
ENSG00000072110	ACTN1	0.73796479	5.56E-08	1.70E-06	up
ENSG00000179041	RRS1	0.77748181	5.63E-08	1.71E-06	up
ENSG00000171241	SHCBP1	0.6084472	5.74E-08	1.74E-06	up
ENSG00000117877	CD3EAP	0.74426174	6.20E-08	1.87E-06	up
ENSG00000169180	XPO6	0.65611183	6.20E-08	1.87E-06	up
ENSG00000140416	TPM1	0.65575469	6.33E-08	1.90E-06	up
ENSG00000169016	E2F6	0.61401717	6.38E-08	1.92E-06	up
ENSG00000108578	BLMH	0.71691933	6.83E-08	2.04E-06	up
ENSG00000237649	KIFC1	0.61972518	7.47E-08	2.21E-06	up
ENSG00000068724	TTC7A	0.66206564	7.59E-08	2.24E-06	up
ENSG00000132819	RBM38	0.67988266	7.58E-08	2.24E-06	up
ENSG00000196497	IPO4	0.72062247	7.90E-08	2.32E-06	up
ENSG00000168461	RAB31	0.73701659	7.93E-08	2.32E-06	up
ENSG00000164163	ABCE1	0.6114603	8.22E-08	2.40E-06	up
ENSG00000066697	MSANTD3	0.77950445	9.16E-08	2.66E-06	up
ENSG00000168496	FEN1	0.58630068	9.59E-08	2.77E-06	up
ENSG00000173621	LRFN4	0.81057512	9.77E-08	2.82E-06	up
ENSG00000197771	MCMBP	0.61177201	1.03E-07	2.95E-06	up
ENSG00000164172	MOCS2	0.628924	1.10E-07	3.15E-06	up
ENSG00000011422	PLAUR	1.25431684	1.11E-07	3.17E-06	up
ENSG00000037474	NSUN2	0.64136643	1.11E-07	3.18E-06	up
ENSG00000168411	RFWD3	0.59211453	1.11E-07	3.19E-06	up
ENSG00000023909	GCLM	0.77839426	1.15E-07	3.28E-06	up
ENSG00000165490	DDIAS	0.72684708	1.17E-07	3.33E-06	up
ENSG00000214517	PPME1	0.65673958	1.17E-07	3.33E-06	up
ENSG00000149798	CDC42EP2	0.93371887	1.18E-07	3.36E-06	up

ENSG00000188536	HBA2	0.94733642	1.20E-07	3.40E-06	up
ENSG00000121152	NCAPH	0.76895486	1.25E-07	3.54E-06	up
ENSG00000136875	PRPF4	0.65619649	1.25E-07	3.54E-06	up
ENSG00000134684	YARS	0.70196149	1.33E-07	3.75E-06	up
ENSG00000111907	TPD52L1	0.59917791	1.38E-07	3.86E-06	up
ENSG00000160193	WDR4	0.71845004	1.43E-07	3.98E-06	up
ENSG00000119714	GPR68	1.01523518	1.49E-07	4.11E-06	up
ENSG00000124302	CHST8	0.91902746	1.55E-07	4.27E-06	up
ENSG00000175793	SFN	0.70967357	1.59E-07	4.36E-06	up
ENSG00000213024	NUP62	0.62297278	1.68E-07	4.58E-06	up
ENSG00000072062	PRKACA	0.63419041	1.69E-07	4.60E-06	up
ENSG00000168268	NT5DC2	0.61309677	1.74E-07	4.71E-06	up
ENSG00000132688	NES	0.75802494	1.80E-07	4.87E-06	up
ENSG00000167723	TRPV3	1.30507815	1.84E-07	4.94E-06	up
ENSG00000176170	SPHK1	0.76141535	2.05E-07	5.44E-06	up
ENSG00000076382	SPAG5	0.61702193	2.15E-07	5.71E-06	up
ENSG00000175785	PRIMA1	1.10365459	2.20E-07	5.82E-06	up
ENSG00000087263	OGFOD1	0.64999561	2.21E-07	5.84E-06	up
ENSG00000237330	RNF223	0.72185287	2.28E-07	6.01E-06	up
ENSG00000072422	RHOBTB1	0.87238742	2.48E-07	6.49E-06	up
ENSG00000144354	CDCA7	0.84360277	2.62E-07	6.84E-06	up
ENSG00000111602	TIMELESS	0.64440897	2.65E-07	6.92E-06	up
ENSG00000155380	SLC16A1	0.85472315	2.66E-07	6.93E-06	up
ENSG00000132780	NASP	0.60351367	2.70E-07	7.01E-06	up
ENSG00000108344	PSMD3	0.61528698	2.82E-07	7.30E-06	up
ENSG00000179241	LDLRAD3	0.82108224	2.89E-07	7.48E-06	up
ENSG00000184009	ACTG1	0.75999808	2.99E-07	7.69E-06	up
ENSG00000143401	ANP32E	0.59094094	3.05E-07	7.83E-06	up
ENSG00000167900	TK1	0.62094245	3.11E-07	7.97E-06	up
ENSG00000198826	ARHGAP11A	0.5945921	3.20E-07	8.17E-06	up
ENSG00000176619	LMNB2	0.59341764	3.51E-07	8.90E-06	up
ENSG00000139734	DIAPH3	0.7520555	3.64E-07	9.24E-06	up
ENSG00000162073	PAQR4	0.59202358	3.73E-07	9.44E-06	up
ENSG00000174437	ATP2A2	0.64379059	3.76E-07	9.51E-06	up
ENSG00000168453	HR	0.61645844	3.88E-07	9.79E-06	up
ENSG00000140545	MFGE8	0.74092942	4.08E-07	1.02E-05	up
ENSG00000198176	TFDP1	0.5947683	4.32E-07	1.08E-05	up
ENSG00000234964	FABP5P7	1.34262037	4.41E-07	1.10E-05	up
ENSG00000178966	RMI1	0.687913	4.51E-07	1.12E-05	up
ENSG00000213397	HAUS7	0.70913262	4.71E-07	1.17E-05	up
ENSG00000173540	GMPPB	0.61184326	4.80E-07	1.19E-05	up

ENSG00000111667	USP5	0.607085	4.96E-07	1.22E-05	up
ENSG00000123473	STIL	0.59689892	4.98E-07	1.23E-05	up
ENSG00000163485	ADORA1	0.74233134	5.08E-07	1.25E-05	up
ENSG00000136811	ODF2	0.65776163	5.25E-07	1.29E-05	up
ENSG00000244405	ETV5	1.15421147	5.36E-07	1.31E-05	up
ENSG00000139514	SLC7A1	0.68989689	5.53E-07	1.35E-05	up
ENSG00000168061	SAC3D1	0.65891362	5.55E-07	1.35E-05	up
ENSG00000196449	YRDC	0.784726	5.73E-07	1.38E-05	up
ENSG00000160211	G6PD	0.70203652	5.74E-07	1.38E-05	up
ENSG00000139352	ASCL1	0.59298634	5.91E-07	1.42E-05	up
ENSG00000073282	TP63	1.3088023	5.96E-07	1.43E-05	up
ENSG00000104889	RNASEH2A	0.62898058	6.01E-07	1.44E-05	up
ENSG00000141076	UTP4	0.59454392	6.05E-07	1.45E-05	up
ENSG00000143179	UCK2	0.59903699	6.16E-07	1.47E-05	up
ENSG00000155561	NUP205	0.63464245	6.32E-07	1.50E-05	up
ENSG00000127589	TUBBP1	0.7347889	6.35E-07	1.51E-05	up
ENSG00000183955	KMT5A	0.59953266	6.54E-07	1.55E-05	up
ENSG00000130309	COLGALT1	0.60181302	6.55E-07	1.55E-05	up
ENSG00000156299	TIAM1	0.71581259	6.67E-07	1.58E-05	up
ENSG00000062485	CS	0.62991743	6.81E-07	1.61E-05	up
ENSG00000116871	MAP7D1	0.71309917	6.94E-07	1.63E-05	up
ENSG00000131873	CHSY1	0.64359309	6.96E-07	1.63E-05	up
ENSG00000007923	DNAJC11	0.65591061	7.14E-07	1.67E-05	up
ENSG00000184164	CRELD2	0.64805838	7.33E-07	1.71E-05	up
ENSG00000154310	TNIK	1.05480354	7.51E-07	1.74E-05	up
ENSG00000204060	FOXO6	0.81065089	7.60E-07	1.76E-05	up
ENSG00000110880	CORO1C	0.70760626	7.63E-07	1.77E-05	up
ENSG00000205352	PRR13	0.61162571	7.68E-07	1.78E-05	up
ENSG00000184675	AMER1	0.83047393	7.71E-07	1.78E-05	up
ENSG00000129810	SGO1	0.65096726	7.71E-07	1.78E-05	up
ENSG00000176903	PNMA1	0.6009817	8.63E-07	1.98E-05	up
ENSG00000247077	PGAM5	0.60975723	8.68E-07	1.99E-05	up
ENSG00000146242	TPBG	0.71863843	8.89E-07	2.03E-05	up
ENSG00000106683	LIMK1	0.65889272	8.99E-07	2.06E-05	up
ENSG00000090861	AARS	0.6062182	9.02E-07	2.06E-05	up
ENSG00000174371	EXO1	0.70241693	9.23E-07	2.10E-05	up
ENSG00000104368	PLAT	1.36172705	9.28E-07	2.11E-05	up
ENSG00000091651	ORC6	0.65488961	9.41E-07	2.13E-05	up
ENSG00000213780	GTF2H4	0.65679949	9.63E-07	2.17E-05	up
ENSG00000140650	PMM2	0.64025522	9.72E-07	2.19E-05	up
ENSG00000106772	PRUNE2	0.91508317	9.76E-07	2.20E-05	up

ENSG00000054598	FOXC1	0.96538975	1.02E-06	2.28E-05	up
ENSG00000134595	SOX3	0.64102346	1.02E-06	2.28E-05	up
ENSG00000110400	NECTIN1	0.71576879	1.05E-06	2.35E-05	up
ENSG00000166908	PIP4K2C	0.6384014	1.08E-06	2.41E-05	up
ENSG00000253125	AC055854.1	0.90560146	1.11E-06	2.47E-05	up
ENSG00000113273	ARSB	0.85668738	1.17E-06	2.58E-05	up
ENSG00000167513	CDT1	0.63683866	1.21E-06	2.67E-05	up
ENSG00000149136	SSRP1	0.62224767	1.22E-06	2.69E-05	up
ENSG00000152137	HSPB8	0.70925875	1.23E-06	2.70E-05	up
ENSG00000106123	EPHB6	0.7829281	1.32E-06	2.90E-05	up
ENSG00000143845	ETNK2	0.68812584	1.34E-06	2.93E-05	up
ENSG00000131504	DIAPH1	0.61462777	1.39E-06	3.02E-05	up
ENSG00000108671	PSMD11	0.62244251	1.41E-06	3.07E-05	up
ENSG00000154146	NRGN	0.73228158	1.42E-06	3.08E-05	up
ENSG00000075420	FNDC3B	0.66458819	1.46E-06	3.14E-05	up
ENSG00000140534	TICRR	0.64309712	1.50E-06	3.21E-05	up
ENSG00000163918	RFC4	0.61617897	1.50E-06	3.22E-05	up
ENSG00000181026	AEN	0.69261981	1.57E-06	3.35E-05	up
ENSG00000189091	SF3B3	0.6055158	1.57E-06	3.36E-05	up
ENSG00000163235	TGFA	0.74611195	1.59E-06	3.38E-05	up
ENSG00000130810	PPAN	0.62972438	1.66E-06	3.52E-05	up
ENSG00000109501	WFS1	0.62426669	1.67E-06	3.54E-05	up
ENSG00000116670	MAD2L2	0.59965074	1.67E-06	3.54E-05	up
ENSG00000131759	RARA	0.7563297	1.74E-06	3.66E-05	up
ENSG00000167670	CHAF1A	0.67077679	1.75E-06	3.68E-05	up
ENSG00000160214	RRP1	0.59818373	1.79E-06	3.75E-05	up
ENSG00000007968	E2F2	0.6890783	1.82E-06	3.79E-05	up
ENSG00000141499	WRAP53	0.6539592	1.84E-06	3.83E-05	up
ENSG00000151640	DPYSL4	0.82746589	1.95E-06	4.03E-05	up
ENSG00000111206	FOXM1	0.680354	2.25E-06	4.59E-05	up
ENSG00000111665	CDCA3	0.74560295	2.43E-06	4.92E-05	up
ENSG00000178921	PFAS	0.64524676	2.49E-06	5.03E-05	up
ENSG00000067225	PKM	0.61799827	2.52E-06	5.06E-05	up
ENSG00000185090	MANEAL	0.64783991	2.63E-06	5.24E-05	up
ENSG00000177303	CASKIN2	0.58732622	2.69E-06	5.37E-05	up
ENSG00000138821	SLC39A8	0.64521411	2.74E-06	5.43E-05	up
ENSG00000162377	COA7	0.6162633	2.75E-06	5.44E-05	up
ENSG00000103876	FAH	0.70249288	2.81E-06	5.54E-05	up
ENSG00000188807	TMEM201	0.67189585	2.81E-06	5.54E-05	up
ENSG00000091409	ITGA6	0.83112823	2.91E-06	5.72E-05	up
ENSG00000172927	MYEOV	1.10005342	2.91E-06	5.72E-05	up

ENSG00000250479	CHCHD10	0.65771859	2.94E-06	5.76E-05	up
ENSG00000127527	EPS15L1	0.59683267	2.98E-06	5.82E-05	up
ENSG00000269190	FBXO17	0.62353884	3.14E-06	6.06E-05	up
ENSG00000273445	AC133644.2	1.16660516	3.23E-06	6.22E-05	up
ENSG00000178531	CTXN1	0.62485291	3.37E-06	6.45E-05	up
ENSG00000277161	PIGW	0.76886101	3.37E-06	6.45E-05	up
ENSG00000107130	NCS1	0.61683122	3.48E-06	6.61E-05	up
ENSG00000023902	PLEKHO1	1.01312864	3.49E-06	6.64E-05	up
ENSG00000101331	CCM2L	0.79628624	3.56E-06	6.76E-05	up
ENSG00000183763	TRAIP	0.64482237	3.68E-06	6.96E-05	up
ENSG00000148459	PDSS1	0.70429724	3.69E-06	6.98E-05	up
ENSG00000106397	PLOD3	0.60366621	3.83E-06	7.21E-05	up
ENSG00000135476	ESPL1	0.60555124	3.88E-06	7.30E-05	up
ENSG00000166889	PATL1	0.69377265	4.00E-06	7.48E-05	up
ENSG00000256500	AL139300.1	0.60920377	4.00E-06	7.48E-05	up
ENSG00000170100	ZNF778	0.60516317	4.40E-06	8.19E-05	up
ENSG00000048991	R3HDM1	0.62161516	4.40E-06	8.19E-05	up
ENSG00000107815	TWNK	0.66785099	4.51E-06	8.37E-05	up
ENSG00000082516	GEMIN5	0.60924366	4.54E-06	8.41E-05	up
ENSG00000151849	CENPJ	0.62543092	4.72E-06	8.69E-05	up
ENSG00000114737	CISH	0.74900674	4.77E-06	8.77E-05	up
ENSG00000129245	FXR2	0.60704477	4.79E-06	8.79E-05	up
ENSG00000135723	FHOD1	0.68868361	4.98E-06	9.10E-05	up
ENSG00000073008	PVR	0.59837431	5.00E-06	9.11E-05	up
ENSG00000187243	MAGED4B	0.93907353	5.06E-06	9.19E-05	up
ENSG00000172789	HOXC5	1.2436683	5.23E-06	9.47E-05	up
ENSG00000160803	UBQLN4	0.58524612	5.25E-06	9.51E-05	up
ENSG00000261026	AC105046.1	1.24297497	5.35E-06	9.66E-05	up
ENSG00000141456	PELP1	0.59523974	5.49E-06	9.89E-05	up
ENSG00000114767	RRP9	0.64374571	5.50E-06	9.89E-05	up
ENSG00000169684	CHRNA5	0.63013077	5.51E-06	9.89E-05	up
ENSG00000059145	UNKL	0.68151549	5.64E-06	0.00010068	up
ENSG00000175166	PSMD2	0.62419914	5.70E-06	0.00010166	up
ENSG00000143368	SF3B4	0.70341994	5.72E-06	0.00010186	up
ENSG00000130725	UBE2M	0.63538341	5.80E-06	0.00010312	up
ENSG00000184497	TMEM255B	0.91329612	5.89E-06	0.00010452	up
ENSG00000105290	APLP1	0.6870142	6.01E-06	0.00010623	up
ENSG00000120158	RCL1	0.67401634	6.04E-06	0.00010657	up
ENSG00000090924	PLEKHG2	0.65812143	6.09E-06	0.00010717	up
ENSG00000011332	DPF1	0.8493648	6.57E-06	0.00011504	up
ENSG00000165632	TAF3	0.59862578	6.66E-06	0.00011628	up

ENSG00000169181	GSG1L	1.15019769	6.80E-06	0.00011819	up
ENSG00000273604	EPOP	0.66967359	6.99E-06	0.00012106	up
ENSG00000155090	KLF10	0.6499449	7.13E-06	0.00012323	up
ENSG00000013619	MAMLD1	0.80297032	7.50E-06	0.00012887	up
ENSG00000122679	RAMP3	0.74372257	7.56E-06	0.00012936	up
ENSG00000198805	PNP	0.58604679	7.59E-06	0.00012975	up
ENSG00000183036	PCP4	0.7605952	7.63E-06	0.00013018	up
ENSG00000106688	SLC1A1	0.68546306	8.11E-06	0.00013771	up
ENSG00000135632	SMYD5	0.61131981	8.30E-06	0.00014054	up
ENSG00000259803	SLC22A31	1.13850274	8.33E-06	0.00014086	up
ENSG00000151090	THRB	0.59434987	8.74E-06	0.00014741	up
ENSG00000065320	NTN1	0.65420155	9.32E-06	0.00015639	up
ENSG00000168754	FAM178B	0.91976477	9.77E-06	0.00016323	up
ENSG00000275700	AATF	0.60776961	9.90E-06	0.00016491	up
ENSG00000176438	SYNE3	0.84985377	1.01E-05	0.000167	up
ENSG00000135045	C9orf40	0.64122872	1.03E-05	0.00017017	up
ENSG00000101945	SUV39H1	0.59304611	1.09E-05	0.00017866	up
ENSG00000070495	JMJD6	0.77664557	1.09E-05	0.00017871	up
ENSG00000118894	EEF2KMT	0.60358727	1.13E-05	0.00018548	up
ENSG00000102879	CORO1A	0.62483613	1.16E-05	0.00018996	up
ENSG00000146410	MTFR2	0.74410533	1.17E-05	0.00019159	up
ENSG00000164045	CDC25A	0.65677103	1.28E-05	0.00020601	up
ENSG00000106477	CEP41	0.6024664	1.41E-05	0.00022581	up
ENSG00000124216	SNAI1	1.09859555	1.46E-05	0.00023257	up
ENSG00000137337	MDC1	0.5973785	1.51E-05	0.00023928	up
ENSG00000160360	GPSM1	0.58958027	1.52E-05	0.00023955	up
ENSG00000105255	FSD1	0.66608129	1.52E-05	0.00023955	up
ENSG00000101146	RAE1	0.59159126	1.52E-05	0.00024003	up
ENSG00000129932	DOHH	0.66940667	1.52E-05	0.00024006	up
ENSG00000275464	FP565260.1	0.66874839	1.54E-05	0.00024284	up
ENSG00000108448	TRIM16L	0.65581953	1.57E-05	0.00024601	up
ENSG00000121281	ADCY7	1.09401979	1.59E-05	0.00024961	up
ENSG00000129195	PIMREG	0.62671931	1.62E-05	0.00025227	up
ENSG00000053372	MRTO4	0.58836582	1.66E-05	0.0002584	up
ENSG00000141994	DUS3L	0.61460325	1.71E-05	0.0002636	up
ENSG00000151503	NCAPD3	0.60709456	1.82E-05	0.00027946	up
ENSG00000205002	AARD	0.66863847	1.83E-05	0.00028069	up
ENSG00000248101	AC002116.1	1.14965623	1.86E-05	0.0002842	up
ENSG00000138646	HERC5	0.88489299	1.88E-05	0.00028642	up
ENSG00000120254	MTHFD1L	0.72398232	1.99E-05	0.0002998	up
ENSG00000096968	JAK2	0.63979812	1.99E-05	0.0002998	up

ENSG00000117148	ACTL8	1.12163806	2.00E-05	0.00030136	up
ENSG00000184602	SNN	0.61021574	2.05E-05	0.00030633	up
ENSG00000106290	TAF6	0.62510614	2.12E-05	0.00031543	up
ENSG00000159147	DONSON	0.64066005	2.25E-05	0.00033231	up
ENSG00000249115	HAUS5	0.5905509	2.41E-05	0.00035312	up
ENSG00000196839	ADA	0.97803577	2.44E-05	0.00035661	up
ENSG00000091127	PUS7	0.60602872	2.63E-05	0.00037844	up
ENSG00000105559	PLEKHA4	0.74859421	2.67E-05	0.00038348	up
ENSG00000143847	PPFIA4	0.88586993	2.72E-05	0.00038937	up
ENSG00000197063	MAFG	0.5975893	2.73E-05	0.00039035	up
ENSG00000103154	NECAB2	1.17259096	2.73E-05	0.00039035	up
ENSG00000079393	DUSP13	1.1044387	2.78E-05	0.00039702	up
ENSG00000088305	DNMT3B	0.67821439	3.05E-05	0.00042952	up
ENSG00000160999	SH2B2	0.75458632	3.09E-05	0.00043408	up
ENSG00000109674	NEIL3	0.69104096	3.25E-05	0.00045242	up
ENSG00000100065	CARD10	0.63703954	3.28E-05	0.00045563	up
ENSG00000024422	EHD2	0.61125786	3.56E-05	0.00049107	up
ENSG00000158747	NBL1	0.62005752	3.58E-05	0.00049268	up
ENSG00000226777	FAM30A	1.19100961	3.62E-05	0.00049786	up
ENSG00000053747	LAMA3	0.65137967	3.67E-05	0.00050377	up
ENSG00000162891	IL20	0.92638663	3.70E-05	0.00050687	up
ENSG00000109107	ALDOC	0.82676604	3.78E-05	0.00051583	up
ENSG00000115414	FN1	0.60148259	3.83E-05	0.00051968	up
ENSG00000170345	FOS	0.71029256	3.83E-05	0.00051973	up
ENSG00000136883	KIF12	0.65096065	4.06E-05	0.00054536	up
ENSG00000249346	LINC01016	1.09703414	4.19E-05	0.00056158	up
ENSG00000145832	SLC25A48	0.82174845	4.25E-05	0.00056805	up
ENSG00000164741	DLC1	0.62573528	4.28E-05	0.00057026	up
ENSG00000127423	AUNIP	0.66860485	4.55E-05	0.00060247	up
ENSG00000183092	BEGAIN	0.77274418	5.03E-05	0.00065605	up
ENSG00000112578	BYSL	0.59854503	5.04E-05	0.00065643	up
ENSG00000179431	FJX1	0.74243776	5.07E-05	0.00065849	up
ENSG00000119698	PPP4R4	1.12032917	5.36E-05	0.00069001	up
ENSG00000137404	NRM	0.64943587	5.39E-05	0.00069243	up
ENSG00000131470	PSMC3IP	0.87810235	6.25E-05	0.00078742	up
ENSG00000074582	BCS1L	0.5919975	6.32E-05	0.00079375	up
ENSG00000253276	CCDC71L	0.63125233	6.34E-05	0.00079553	up
ENSG00000069535	MAOB	0.63153077	6.38E-05	0.00079934	up
ENSG00000137124	ALDH1B1	0.62966057	6.49E-05	0.00081083	up
ENSG00000075131	TIPIN	0.61582429	6.51E-05	0.00081248	up
ENSG00000177602	GSG2	0.69941123	6.95E-05	0.00086063	up

ENSG00000169218	RSPO1	1.14654183	7.11E-05	0.00087667	up
ENSG00000139438	FAM222A	0.6375932	7.27E-05	0.00089471	up
ENSG00000107104	KANK1	0.74000124	7.30E-05	0.00089808	up
ENSG00000141068	KSR1	0.79531194	7.35E-05	0.00090131	up
ENSG00000163132	MSX1	0.89062628	7.35E-05	0.00090131	up
ENSG00000151224	MAT1A	1.14787783	7.39E-05	0.00090544	up
ENSG00000221926	TRIM16	0.65685198	8.01E-05	0.00097348	up
ENSG00000163888	CAMK2N2	0.75483185	8.34E-05	0.00100588	up
ENSG00000178718	RPP25	0.62550498	9.42E-05	0.00112096	up
ENSG00000167771	RCOR2	0.96799912	9.72E-05	0.00114594	up
ENSG00000122591	FAM126A	0.73115653	9.88E-05	0.00116118	up
ENSG00000164294	GPX8	0.68340013	0.00010406	0.00121366	up
ENSG00000164638	SLC29A4	0.6864798	0.00010435	0.00121617	up
ENSG00000116833	NR5A2	1.0385313	0.00010532	0.00122492	up
ENSG00000100629	CEP128	0.64771034	0.00010805	0.00125142	up
ENSG00000162894	FCMR	0.81730431	0.00011057	0.00127626	up
ENSG00000186862	PDZD7	0.88590918	0.00011747	0.00134205	up
ENSG00000180739	S1PR5	0.95233684	0.00011782	0.00134421	up
ENSG00000160712	IL6R	0.76070894	0.00012416	0.00141088	up
ENSG00000006453	BAIAP2L1	0.65344497	0.00012438	0.00141242	up
ENSG00000160072	ATAD3B	0.64934089	0.00012555	0.00142282	up
ENSG00000079335	CDC14A	0.60528956	0.00012583	0.001424	up
ENSG00000103047	TANGO6	0.73896431	0.00013392	0.00149847	up
ENSG00000164949	GEM	0.83239278	0.00013375	0.00149847	up
ENSG00000118515	SGK1	0.73155496	0.00013389	0.00149847	up
ENSG00000203999	LINC01270	0.90609706	0.0001355	0.00150906	up
ENSG00000129173	E2F8	0.65074265	0.00013574	0.00150972	up
ENSG00000091732	ZC3HC1	0.59078092	0.00014004	0.00155036	up
ENSG00000132017	DCAF15	0.59323548	0.00014021	0.00155126	up
ENSG00000128266	GNAZ	0.64884002	0.00015032	0.00164791	up
ENSG00000171236	LRG1	0.94371963	0.00015333	0.00167442	up
ENSG00000143512	HHIPL2	0.84885255	0.00015484	0.00168811	up
ENSG00000187713	TMEM203	0.75918719	0.00015978	0.0017311	up
ENSG00000127954	STEAP4	0.68162995	0.00016306	0.00175886	up
ENSG00000164053	ATRIP	0.63778652	0.00016455	0.00177271	up
ENSG00000129911	KLF16	0.59134911	0.00017087	0.00183259	up
ENSG00000077152	UBE2T	0.5914752	0.00017816	0.0018962	up
ENSG00000064666	CNN2	0.69237458	0.00018823	0.00198173	up
ENSG00000198488	B3GNT6	1.03998404	0.00019048	0.00199946	up
ENSG00000110811	P3H3	0.98317611	0.00020052	0.00208789	up
ENSG00000004660	CAMKK1	0.76955976	0.00020151	0.00209691	up

ENSG00000261762	AC027228.2	0.70476095	0.00022788	0.00231899	up
ENSG00000124191	TOX2	0.80334319	0.00023245	0.00235332	up
ENSG00000115526	CHST10	0.66024266	0.00024944	0.00250726	up
ENSG00000054967	RELT	0.58972343	0.00026376	0.00263231	up
ENSG00000162769	FLVCR1	0.64057527	0.00027837	0.00276001	up
ENSG00000205363	C15orf59	0.76531464	0.00028135	0.0027781	up
ENSG00000169826	CSGALNACT2	0.59189134	0.00029055	0.00285385	up
ENSG00000251322	SHANK3	0.64517198	0.00029687	0.00290065	up
ENSG00000135083	CCNJL	0.64218536	0.00030003	0.00292608	up
ENSG00000198042	MAK16	0.60106935	0.0003034	0.0029525	up
ENSG00000119862	LGALSL	0.63599954	0.00030432	0.00295969	up
ENSG00000185615	PDIA2	0.91414921	0.00031087	0.00300946	up
ENSG00000243302	AC018638.4	1.04200252	0.00031258	0.00302245	up
ENSG00000102302	FGD1	0.72019633	0.00031655	0.0030487	up
ENSG00000102781	KATNAL1	0.63473071	0.0003226	0.00309456	up
ENSG00000154920	EME1	0.62163972	0.00032363	0.00310265	up
ENSG00000177542	SLC25A22	0.60770856	0.00033775	0.00320868	up
ENSG00000136167	LCP1	0.62405896	0.00034114	0.00323722	up
ENSG00000204516	MICB	0.59103677	0.00034153	0.0032373	up
ENSG00000263513	FAM72C	0.99823265	0.00035986	0.00337681	up
ENSG00000169884	WNT10B	1.00322728	0.00036161	0.00339001	up
ENSG00000169258	GPRIN1	0.59863885	0.00036711	0.00343135	up
ENSG00000205534	SMG1P2	0.59854705	0.00036692	0.00343135	up
ENSG00000101463	SYNDIG1	0.88420878	0.00042	0.0038195	up
ENSG00000180176	TH	0.9465542	0.00042129	0.00382871	up
ENSG00000198934	MAGEE1	0.97448813	0.00045871	0.00410495	up
ENSG00000183785	TUBA8	1.01639125	0.00046198	0.00413201	up
ENSG00000187627	RGPD1	1.0108526	0.00048649	0.00430085	up
ENSG00000246465	AC138904.1	0.75933346	0.0005181	0.00451854	up
ENSG00000154640	BTG3	0.85828574	0.00054231	0.00469795	up
ENSG00000196092	PAX5	0.88170335	0.00054917	0.00474939	up
ENSG00000213023	SYT3	0.74724744	0.00055239	0.00477056	up
ENSG00000111252	SH2B3	0.67200809	0.00056556	0.00487428	up
ENSG00000186185	KIF18B	0.6732352	0.00058228	0.00499273	up
ENSG00000139800	ZIC5	0.86102575	0.00058714	0.00502931	up
ENSG00000154277	UCHL1	0.82896267	0.00058712	0.00502931	up
ENSG00000187678	SPRY4	0.88575681	0.00058882	0.00504112	up
ENSG00000131746	TNS4	0.98077793	0.00064926	0.00547425	up
ENSG00000082212	ME2	0.66221945	0.0006628	0.00557505	up
ENSG00000092421	SEMA6A	0.68963665	0.00068657	0.00572952	up
ENSG00000130768	SMPDL3B	0.7343792	0.00069706	0.00579656	up

ENSG00000249992	TMEM158	0.95171158	0.00073876	0.00606915	up
ENSG00000162676	GFI1	0.90476156	0.00074216	0.00609071	up
ENSG00000141682	PMAIP1	0.79131702	0.0007747	0.00630394	up
ENSG00000124749	COL21A1	0.81021144	0.00079024	0.00639422	up
ENSG00000116285	ERRFI1	0.64634917	0.00079742	0.00644303	up
ENSG00000203685	STUM	0.90613727	0.00080325	0.0064745	up
ENSG00000162892	IL24	0.92156545	0.000904	0.0071596	up
ENSG00000139269	INHBE	0.93509746	0.00092487	0.00728028	up
ENSG00000154839	SKA1	0.62236572	0.00096272	0.00753661	up
ENSG00000106633	GCK	0.95438989	0.00096999	0.0075681	up
ENSG00000131015	ULBP2	0.63273792	0.00099671	0.00774063	up
ENSG00000116717	GADD45A	0.62783604	0.00103025	0.00793935	up
ENSG00000170231	FABP6	0.93508661	0.00104614	0.00801705	up
ENSG00000129455	KLK8	0.7971578	0.00106646	0.00813567	up
ENSG00000176749	CDK5R1	0.63163869	0.00108697	0.0082584	up
ENSG00000198825	INPP5F	0.59086349	0.00110337	0.00836036	up
ENSG00000100292	HMOX1	0.65416949	0.00118821	0.00888696	up
ENSG00000116329	OPRD1	0.63932782	0.00119335	0.0089175	up
ENSG00000120322	PCDHB8	0.62837669	0.00120847	0.0090042	up
ENSG00000039560	RAI14	0.68190129	0.00128452	0.00945582	up
ENSG00000099625	CBARP	0.65481132	0.00130624	0.00958635	up
ENSG00000128965	CHAC1	0.86711786	0.00132809	0.00970853	up
ENSG00000167103	PIP5KL1	0.62964511	0.00136193	0.00992362	up
ENSG00000137285	TUBB2B	0.85417205	0.00137732	0.01000319	up
ENSG00000175832	ETV4	0.7296181	0.00139804	0.01012298	up
ENSG00000278535	DHRS11	0.66939601	0.00141268	0.01020263	up
ENSG00000149489	ROM1	0.68881478	0.0014597	0.01047629	up
ENSG00000132554	RGS22	0.88155469	0.00146039	0.01047629	up
ENSG00000164077	MON1A	0.63860798	0.00147666	0.01056033	up
ENSG00000105991	HOXA1	0.90183086	0.00156305	0.01107693	up
ENSG00000117407	ARTN	0.83945349	0.00160594	0.01132104	up
ENSG00000023892	DEF6	0.64476534	0.00167091	0.01169082	up
ENSG00000100167	Sep-03	0.59504926	0.00168804	0.01177644	up
ENSG00000196427	NBPF4	0.7964635	0.00172688	0.01199515	up
ENSG00000204539	CDSN	0.87660273	0.00175931	0.01218161	up
ENSG00000175592	FOSL1	0.84128069	0.00179064	0.01235367	up
ENSG00000125434	SLC25A35	0.68933606	0.00187768	0.01284866	up
ENSG00000166831	RBPMS2	0.89718872	0.00189081	0.01291743	up
ENSG00000128011	LRFN1	0.64224067	0.00195769	0.01326647	up
ENSG00000137094	DNAJB5	0.59499492	0.00203436	0.01365396	up
ENSG00000176153	GPX2	0.65258658	0.0020635	0.01379989	up

ENSG00000170425	ADORA2B	0.78112195	0.00211285	0.01406098	up
ENSG00000153976	HS3ST3A1	0.60265781	0.0021549	0.01427746	up
ENSG00000248946	MTND3P22	0.80541578	0.00216572	0.01432391	up
ENSG00000168404	MLKL	0.60486782	0.00227242	0.01490059	up
ENSG00000103044	HAS3	0.83325561	0.00230589	0.01505544	up
ENSG00000108370	RGS9	0.69586515	0.00237042	0.01536934	up
ENSG00000132031	MATN3	0.64299389	0.00240621	0.01555335	up
ENSG00000223799	IL10RB-AS1	0.63252127	0.00242945	0.01567944	up
ENSG00000163710	PCOLCE2	0.69480714	0.0025664	0.01643764	up
ENSG00000172244	C5orf34	0.59153489	0.00268019	0.01698238	up
ENSG00000196756	SNHG17	0.58700233	0.00277675	0.01749103	up
ENSG00000280164	CU638689.5	0.84365747	0.00280039	0.01760696	up
ENSG00000165887	ANKRD2	0.86091137	0.00289795	0.01809844	up
ENSG00000185338	SOCS1	0.66211004	0.00294148	0.01831586	up
ENSG00000137474	MYO7A	0.74014155	0.00295963	0.01840841	up
ENSG00000139318	DUSP6	0.64831625	0.00299463	0.0185711	up
ENSG00000170819	BFSP2	0.71414001	0.00317977	0.01953189	up
ENSG00000168491	CCDC110	0.84296291	0.00326805	0.01996471	up
ENSG00000157833	GAREM2	0.81863712	0.00344689	0.02079267	up
ENSG00000019186	CYP24A1	0.84386986	0.00345981	0.0208591	up
ENSG00000214336	FOXI3	0.64240611	0.00349487	0.02102174	up
ENSG00000043039	BARX2	0.62716124	0.00350968	0.02108821	up
ENSG00000058085	LAMC2	0.66907888	0.00358502	0.02144692	up
ENSG00000282021	AC100810.3	0.83758086	0.00369516	0.02192746	up
ENSG00000158301	GPRASP2	0.8396365	0.00376773	0.0222724	up
ENSG00000166159	LRTM2	0.83854066	0.00382121	0.02251729	up
ENSG00000113356	POLR3G	0.644505	0.00392484	0.0229509	up
ENSG00000279673	AC092919.2	0.82038538	0.00392417	0.0229509	up
ENSG00000242265	PEG10	0.73150426	0.00409496	0.02372283	up
ENSG00000132481	TRIM47	0.68988811	0.0043664	0.0249513	up
ENSG00000265763	ZNF488	0.74713129	0.00459665	0.02604561	up
ENSG00000154127	UBASH3B	0.77723143	0.00467203	0.02641928	up
ENSG00000131016	AKAP12	0.60740781	0.00468517	0.02645844	up
ENSG00000115318	LOXL3	0.58522206	0.00484602	0.02715644	up
ENSG00000102385	DRP2	0.80702181	0.00486359	0.0272277	up
ENSG00000228830	AL160408.2	0.73532298	0.00507311	0.02820332	up
ENSG00000065989	PDE4A	0.74110304	0.00511315	0.02835091	up
ENSG00000152969	JAKMIP1	0.76758142	0.00523146	0.02884513	up
ENSG00000125657	TNFSF9	0.78203028	0.00536281	0.02937661	up
ENSG00000256663	AC112777.1	0.65522658	0.00540915	0.02953341	up
ENSG00000197576	HOXA4	0.72350438	0.00544847	0.02971027	up

ENSG00000140931	CMTM3	0.65756255	0.005452	0.02971984	up
ENSG00000227811	FAM212B-AS1	0.79729345	0.00555835	0.03020551	up
ENSG00000178752	ERFE	0.6121836	0.00562642	0.03048281	up
ENSG00000183850	ZNF730	0.78474456	0.00571155	0.03085448	up
ENSG00000101197	BIRC7	0.74317899	0.00589572	0.03166619	up
ENSG00000241361	SLC25A24P1	0.77938435	0.00628221	0.03322178	up
ENSG00000260807	AC009041.2	0.69479496	0.00650955	0.03417665	up
ENSG00000268736	MTCO3P39	0.78022235	0.0065173	0.03420666	up
ENSG00000232445	AC006329.1	0.64310082	0.00659042	0.03446134	up
ENSG00000167754	KLK5	0.78779948	0.00663048	0.0345754	up
ENSG00000102445	RUBCNL	0.76288385	0.00666349	0.03471375	up
ENSG00000101336	HCK	0.63220982	0.00668351	0.03479648	up
ENSG00000100078	PLA2G3	0.5972728	0.00689965	0.03568958	up
ENSG00000237424	FOXD2-AS1	0.67171473	0.00709833	0.03649265	up
ENSG00000198873	GRK5	0.68344869	0.00711327	0.03654711	up
ENSG00000269096	CT45A3	0.78020826	0.00717364	0.03677859	up
ENSG00000164778	EN2	0.63325036	0.00745033	0.03785071	up
ENSG00000198576	ARC	0.67448252	0.00755874	0.03829729	up
ENSG00000143494	VASH2	0.76538926	0.00756268	0.03830574	up
ENSG00000136010	ALDH1L2	0.72349631	0.00789391	0.03972091	up
ENSG00000168389	MFSD2A	0.62207203	0.00837161	0.04163753	up
ENSG00000140807	NKD1	0.75632095	0.00854854	0.04226801	up
ENSG00000100385	IL2RB	0.76074491	0.00857594	0.04234769	up
ENSG00000066382	MPPED2	0.63614413	0.00865883	0.04269962	up
ENSG00000196932	TMEM26	0.67026731	0.00868029	0.04276781	up
ENSG00000189280	GJB5	0.6740983	0.008887	0.04352618	up
ENSG00000269940	AL049840.3	0.71131328	0.00937171	0.04541659	up
ENSG00000254290	AC124067.4	0.6558391	0.0094339	0.04569054	up
ENSG00000204710	SPDYC	0.66669564	0.00978617	0.04686986	up
ENSG00000095370	SH2D3C	0.74835112	0.00991933	0.04737264	up
ENSG00000159958	TNFRSF13C	0.74419974	0.01024674	0.04859104	up
ENSG00000255031	AP002807.1	0.70476231	0.01038575	0.04907028	up